Propagation and Scattering of Waves by Terrain Features

by

Bradley A. Davis

Dissertation submitted to the Faculty of the Virginia Polytechnic Institute and State University in partial fulfillment of the requirements for the degree of

Doctor of Philosophy

in

Electrical and Computer Engineering

Dr. Gary S. Brown, Chair

Dr. Ioannis M. Besieris

Dr. David A. DeWolf

Dr. Werner E. Kohler

Dr. Warren L. Stutzman

June 13, 2000

Blacksburg, Virginia

Keywords: Scattering, Propagation, Random Media

Propagation and Scattering of Waves by Terrain Features

Bradley A. Davis

(Abstract)

The intent of this dissertation is to obtain estimates of the effects of natural terrain features on the propagation and scattering of waves. It begins with the rough knife obstruction case, moves into rough surfaces and finally concludes with several approaches to a foliage covered rough surface. Each of these problems is encountered in radar, remote sensing and communication systems.

The first topic in this dissertation is the study of the effect of random edge roughness on the diffraction of a wave. This has been accomplished by approximating the field beyond the diffracting half-plane through the use of spectral techniques and the Kirchhoff approximation. The relationships developed for the mean or average diffracted field and the incoherent diffracted power are studied for a range of electrophysical parameters that are representative of the situation encountered in a point-to-point communications link with blockage by a rough edged half plane. The interpretation of the results is facilitated by the observation that the total diffracted field is a superposition of the incident field and the edge-diffracted field. When the roughness on the edge increases, the edge diffracted-field becomes more incoherent and the phase interference consequently diminishes, leading to an attenuation of the oscillations in the coherent or mean total field. The model also addresses the effects of the knife edge in directions off the line-of-sight path as well as its effects on pulse propagation.

Next, rough surface scattering effects are addressed. Extending the idea of the knife edge diffraction, this dissertation builds on the topic of a wedge on a plane by adapting the Method of Multiple Ordered Interactions (MOMI) to the dielectric surface. In this

development, the coupled integral equations governing the scattering by a dielectric surface are combined into a single equation wherein the lossy dielectric enters the solution as a perturbation of the result for a perfectly conducting surface. Hence, the solution is not only exact, but as the loss increases, the convergence is rapid. Next, the Kirchhoff approximation is expanded to a two-frequency form for use with the later chapters which deal with pulse scattering by rough surfaces. Example waveform calculations are given.

Propagation and scattering by a volume of scatterers over a surface is then examined. Starting from the radiative transfer equations, a model is developed herein for scattering from vegetated rough terrain. It assumes completely incoherent scattering and includes contributions from both the vegetation and the surface scattering along with a relatively simple accounting for their interaction. The model is developed into a form that easily separates the three primary components of the scattering problem – the radar system, the geometry, and the environment, and then recombines them through a multiple convolution.

Extending the basic model to volumes for which multiple scattering is important is accomplished through the use of effective parameters. These effective parameters are obtained by comparing the model with pulsed radar data at normal incidence, i.e., looking directly down through the foliage and onto the ground. Hence, our overall model is a hybrid approach wherein the basic physics are retained in the simple solution. It is then extended to a more complicated environment through the use of these effective parameters. Example waveform calculations are given.

The simple model assumes that multiple interactions are insignificant and that only narrow-band signals and narrow-beamwidth antenna patterns are used. Consequently, a more general radiative transfer approach is applied to the propagation of a beam through the random medium. This effort is a test of the narrow beamwidth and forward-backward scattering approximations implicit in the convolutional model. Next, the same convolutional model is developed using wave theory in order to clarify the assumptions and lend some physical meaning to the free parameters of the convolutional model. First the single scatter theory, with strictly forward and backward scattering is shown to be equivalent to the convolutional approach derived with radiative transfer theory. Next,

multiple scattering in a discrete random medium is investigated in the "extended" Twersky approximation [Tsolakis, 1985]. This development leads to the mean Green's function for the medium, a form of the Distorted Wave Born Approximation and to a two-frequency radiative transfer equation. This transfer equation is then shown to simplify under the forward-backward assumption, eventually leading to a form which is compatible with the convolutional result.

Finally, the effects of multiple scattering between the volume and its boundary, the rough surface, have been investigated. Using a numerical implementation (MOMI) of a scatterer over a rough surface, the orders of significant multiple interactions between the rough surface and the volume scattering components have been simulated. It is demonstrated that foliage components well above the rough surface may be treated as non-interacting; this includes components other than the trunks, which were not simulated. However, it is evident that multiple scattering effects may be significant for large objects near the rough surface.

This work has been supported by grants from the Bradley Department of Electrical and Computer Engineering, National Science Foundation, and the Virginia Space Grant Consortium. Additional support has been provided by the U.S. Air Force at Hansom Airforce Base under grant F19628-96-C-0071, and U.S. Army Research Office under grant DAAG55-97-1-0164.

Dedication

I would like to dedicate this work to my family. Only their helpful support, understanding and kindness have made this work possible.

Acknowledgments

I would like to express my sincere thanks to my advisor, Dr. Gary S. Brown for his guidance, time and efforts on my behalf. I could not have started or finished without his encouragement and assistance. His friendship and gentle supervision and the working environment of the ElectroMagnetic Interactions Laboratory have made this experience exciting and challenging.

I would like to thank Dr. Ioannis Besieris for introducing me to the area of electromagnetics so many years ago. He is a masterful teacher and certainly has made one of the most feared subjects both exciting and comprehensible. In addition, I must thank him for his constant friendship, encouragement and our long talks. I also express my warmest appreciation to the rest of my committee. Dr Werner Kohler opened the world of applied mathematics to me. His classes and counsel gave me the mathematical tools and maturity to complete my research. Dr. Warren Stutzman has opened the world of applied electromagnetics and inspired me to my first job in antennas. His practical approach to the discipline has always kept me on track. Finally, I would like to thank Dr. David DeWolf for his time and the many discussions we had. His deep insight into my thesis subject has been a constant source of new ideas and instruction.

Special thanks are also due to my friends and teachers in the ElectroMagnetic Interactions Laboratory. First and foremost, I must thank my good friend, Dr. Robert Adams for his encouragement, commiseration and instruction. He is a constant source of new ideas and insight. Next, I must thank Dr. Raid Awadallah for his instruction and kindness through this experience. In addition to being a great friend, he is a natural-born teacher. Finally, I would like to thank the remainder of the ElectroMagnetic Interactions Laboratory: Bryan Browe, Dr. Jakov Toporkov, Dr. Roger Marchand, and Dr. David Kapp for their friendship and assistance. This entire group of friends and coworkers have made this experience as enjoyable as possible.

Finally, my deepest appreciation goes to my wife, Monica and my children Ian and Connor who have endured over four years of neglect. Their constant diversion and love have made my life complete. Retribution for lost time and lost kindness is required. I am unable express my regret for lost time with them. In addition, I thank my parents, Richard and Isabelle Davis for their rich support and encouragement throughout the years. I look forward to more time to spend with my entire family.

I would like to thank all of the following sponsors for their generous support. This research was supported by many different groups. First, I would like to thank Dr Ferrari and the entire faculty and staff of the Bradley Department of Electrical and Computer Engineering for my selection as a the Bradley Fellow. Next, I would like to thank Dr Richard Weyers for his support for me through his Civil Infrastructure grant sponsored by the National Science Foundation. Next I would like to thank Mr. William Stevens of the U.S. Air Force at Hansom Airforce Base for his support, and Dr. James Harvey of the U.S. Army Research Office. The author to these is indebted to individuals for technical guidance and discussions on this problem. Finally, I would like to thank the Virginia Space Grant Consortium for their support.

Table of Contents

List of Figures

Chapter 1 Introduction and Literature Survey

The modeling and prediction of electromagnetic wave interaction with natural terrain features is the subject of a vast body of literature covering a large array of topics. The prediction of forward and/or backscattered waveforms is addressed in this thesis in three arenas: past edges, over the terrain, and through vegetation. Propagation through vegetation is actually in combination with the surface scattering, particularly in radar studies.

In Chapter 2 , the propagation in a mountainous region is examined using the physical optics and the knife edge approximations. The effects of roughness are examined to varying degrees along the line-of-sight, wide angle, and for pulse propagation. This work is continued in Chapter 3 with moment method (MOM) simulations of scattering by a one-dimensional rough surface which is either perfectly conducting or dielectric; this study is work in progress. In addition, as a precursor to the volume-surface interaction of the next several sections, this chapter reviews other methods of predicting surface scattering, including the impulse response method [Brown, 1997] and a two-frequency Kirchhoff scattering result.

Chapter 4 begins the examination of the interaction with a vegetated terrain. In this chapter, the problem is examined with a radiative transfer approach and is quickly reduced to a simple, computationally efficient solution method; henceforth referred to as the *convolutional model*. The next chapter examines the possibility of beam spread within the volume using more generalized transfer theory results. The following two chapters present a reconciliation of the radiative transfer approach with wave theory. Chapter 6 attacks this problem using single scatter theory. Under limiting assumptions, the single scatter solution is shown to reduce to the convolutional model. Chapter 7 develops the multiple scattering equations and then presents a slight variation on existing, two-frequency radiative transfer equations. Under the assumptions common to the previous two chapters, this formulation also leads to a form similar to the convolutional model. Finally, Chapter 8 examines the consequences of the interaction of the surface and volume components using numerical methods and an analytical method that remains a work in progress.

1.1 Propagation Over a Rough Knife Edge

Diffraction by a knife edge boundary has long been used as a model to estimate the effect of path-obstructing ridges, mountains, and other natural obstacles in terrestrial-based communication links. The use of this approximation is now of interest in assessing blockage effects involving much shorter paths, e.g., such as in propagation in an urban environment where buildings and other man-made obstacles cause the path blockage. Although the knife edge boundary solution has been used extensively to model natural and man-made diffracting objects, there has always been an uncertainty associated with estimating the effects of *edge roughness* on the diffraction pattern.

Previous efforts for modeling the diffraction by a rough edge using aperture integration have appeared in the literature. Two papers in particular address the communication problem by modeling the diffraction by edges using the Kirchhoff approximation and nontransparent absorbing screens [Polishchuk, 1971] and [Polishchuk, 1974]. The paper by Dagurov, *et al.* [Dagurov, 1994] presents a method in which real terrain data may be used to predict the propagation over rough edges using the Kirchhoff approximation. On the other hand, the paper by George and Morris [George, 1989] which addresses diffraction by serrated apertures in the optical limit, most closely resembles the approach presented in this study. The application in this case addresses the statistical properties of a converging lens modeled as a serrated aperture.

The results presented herein are noteworthy relative to these previous works for their simplicity, their straightforward design implications, and their robustness. In addition, they give, for the first time, the communication system designer the ability to estimate the *degree of variability* possible in the received power levels resulting from a mid-path diffracting object with rough edges. It is not possible to predict exactly what the received power levels will be because the edge-diffracted field is a random process resulting from the randomly rough edge. Once the system is set in place, the received power will comprise *only one realization* of this random process. Without some method that *either* simulates averaging, e.g. moving the transmitter and/or the receiver or dithering the carrier frequency, *or* provides a detailed description of the rough edge profile, this one realization is what must be worked with. However, the equation for the incoherent power developed in this paper is appropriate for estimating the degree of variability that should be expected. If this degree of variability (uncertainty) is too large, adjustments in the system parameters will have to be undertaken during the link design phase to reduce it. The important point is that engineers now have the ability to determine exactly what can be changed to diminish the uncertainty!

1.2 Foliage above a Rough Surface: An Approach Rationale

When studying scattering from the combination of a foliage layer above a rough surface, one must deal with the scattering from the foliage, the rough surface, and the interaction between the two. Of these three components to the fundamental scattering problem, the foliage scattering and the interaction scattering are the most difficult to analyze.

Foliage by itself presents a challenge to the analyst because of the many-body aspects of the problem. In addition, modeling foliage scattering from first principles is further complicated by the fact that the scatterers are irregular at best and generally ill-defined. From an electromagnetic point of view, leaves do not all look to be identical and twigs, branches, and limbs conform to no particular shape! Thus, except for very low and very high frequency limits, it is almost impossible to compute the scattering pattern of the basic "constituents" of foliage. Some details are known about the typical volume fraction of foliage and how this is partitioned between leaves and the woody components, and we have some idea of the range of complex dielectric constant variation for wood and leaf materials [Brown, 1982]. Yet another unknown is the variation of foliage density with depth into a canopy. Finally, even though foliage is quite frequently classified as on the edge of being a volumetrically sparse medium, this does not mean that there is a lack of strong electromagnetic interactions between the various scattering components, e.g., twigs, branches, leaves, etc. Furthermore, for European forests that have been well managed and not logged (also called old growth forests), the volume fractional density of the biomaterial may be as large as 5%.

When dealing with independently scattering objects and scattering from rough surfaces, it is possible to convert single-frequency models of the individual scattering cross sections (for the discrete objects) and the scattering cross section per unit area (for the extended surface scattering) into models for the incoherent time-dependent scattered waveform produced under pulse illumination. For strongly interacting individual scatterers, this simplification is not usually possible, the reason being that it is not sufficient to know that the scatterer is in a volume because its *location within the volume* must also be known.

What can be done then to resolve this dilemma? First, an effective “scattering cross section per unit illuminated volume, σ_v” may be extracted from airborne radar data, e.g., the scattered power P_r received by a pulsed radar is given by

$$P_r = P_t \frac{G^2(\theta_i, \phi_i)\lambda^2}{(4\pi)^2 R^4}\sigma$$

Equation 1.2-1

where the effective scattering cross is given by

$$\sigma = (cT/2)(R\Phi_{az})(R\Theta_{el})\sigma_v$$

Equation 1.2-2

Solving Equation 1.2-1 and Equation 1.2-2 for σ_v yields

$$\sigma_v = \frac{P_r}{P_t}\frac{(4\pi)^2 R^2}{G^2(\theta_i, \phi_i)\,(cT/2)(\Phi_{az}\Theta_{el})}$$

Equation 1.2-3

In the above equations P_r is the received or scattered power, P_t is the transmitted power, $G^2(\theta_i, \phi_i)$ is the two-way antenna gain in the indicated direction, c is the speed of light, T is the pulse length, R is the range to the volume, Φ_{az} is the antenna's azimuthal beamwidth, and Θ_{el} is its elevation beamwidth. Of course, some of these factors are a function of time indicating what portion of the volume scatterers are being illuminated by the incident pulse waveform as it passes through the scattering medium. Equation 1.2-3 is actually an approximation in that one should integrate over the volume bounded by the antenna gain pattern weighting and the pulse width extent. The important point is that incoherent power waveform data from a pulsed radar can be converted into an effective "scattering cross section per unit illuminated volume". It should be noted that, within the resolution limits imposed by the radar pulse width and antenna beamwidth, the σ_v extracted from the data may be a function of the slant path distance (R) into the medium.

The approach rationale followed in developing the model presented in this dissertation is as follows. First, it is well known that the end users of such models are extremely skeptical of any model that does not contain some measurements in its development. That is, they are concerned that the model be designed so that it is capable of at least reproducing known measurements. Consequently, it is essential to involve measured data in the model. The second element of this model is based upon the realization that it is possible to develop a somewhat general model for media that is not too strongly interacting and this model may be "matched" to data to determine the actual parameters that are embedded in the model and, perhaps, to extend it beyond its known range of validity. In short, the model parameters can be determined by matching actual measured data to the scattering results predicted by the model. It should be noted that such an approach avoids long and questionable computations based on one's *estimate* of what actually causes the scattering and how it does this. The reason for avoiding such computations is very simple – there is no way to estimate how applicable they will be since the accuracy of the overall model is unknown. By matching the model to data, the model's accuracy is extended through the use of "effective parameters" that are "calibrated" by the data. In summary then, the approach has been to develop a model that is accurate but not overly (computationally) detailed, match it to measured foliage scattering data to generate the model parameters ("effective parameters"), and then investigate the accuracy of extending the model to other situations using the existing "effective parameters".

1.3 The Waveform Scattered by a Vegetated Rough Surface

Ideally, in estimating the returned signal from foliage covered terrain, scattering models should include self and mutual interactions among all of the constituent components. These would include interactions among the discrete scatterers comprising the volume, the interactions between each surface element and finally the interactions between the surface and the volume. In the following sections, a brief introduction to the literature surrounding these components will be presented.

Beginning with full interaction problem, the incident field, $\vec{E}^{inc}$, see Figure 1.3-1, is defined as the field that would exist in free space in the absence of the foliage and the surface. With introduction of a scatterer, i.e. foliage, the total field is found to be a superposition of the incident field $\vec{E}^{inc}$ and the field scattered by the scatterer, $\vec{E}^{s}$.

$$\vec{E}^{total} = \vec{E}^{inc} + \vec{E}^{s}$$

Consequently, our first task will be the construction of the scattered field produced by the ith scatterer, $\vec{E}_i^s$, of the N objects which comprise the volume of scatterers.

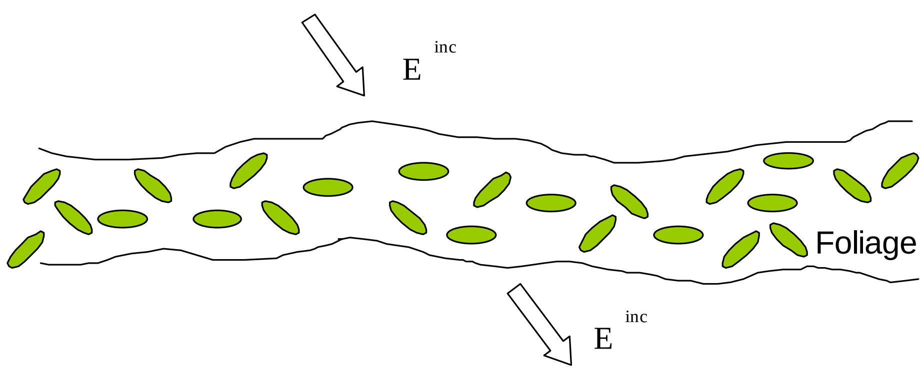

Figure 1.3-1: The Incident Field

Each component of the foliage (leaves, twigs, branches, etc.) will scatter the energy from the incident field. Isolated, each scatterer's effect can be assessed using an integral equation approach that leads to a Method of Moments (MOM) formulation. However, considered as one system, a full solution to the interaction of waves with the foliage-surface combination quickly out-paces present computing capabilities. Consequently, approximate, analytical methods are employed.

1.3.1 Volume Scattering

Modeling of scattering from a volume of scatterers has been handled in the literature in one of two ways: phenomenological models (radiative transfer) or physical models (wave theory). Extensive literature exists for scattering from vegetation and more generally, random media. Consequently, the reader is referred to other sources for complete literature reviews [Ishimaru, 1997], [Tsang, 1985]. In this review, only a few recent works will be briefly discussed.

Radiative transfer approach

The analytical, full wave approach to the multiple scattering problem presents many mathematical challenges even in tenuous, i.e. sparse, medium; consequently, the simpler ideas and the more tractable numerics of radiative transfer present an appealing alternative. However, since phase information is lost, the multiple scattering phenomena described by transfer theory are not well understood. In addition, transfer theory may only have a certain range of validity because of the following assumptions:

- interactions are considered incoherent
- interactions are considered to be far field
- extinction, scattering and propagation parameters have no direct physical interpretation
- frequency dependence is not accurately modeled
- certain multiple scattering processes are neglected, e.g. the so called “enhanced backscatter”

There exist at least two different levels of modeling the environment in radiative transfer theory. The first and most abundant in the literature is a level that can become quite detailed. Typical examples of this are found in references [Ulaby, 1990] and [Karam, 1992, 1997]. Ulaby, et al., solves the vector radiative transfer equations iteratively. Their model has been taken to the "second order" which is simply the second iterate of the radiative transfer equations. Their major assumptions, *beyond those inherent in the radiative transfer method itself*, include

- flat surface, i.e., specular boundary
- strongly forward scattering medium

Although in some cases, these approximations are valid, this model is not applicable (because of the medium assumptions) for lower frequencies nor, to a lesser degree at high frequencies because of the flat surface assumption. The deficiencies of previous models that this one claims to address are as follows [Ulaby, 1990]

- canopy is not treated as a continuous layer in the horizontal direction
- crown and foliage regions have the same scattering characteristics
- uniform dielectric constant and size, etc. are assumed

This model is created from the vector transfer equations for a two-layer medium. In the "Michigan" model, the extinction and scattering matrices are based on measured values of number density, extinction, etc. of leaves, needles, trunks and branches of all sizes. After great effort, these values are all combined to form an effective extinction matrix, $\bar{\bar{\mathrm{k}}}_{\mathrm{layer}}$, and an effective phase/power scattering matrix, $\bar{\bar{\mathrm{P}}}_{\mathrm{layer}}$, for each layer. In addition, the tree canopies are modeled as spheroidal in shape, rather than planar. They create transfer equations for the crown, trunk region and finally the underlying surface all of the following form (for upward and downward propagating intensities, see Figure 1.3-2):

$$\text{(upward)} \qquad \frac{d}{dz}\bar{I}^{+}_{layer}(\mu,\phi,z) = -\frac{1}{\mu}\bar{\bar{k}}^{+}_{e}\,\bar{I}^{+}_{layer}(\mu,\phi,z)$$

$$+\frac{1}{\mu}\int_0^1\int_0^{2\pi}\bar{\bar{P}}_{layer}\,\bar{I}^{+}_{layer}(\mu',\phi',z)\,d\Omega' + \frac{1}{\mu}\int_0^1\int_0^{2\pi}\bar{\bar{P}}_{layer}\,\bar{I}^{-}_{layer}(-\mu',\phi',z)\,d\Omega'$$

$$\text{(downward)} \qquad -\frac{d}{dz}\bar{I}^{-}_{layer}(\mu,\phi,z) = -\frac{1}{\mu}\bar{\bar{k}}^{+}_{e}\,\bar{I}^{-}_{layer}(\mu,\phi,z)$$

$$+\frac{1}{\mu}\int_0^1\int_0^{2\pi}\bar{\bar{P}}_{layer}\,\bar{I}^{+}_{layer}(-\mu',\phi',z)\,d\Omega' + \frac{1}{\mu}\int_0^1\int_0^{2\pi}\bar{\bar{P}}_{layer}\,\bar{I}^{+}_{layer}(\mu',\phi',z)\,d\Omega'$$

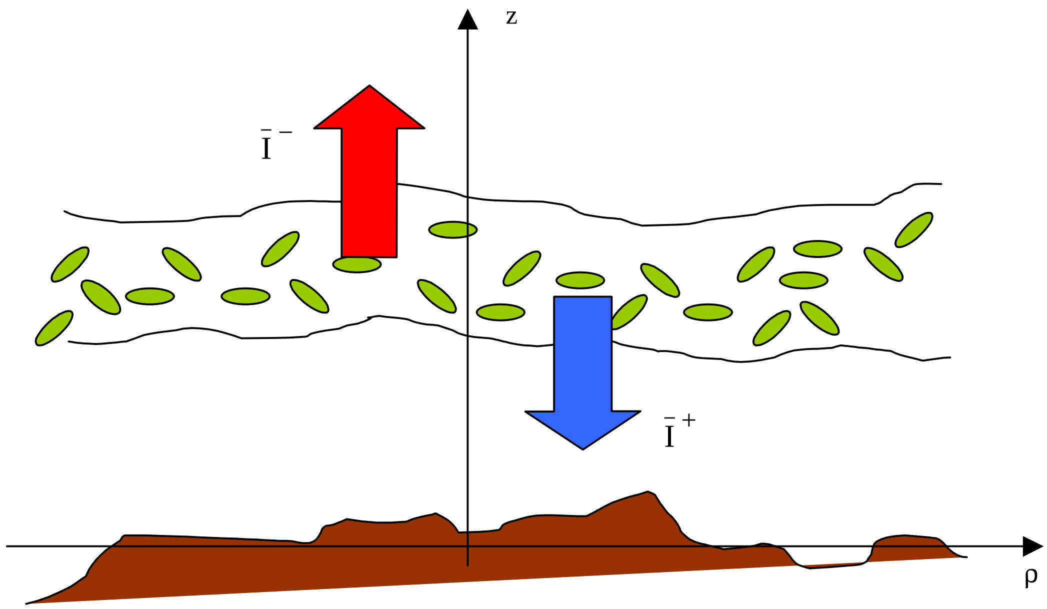

Figure 1.3-2: Upward and downward propagating power density

Given three sets of the above equations (one set each for the crown, trunk, ground), Ulaby's first order approximation to the radiative transfer equations is essentially a single scatter model. Solution is accomplished through iteration and at this point, up to two iterations have been reported [Ulaby, 1990], [McDonald, 1993]. Consequently, aside from the extra work to characterize the contributions to the propagation matrices, the result is the same as the bulk parameter models such as Schwering's [1985,1986] and the one described in this report. The difference is that the bulk parameters are characterized before the computation in the Michigan model and after-the-fact in the bulk parameter models.

The second approach to the radiative transfer deals in bulk media and effective parameters. A typical example of this approach would be the work of Johnson and Schwering [1985, 1986]. This approach creates a simple, random medium with a single type of scatterer. For millimeter wave propagation, they have assumed that the constituents of the random medium will scatter energy primarily in the forward direction. Hence, they define a scattering pattern that consists of a forward-directed (Gaussian) lobe superimposed on a greatly reduced isotropic background level for all other directions. This scattering pattern has subsequently been measured by Ulaby [1990] while in this dissertation, the scattering pattern (or function) is often assumed or even simplified to strictly forward-backward scattering. Using this simple model, Johnson and Schwering solve the classical radiative transfer equation using a Legendre polynomial expansion of the scattering pattern. Their results are straightforward and the model's free parameters allow simple matching to measured data. Whitman and Schwering have extended the same work to pulse propagation by simple Fourier decomposition of the time domain waveform [Whitman, 1996]. The response to each frequency component is determined using the previously developed solution to the radiative transfer equations and finally, the pulsed solution is synthesized by transforming back into the time domain. This study will address the scattering by a vegetated rough surface using the bulk parameter idea in Chapter 4 .

The final topic addressed in the radiative transfer development is the propagation of beams in the radiative transfer formulation. This topic was chosen since the effects of beam spread within the random media are neglected in the "convolutional model" of Chapter 4 , by default, when the scattering is assumed to be exclusively forward-backward. Simulating the beam spread in a random medium requires the solution of the full radiative transfer equations since the scattering pattern of the scatterers is arbitrary. This solution accounts for multiple scattering within the context of the radiative transfer theory. A few works have been performed in this area, the first was by Chang and Ishimaru [1987] and the only other relevant example is given by Zardecki [1985]. In each case, the solution method is similar to the one presented in this dissertation; however, the boundary conditions are different and the cases presented for comparison are unique to this dissertation.

Wave scattering approach

If multiple scattering within the volume is expected to play an important role, interactions among the discrete scatterers must be considered. Like the radiative transfer approach, the wave approach encompasses a great deal of literature. Starting with Maxwell's equations or the wave equation, a wave approach will include all multiple scattering, diffraction and interference effects. A full solution, however, quickly becomes intractable and approximations must be made. Single scatter theory is the simplest approach to the wave problem in a random medium. In scattering theory, the total field can be written as a sum of the free-space incident field and the scattered field due to each scatterer. The scattered field in a tenuous medium is a product of the dyadic scattering amplitude, f, and the applicable (far-field) Green's function along with the field incident to the scatterer.

$$\vec{E}(\vec{r}_a) = \vec{E}_i(\vec{r}_a) + \sum_{s=1}^{N} \overline{\overline{f}}(\hat{k}_s, \hat{k}_i) \cdot \vec{E}_i(\vec{r}_s) \frac{e^{-jkR}}{R}$$

Equation 1.3-1

When the incident field at the scatterer number s, (under the summation) is simply given by the *free-space incident field evaluated at the position* $\vec{r}_s$, Equation 1.3-1 is the **single scatter** or **Born Approximation** (often, the Born approximation is attributed to an integral equation, not a summation). In other words, the field incident to each scatterer neglects the fields due to scattering from other scatterers. Often the dyadic scattering matrix, $\overline{\overline{f}}$ in Equation 1.3-1, is written as a product of the Fourier transform of the scattering operator and the remainder of the far-field form of the free space Green's function [Frisch, 1968]

$$\overline{\overline{f}}(\hat{k}_s, \hat{k}_i) = \tilde{S}(\hat{k}_s, \hat{k}_i) e^{-j(\vec{k}_i - \vec{k}_s) \cdot \vec{r}_s} = \frac{[\overline{\overline{I}} - \hat{k}_s \hat{k}_s]}{4\pi} \cdot \int \int e^{-j\vec{k}_s \cdot \vec{r}_a} S(\vec{r}_a, \vec{r}_s) e^{j\vec{k}_s \cdot \vec{r}_s} d\vec{r}_a d\vec{r}_s$$

Equation 1.3-2

Other assumptions in this method are that the location, shape or sizes of the individual scatterers are uncorrelated. Hence, a simple summation of the scattered power waveform from each scatterer is possible. Single scattering theory plays a central role in the model proposed in this report. A great deal of literature exists for the single scatter theory; however, this literature will not be reviewed here. The single scatter approach, however, will be reviewed and applied in Chapter 6 .

An exact solution would consider not only the scattering from each individual object, but the full interaction between them; this alters the field incident on each scatterer. One method of solution that accounts for full interaction between N objects is the solution of the associated N-coupled integral equations. Using the equivalence principle, the scatterers may be replaced by equivalent currents that radiate in free space. In addition to the requirement for more computing power than is commonly available, the exact solution for the N-coupled integral equations for propagation through the foliage would require an abundance of detailed data and a number of realizations to create acceptable averages. Consequently, some approximations must be made.

There is a multitude of these approximate wave approaches reported in the literature. In continuous random media, the literature is well represented in the books by Ishimaru [1997] and Tsang [1985]. Most notable for this dissertation are the papers by Barabanenkov *et al.* [1971] and Besieris and Kohler [1981] in which a radiative transfer equation is developed from the wave approach. Renormalization approaches are well represented in the work of Frisch [1968] and DeWolf [1971]. For discrete random media, many researchers have considered the effects of multiple scattering due to random inhomogeneities. These methods perform a summation of the scattering effects in the ensemble, then average the result. However, in order to retrieve a closed form result, they have made basic assumptions about the scattering processes. Twersky has developed integral equations that describe the higher order moments by neglecting multiple scattering involving the same particle; various approximate solutions exist for these equations [Twersky, 1964]. Tsolakis [1985] (among others) has created a transfer equation from wave theory. This approach will be examined in detail and implemented for a forward scattering medium in Chapter 7 .

One popular method beyond the single scatter approach is the Distorted Wave Born Approximation (DWBA) [Lang, 1981]. Beginning with the expression for the total field, Lang derives a polarization-sensitive operator formulation for scattering from discrete random media. After considerable effort in deriving the integral equations for the field, he invokes the Foldy approximation for the mean field. In this approximation, the incident field at scatterer, s, (under the summation) is given by the *average field evaluated at the position* $\vec{r}_s$,

$$\left\langle \vec{E}(\vec{r}_a) \right\rangle = \vec{E}_i(\vec{r}_a) + \sum_{s=1}^{N} \overline{\overline{f}}(\hat{k}_s, \hat{k}_i) \cdot \left\langle \vec{E}(\vec{r}_s) \right\rangle \frac{e^{-jkR}}{R}$$

Equation 1.3-3

The Foldy formulation is equivalent to the assumption of scatterers with no correlation and scattering amplitudes that are isotropic [Frisch, 1968]. In summary, the scattered field is found by iterating the multiple scattering formulation and then assuming that the effective incident field at each scatterer is the mean field (Foldy). Lang then embeds the scatterers in the equivalent (mean) medium (DWBA) and scattered power is computed in the single scatter approximation. The mean medium has an effective, tensor dielectric constant which in turn, is a function of the scattering amplitudes of the individual scatterers. This use of an equivalent medium creates an environment where both the incident and scattered fields attenuate while propagating. The scattered field derived from the scatterers embedded in the equivalent medium results in solving the multiple scattering equations in the first-order Born approximation. This solution is valid in a medium in which the scatterers have a small albedo (ratio of the scattering cross section to the total cross section) [Lang, 1981].

Whether single scatter theory or multiple scatter theory is used, we will construct a composite scattered field, $\vec{E}_f^s$, due to the volume of scatterers, see Figure 1.3-3. In the integral equation formulation, the scattered field results from an induced current, J_{sn}, on each of the N scatterers; see Figure 1.3-3.

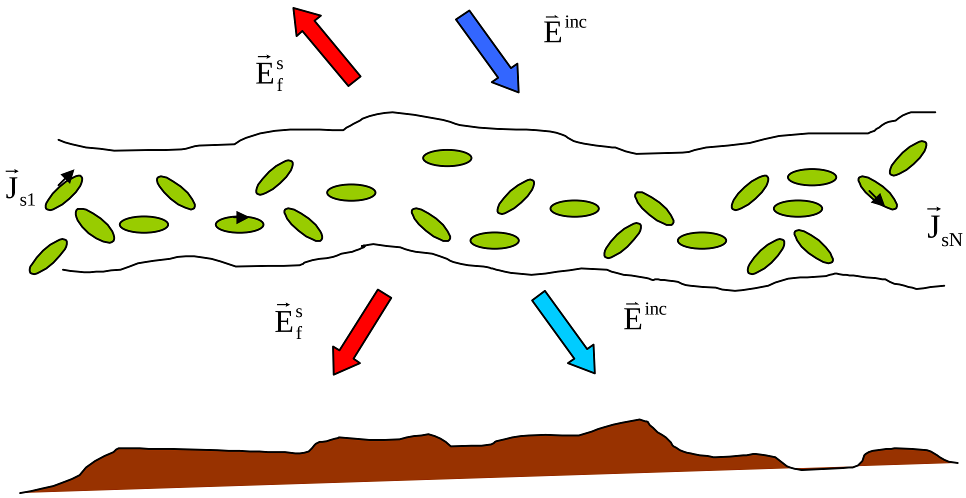

Figure 1.3-3: The total incident field with respect to the surface

Initially, we present a derivation of the scattered field from the volume using a reduced form of the radiative transfer approach that results in a form of the first order multiple scattering result. The limitations of this result are apparent in the context of the first order multiple scattering results.

1.3.2 Scattering from a Rough Surface

Modeling the multiple scattering that takes place along the surface is also widely addressed in the literature. Numerical implementations typically use the integral equation formulation. Given a field incident on a statistically rough terrain, the integral equation technique, typically implemented with the Method of Moments (MOM), can yield exact results for a given surface. Average results for a collection of realizations are found using Monte Carlo methods. The solution method used here is the MOM formulation accelerated by the Method of Ordered Multiple Interactions (MOMI) [Kapp, 1996]. It will be explored in Section 3.1 and is used to verify some assumptions in the model developed in this report. Analytical results, including Kirchhoff and perturbation approximations, may also be useful in an analytically reduced integral equation formulation. The Kirchhoff approximation is discussed in Section 3.4.1.

A time dependent analytical approach for the calculation of the incoherent power waveform scattered by an extended rough surface that is consistent with the single scatter approach is the Impulse Response Method. This method is derived under the assumption that there exist a continuum of scattering facets on the surface that reflect a radar power waveform [Brown, 1977]. Under certain assumptions, the return *power* from each properly oriented surface facet enters a summation. The number of these properly oriented facets per unit area of the surface defines a cross section per unit area. Section 3.3 presents a brief discussion of the impulse response method for calculating the scattering from terrain in free space, i.e. no foliage cover.

1.3.3 Interaction between the Foliage and the Rough Surface

Regardless of the modeling method used for the terrain and the volume scattering individually, there will be an additional source of multiple interactions (or multiple scattering): the interaction between the volume and the surface. This interaction mechanism is not well explored in the literature. In addition, when it is addressed, only a single interaction is discussed and in most cases only flat surfaces are considered [Le Vine, 1992; Karam, 1997; Ulaby, 1990; McDonald, 1993].

Once the surface scattered field, E^s_{fs}, due to the currents induced on the surface, $\vec{J}_s$, is calculated, it can act as an additional field incident upon the foliage on its path back through the foliage to the radar. See the field $\vec{E}^s_{fs}$ in Figure 1.3-4. This single passage (from foliage to surface, and back to foliage) does not account for the full interaction between the current induced in the foliage and the current on the surface. This single passage approximation to the interaction between the foliage and the surface represents a single interaction: the foliage-scattered field that creates the surface currents is due only to the field incident from the radar. This approximation is explored in Chapter 8 through a comparison with the exact results for a single scatterer above a rough surface. A full interaction formulation requires that the currents on the surface and on each scatterer in the foliage be coupled. Additional interaction terms would include corrections to the foliage currents due to the surface scattered field that, in turn, will produce corrections to the surface currents: an infinite series of these corrections will produce the full interaction results. Alternatively, a coupled integral equation formulation relating the induced currents will also produce the full interaction result.

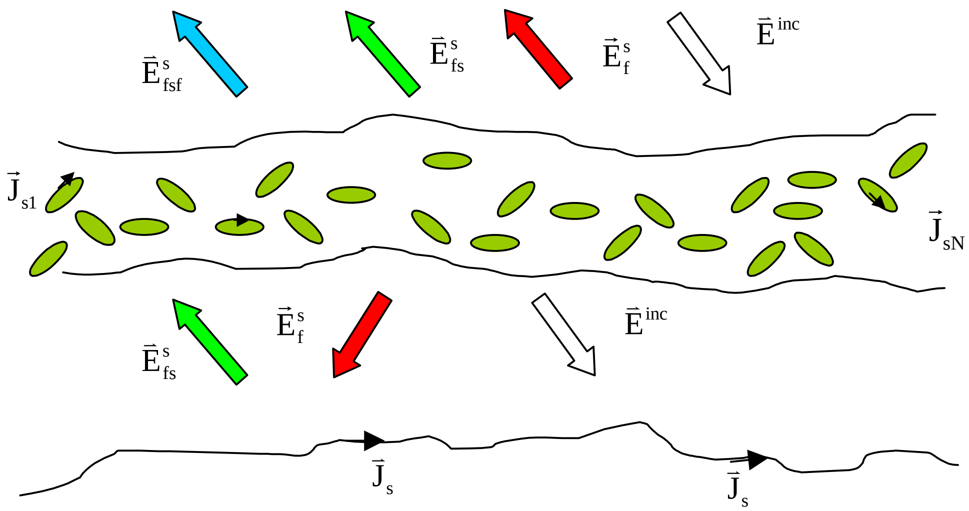

Figure 1.3-4: Surface to Foliage Interaction

Assuming that the integral equation approach is followed, the solution for the passage from the surface through the foliage can be formulated using the equivalence principle. The *surface current*, $\vec{J}_s$, is permitted to radiate in free space and the resulting field acts as an additional incident field with respect to the foliage. Hence, the surface scattered field, E^s_{fs}, will induce a corrective current, $\vec{J}^s_{sn}$, on the n^th^ scatterer which must be vectorially added to the previous current. This current radiates a second field scattered from the foliage, $\vec{E}^s_{fsf}$, in addition to the scattered field due only to the foliage, $\vec{E}^S_f$. See Figure 1.3-5. This is a first approximation to the foliage-surface-foliage interaction.

A second order correction to the surface current will treat the incident field on the surface as

$$\vec{E}^{\text{inc on surface}} = \vec{E}^{inc} + \vec{E}^s_f + \vec{E}^s_{fsf}$$

Consequently, a new surface current $\vec{J}_s$ is found. This current will produce a new value for the surface scattered field, $\vec{E}^s_{fs}$, and a new value for the field incident to the foliage from the surface. Continuing this process of iteration will produce the full interaction result.

Alternatively, like the first passage through the vegetation, this second field scattered from the foliage, $\vec{E}^{s}_{fsf}$, can be found using the single scatter approximation. This result may also be iterated, correcting the surface currents producing scattered fields. However, this result will suffer the limitations of the single scatter theory.

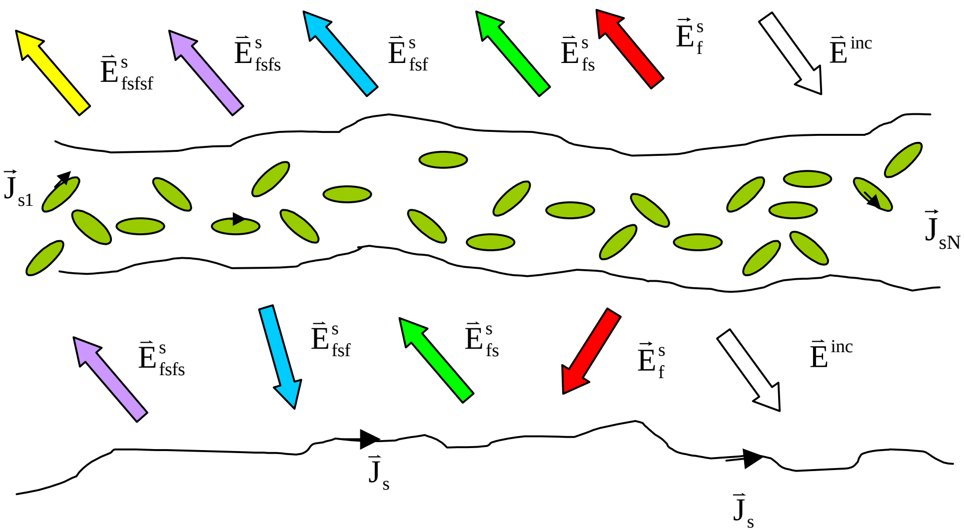

Figure 1.3-5: the second order approximate scattered field from the foliage and surface combination

1.4 Goals of this Research

The goals of this research are to produce usable engineering models for the propagation of waves in natural terrain features. Many numerically efficient codes have been developed for the propagation past a rough knife edge, dielectric surfaces, and foliage over a rough surface. The foliage-surface model can incorporate measured data for calibration and accurately reproduce the general trends of an average returned waveform from terrain and foliage with similar statistics and constituents as the calibration data. Numerical efficiency is best served with the impulse response approach, which casts the returned waveform into a series of convolutions and uses empirically derived parameters. Through its relation to first order multiple scattering theory, this model was found to incorporate some limiting assumptions. These assumptions are exposed and the model is improved by the wave derivation of the same equations in single scattering Chapter 6 and multiple scattering Chapter 7 .

Chapter 2 Rough Knife Edge Diffraction

Diffraction by a knife edge boundary has long been used as a model to estimate the effect of path-obstructing ridges, mountains, and other natural obstacles in terrestrial-based communication links. The use of this approximation is now of interest in assessing blockage effects involving much shorter paths, e.g., such as in propagation in an urban environment where buildings and other man-made obstacles cause the path blockage. R.E. Collin developed a particularly simple yet very powerful approximate solution to the problem of diffraction by a knife edge boundary [Collin, 1985]. The robustness of his solution is due in part to (a) the careful manner in which he developed the approximation and (b) the general tolerance of the knife edge diffraction problem to approximation.

Although the knife edge boundary solution has been used extensively to model natural and man-made diffracting objects, there has always been an uncertainty associated with estimating the effects of *edge roughness* on the diffraction pattern. The purpose of this chapter is to present an approximate solution to this edge-roughness problem when the roughness is random in nature. The solution will use Collin's approximate formulation of the problem so that the fundamental physics of the distance-dependent phase interference between the direct and diffracted fields is preserved [Collin, 1985].

The roughness on the knife edge boundary is assumed to comprise a non-zero mean, second order process with jointly Gaussian probability density function and a Gaussian spectrum. The latter is used for demonstration purposes but the theory is not limited to this spectral form. Using this approach, an expression is derived for the mean or coherent field at a receiver on the side of the knife edge opposite to the transmitter; this result is cast in terms of the error function of a complex argument. As might be expected, the most important parameters in this result are the separation distances of the transmitter and receiver from the knife edge, the degree of path blockage present, the edge roughness parameters, and the antenna pattern of the transmitter. Numerical calculations demonstrate the interplay of these factors and illustrate the effect of the roughness relative to a knife edge without roughness. The calculation of the total and the diffuse received power is reduced to two integrations, but it is shown that these can be considerably simplified due to the effective lack of any strong dependence on many of the problem parameters. Computations illustrate the increase in the diffuse or incoherent power at the expense of the coherent power and confirm the fact that if phase coherence is not needed it may still be possible to use the averaged incoherent power to achieve a transfer of power.

2.1 Review of the Approximations for a Smooth Knife Edge

The power transferred between transmitter and receiver antennas when there is a knife edge half-plane conductor located in the vicinity of the line connecting the two, may be derived as follows [Collin, 1985]. Assuming that the total field above the knife edge is simply the incident field, a scattered plane wave spectrum may be constructed and this in turn may be used to produce results for the knife edge diffraction. In this construction, the line-of-sight (LOS) path coincides with the z-axis and the x-axis is parallel to the edge of the infinite half plane (the knife edge), see Figure 2.1-1.

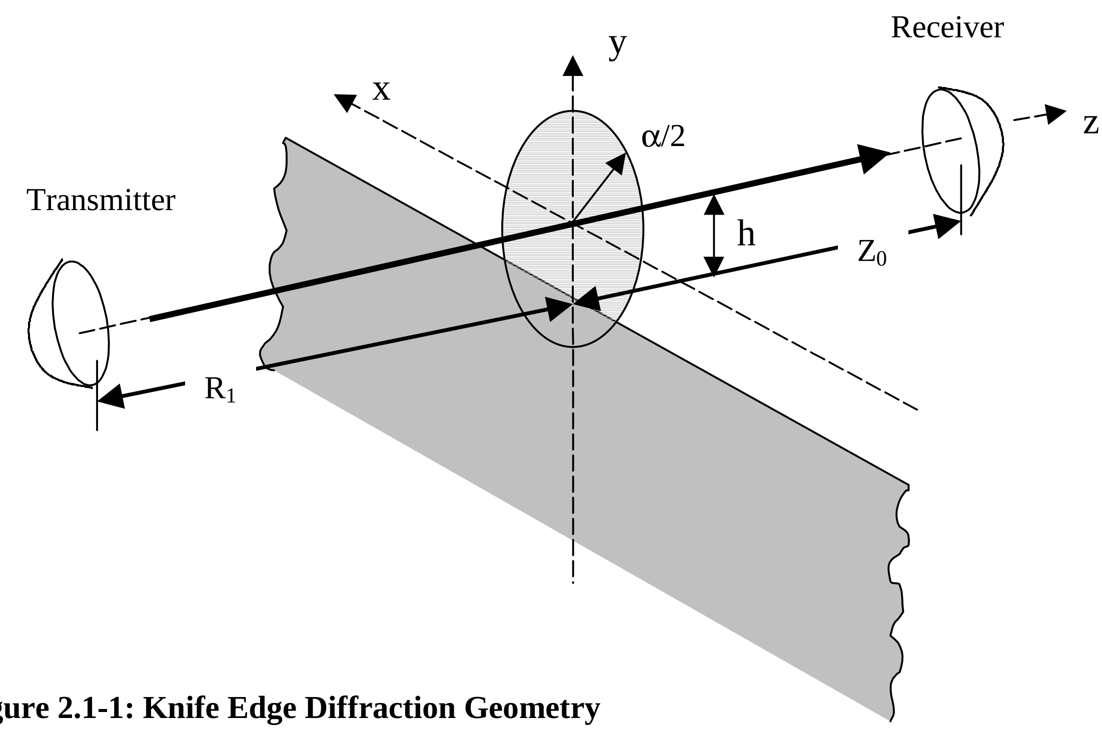

Figure 2.1-1: Knife Edge Diffraction Geometry

Within this framework, a Gaussian tapered beam with a beam-waist α is assumed to be incident on the knife edge from a transmitter placed a distance R_1 from the knife edge as measured along the LOS path. Referring to Figure 2.1-1, the heavy line represents the LOS path. The height, h, is the perpendicular distance from the LOS to the knife edge below. The distance z_0 describes the distance from the knife edge to the receiver as measured along the LOS path.

Consider that the z = 0 plane is an aperture bounded on only one side by the knife edge which is a distance h below the LOS (z-axis). Assume that a source, placed a finite distance from the knife edge, produces a field in the aperture as shown in Figure 2.1-2. It is assumed that the main beam of the transmitting antenna pattern may be approximated as a Gaussian beam.

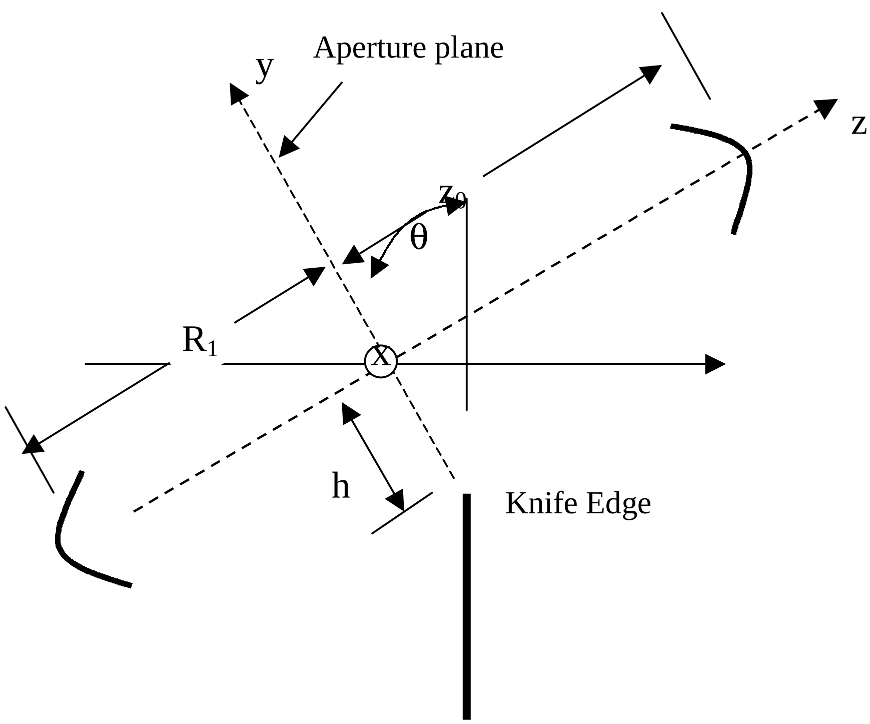

Figure 2.1-2: Knife Edge Geometry, the “Aperture” Definition

Hence, in order to account for the spherical and Fresnel phase effects in the incident field over the aperture (z = 0) in combination with a Gaussian taper, this field is constructed as follows:

$$\vec{E}^{inc}(x,y,z=0) = \frac{E_0(\hat{x}+\hat{y})e^{-jk_0R_1}}{R_1}\exp\left\{-jk_0\left(\frac{\left(x^2+y^2\right)}{2R_1}\right)\right\}\exp\left\{-\frac{\left(x^2+y^2\right)}{\alpha^2}\right\}$$

Equation 2.1-1

In this expression, the first and second exponential are due to the expansion of the incident spherical wave's phase while the third accounts for the tapering of the field.

The transverse plane wave spectrum can be derived starting with the following Fourier transform relation:

$$A_x(k_x,k_y)\hat{x}+A_y(k_x,k_y)\hat{y} = \left(E_x\hat{x}+E_y\hat{y}\right)\frac{e^{-jk_0R_1}}{4\pi R_1}$$

$$\cdot \iint_{\substack{\text{aperture}\\ \text{area}}} \left\{ e^{-jk_0\left(\rho^2/2R_1\right)} e^{-\left(\rho^2/\alpha^2\right)} \right\} e^{+j(k_x x+k_y y)}\, dx\, dy$$

Equation 2.1-2

where $\rho^2 = \sqrt{x^2+y^2}$. Once the plane wave spectrum is found, the diffracted plus the direct transverse field at a given observation point ($z_0 > 0$) can be found via the inverse Fourier transform relation:

$$\vec{E}_t(x_0,y_0,z_0) = \frac{1}{(2\pi)^2}\iint_{\substack{\text{all}\\ k-\text{space}}} \left\{A_x(k_x,k_y)\hat{x}+A_y(k_x,k_y)\hat{y}\right\}e^{-j\vec{k}\cdot\vec{r}_0}\, dk_x\, dk_y$$

where $\vec{k} = k_x\hat{x}+k_y\hat{y}+k_z\hat{z}$, $\quad k_0{}^2 = k_x{}^2+k_y{}^2+k_z{}^2$, and $\quad \vec{r}_0 = x_0\,\hat{x}+y_0\,\hat{y}+z_0\,\hat{z}$

Equation 2.1-3

Typically in near-field to far-field transformation, the relationship in Equation 2.1-3 is evaluated approximately via stationary phase to obtain the fields in the far field. However, since we may be interested in fields in the Fresnel region, the exact form of Equation 2.1-3 is used in conjunction with the following simplification: the fields of interest will be measured near the z-axis. Hence, for an observation point at $\left(x_0,y_0,z_0\right)$ with $z_0^2 >> \left(x_0^2 + y_0^2\right)$ we expect only a small k_z component in the transverse plane at the observation point. Under these conditions and using a binomial expansion, the wave number vector can be written approximately as:

$$\vec{k} = k_x\hat{x} + k_y\hat{y} + \sqrt{k_0^2 - \left(k_x{}^2 + k_y{}^2\right)}\ \hat{z} \ \approx\ k_x\hat{x} + k_y\hat{y} + k_0\left(1 - \frac{k_x{}^2 + k_y{}^2}{2k_0^2}\right)\hat{z}$$

Equation 2.1-4

which leads to the paraxial approximation for the phase function

$$\exp\left\{-\,j\vec{k}_0 \cdot \vec{r}_0\right\} \approx \exp\left(-\,j\left\{\ k_x x_0 + k_y y_0 + k_0 z_0\left(1 - \frac{k_x^2 + k_y^2}{2k_0^2}\right)\right\}\right)$$

Equation 2.1-5

Consequently, using the paraxial approximation and substituting the plane wave spectrum Equation 2.1-2 into the expression for the transverse field Equation 2.1-3, the field in the half space, $z_0 > 0$, along the z-axis (LOS) may be written as;

$$\vec{E}_t(x_0, y_0, z_0) = \iint\limits_{\substack{\text{all}\\ k-\text{space}}} \left\{\left(E_x\hat{x} + E_y\,\hat{y}\right)\frac{e^{-jk_0R_1}}{4\pi R_1}\iint\limits_{\substack{\text{aperture}\\ \text{area}}}\left\{e^{-jk_0\left(\rho^2/2R_1\right)}e^{-\left(\rho^2/\alpha^2\right)}\right\}\right\}$$
$$\cdot\frac{e^{-jk_0z_0}}{(2\pi)^2}e^{+j(k_x x + k_y y)}\,dx\,dy\,e^{-j\left\{k_x x_0 + k_y y_0 - k_0 z_0\left(\frac{k_x{}^2 + k_y{}^2}{2k_0^2}\right)\right\}}\,dk_x\,dk_y$$

Equation 2.1-6

Rearranging the order of integration, removing those terms that are constant, and using the following identity (to be used extensively in subsequent sections),

$$\int_{-\infty}^{\infty} e^{-\left(ax^2 + bx + c\right)}dx = \sqrt{\frac{\pi}{a}}\,e^{\left(\frac{b^2 - 4ac}{4a}\right)}$$

Equation 2.1-7

we can perform the integration over k-space with the final result, assuming that the field measurements are performed on axis $(x_0 = 0,\ y_0 = 0,\ z_0 > 0)$

$$\vec{E}_t(0,0,z_o) = \frac{jk_o e^{-jk_o(z_o + R_1)}}{2\pi R_1 z_o}\left(E_x\hat{x} + E_y\,\hat{y}\right)\int_{-\infty}^{\infty}\int_{-h}^{\infty} e^{-a\left(x^2+y^2\right)}dy\,dx$$

$$\text{where}: \qquad a \equiv \frac{1}{\alpha^2} + jk_o\left(\frac{1}{2R_1} + \frac{1}{2\,z_o}\right) \equiv \frac{1}{\alpha^2} + j\frac{k_o}{d_o}$$

Equation 2.1-8

Note that a new distance d_0 has been defined as follows

$$d_0 \equiv \frac{2R_1\,z_0}{R_1 + z_0}$$

Hence, the diffracted field as measured along the LOS path $(x_0 = 0, y_0 = 0, z_0 > 0)$ can be written [Collin, 1985] as

$$\begin{aligned}\vec{E}_t(0,0,z_o) &= \frac{j\,k_o e^{-jk_o(z_o + R_1)}}{2\pi R_1 z_o}\left(E_x\hat{x} + E_y\,\hat{y}\right)\sqrt{\frac{\pi}{a}}\ \int_{-h}^{\infty} e^{-a\,y^2}\,dy \\ &= \frac{j\,k_o e^{-jk_o(z_o + R_1)}}{4R_1 a\,z_o}\left(E_x\hat{x} + E_y\,\hat{y}\right)\left[\mathrm{erf}\left(-h\sqrt{a}\right) + 1\right]\end{aligned}$$

Equation 2.1-9

where the function erf(z) is the error function used as defined in Abramowitz and Stegun [1972]. Since the parameter, a, is complex, this will be evaluated using the error function of a complex argument. The free space power along the LOS direction may be calculated through the use of the following (in terms of the mean separation, h_c)

$$\begin{aligned}\left[P_{coherent}\right]_{h_c \to \infty} &= \left[\vec{E}(x_o, y_o)\vec{E}(x_o, y_o)^*\right]_{h_c \to \infty} \\ &= \frac{|K|^2}{4}\,\frac{\pi^2}{aa^*}\left(\mathrm{erf}\left(-\infty\right) + 1\right)^2 = |K|^2\ \frac{\pi^2}{aa^*}\end{aligned}$$

$$\text{where: } \quad |K|^2 = \vec{K}\cdot\vec{K}^* = \left[\frac{k_0^2 e^{-jk_o(z_o+R_1)} e^{+jk_o(z_o+R_1)}}{4\pi^2 R_1^2 z_0^2}\right]\left(E_x^2 + E_y^2\right) = \frac{k_0^2\left(E_x^2 + E_y^2\right)}{4\pi^2 R_1^2 z_0^2}$$

Equation 2.1-10

If the beamwidth parameter, α, (a distance measure of the beamwidth at the knife edge) is large with respect to the distance d_0, the real part in the expression for a can be dropped and the field can be evaluated using the Fresnel integral.

$$\begin{aligned}\bar{E}_t(0,0,z_o) &\cong \frac{j k_0 e^{-jk_0(z_0+R_1)}}{2R_1 z_0}\left(E_x\hat{x} + E_y\hat{y}\right)\sqrt{\frac{\pi d_0}{jk_0}} \int_{-h}^{\infty} e^{-j\frac{k_0}{d_0}y^2}\,dy \\ &\cong \frac{d_0 e^{-jk_0(z_0+R_1)} e^{j\frac{\pi}{4}}}{2\sqrt{2}R_1 z_0}\left(E_x\hat{x} + E_y\hat{y}\right)\left[C\left(-h\sqrt{\frac{2k_0}{\pi d_0}}\right) - jS\left(-h\sqrt{\frac{2k_0}{\pi d_0}}\right)\right]\end{aligned}$$

Equation 2.1-11

where the functions C(z) and S(z) are the Fresnel integrals as defined in Abramowitz and Stegun [1972].

Given the system parameters listed in Table I (in the example from the final section) for a typical terrestrial microwave communication link, the argument of the exponential, in Equation 2.1-11, will affect the resulting coherent power as the beamwidth parameter, α, becomes smaller, the frequency increases, or the separation distances decrease. For the system parameters of Table I, there are only slight differences in the coherent power as given in the approximation Equation 2.1-11 with respect to the more exact solution Equation 2.1-9. However, as α decreases, a disparity in the oscillations becomes evident. For example, Figure 2.1-3 demonstrates that if α is reduced to 50 m (which corresponds to reducing the beamwidth or placing the transmitter closer to the knife edge), the use of the approximation Equation 2.1-10 may not always yield adequate results. This figure compares the approximate solution for the power using the Fresnel integral to the complete solution using the error function of a complex argument.

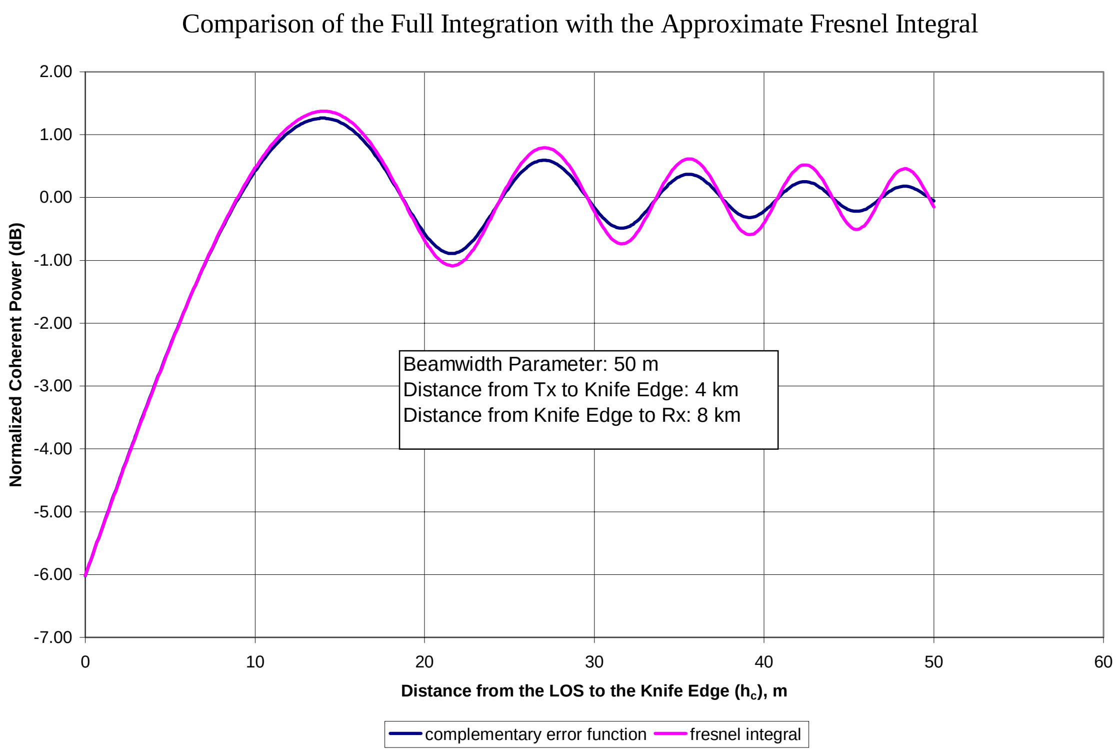

Figure 2.1-3: Coherent Field as a Function of the Displacement of the Mean Height, h_c, of the knife edge from the LOS.

2.2 *Roughness on the Knife Edge*

Consider the case when there is roughness along the knife edge, i.e. the knife edge is rough along the x-direction transverse to the LOS path. The geometry in this case is depicted in Figure 2.2-1. The height h is now a function of x and relates the displacement of the knife edge level with respect to the LOS path. In addition, this height is taken to be a zero-mean stochastic variable. Assuming Gaussian statistics for the height roughness of the knife edge, we can divide this height into two parts

$$h = h_c + \delta h_c$$

Equation 2.2-1

Hence, we have split the random height, *h*, into its mean (*h_c*) and its fluctuating portion δh_c (with zero mean). The fluctuating portion is assumed to have a Gaussian probability density function defined by $p(\delta h_c)$ and standard deviation σ as given below

$$p(\delta h_c) = \frac{1}{\sqrt{2\pi}\sigma} e^{-\frac{1}{2\sigma^2}\delta h_c{}^2}$$

Equation 2.2-2

The statistics of the roughness are assumed independent of x, i.e. h is a spatially stationary process.

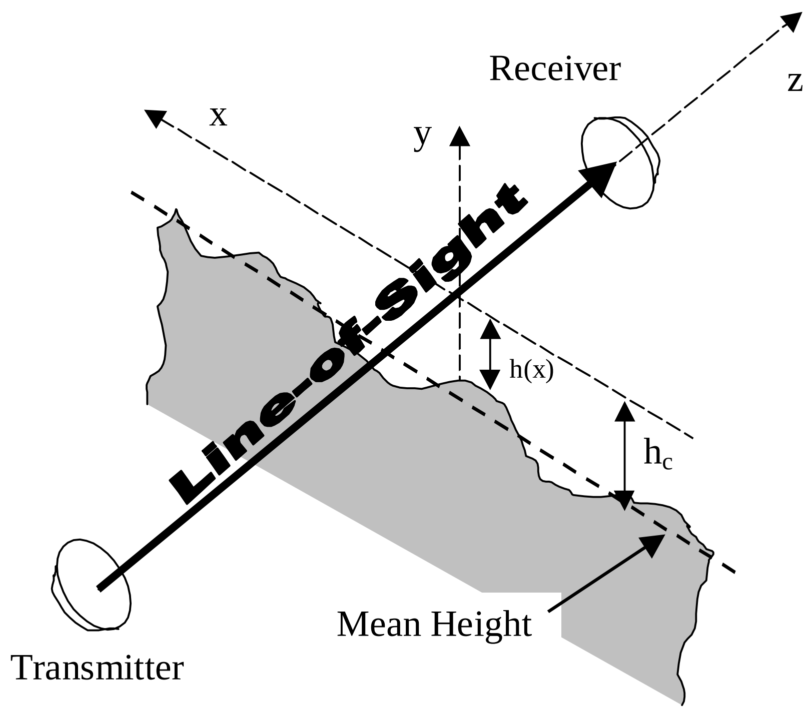

Figure 2.2-1: Geometry for the Rough Knife Edge

2.2.1 The Coherent Field

The average total field, also referred to as the coherent total field, is found by forming the first moment of the transverse field (z > 0). Making a change of variables in order to bring the fluctuating portion of the integration limit into the integrand, the integral expression for the coherent field is rewritten as follows

$$\left\langle \vec{E}(0,0,z_0) \right\rangle = \int_{-\infty}^{\infty} \frac{jk_o e^{-jk(z_0+R_1)}}{2\pi R_1 z_0} \left(E_x \hat{x} + E_y \hat{y} \right) \cdot \int_{-\infty}^{\infty} \int_{-h_c}^{\infty} e^{-a\left(x^2+[u-\delta h_c]^2\right)} \frac{1}{2\pi\sigma} e^{-\frac{1}{2\sigma^2}\delta h_c^2} \, du\, dx\, d\delta h_c$$

Equation 2.2-3

Note the lower limit for the u integration is now the mean height from the LOS to the knife edge h_c. After interchanging the order of integrations, gathering terms, and performing the δh_c integration, we can then perform the integration in the transverse coordinate x leading to the following result for the coherent field along the LOS direction:

$$\left\langle \vec{E}(0,0,z_0) \right\rangle = \frac{jk_0 e^{-jk_o(z_0+R_1)}}{2\pi R_1 z_0} \sqrt{\frac{\pi}{a\left(2\sigma^2 a+1\right)}} \left(E_x \hat{x} + E_y \hat{y} \right) \int_{-h_c}^{\infty} e^{-\left(\frac{a}{2\sigma^2 a+1}\right)u^2} du$$

Equation 2.2-4

Note that this expression reduces to that given above in Equation 2.1-10 as the height variance is reduced to zero. Finally, this integral can be split and written in terms of the error function of a complex argument or the complementary error function of a complex argument:

$$\int_{-h_c}^{\infty} e^{-\left(\frac{a}{2\sigma^2 a+1}\right)u^2} du = \frac{1}{2}\sqrt{\frac{\pi\left(2\sigma^2 a+1\right)}{a}} \left(1 + \operatorname{erf}\left\{ h_c \sqrt{\frac{a}{2\sigma^2 a+1}} \right\} \right)$$
$$= \frac{1}{2}\sqrt{\frac{\pi\left(2\sigma^2 a+1\right)}{a}} \operatorname{erfc}\left\{ -h_c \sqrt{\frac{a}{2\sigma^2 a+1}} \right\}$$

Equation 2.2-5

Substituting this result for the integral, the final expression for the coherent field is written as follows

$$\left\langle \vec{E}(0,0,z_0) \right\rangle = \frac{jk_o e^{-jk_0(z_0+R_1)}}{4aR_1 z_0} \left(E_x \hat{x} + E_y \hat{y}\right) \mathrm{erfc}\left\{ -h_c \sqrt{\frac{a}{2\sigma^2 a + 1}} \right\}$$

Equation 2.2-6

where $\quad a \equiv \frac{1}{\alpha^2} + jk_o \left(\frac{1}{2R_1} + \frac{1}{2z_o} \right) \equiv \frac{1}{\alpha^2} + j\frac{k_o}{d_o}$

From this result for the mean or coherent field, the power in the coherent field may be easily calculated. This power, $P_{coherent}$, is given by (for simplicity, we assume the intrinsic impedance of the medium is unity throughout this work)

$$\begin{aligned} P_{coherent} &= \left\langle \vec{E}(0,0,z_0) \right\rangle \left\langle \vec{E}(0,0,z_0) \right\rangle^* \\ &= \frac{|K|^2}{4} \frac{\pi^2}{aa^*} \mathrm{erfc}\left(-h_c \sqrt{\frac{a}{2\sigma^2 a + 1}} \right) \mathrm{erfc}\left(-h_c \sqrt{\frac{a^*}{2\sigma^2 a^* + 1}} \right) \end{aligned}$$

$$\text{where}: |K|^2 = \vec{K} \cdot \vec{K}^* = \left[\frac{k_0^2 e^{-jk_o(z_o+R_1)} e^{+jk_o(z_o+R_1)}}{4\pi^2 R_1^2 z_0^2} \right] \left(E_x^2 + E_y^2\right) = \frac{k_0^2 \left(E_x^2 + E_y^2\right)}{4\pi^2 R_1^2 z_0^2}$$

Equation 2.2-7

It can be easily seen that as the roughness becomes negligible, i.e., $\sigma \to 0$, the coherent power becomes equivalent to Collin's result [Collin, 1985], i.e.

$$\left[\left\langle \vec{E}(0,0,z_0) \right\rangle \right]_{\sigma \to 0} = j\frac{K}{2}\frac{\pi}{a} \mathrm{erfc}\left(-h\sqrt{a}\right)$$

while the expression for the coherent power is given by

$$\begin{aligned} \left[P_{coherent}\right]_{\sigma \to 0} &= \left[\left\langle \vec{E}(0,0,z_0) \right\rangle \left\langle \vec{E}(0,0,z_0) \right\rangle^* \right]_{\sigma \to 0} \\ &= \frac{|K|^2}{4} \frac{\pi^2}{aa^*} \mathrm{erfc}\left(-h_c \sqrt{a} \right) \mathrm{erfc}\left(-h_c \sqrt{a^*} \right) \end{aligned}$$

Equation 2.2-8

Additionally, as the knife edge itself is withdrawn to infinity, we find a second limit: the free space power along the LOS direction.

$$[P_{coherent}]_{h_c\to\infty} = \left[\left\langle \vec{E}(0,0,z_0)\right\rangle\left\langle \vec{E}(0,0,z_0)\right\rangle^*\right]_{h_c\to\infty}$$
$$= \frac{|K|^2}{4}\frac{\pi^2}{aa^*}\operatorname{erfc}(-\infty)\operatorname{erfc}(-\infty) = |K|^2\,\frac{\pi^2}{aa^*}$$

Equation 2.2-9

As expected, in this limit the roughness along the knife edge is inconsequential.

2.2.2 *The Total Power*

The total mean power on the z-axis (LOS path) at $z = z_0$ is given in terms of the two-point probability function, $p(\delta h_1, \delta h_{c2})$, as shown in the equation below

$$\left\langle \vec{E}(0,0,z_0)\cdot\vec{E}^*(0,0,z_0)\right\rangle = |K|^2\int_{-\infty}^{\infty}\int_{-\infty}^{\infty}\int_{-\infty}^{\infty}\int_{-\infty}^{\infty}\int_{-\infty}^{\infty}\int_{-\infty}^{\infty} p(\delta h_1, \delta h_{c2})$$
$$\cdot\, e^{-a\left(x_1{}^2+[u_1-\delta h_{c1}]^2\right)}e^{-a^*\left(x_2{}^2+[u_2-\delta h_{c2}]^2\right)}du_1du_2\;dx_1dx_2\;d\delta h_{c1}\;d\delta h_{c2}$$
$$\text{where}: |K|^2=\vec{K}\cdot\vec{K}^* = \left[\frac{k_0^2e^{-jk_o(z_o+R_1)}e^{+jk_o(z_o+R_1)}}{4\pi^2R_1^2z_0^2}\right]\left(E_x^2+E_y^2\right) = \frac{k_0^2\left(E_x^2+E_y^2\right)}{4\pi^2R_1^2z_0^2}$$

Equation 2.2-10

The asterisk (*) denotes a complex conjugate. The joint probability density function (pdf) for the Gaussian heights is expressed as

$$p(\delta h_{c1}, \delta h_{c2}) = \frac{1}{2\pi\sigma\sqrt{1-C_n{}^2}}\,e^{-\frac{1}{2\sigma^2\left(1-C_n{}^2\right)}\left[\delta h_{c1}^2-2C_n\delta h_{c1}\delta h_{c2}+\delta h_{c2}^2\right]}$$

Equation 2.2-11

where $C_n(x)$ is their normalized correlation function. Substituting for the joint pdf, we find the average total power can be expressed as follows

$$\left\langle \left|\vec{E}(0,0,z_0)\right|^2 \right\rangle = \left\langle \vec{E}(0,0,z_0) \cdot \vec{E}^*(0,0,z_0) \right\rangle$$

$$= \frac{|K|^2}{2\pi\sigma} \int_{-\infty}^{\infty} \int_{-\infty}^{\infty} \int_{-\infty}^{\infty} \int_{-\infty}^{\infty} \int_{-h_c}^{\infty} \int_{-h_c}^{\infty} \frac{1}{\sqrt{1-C_n{}^2}}\, e^{-\frac{1}{2\sigma^2\left(1-C_n{}^2\right)}\left[\delta h_{c1}^2 - 2C_n \delta h_{c1} \delta h_{c2} + \delta h_{c2}^2\right]}$$

$$\cdot\, e^{-a\left(x_1{}^2 + [u_1 - \delta h_{c1}]^2\right)} e^{-a^*\left(x_2{}^2 + [u_2 - \delta h_{c2}]^2\right)}\, du_1 du_2\, dx_1 dx_2\, d\delta h_{c1}\, d\delta h_{c2}$$

Equation 2.2-12

The normalized correlation function for the knife edge roughness may be expressed in the form

$$C_n = \frac{\langle h(x_1) h(x_2) \rangle}{\sigma^2} = \frac{C(\Delta x)}{\sigma^2}$$

Equation 2.2-13

where $C(\Delta x)$, the correlation function for the knife edge roughness, is a function of the separation distance Δx along the knife edge. Expanding the integrand in Equation 2.2-12, collecting terms, interchanging the order of the integrations, the δh_{c1} and δh_{c2} integrations can be accomplished yielding

$$\left\langle \left|\vec{E}(0,0,z_0)\right|^2 \right\rangle = |K|^2 \int_{-\infty}^{\infty} \int_{-\infty}^{\infty} \int_{-h_c}^{\infty} \int_{-h_c}^{\infty} e^{-ax_1^2 - a^* x_2^2} \sqrt{\frac{1}{4aa^*\left(\sigma^4 - C^2(\Delta x)\right) + 2\sigma^2\left(a + a^*\right) + 1}}$$

$$\cdot \exp\left\{ \frac{-\left[a u_1^2\left(2\sigma^2 a^* + 1\right) + a^* u_2^2\left(2\sigma^2 a + 1\right) - 4aa^* u_1 u_2 C(\Delta x)\right]}{4aa^*\left(\sigma^4 - C^2(\Delta x)\right) + 2\sigma^2\left(a + a^*\right) + 1} \right\} du_1 du_2\, dx_1 dx_2$$

After some simplification and a change of variables: $\Delta x = x_1 - x_2$ *or* $x_1 = \Delta x + x_2$, the x_2 integration can be performed, reducing the number of integrations to three. Again a change of variables is employed in order to bring h_c into the integrands: $y_1 = u_1 + h_c$

and $y_2 = u_2 + h_c$. Upon performing this change, the y_1 integration can be evaluated, resulting in the following double integral

$$\left\langle \vec{E}\cdot\vec{E}^* \right\rangle = |K|^2 \frac{\pi}{\sqrt{a(a+a^*)(2\sigma^2 a^*+1)}} \int_{-\infty}^{\infty} e^{-\frac{aa^*}{(a+a^*)}\Delta x^2} \int_0^{\infty} e^{-\frac{a^*}{(2\sigma^2 a^*+1)}(y_2-h_c)^2}$$
$$\cdot \operatorname{erfc}\left\{ \frac{-\sqrt{a}[h_c(2\sigma^2 a^*+1)] + 2a^* C(\Delta x)(y_2-h_c)}{\sqrt{(2\sigma^2 a^*+1)[4aa^*(\sigma^4 - C^2(\Delta x)) + 2\sigma^2(a+a^*)+1]}} \right\} dy_2\, d\Delta x$$

Equation 2.2-14

This is the extent of our analytical evaluation. To further reduce Equation 2.2-14, we must first rearrange the order of integration since the form in Equation 2.2-14 appears to yield little insight into the important terms in the integrand. Interchanging the order, we find

$$\left\langle \vec{E}\cdot\vec{E}^* \right\rangle = |K|^2 \frac{\pi}{\sqrt{a(a+a^*)(2\sigma^2 a^*+1)}} \int_0^{\infty} e^{-\frac{a^*}{(2\sigma^2 a^*+1)}(y_2-h_c)^2} \int_{-\infty}^{\infty} e^{-\frac{aa^*}{(a+a^*)}\Delta x^2}$$
$$\cdot \operatorname{erfc}\left\{ \frac{-\sqrt{a}[h_c(2\sigma^2 a^*+1)] + 2a^* C(\Delta x)(y_2-h_c)}{\sqrt{(2\sigma^2 a^*+1)[4aa^*(\sigma^4 - C^2(\Delta x)) + 2\sigma^2(a+a^*)+1]}} \right\} d\Delta x\, dy_2$$

Equation 2.2-15

Examining the integrand, we see the complementary error function is an apparently complicated function of Δx. However, note that the Δx integration contains an exponential decay (as the square of the Δx variable), particularly as the value of the positive real constant

$$\frac{aa^*}{\left(a+a^*\right)} = \frac{1}{2\alpha^2} + \frac{k_0^2\,\alpha^2}{2d_0^2}$$

Equation 2.2-16

becomes large. Obviously, the beamwidth parameter is much larger than zero ($\alpha >> 0$) since it represents the incident field spread in the aperture plane; hence, the first term in

Equation 2.2-16 may be neglected. Laplace's method may then be employed if the second term may be treated as a large parameter. Consequently, if we assume microwave frequencies and an illuminated spot of at least $\alpha = 100$ meters, we can set an upper limit on d_0, a distance related to the separation between the receiver and transmitter. Figure 2.2-2 shows the required separation between the knife edge and the receiver (in order to maintain the unity coefficient in the exponential) as a function of frequency and beamwidth for a fixed distance from the transmitter to knife edge distance (4 km). As expected, the support for the Δx integration decreases as the frequency and beamwidth increase or the separation distance parameter d_0 decreases.

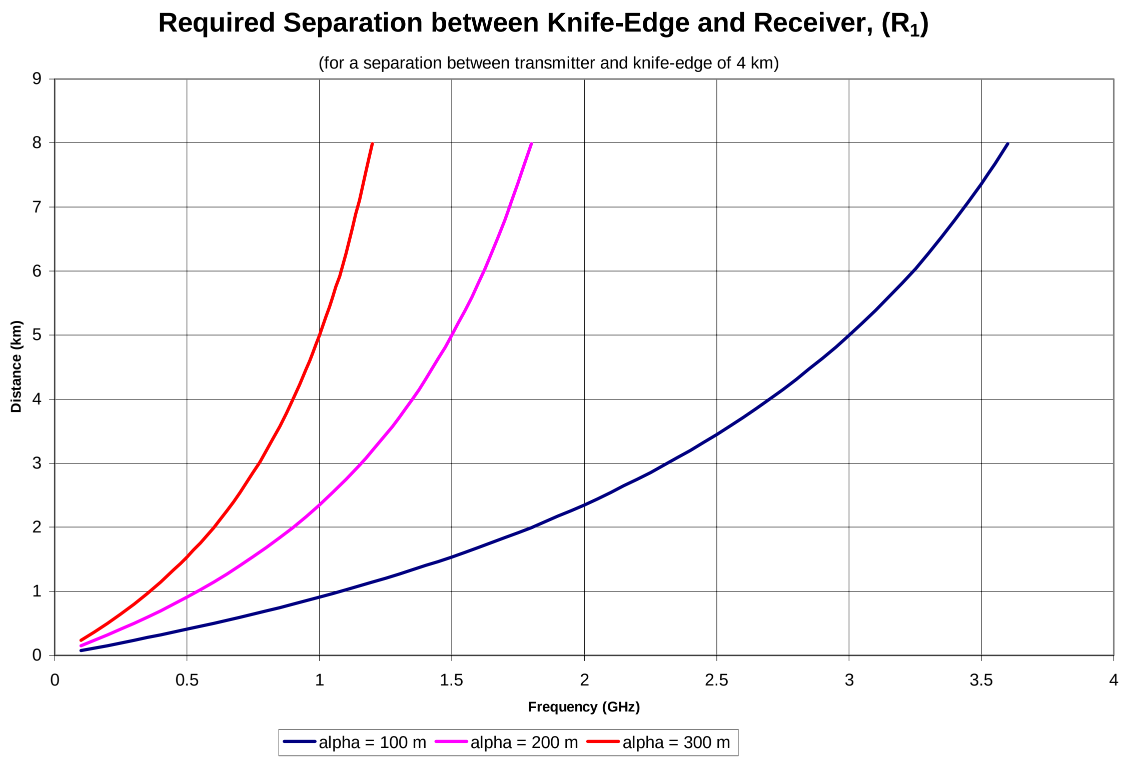

Figure 2.2-2: The maximum distance from the knife edge to the receiver (R_1) which results in a coefficient in the exponent greater than 1

Note that unity is not a strict limit, only a convenient assignment. Once the Δx integration is constructed such that Laplace's Method is applicable, we investigate the behavior of the complementary error function. If the complementary error function is a slowly varying function with respect to Δx over the integration interval before the exponential drives the integrand to zero, it may be removed from the inner integrand and evaluated at $\Delta x = 0$. Consequently, the Δx integration can be easily performed. This elementary implementation of Laplace's method may be justified through the following observations.

Since the correlation function, $C(\Delta x)$, is directly proportional to square of the roughness σ, it becomes negligible as the roughness becomes approaches zero. Hence, in this limit the complementary error function in Equation 2.2-15 is slowly varying with respect to the variable of integration, Δx, and may be removed from under the integral and evaluated at the peak of the integrand, $\Delta x = 0$. Conversely, if the roughness is very large, the correlation function will strongly influence the behavior of the complementary error function in Equation 2.2-15, which may become a rapidly varying function of the integration variable. Hence, with all other parameters held constant, we expect that if σ is small, we can remove the complementary error function from the integrand; whereas for σ large, this may not be possible.

For intermediate values of the roughness σ, we must more closely examine the correlation function's dependence on Δx. For example, if we choose a Gaussian form, the correlation function $C(\Delta x)$ has the following form

$$C(\Delta x) = \sigma^2 \, e^{-\frac{\Delta x^2}{l_x^2}}$$

Equation 2.2-17

where l_x is the correlation length. Since this function will peak at $\Delta x = 0$ and decay to zero at infinity, we can investigate its influence on the argument of the complementary error function by examining the relevant arguments: h_c, σ, l_x and y_2. Through extensive numerical investigation, it has been found that the variation of the complementary error function with Δx is strongly dependent on the correlation length l_x. Rearranging the argument of the complementary error function as shown below

$$\frac{-2aa^*\left[\left(\sigma^2 - C(\Delta x)\right)h_c + C(\Delta x)y_2\right] - h_c a}{\sqrt{(2\sigma^2 a^* a + a)[4aa^*(\sigma^4 - C^2(\Delta x)) + 2\sigma^2(a + a^*) + 1]}}$$

we can see that this expression depends on Δx in two ways: first, directly with y_2, the variable of integration in the outer integral, and second, as in the difference $\left(\sigma^2 - C(\Delta x)\right)$. If $\Delta x \approx 0$ or if $\Delta x << l_x$, these dependencies will be constant (first case) and roughly zero (second case) and the complementary error function will vary little with Δx in the region of interest. By construction, we have created the Δx interval over which there is a significant contribution, dictated by the exponential portion of the integrand

$$\int_{-\infty}^{\infty} e^{-\frac{aa^*}{\left(a+a^*\right)}\Delta x^2} \operatorname{erfc}\left\{\frac{-2aa^*\left[\left(\sigma^2 - C(\Delta x)\right)h_c + C(\Delta x)y_2\right] - h_c a}{\sqrt{(2\sigma^2 a^* a + a)[4aa^*(\sigma^4 - C^2(\Delta x)) + 2\sigma^2(a+a^*) + 1]}}\right\} d\Delta x$$

Hence, if we can construct the correlation function in Equation 2.2-17 such it does not vary significantly in the Δx interval of interest then the argument of the complementary error function and consequently the complementary error function itself will remain constant over the significant Δx interval. In other words, we must compare the following exponential functions

$$e^{-\frac{aa^*}{\left(a+a^*\right)}\Delta x^2} \quad \text{vs.} \quad e^{-\frac{\Delta x^2}{l_x^2}}$$

Equation 2.2-18

with the first required to decay much more rapidly than the second must. Hence, the following inequality has been constructed which sets limits on the correlation length

$$\frac{1}{l_x^2} << \frac{aa^*}{a+a^*} \quad \Rightarrow \quad l_x >> \sqrt{\frac{2\alpha^2 d_0^2}{d_0^2 + \alpha^4 k_0^2}}$$

Equation 2.2-19

Figure 2.2-3 graphically portrays this requirement for the correlation length ten times greater in the inequality above as a function of the distance d_0 and the beamwidth at a frequency (3 GHz).

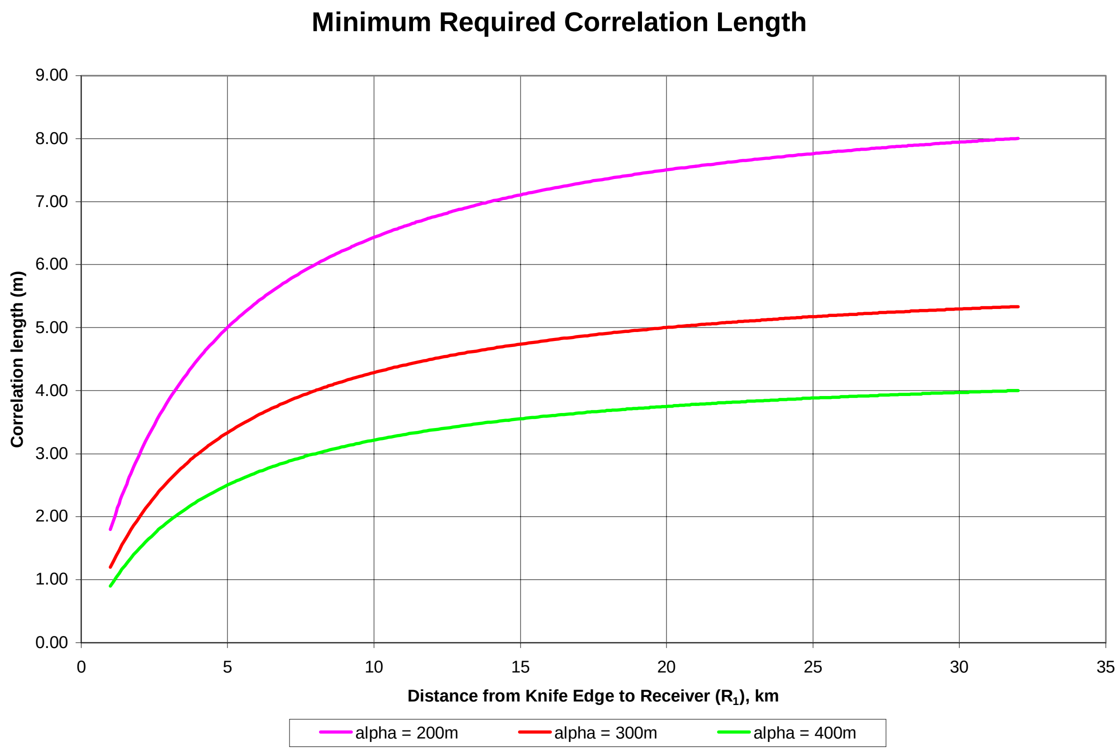

Figure 2.2-3: Correlation length that satisfies the inequality of Equation 2.2-19 by a conservative factor of 10 for a carrier frequency of 3 GHz

Figure 2.2-4 gives a representative picture of the complementary error function for the communication system described in Table 1 of a later section. As a reference, the first exponential function of Equation 2.2-18 is included. Recall that this exponential function will define the significant range for Δx if Laplace's Method is to apply. Note how the complementary error function is relatively constant over the non-zero Δx region defined by the exponential, particularly as the correlation length increases.

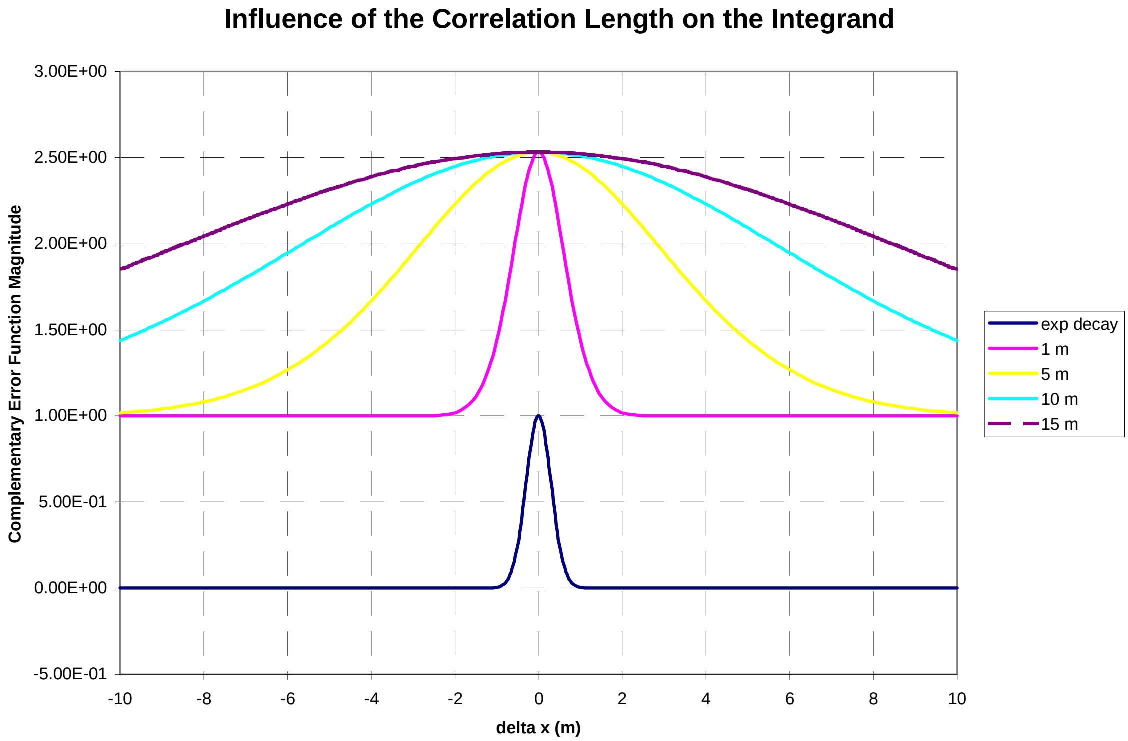

Figure 2.2-4: Comparison of the exponential decay with the behavior of the complementary error function

When the complementary error function is essentially independent of Δx, the Δx integration is easily performed. Then using the form of the correlation function in equation Equation 2.2-17, this expression further reduces to (choosing a value of $\Delta x = 0$ meters and noting that $C(\Delta x) = \sigma^2$)

$$\left\langle \vec{E}\cdot\vec{E}^* \right\rangle \approx K^2 \frac{\pi\sqrt{\pi}}{\sqrt{a^2 a*\left(2\sigma^2 a^* + 1\right)}} \int_0^\infty e^{-\frac{a^*}{\left(2\sigma^2 a^*+1\right)}(y_2-h_c)^2} \cdot \mathrm{erfc}\left\{ \frac{-\sqrt{a}\left[2a^*\sigma^2 y_2 + h_c\right]}{\sqrt{\left(2\sigma^2 a^*+1\right)\left[2\sigma^2\left(a+a^*\right)+1\right]}} \right\} dy_2$$

Equation 2.2-20

We can see that the exponential portion in the remaining y_2 integral produces its most significant result about $y_c = h_c$. However, Laplace's Method stationary phase and saddle point techniques will not be applicable in the majority of cases due to the magnitude of the coefficient in the exponential and its complex nature; it is not a large parameter. Consequently, Equation 2.2-20 will be considered the final reduced form for most reasonable physical situations.

We may next investigate the limiting forms of the mean square field. First, as the edge is removed to infinity $(h_c \to \infty)$, the mean square field will reduce to the square of the coherent field as given in Equation 2.2-7. This can be seen starting with the exact form for the mean square field given in Equation 2.2-15 and allowing the condition $(h_c \to \infty)$

$$\left\langle \vec{E} \cdot \vec{E}^* \right\rangle = K^2 \frac{\pi}{\sqrt{a(a+a^*)(2\sigma^2 a^*+1)}} \int_0^\infty e^{-\frac{a^*}{(2\sigma^2 a^*+1)}(y_2-h_c)^2} \cdot \int_{-\infty}^{\infty} e^{-\frac{aa^*}{(a+a^*)}\Delta x^2} \operatorname{erfc}\{-\infty\} d\Delta x \, dy_2$$

Equation 2.2-21

and since $\operatorname{erfc}\{-\infty\} = 2$, the two integrals may be evaluated exactly yielding the free space result for the mean square field

$$\left[\left\langle \bar{E}(0,0,z_0) \cdot \bar{E}^*(0,0,z_0) \right\rangle\right]_{h_c \to \infty} = \left\langle \bar{E}(0,0,z_0)\right\rangle \left\langle \bar{E}(0,0,z_0)\right\rangle^* = \frac{|K|^2 \pi^2}{aa^*}$$

Equation 2.2-22

which is identical to the square of the mean field or the coherent field.

A second limit that requires investigation is that of the smooth edge. As expected, as the roughness height tends toward zero, i.e. $\sigma \to 0$, the resulting mean square field becomes equal to the magnitude of the square of the coherent power from Equation 2.2-7.

Again starting with the exact form for the mean square field given in Equation 2.2-15 and allowing the condition $\sigma \to 0$

$$\left\langle \vec{E} \cdot \vec{E}^* \right\rangle = K^2 \frac{\pi}{\sqrt{a(a+a^*)}} \int_0^\infty e^{-a^*(y_2-h_c)^2} \int_{-\infty}^\infty e^{-\frac{aa^*}{(a+a^*)}\Delta x^2} \operatorname{erfc}\left\{-\sqrt{a}\, h_c\right\} d\Delta x \, dy_2$$

Equation 2.2-23

which reduces to the familiar form of Equation 2.2-7 for the square of the absolute value of the mean field or to within a constant, the coherent power

$$\left\langle \vec{E}(0,0,z_0) \cdot \vec{E}^*(0,0,z_0) \right\rangle = \left\langle \vec{E}(0,0,z_0) \right\rangle \left\langle \vec{E}(0,0,z_0) \right\rangle^*$$
$$= \frac{|K|^2}{4} \frac{\pi^2}{aa^*} \operatorname{erfc}\left(-h_c \sqrt{a}\right) \operatorname{erfc}\left(-h_c \sqrt{a^*}\right)$$

Equation 2.2-24

Consequently, as we suspected, the total power reduces to the power in the coherent field for both the absence of the knife edge and for the smooth knife edge.

Finally, we may express the power in the incoherent field using the expressions:

$$P_{incoherent} = \left\langle \vec{E}(0,0,z_0) \cdot \vec{E}^*(0,0,z_0) \right\rangle - \left\langle \vec{E}(0,0,z_0) \right\rangle \left\langle \vec{E}(0,0,z_0) \right\rangle^*$$
$$= |K|^2 \frac{\pi}{\sqrt{a(a+a^*)(2\sigma^2 a^*+1)}} \int_0^\infty e^{-\frac{a^*}{(2\sigma^2 a^*+1)}(y_2-h_c)^2} \int_{-\infty}^\infty e^{-\frac{aa^*}{(a+a^*)}\Delta x^2}$$
$$\cdot \operatorname{erfc}\left\{ \frac{-\sqrt{a}[h_c(2\sigma^2 a^*+1)] + 2a^* C(\Delta x)(y_2-h_c)}{\sqrt{(2\sigma^2 a^*+1)[4aa^*(\sigma^4 - C^2(\Delta x)) + 2\sigma^2(a+a^*)+1]}} \right\} d\Delta x \, dy_2$$
$$- \frac{|K|^2}{4} \frac{\pi^2}{aa^*} \operatorname{erfc}\left(-h_c \sqrt{\frac{a}{2\sigma^2 a+1}}\right) \operatorname{erfc}\left(-h_c \sqrt{\frac{a^*}{2\sigma^2 a^*+1}}\right)$$

Equation 2.2-25

under the assumptions mentioned in the previously, this expression may be reduced using the approximations in Equation 2.2-20.

2.3 Example Results

Consider the communication system described in Table 2.3-1 and whose system parameters represent a model of a terrestrial microwave link.

Table 2.3-1. Terrestrial Microwave Link-to-Link Example

• Frequency:	$f = 3\text{GHz}$	($\lambda = 0.1$ m)
• Distance from the transmitter to the knife edge:	$R_1 = 4$ km	
• Distance from the knife edge to the receiver:	$z_o = 8$ km	
• Beamwidth parameter:	$\alpha = 200$ m	(beamwidth $\cong 2°$)
(refer to Figure 2.1-2)		

Figure 2.3-1 compares the total mean power to the knife edge roughness or the standard deviation of the heights.

Note that as the rms roughness on the knife edge increases, the amplitude oscillations decreased due to the destruction of the phase interference between the direct and the scattered fields.

In the next several figures, the results for the mean power are given for knife edge to receiver separation of 4 km. These values for power are given in dB and have been normalized by the free-space result; the normalization for the power when the roughness σ is varied is

$$\frac{\pi^2 |K|^2}{aa^*}$$

Equation 2.3-1

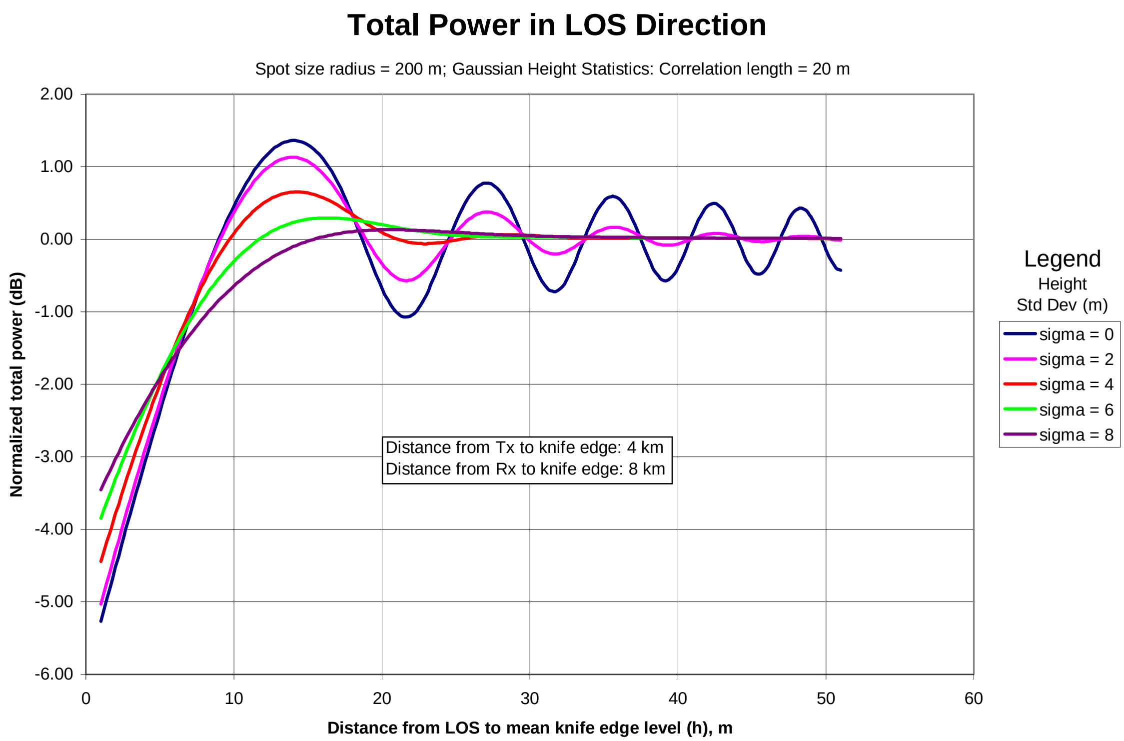

Figure 2.3-1: Total mean power (receiver to knife edge: z_o = 8 km).

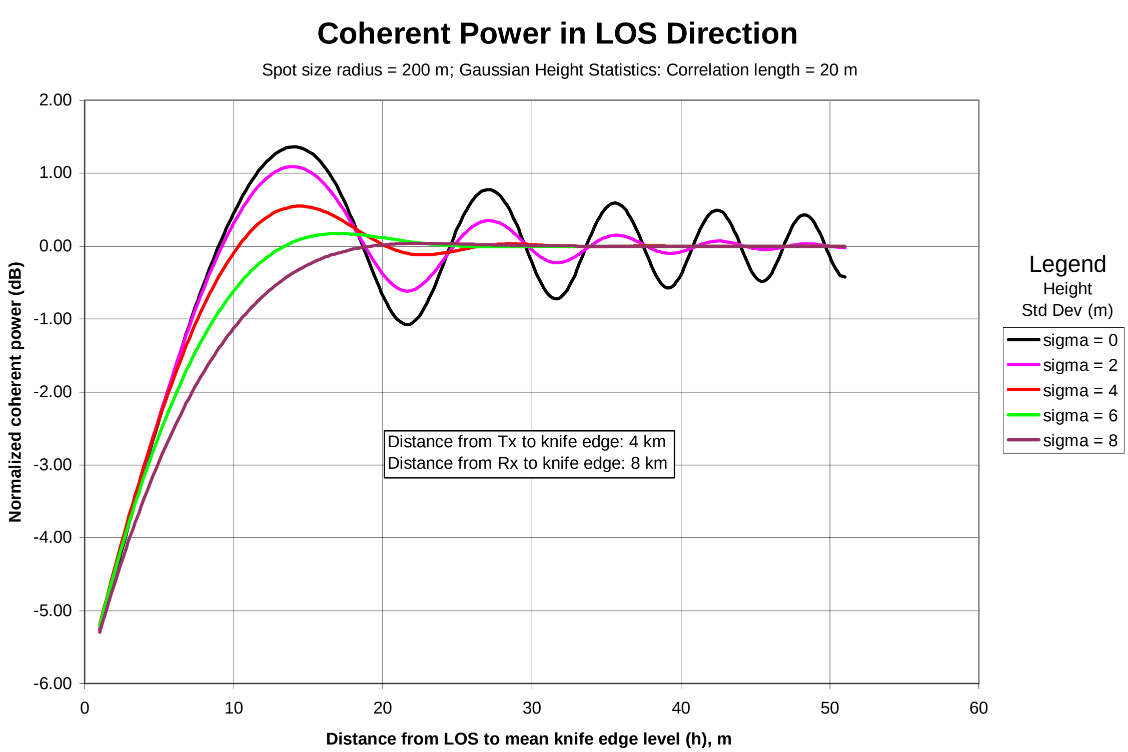

Figure 2.3-2: Coherent power (receiver to knife edge: z_o = 8 km).

In Figure 2.3-2 we present the coherent power in which we can see a slight variation from the total power of Figure 2.3-1. The total power is significantly larger than the coherent power when the knife edge is nearer the LOS and σ is large. It remains greater than or equal to this power throughout the calculations as would be expected. Note that each of these figures shows that as roughness is increased and as the knife edge is closer to the LOS, the power in the coherent field is lost to the incoherent field.

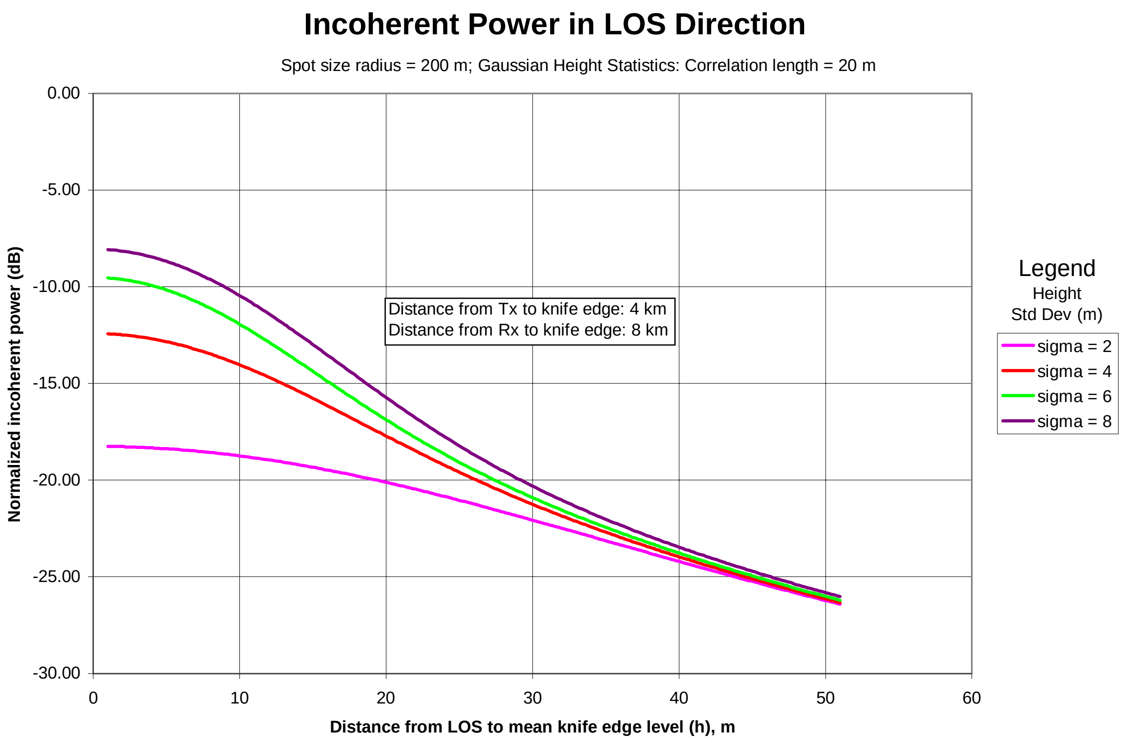

Figure 2.3-3: Incoherent power (receiver to knife edge: z_o = 8 km).

The incoherent power is given in Figure 2.3-3. In addition, the constructive and destructive interference in the total power that is usually predicted by conventional knife edge theory is lost as roughness is introduced. The total diffracted field is a superposition of the incident field and the edge-diffracted field; thus, the conventional oscillating behavior of the total field as the point of observation is moved away from the edge is due to the phase interference between these two fields. When the roughness on the edge increases, the edge diffracted-field becomes more incoherent and the phase interference consequently diminishes leading to an attenuation of the oscillations in the coherent or mean total field.

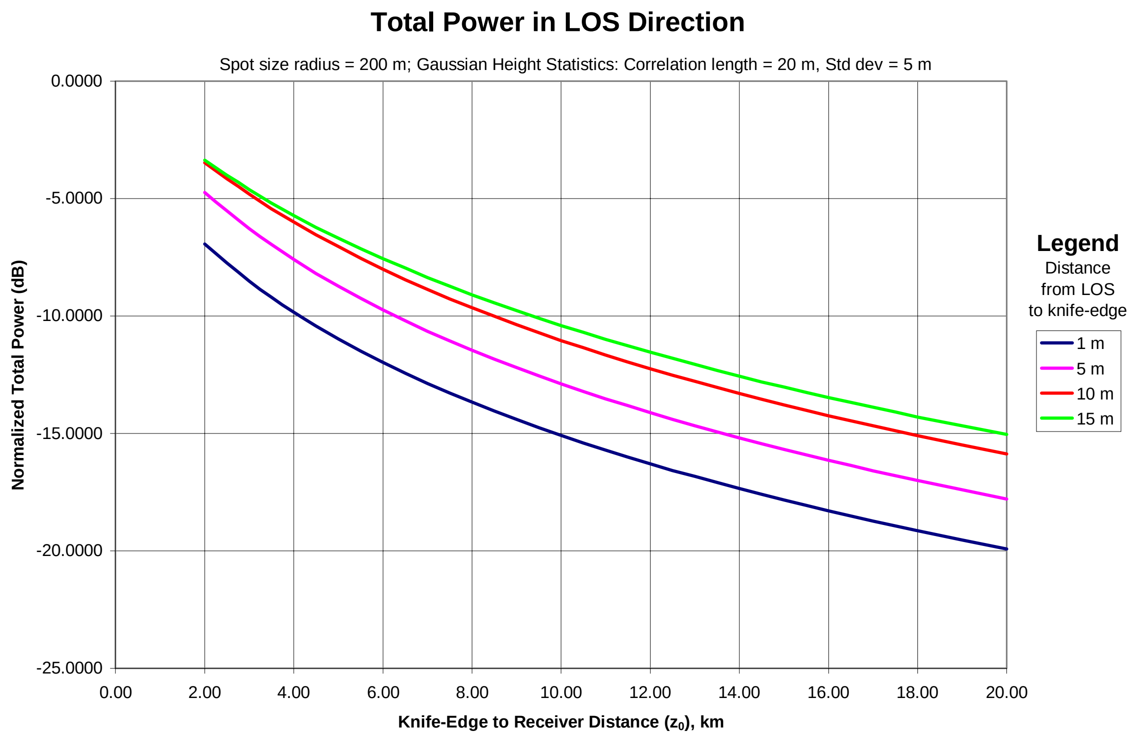

Figure 2.3-4: Total mean power (knife edge height standard deviation: σ = 5 m)

In the next several figures, we present the total mean and the incoherent power as a function of distance from the knife edge for two different roughness values: σ = 5 m (Figure 2.3-4 and Figure 2.3-5) and σ = 10 m (Figure 2.3-6 and Figure 2.3-7). The normalization for distance variation is simply:

$$\frac{|E_0|^2}{R_1^2}$$

Equation 2.3-2

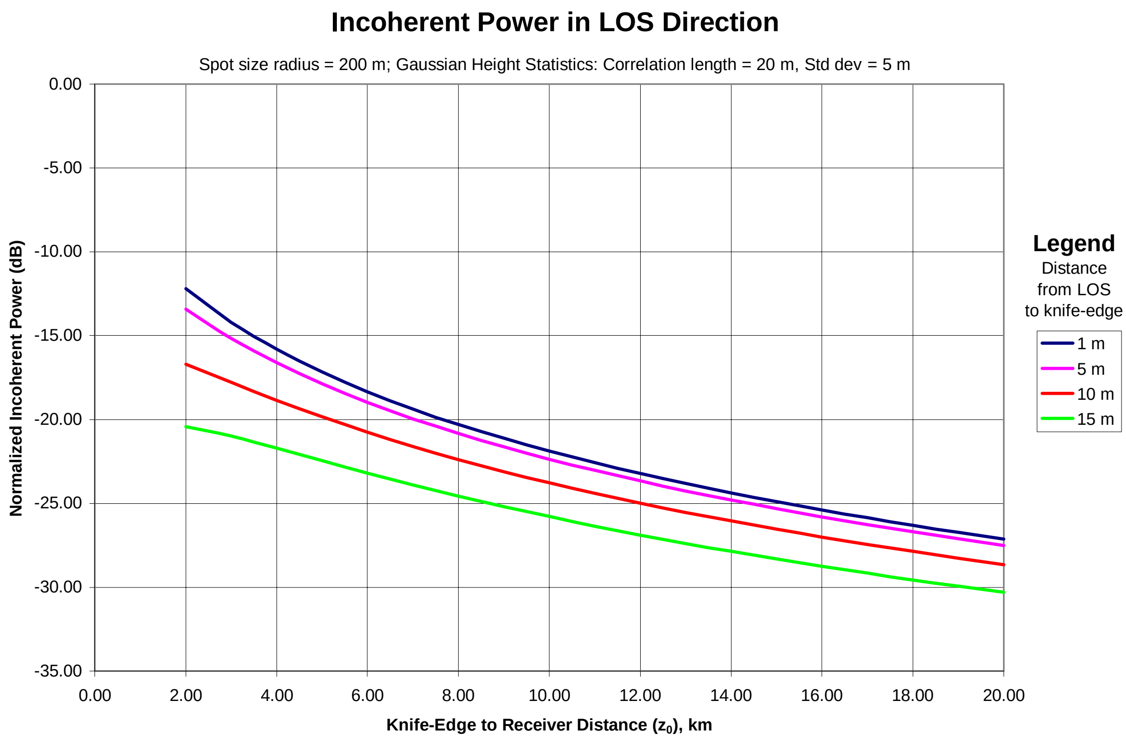

Figure 2.3-5: Incoherent power (knife edge height standard deviation: σ = 5 m)

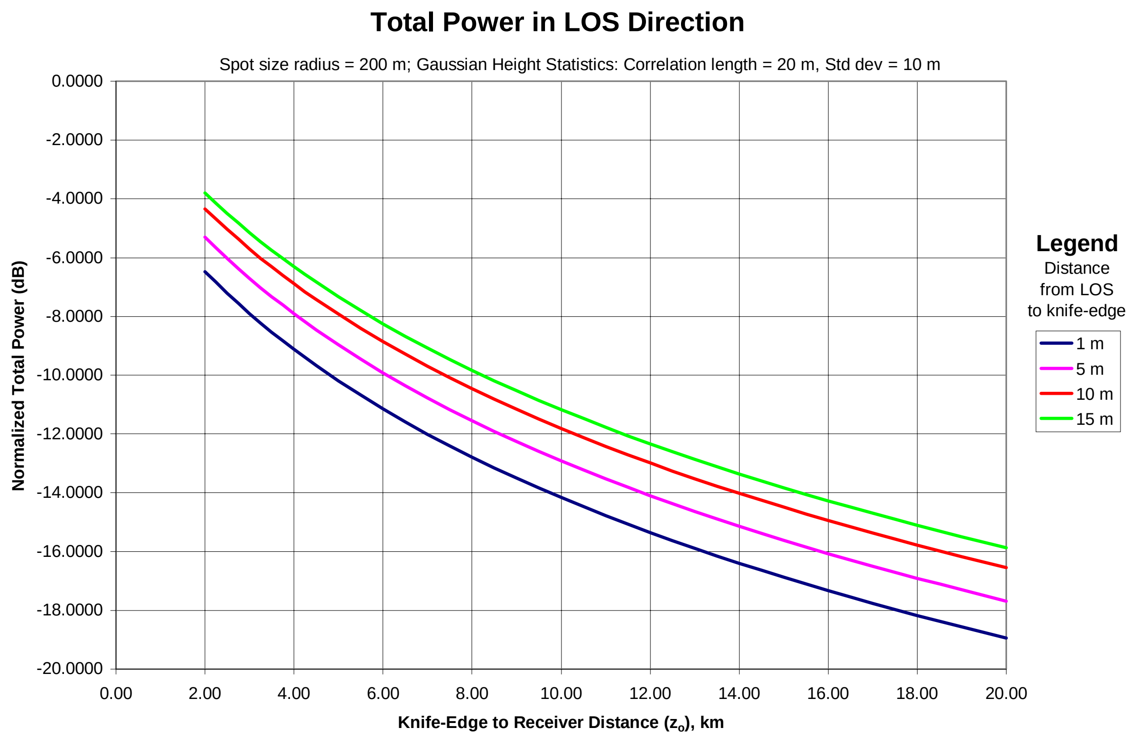

Figure 2.3-6: Total mean power (knife edge height standard deviation: σ = 10 m)

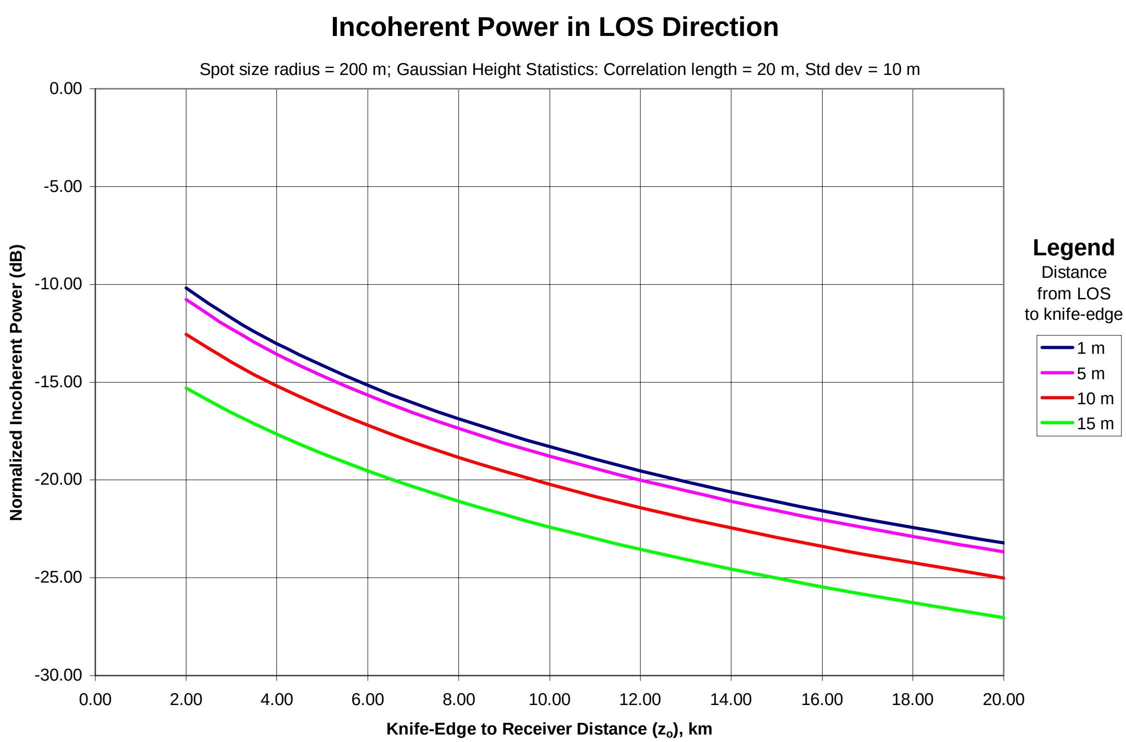

Figure 2.3-7: Incoherent power (knife edge height standard deviation: σ = 10 m)

2.4 Wide Angle Scattering by Randomly Rough Knife Edge

In the previous sections, we saw the results for scattering from a rough knife edge along the line-of-sight (LOS) coordinate. Nevertheless, there are often multiple transmitters or receivers and consequently, the power is desired in other directions. In this section, we consider the field lying on points outside the LOS direction. This will be accomplished primarily using the paraxial approximation, but will also be checked using the method of stationary phase. The solution was also sought in terms of the saddle point method; however, although it is more widely applicable than the stationary phase result, the solution becomes very cumbersome. The saddle point solution was compared for a smooth knife edge (two-dimensional problem) with favorable results; however, in three dimensions, the solution has branch cuts similar to those found in Banos [1966]. This solution has not been pursued at this point, yet it remains a topic of future exploration.

2.4.1 Paraxial approximation in wide angle scattering

The paraxial approximation is expected to hold only for those directions near the LOS. However, as we shall see, the spectral content of reasonably sized beams allows the paraxial approximation to be used in most cases. The paraxial approximation breaks down, as the beam becomes very narrow, consequently with increasing the spectral content of the beam.

We begin with the four dimensional, space/spectral integral from the previous section. This describes the spectral summation of the beam components integrated over the "aperture" region.

$$\vec{E}(\vec{r}_o) = \frac{e^{-jk_0 R_1}}{(2\pi)^2 4\pi R_1} \int_{-\infty}^{\infty}\int_{-\infty}^{\infty}\int_{-\infty}^{\infty}\int_{-h_c}^{\infty} e^{-\frac{(x^2+y^2)}{\alpha^2}} e^{+jk_x(x-x_o)} e^{+jk_y(y-y_o)} \cdot e^{+j\sqrt{k^2-k_x^2-k_y^2}\,z_o}\, dx\, dy dk_x dk_y$$

Equation 2.4-1

As before, we implement the paraxial approximation which is essentially the binomial expansion of the square root expression of the phase function

$$e^{+j\sqrt{k^2-k_x^2-k_y^2}\,z_o} \approx e^{-jkz_o} e^{+j\frac{\left(k_x^2+k_y^2\right)}{2k}z_o}$$

and substituting into Equation 2.4-1, we find a function which can be integrated.

$$\vec{E}(\vec{r}_o)=\frac{e^{-jk_0(z_o+R_1)}}{(2\pi)^2 4\pi R_1}\int_{-\infty}^{\infty}\int_{-h_c}^{\infty}\int_{-\infty}^{\infty}\int_{-\infty}^{\infty} e^{-\frac{\left(x^2+y^2\right)}{\alpha^2}} e^{jk_x(x-x_o)} e^{jk_y(y-y_o)} e^{+j\frac{\left(k_x^2+k_y^2\right)}{2k}z_o}\,dx\,dy\,dk_x\,dk_y$$

Equation 2.4-2

The spectral integrals are easily accomplished since the spatial components of the spectrum are no longer coupled. We have two similar integrals in the k_x and k_y integrations

$$\int_{-\infty}^{\infty} e^{-j\frac{z_o}{2k}k_x^2} e^{+jk_x(x-x_o)}dk_x = \sqrt{\frac{2\pi k}{-jz_o}}\, e^{\frac{-jk(x-x_o)^2}{2z_o}}$$

Replacing the x and y spectral integrals by the above results (for x and y, respectively), we find the total field after diffraction by the knife edge (in the physical optics approximation)

$$\vec{E}(\vec{r}_o)=j\frac{ke^{-jk_0R_1}}{8\pi^2R_1z_o} e^{\frac{-jk\left(x_o^2+y_o^2\right)}{2z_o}} \int_{-\infty}^{\infty}\int_{-h_c}^{\infty} e^{-a\left(x^2+y^2\right)} e^{\frac{-jk(x-x_o)^2}{2z_o}}\, e^{\frac{-jk(y-y_o)^2}{2z_o}}\,dx\,dy$$

where $a=\left(\frac{1}{\alpha^2}+j\frac{k}{2z_o}\right)$

Equation 2.4-3

Next we must integrate the incident field over the aperture region, thus implementing the physical optics approximation. Making a change of variables, $u = y + h_c;\ du = dy$, and evaluating the integral, we find the closed form solution.

$$\vec{E}(\vec{r}_o) = j\frac{ke^{-jk_0R_1}}{8\pi^2 R_1 z_o} e^{\frac{-jk\left(x_o^2+y_o^2\right)}{2z_o}} e^{\frac{-k^2 x_o^2}{4az_o^2}} \sqrt{\frac{\pi}{a}} \int_0^\infty e^{-a(u-h_c)^2 - \left(-j\frac{ky_o}{z_o}\right)(u-h_c)} du$$

$$= j\frac{ke^{-jk_0R_1}}{16\pi R_1 z_o a} e^{\frac{-jk\left(x_o^2+y_o^2\right)}{2z_o}} e^{\frac{-k^2\left(x_o^2+y_o^2\right)}{4az_o^2}} \operatorname{erfc}\left[-\sqrt{a}h_c - \frac{jky_o}{2\sqrt{a}z_o}\right]$$

Equation 2.4-4

This is the final result for the smooth edge in terms of the complementary error function of a complex argument.

The rough knife edge has a similar development. Again, we start with the Kirchhoff diffraction integral in the spectral domain, and implementing the paraxial approximation,

$$\vec{E}(\vec{r}_o) = j\frac{ke^{-jk_0R_1}}{8\pi^2 R_1 z_o} e^{\frac{-jk\left(x_o^2+y_o^2\right)}{2z_o}} \int_{-\infty}^{\infty} \int_{-(h_c+\delta h_c)}^{\infty} e^{-a\left(x^2+y^2\right)} e^{\frac{-jk(x-x_o)^2}{2z_o}} e^{\frac{-jk(y-y_o)^2}{2z_o}} dx\,dy$$

$$\text{where } a = \left(\frac{1}{\alpha^2} + j\frac{k}{2z_o}\right)$$

Equation 2.4-5

Next we make the change of variables, $u = y + \delta h_c; du = dy$, and averaging over the fluctuating portion of the roughness on the knife edge.

$$\left\langle \vec{E}(\vec{r}_o) \right\rangle = j\frac{ke^{-jk_0R_1}}{8\pi^2 R_1 z_o} e^{\frac{-jk\left(x_o^2+y_o^2\right)}{2z_o}} \int_{-\infty}^{\infty} e^{-ax^2} e^{\frac{-jk(x-x_o)^2}{2z_o}} dx$$

$$\cdot \int_{-h_c}^{\infty} \left\langle e^{a(u-\delta h_c)^2 - jk\frac{(u-\delta h_c - y_o)^2}{2z_o}} \right\rangle du$$

where $a = \left(\frac{1}{\alpha^2} + j\frac{k}{2R_1} \right)$

Equation 2.4-6

This average over the fluctuating portion of the knife edge is evaluated using a Gaussian probability density function

$$p(\delta h_c) = \frac{1}{\sqrt{2\pi}\sigma} e^{-\frac{1}{2\sigma^2}\delta h_c{}^2}$$

Consequently, the integral for the mean field is evaluated to yield the following result for total field due to the diffraction by a rough, knife edge obstruction: in the physical optics approximation.

$$\left\langle \vec{E}(\vec{r}_o) \right\rangle = j\frac{ke^{-jk_0R_1}}{16\pi R_1 z_o a_1} e^{\frac{-jk\left(x_o^2+y_o^2\right)}{2z_o}} e^{\frac{-k^2\left(x_o^2+y_o^2\right)}{4a_1 z_o^2}} \operatorname{erfc}\left[\frac{-2a_1 h_c z_o - jky_o}{2z_o\sqrt{2z_o\left(2\sigma^2 a_1 + 1\right)}} \right]$$

Equation 2.4-7

From Equation 2.4-7, we see that the effects of the roughness only enter through the error function. Of greater interest is the mean power or coherent power; this can be written as

$$P(\vec{r}_o) = \left\langle \vec{E}(\vec{r}_o) \right\rangle \left\langle \vec{E}^*(\vec{r}_o) \right\rangle$$

$$= \frac{ke^{\frac{-k^2\left(x_o^2+y_o^2\right)}{4a_1 z_o^2}} e^{\frac{-k^2\left(x_o^2+y_o^2\right)}{4a_1^* z_o^2}}}{(16\pi R_1 z_o)^2 a_1 a_1^*} \operatorname{erfc}\left[\frac{-2a_1 h_c z_o - jky_o}{2z_o\sqrt{2z_o\left(2\sigma^2 a_1 + 1\right)}} \right] \operatorname{erfc}\left[\frac{-2a_1^* h_c z_o - jky_o}{2z_o\sqrt{2z_o\left(2\sigma^2 a_1^* + 1\right)}} \right]$$

Equation 2.4-8

Figure 2.4-1 through Figure 2.4-4 show the results for scattering by a rough knife edge.

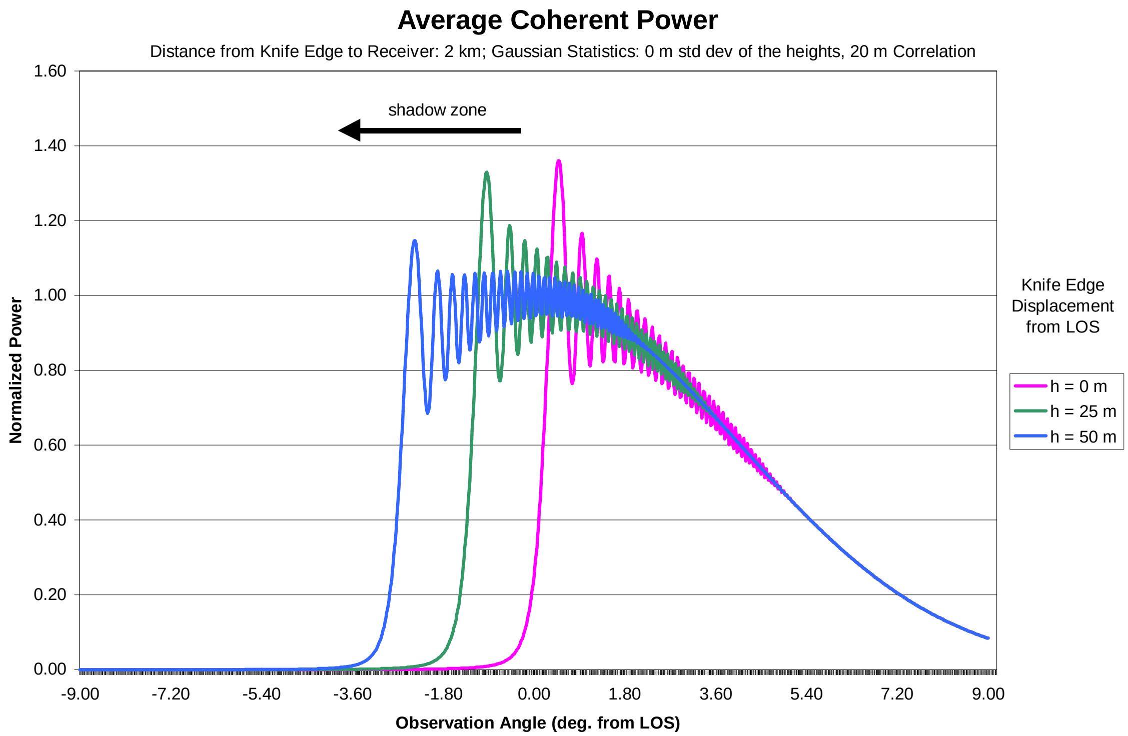

Figure 2.4-1: Average Coherent Power; Varying Heights

Figure 2.4-1 shows the effect that varying the height of the knife edge, relative to the line-of-sight path, has on the coherent power. From this figure, it can be seen that as the knife edge is pulled away from the line-of-sight path toward infinity, the effect of this obsticle diminishes. This is seen since the height of the oscillations is decreasing with increasing distance. Figure 2.4-2 shows the effects of the roughness of the knife edge. From this figure, the phase interference effects are damped out as the roughness is increased. Just as was seen with the power along the line-of-sight path, this effect is due to the destruction of the phase coherence of the energy scattered by the edge.

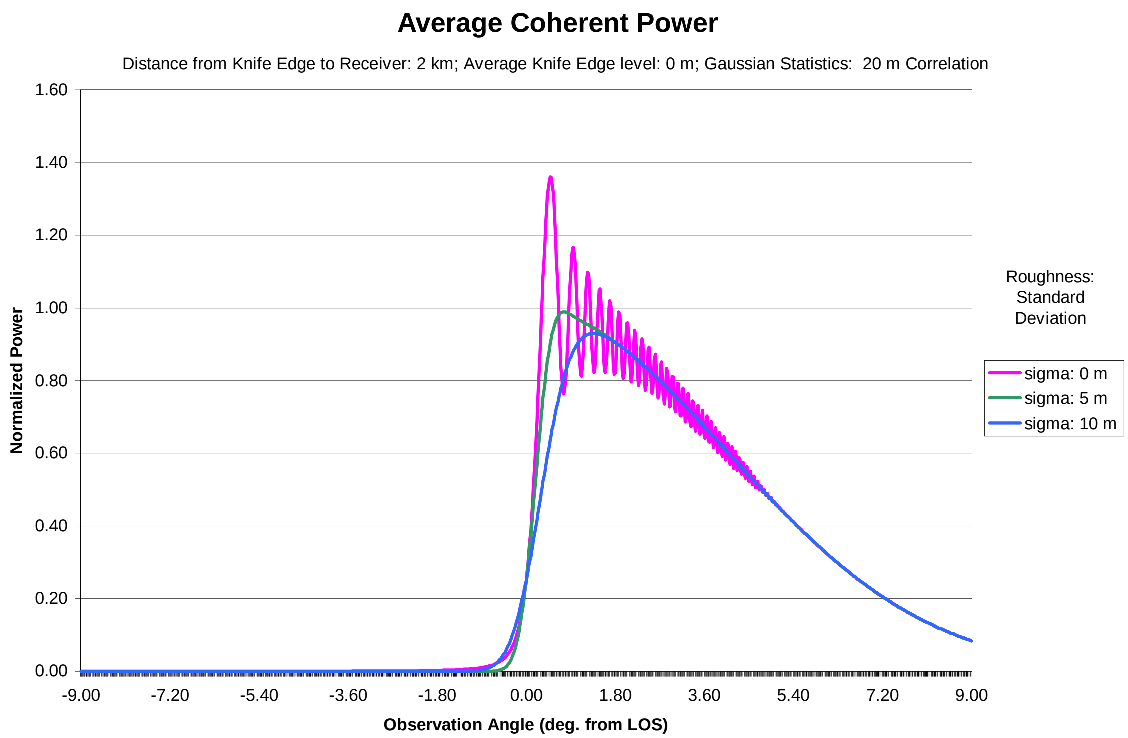

Figure 2.4-2: Average Coherent Power; Varying Knife Edge Roughness

Figure 2.4-3 is very similar to that of Figure 2.4-2 since it shows the same effect. This figure, however, was included since it also combines the effect of edge roughness with the effect of mean edge displacement. Essentially, it demonstrates that the curves are simply shifted and are slightly smaller in amplitude.

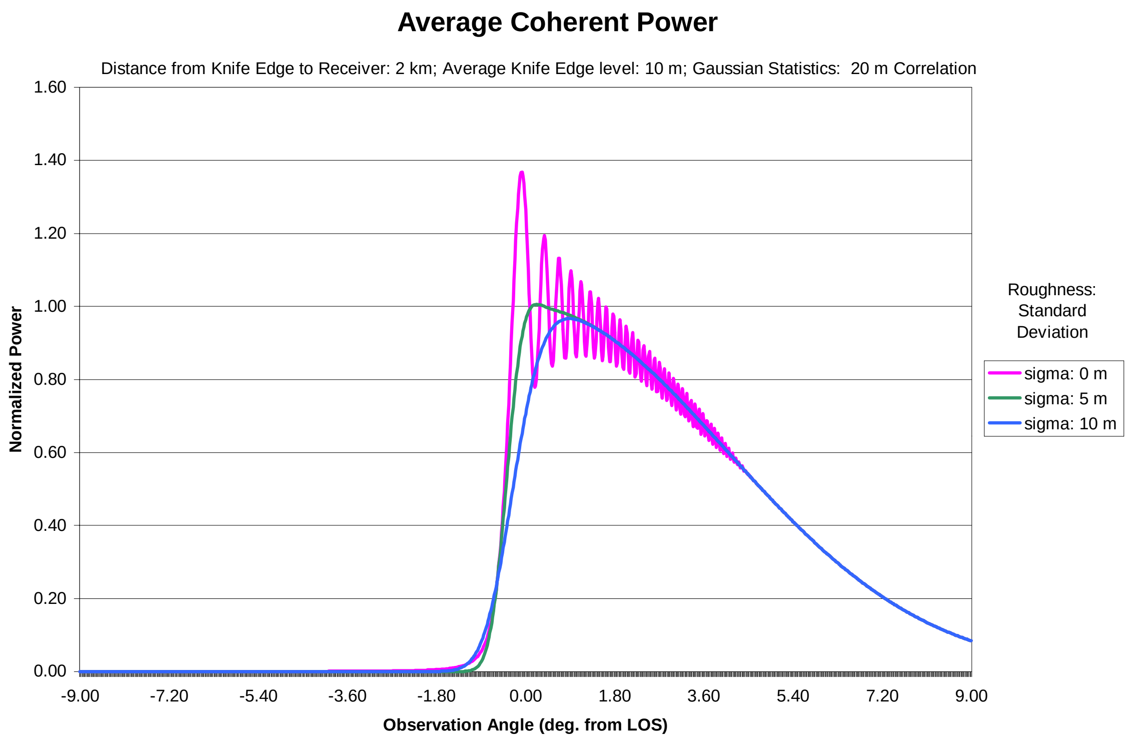

Figure 2.4-3: Average coherent power for varying roughness, knife edge displaced by 10 meters

Finally, Figure 2.4-4 shows the effect of changing the mean height from the line-of-sight path for a rough edge. This figure is similar to Figure 2.4-1 in that the curves appear to be truncated at different points. For very rough edge, the effects are more closely approaching the effect expected in geometrical optics, where the shadowing is distinct and does not include the phase interference effects in the transition zones demonstrated in classical diffraction by a smooth edge, see Figure 2.4-1.

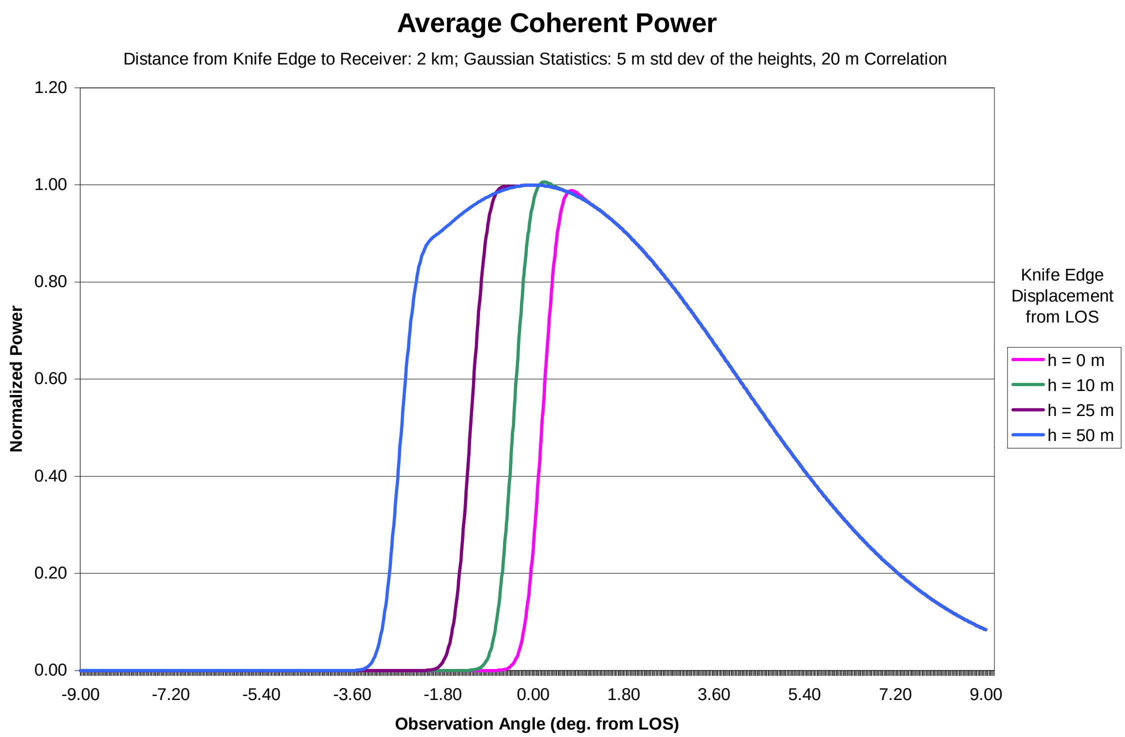

Figure 2.4-4: Average Coherent Power; Varying Mean Displacement from LOS

2.4.2 Stationary Phase Approximation to Wide-angle Scattering

Alternatively, we can formulate the wide-angle scatter using the method of stationary phase or saddle point integration, as needed. In this approach, we begin by performing the spatial integral (i.e. the integral over the aperture). From this effort, we find the result

$$\vec{E}(\vec{r}_o)=\frac{e^{-jk_0R_1}}{(2\pi)^2 4\pi R_1}\int_{-\infty}^{\infty}\int_{-\infty}^{\infty} e^{-jk_x x_o - jk_y y_o} e^{+j\sqrt{k^2-k_x^2-k_y^2}\, z_o} \cdot\left(\alpha\sqrt{\pi}e^{-\frac{k_x^2\alpha^2}{4}}\right)\left(\frac{\alpha\sqrt{\pi}}{2}e^{-\frac{k_y^2\alpha^2}{4}}\operatorname{erfc}\left[-\frac{h_c}{\alpha}-j\frac{k_y\alpha}{2}\right]\right)dk_x dk_y$$

Equation 2.4-9

The error function of a complex argument yields a complex function. Combining terms, rearranging and substituting for the complementary error function,

$$\vec{E}(\vec{r}_o)=\frac{e^{-jk_0R_1}\alpha^2}{8(2\pi)^2R_1}C_1\int_{-\infty}^{\infty}\int_{-\infty}^{\infty}e^{-jk_xx_o-jk_yy_o}e^{+j\sqrt{k^2-k_x^2-k_y^2}\,z_o}e^{-\frac{\left(k_x^2+k_y^2\right)\alpha^2}{4}}dk_xdk_y$$
$$-\frac{e^{-jk_0R_1}\alpha^2}{8(2\pi)^2R_1}\int_{-\infty}^{\infty}\int_{-\infty}^{\infty}e^{-jk_xx_o-jk_yy_o}e^{+j\sqrt{k^2-k_x^2-k_y^2}\,z_o}e^{-\frac{\left(k_x^2+k_y^2\right)\alpha^2}{4}}g\left(k_y\right)e^{-jk_yh_c}dk_xdk_y$$

Equation 2.4-10

Where we have substituted the series expansion for the error function of a complex argument [Abromowitz, 1972]

$$C_1=1+\operatorname{erf}\left(\frac{h_c}{\alpha}\right)+\frac{1}{\pi}\left[\frac{\alpha}{2h_c}+\frac{4h_c}{\alpha}\sum_{n=1}^{\infty}\frac{e^{-\frac{n^2}{4}}}{n^2+4\frac{h_c^2}{\alpha^2}}\right]$$

$$g\left(k_y\right)=\frac{e^{-\frac{h_c^2}{\alpha^2}}}{\pi}\left[\frac{\alpha}{2h_c}+\frac{4h_c}{\alpha}\sum_{n=1}^{\infty}\frac{e^{-\frac{n^2}{4}}}{n^2+4\frac{h_c^2}{\alpha^2}}\cosh\left(\frac{nk_y\alpha}{2}\right)-j2\sum_{n=1}^{\infty}\frac{e^{-\frac{n^2}{4}}}{n^2+4\frac{h_c^2}{\alpha^2}}n\sinh\left(\frac{nk_y\alpha}{2}\right)\right]$$

Each of these integrals is to be evaluated by the method of stationary phase.

$$\vec{E}(\vec{r}_o)=\frac{e^{-jkR_1}\alpha^2}{8(2\pi)^2R_1}\int_{-\infty}^{\infty}\int_{-\infty}^{\infty}g_1\left(k_y\right)e^{-jk_xx_o-jk_yy_o}e^{+j\sqrt{k^2-k_x^2-k_y^2}\,z_o}dk_xdk_y$$
$$-\frac{e^{-jkR_1}\alpha^2}{8(2\pi)^2R_1}\int_{-\infty}^{\infty}\int_{-\infty}^{\infty}g_2\left(k_y\right)e^{-jk_xx_o-jk_yy_o}e^{+j\sqrt{k^2-k_x^2-k_y^2}\,z_o}e^{-jk_yh_c}dk_xdk_y$$

Equation 2.4-11

where

$$g_1\left(k_x,k_y\right)=e^{-\frac{\left(k_x^2+k_y^2\right)\alpha^2}{4}}\left(1+\operatorname{erf}\left(\frac{h_c}{\alpha}\right)+\frac{e^{-\frac{h_c^2}{\alpha^2}}}{\pi}\left[\frac{\alpha}{2h_c}+\frac{4h_c}{\alpha}\sum_{n=1}^{\infty}\frac{e^{-\frac{n^2}{4}}}{n^2+4\frac{h_c^2}{\alpha^2}}\right]\right)$$

$$g_2\left(k_x, k_y\right) = \frac{e^{-\frac{h_c^2}{\alpha^2}} e^{-\frac{\left(k_x^2+k_y^2\right)\alpha^2}{4}}}{\pi} \left[\begin{array}{r} \dfrac{\alpha}{2h_c} + \dfrac{4h_c}{\alpha} \sum\limits_{n=1}^{\infty} \dfrac{e^{-\frac{n^2}{4}}}{n^2 + 4\frac{h_c^2}{\alpha^2}} \cosh\left(\dfrac{nk_y\alpha}{2}\right) \\ - j2 \sum\limits_{n=1}^{\infty} \dfrac{e^{-\frac{n^2}{4}}}{n^2 + 4\frac{h_c^2}{\alpha^2}} n \sinh\left(\dfrac{nk_y\alpha}{2}\right) \end{array} \right]$$

Stationary phase evaluation of the first integral yields (see Appendix 2.4.3)

$$\begin{aligned} &\frac{e^{-jkR_1}\alpha^2}{8(2\pi)^2 R_1} \int\limits_{-\infty}^{\infty}\int\limits_{-\infty}^{\infty} g_1\left(k_y\right) e^{-jk_x x_o - jk_y y_o} e^{+j\sqrt{k^2-k_x^2-k_y^2}\, z_o} dk_x dk_y \\ &\quad\cong \quad j\frac{\alpha^2\, k\cos\theta_o\, e^{-jk\left(R_1+r_o\right)}}{8\pi R_1 r_o} g_1\left(k_{xs}, k_{ys}\right) \end{aligned}$$

and the second integral yields a similar result with slightly shifted stationary points due to the extra phase term (see Appendix 2.4.3)

$$\begin{aligned} &\frac{e^{-jkR_1}\alpha^2}{8(2\pi)^2 R_1} \int\limits_{-\infty}^{\infty}\int\limits_{-\infty}^{\infty} g_2\left(k_x, k_y\right)\ e^{-jk_x x_o - jk_y y_o} e^{+j\sqrt{k^2-k_x^2-k_y^2}\, z_o} e^{-jk_y h_c} dk_x dk_y \\ &\quad\cong\ j g_2\left(k_{xs}, k_{ys}\right)\frac{\alpha^2\, e^{-jkR_1}}{8\pi R_1 r_o}\sqrt{k^2 - k_{xs}^2 - k_{ys}^2}\ e^{-j\phi\left(k_{xs}, k_{ys}\right) r_o} \end{aligned}$$

$$\text{where } \phi\left(k_x, k_y\right) = k_x \sin\theta_o \cos\phi_o + k_y\left(\sin\theta_o \sin\phi_o + \frac{h_c}{r_o}\right) + \sqrt{k^2 - k_x^2 - k_y^2}\cos\theta_o$$

Equation 2.4-12

One computational note: the above exponential factor should be distributed into the hyperbolic sine and cosine within the function $g(k_y)$ so that these functions do not “blow up.” Hence,

$$
g_2(k_x,k_y) = \frac{e^{-\frac{h_c^2}{\alpha^2}}}{\pi}\left[\begin{array}{l} \left(\dfrac{\alpha}{2h_c} + \dfrac{4h_c}{\alpha}\displaystyle\sum_{n=1}^{\infty}\dfrac{e^{-\frac{n^2}{4}}}{n^2+4\frac{h_c^2}{\alpha^2}}\right)\left(\dfrac{e^{\frac{nk_y\alpha}{2}-\frac{(k_x^2+k_y^2)\alpha^2}{4}}+e^{-\frac{nk_y\alpha}{2}-\frac{(k_x^2+k_y^2)\alpha^2}{4}}}{2}\right) \\ -j2\displaystyle\sum_{n=1}^{\infty}\dfrac{e^{-\frac{n^2}{4}}}{n^2+4\frac{h_c^2}{\alpha^2}}\, n\left(\dfrac{e^{\frac{nk_y\alpha}{2}-\frac{(k_x^2+k_y^2)\alpha^2}{4}}-e^{-\frac{nk_y\alpha}{2}-\frac{(k_x^2+k_y^2)\alpha^2}{4}}}{2}\right)\end{array}\right]
$$

Equation 2.4-13

The figures demonstrate the use of the stationary phase result.

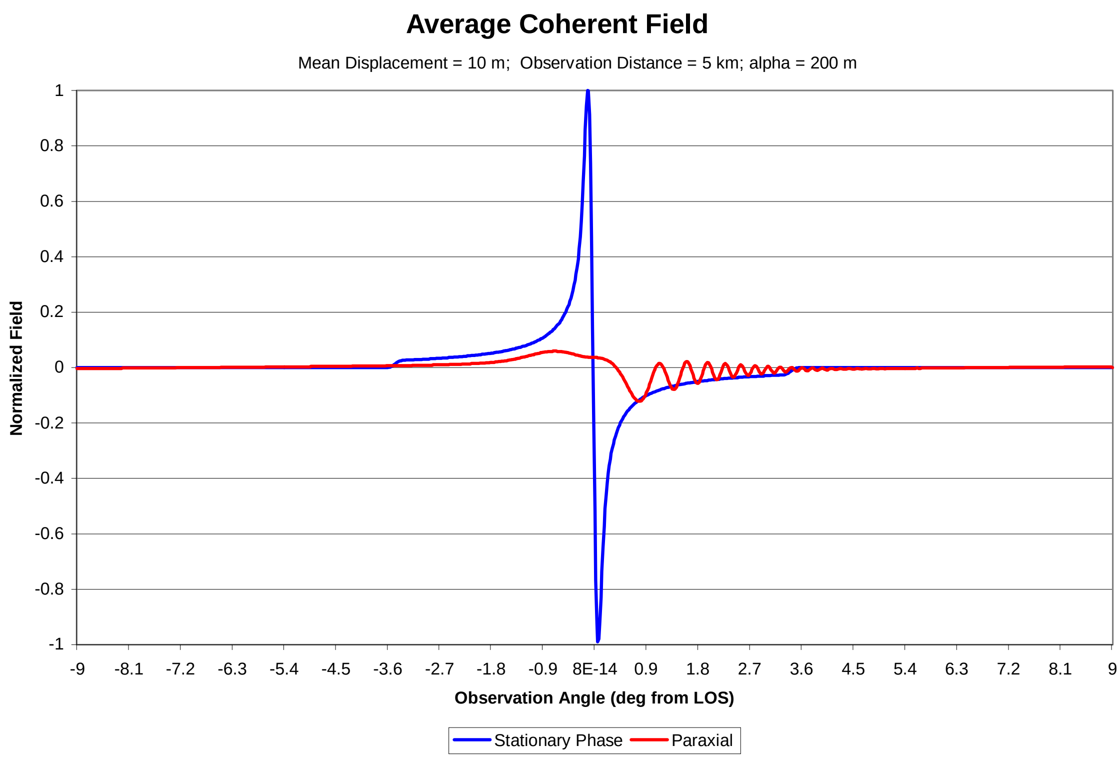

Figure 2.4-5: Failure of the stationary phase result.

Figure 2.4-5 shows a case of poor agreement. If the observation distance is not large, the stationary phase approximation does not provide a good estimate for the average coherent field. Figure 2.4-5 shows an example of the failure of the stationary phase result. It was predicted that the stationary phase result should provide a good estimate when the observation distance is large and the beam width factor is small.

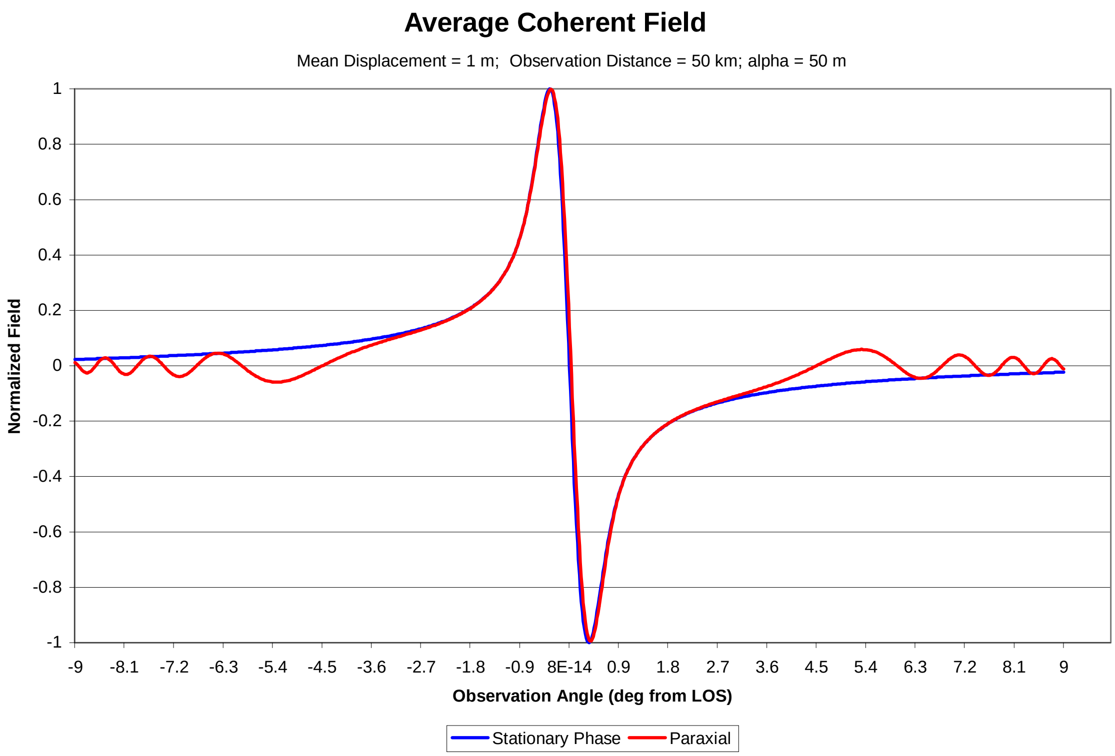

Figure 2.4-6: Agreement of stationary phase and paraxial approximations, h = 1 m

Figure 2.4-6 shows reasonably good agreement for a large observation distance and a small beamwidth. The stationary phase agrees in magnitude with the paraxial result. The ripples in the paraxial result may be a matter of further investigation since the stationary phase result should hold as the angles get larger, whereas the paraxial should break down. However, the angles explored are small enough so that the paraxial should also be accurate.

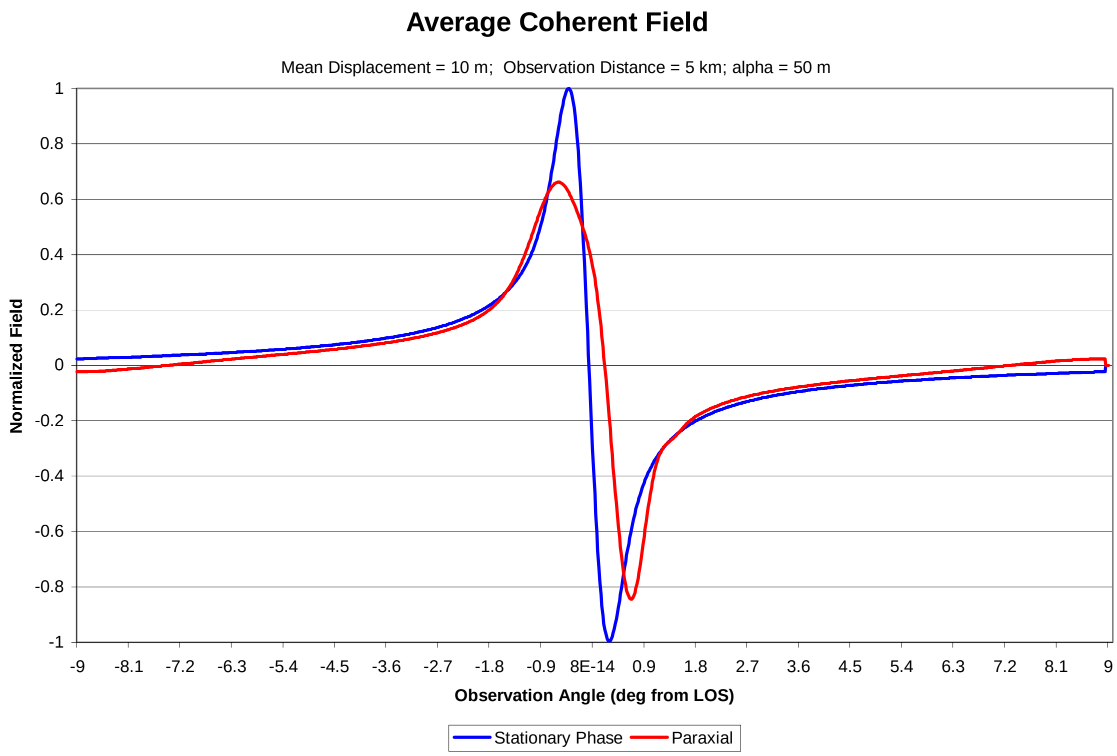

Figure 2.4-7: Degradation of the stationary phase result by observation distance

Figure 2.4-7 has the same parameters as Figure 2.4-6 but the observation distance is smaller. The degradation of the stationary phase result is obvious from this comparison. This is seen in the magnitude of the peak and the alignment in the "lit" region. As the beam width becomes larger, we expect that the saddle point method of integration will become necessary. Figure 2.4-7 shows another case where agreement is expected. In general, the magnitudes do agree (although only the real part is shown). This figure is simply an example showing the effect of increasing the separation from the line-of-sight to the knife edge. Finally, Figure 2.4-8 shows another case where the failure of the stationary phase result has been predicted: increased beamwidth. This result should be compared to the narrower beamwidth result of Figure 2.4-6.

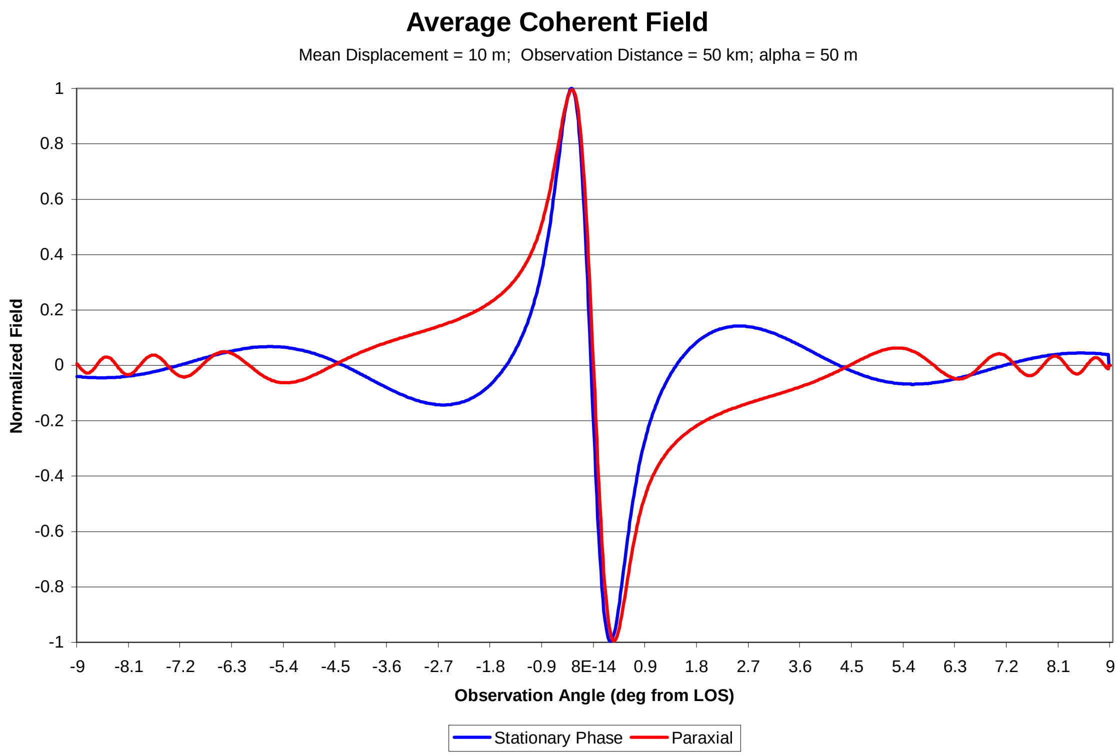

Figure 2.4-8: Agreement of stationary phase and paraxial approximations, h = 10 m

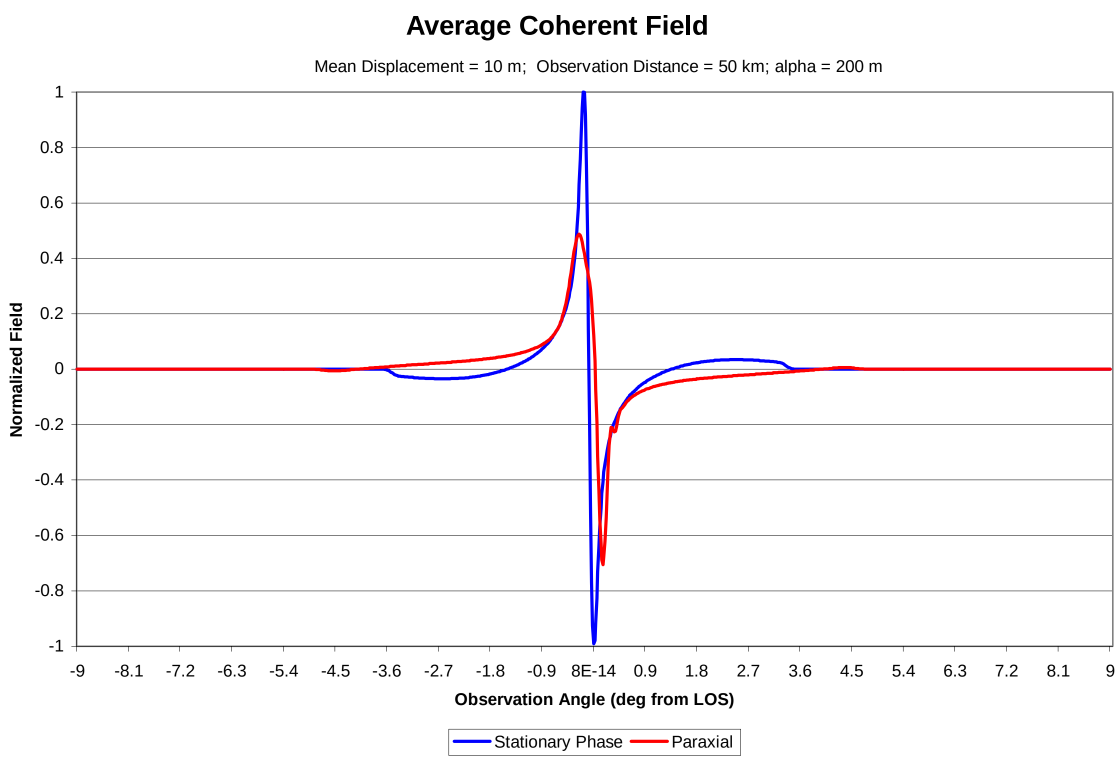

Figure 2.4-9: Degradation due to increased beamwidth

2.4.3 *Appendix: Stationary Phase Evaluation of Equation 2.4-10*

The evaluation of this integral

$$\int_{-\infty}^{\infty}\int_{-\infty}^{\infty} e^{-jk_x x_o - jk_y y_o} e^{+j\sqrt{k^2-k_x^2-k_y^2}\,z_o} e^{-\frac{\left(k_x^2+k_y^2\right)\alpha^2}{4}} dk_x dk_y$$

via stationary phase requires some limiting assumptions; the exponential factors

$$e^{-\frac{\left(k_x^2+k_y^2\right)\alpha^2}{4}}$$

must not force the integrand to zero too quickly with respect to the oscillations. Otherwise Laplace's method must be used when the decay is very rapid and saddle point evaluation becomes necessary in the intermediate case.

Converting the phase of the integrand in the first integral in Equation 2.4-10 to spherical coordinates and choosing range to the observation point as a large parameter,

$$\begin{aligned} &k_x x_o + k_y y_o + \sqrt{k^2 - k_x^2 - k_y^2}\, z_o \\ &\quad \Rightarrow r_o\left(k_x \sin\theta_o \cos\phi_o + k_y \sin\theta_o \sin\phi_o + \sqrt{k^2 - k_x^2 - k_y^2}\cos\theta_o \right) \end{aligned}$$

$$\Rightarrow \int_{-\infty}^{\infty}\int_{-\infty}^{\infty} e^{-\frac{\left(k_x^2+k_y^2\right)\alpha^2}{4}} e^{-jr_o\left(k_x \sin\theta_o \cos\phi_o + k_y \sin\theta_o \sin\phi_o + \sqrt{k^2-k_x^2-k_y^2}\cos\theta_o \right)} dk_x dk_y$$

Next we find the stationary point

$$\left(\frac{\partial\left(k_x \sin\theta_o \cos\phi_o + k_y \sin\theta_o \sin\phi_o + \sqrt{k^2 - k_x^2 - k_y^2}\cos\theta_o\right)}{\partial k_x}\right)_{(k_{xs},k_{ys})} = 0$$

$$\Rightarrow \quad \sin\theta_o \cos\phi_o = \frac{k_{xs}\cos\theta_o}{\sqrt{k^2 - k_{xs}^2 - k_{ys}^2}}$$

$$\text{squaring} \Rightarrow \quad \sin^2\theta_o \cos^2\phi_o = \frac{k_{xs}^2 \cos^2\theta_o}{k^2 - k_{xs}^2 - k_{ys}^2}$$

$$\left(\frac{\partial\left(k_x \sin\theta_o \cos\phi_o + k_y \sin\theta_o \sin\phi_o + \sqrt{k^2 - k_x^2 - k_y^2}\cos\theta_o\right)}{\partial k_y}\right)_{(k_{xs},k_{ys})} = 0$$

$$\Rightarrow \quad \sin\theta_o \sin\phi_o = \frac{k_{ys}\cos\theta_o}{\sqrt{k^2 - k_{xs}^2 - k_{ys}^2}}$$

$$\text{squaring} \Rightarrow \quad \sin^2\theta_o \sin^2\phi_o = \frac{k_{ys}^2 \cos^2\theta_o}{k^2 - k_{xs}^2 - k_{ys}^2}$$

forming the matrix equation:

$$\begin{bmatrix} \left(\sin^2\theta_o \cos^2\phi_o + \cos^2\theta_o\right) & \sin^2\theta_o \cos^2\phi_o \\ \sin^2\theta_o \sin^2\phi_o & \left(\sin^2\theta_o \sin^2\phi_o + \cos^2\theta_o\right) \end{bmatrix} \begin{bmatrix} k_{xs}^2 \\ k_{ys}^2 \end{bmatrix} = k^2 \begin{bmatrix} \sin^2\theta_o \cos^2\phi_o \\ \sin^2\theta_o \sin^2\phi_o \end{bmatrix}$$

yields the well-known stationary points

$$k_{xs} = k \sin\theta_o \cos\phi_o$$
$$k_{ys} = k \sin\theta_o \sin\phi_o$$

expanding the phase around the stationary point

$$\phi(k_x, k_y) \cong \phi(k_{xs}, k_{ys}) + 0 + \frac{1}{2!}\begin{bmatrix} [\phi_{xx}(k_x,k_y)](k_x - k_{xs})^2 \\ +2[\phi_{xy}(k_x,k_y)](k_x - k_{xs})(k_y - k_{ys}) \\ + [\phi_{yy}(k_x,k_y)](k_y - k_{ys})^2 \end{bmatrix}$$

where the partial derivatives are given in shorthand notation and evaluated at the stationary point. An approximation to the integration is given below; here the amplitude terms have been expanded to include only the first term of the Taylor series and the phase terms include the first two terms.

$$\int_{-\infty}^{\infty}\int_{-\infty}^{\infty} g_1(k_y) e^{-jr_o\left(k_x \sin\theta_o \cos\phi_o + k_y \sin\theta_o \sin\phi_o + \sqrt{k^2-k_x^2-k_y^2}\cos\theta_o\right)} dk_x dk_y$$

$$\cong g_1(k_{ys}) e^{-j\phi(k_{xs},k_{ys})r_o} \int_{-\infty}^{\infty}\int_{-\infty}^{\infty} \left\{ \begin{array}{l} e^{\frac{jr_o\cos\theta_o}{2\sqrt{k^2-k_{xs}^2-k_{ys}^2}}\left[1+\frac{k_{xs}^2}{\left(k^2-k_{xs}^2-k_{ys}^2\right)}\right](k_x-k_{xs})^2} \\ \cdot e^{\frac{jr_o\cos\theta_o}{2\sqrt{k^2-k_{xs}^2-k_{ys}^2}}\frac{2k_{xs}k_{ys}}{\left(k^2-k_{xs}^2-k_{ys}^2\right)}(k_x-k_{xs})(k_y-k_{ys})} \\ \cdot e^{\frac{jr_o\cos\theta_o}{2\sqrt{k^2-k_{xs}^2-k_{ys}^2}}\left[1+\frac{k_{ys}^2}{\left(k^2-k_{xs}^2-k_{ys}^2\right)}\right](k_y-k_{ys})^2} \end{array} \right\} dk_x dk_y$$

Equation 2.4-14

Substituting for the stationary points and simplifying, this approximation to the integral can be written

$$\cong g_1(k_{ys}) e^{-jkr_o} \int_{-\infty}^{\infty}\int_{-\infty}^{\infty} \left\{ \begin{array}{l} e^{\frac{jr_o}{2k}\left[1+\frac{k^2\sin^2\theta_o\cos^2\phi_o}{k^2\cos^2\theta_o}\right](k_x-k_{xs})^2} \\ \cdot e^{\frac{jr_o}{2k}\frac{2k^2\sin^2\theta_o\sin\phi_o\cos\phi_o}{k^2\cos^2\theta_o}(k_x-k_{xs})(k_y-k_{ys})} \\ \cdot e^{\frac{jr_o}{2k}\left[1+\frac{k^2\sin^2\theta_o\sin^2\phi_o}{k^2\cos^2\theta_o}\right](k_y-k_{ys})^2} \end{array} \right\} dk_x dk_y$$

where $\left(k^2-k_{xs}^2-k_{ys}^2\right)=k^2\cos^2\theta_o$

Equation 2.4-15

Note if we let $k_1 = (k_x - k_{xs}), k_2 = (k_y - k_{ys})$, the phase may be written in the following matrix form:

$$K^T \overline{\overline{\Phi}} K = \begin{bmatrix} k_1 & k_2 \end{bmatrix} \begin{bmatrix} \frac{r_o}{2k}\left[1 + \tan^2\theta_o \cos^2\phi_o\right] & \frac{r_o}{2k}\tan^2\theta_o \cos\phi_o \sin\phi_o \\ \frac{r_o}{2k}\tan^2\theta_o \cos\phi_o \sin\phi_o & \frac{r_o}{2k}\left[1 + \tan^2\theta_o \sin^2\phi_o\right] \end{bmatrix} \begin{bmatrix} k_1 \\ k_2 \end{bmatrix}$$

Equation 2.4-16

Hence, if we diagonalize the matrix, Φ, using the matrix of eigenvectors, $\overline{\overline{P}}$, we find that we map from the vector $K = \begin{bmatrix} k_1 & k_2 \end{bmatrix}$, to $\tilde{K} = \begin{bmatrix} \tilde{k}_1 & \tilde{k}_2 \end{bmatrix}$ as follows:

$$\tilde{K} = T\,K \text{ and } K^T \overline{\overline{\Phi}} K \Rightarrow K^T\left[T^T \overline{\overline{\Phi}} T\right] K = \tilde{K}^T \overline{\overline{\Lambda}} \tilde{K}$$
$$\text{where } \overline{\overline{\Lambda}} = \begin{bmatrix} \lambda_1^2 & 0 \\ 0 & \lambda_1^2 \end{bmatrix} \text{ (matrix of transformed eigenvalues)}$$

Consequently, the integral becomes (after expanding the argument of the exponent from its matrix form)

$$\int_{-\infty}^{\infty}\int_{-\infty}^{\infty} g_1(k_y) e^{-jr_o\left(k_x \sin\theta_o \cos\phi_o + k_y \sin\theta_o \sin\phi_o + \sqrt{k^2 - k_x^2 - k_y^2}\cos\theta_o\right)} dk_x dk_y$$

$$\cong g_1(k_{ys}) e^{-jkr_o} \int_{-\infty}^{\infty}\int_{-\infty}^{\infty} e^{-j\frac{r_o}{2k}\left[\lambda_1^2 \tilde{k}_1^2 + \lambda_2^2 \tilde{k}_2^2\right]} \left|\frac{\partial(dk_x, dk_y)}{\partial(d\tilde{k}_1, d\tilde{k}_2)}\right| d\tilde{k}_1 d\tilde{k}_2$$

where the Jacobian transformation matrix is given by

$$\overline{\overline{J}} = \frac{\partial(dk_x, dk_y)}{\partial(dk_1, dk_2)} = \begin{vmatrix} \frac{\partial k_x}{\partial k_1} & \frac{\partial k_y}{\partial k_1} \\ \frac{\partial k_x}{\partial k_2} & \frac{\partial k_y}{\partial k_2} \end{vmatrix} = |T| = 1$$

hence, using a result from contour integration,

$$\int_{-\infty}^{\infty}\int_{-\infty}^{\infty} e^{-j\frac{r_o}{2k}\left[\lambda_1^2\tilde{k}_1^2+\lambda_2^2\tilde{k}_2^2\right]} d\tilde{k}_1 d\tilde{k}_2 \cong j\frac{2\pi}{\sqrt{\lambda_1^2\lambda_2^2}} \cong j\frac{2\pi}{\sqrt{\left|\overline{\overline{\Lambda}}\right|}}$$

but since $\left|\overline{\overline{\Lambda}}\right| = \left|T^T\overline{\overline{\Phi}}T\right| = \left|T^T\right|\left|\overline{\overline{\Phi}}\right|\left|T\right| = \left|\overline{\overline{\Phi}}\right|$

$$\int_{-\infty}^{\infty}\int_{-\infty}^{\infty} e^{-j\frac{r_o}{2k}\left[\lambda_1^2\tilde{k}_1^2+\lambda_2^2\tilde{k}_2^2\right]} d\tilde{k}_1 d\tilde{k}_2 \cong j\frac{2\pi}{\sqrt{\lambda_1^2\lambda_2^2}} = j\frac{2\pi}{\sqrt{\left|\overline{\overline{\Phi}}\right|}} \cong j\frac{2\pi}{\sqrt{\phi_{xx}\phi_{yy}-\phi_{xy}^2}}$$

$$\cong j2\pi\frac{2k\cos\theta_o}{r_o} = j4\pi\frac{k\cos\theta_o}{r_o}$$

where

$$\phi_{xx}\phi_{yy}-\phi_{xy}^2 = \frac{r_o^2}{4k^2}\left(\left[1+\frac{k_{xs}^2}{\left(k^2-k_{xs}^2-k_{ys}^2\right)}\right]\left[1+\frac{k_{ys}^2}{\left(k^2-k_{xs}^2-k_{ys}^2\right)}\right]-\frac{k_{xs}^2k_{ys}^2}{\left(k^2-k_{xs}^2-k_{ys}^2\right)^2}\right)$$

$$= \frac{r_o^2}{4k^2}\left(1+\frac{\left(k_{xs}^2+k_{ys}^2\right)}{\left(k^2-k_{xs}^2-k_{ys}^2\right)}\right) = \frac{r_o^2}{4k^2}\left(\frac{k^2}{\left(k^2-k_{xs}^2-k_{ys}^2\right)}\right) = \frac{r_o^2}{4k^2\cos^2\theta_o}$$

so that the first integral is evaluated as

$$\int_{-\infty}^{\infty}\int_{-\infty}^{\infty} g_1(k_y) e^{-jr_o\left(k_x\sin\theta_o\cos\phi_o+k_y\sin\theta_o\sin\phi_o+\sqrt{k^2-k_x^2-k_y^2}\cos\theta_o\right)} dk_x dk_y$$

$$\cong j4\pi\frac{k\cos\theta_o}{r_o} g_1(k_{ys}) e^{-jkr_o}$$

Next we evaluate the second integral (rearranged)

$$\int_{-\infty}^{\infty}\int_{-\infty}^{\infty} e^{-\frac{\left(k_x^2+k_y^2\right)\alpha^2}{4}} g(k_y)\, e^{-jk_x x_o-jk_y y_o-jk_y h_c} e^{+j\sqrt{k^2-k_x^2-k_y^2}\,z_o} dk_x dk_y$$

Equation 2.4-17

Next we find the stationary point

$$\frac{\partial\left(k_x \sin\theta_o \cos\phi_o + k_y\left(\sin\theta_o \sin\phi_o + \frac{h_c}{r_o}\right) + \sqrt{k^2 - k_x^2 - k_y^2}\cos\theta_o\right)}{\partial k_x} = 0$$

$$\Rightarrow \quad \sin\theta_o \cos\phi_o \;=\; \frac{k_x \cos\theta_o}{\sqrt{k^2 - k_x^2 - k_y^2}}$$

$$\text{squaring} \;\Rightarrow\; \sin^2\theta_o \cos^2\phi_o \;=\; \frac{k_{xs}^2 \cos^2\theta_o}{k^2 - k_{xs}^2 - k_{ys}^2}$$

Equation 2.4-18

$$\left[\frac{\partial\left(k_x \sin\theta_o \cos\phi_o + k_y\left(\sin\theta_o \sin\phi_o + \frac{h_c}{r_o}\right) + \sqrt{k^2 - k_x^2 - k_y^2}\cos\theta_o\right)}{\partial k_y}\right]_{(k_{xs}, k_{ys})} = 0$$

$$\Rightarrow \quad \sin\theta_o \sin\phi_o + \frac{h_c}{r_o} \;=\; \frac{k_{ys} \cos\theta_o}{\sqrt{k^2 - k_{xs}^2 - k_{ys}^2}}$$

$$\text{squaring} \;\Rightarrow\; \sin^2\theta_o \sin^2\phi_o + 2\frac{h_c}{r_o}\sin\theta_o \sin\phi_o + \left(\frac{h_c}{r_o}\right)^2 = \frac{k_{ys}^2 \cos^2\theta_o}{k^2 - k_{xs}^2 - k_{ys}^2}$$

Equation 2.4-19

adding the squares from Equation 2.4-18 and Equation 2.4-19

$$\sin^2\theta_o + \left[2\frac{h_c}{r_o}\sin\theta_o \sin\phi_o + \left(\frac{h_c}{r_o}\right)^2\right] = \frac{\cos^2\theta_o}{\left(k^2 - k_{xs}^2 - k_{ys}^2\right)}\left(k_{xs}^2 + k_{ys}^2\right)$$

$$\Rightarrow k^2\left(\sin^2\theta_o + 2\frac{h_c}{r_o}\sin\theta_o \sin\phi_o + \left(\frac{h_c}{r_o}\right)^2\right) = \left(k_{xs}^2 + k_{ys}^2\right)\left[1 + 2\frac{h_c}{r_o}\sin\theta_o \sin\phi_o + \left(\frac{h_c}{r_o}\right)^2\right]$$

$$\Rightarrow \left(k_{xs}^2 + k_{ys}^2\right) = \frac{k^2\left(\sin^2\theta_o + 2\frac{h_c}{r_o}\sin\theta_o \sin\phi_o + \left(\frac{h_c}{r_o}\right)^2\right)}{\left[1 + 2\frac{h_c}{r_o}\sin\theta_o \sin\phi_o + \left(\frac{h_c}{r_o}\right)^2\right]}$$

using this relationship, we may now solve for the stationary points

$$k_{xs}^2 = \frac{\sin^2\theta_o \cos^2\phi_o}{\cos^2\theta_o}\left[k^2 - \left(k_{xs}^2 + k_{ys}^2\right)\right]$$

$$k_{ys}^2 = \left[\sin\theta_o \sin\phi_o + \left(\frac{h_c}{r_o}\right)\right]^2 \frac{\left[k^2 - \left(k_{xs}^2 + k_{ys}^2\right)\right]}{\cos^2\theta_o}$$

Since the observation distance is growing large, we expect the third term to become negligible (with the exception of $h_c \to \infty$, free space). The remainder of the development is essentially the same as the previous since the partial derivatives are the same. Restating the approximation to the integration where the amplitude terms have been expanded to include only the first term of the Taylor series and the phase terms include the first two terms.

$$\int_{-\infty}^{\infty}\int_{-\infty}^{\infty} e^{-\frac{\left(k_{xs}^2+k_{ys}^2\right)\alpha^2}{4} - j\phi\left(k_{xs},k_{ys}\right)r_o} \left\{ \begin{array}{l} e^{\frac{j r_o \cos\theta_o}{2\sqrt{k^2-k_{xs}^2-k_{ys}^2}}\left[1+\frac{k_{xs}^2}{\left(k^2-k_{xs}^2-k_{ys}^2\right)}\right]\left(k_x-k_{xs}\right)^2} \\ \cdot\, e^{\frac{j r_o \cos\theta_o}{2\sqrt{k^2-k_{xs}^2-k_{ys}^2}}\frac{2k_{xs}k_{ys}}{\left(k^2-k_{xs}^2-k_{ys}^2\right)}\left(k_x-k_{xs}\right)\left(k_y-k_{ys}\right)} \\ \cdot\, e^{\frac{j r_o \cos\theta_o}{2\sqrt{k^2-k_{xs}^2-k_{ys}^2}}\left[1+\frac{k_{ys}^2}{\left(k^2-k_{xs}^2-k_{ys}^2\right)}\right]\left(k_y-k_{ys}\right)^2} \end{array} \right\} dk_x dk_y$$

Consequently, the integral becomes (after expanding the argument of the exponent from its matrix form)

$$\int_{-\infty}^{\infty}\int_{-\infty}^{\infty} g_2\left(k_y\right) e^{-jk_x x_o - jk_y y_o - jk_y h_c} e^{+j\sqrt{k^2-k_x^2-k_y^2}\, z_o}\, dk_x dk_y$$

$$\cong g_2(k_{ys}) e^{-j\phi(k_{xs},k_{ys})r_o} j \frac{2\pi}{\sqrt{\phi_{xx}\phi_{yy} - \phi_{xy}^2}}$$

$$\cong j4\pi g_2(k_{ys}) \frac{(k^2 - k_{xs}^2 - k_{ys}^2)^{1/2}}{r_o} e^{-j\phi(k_{xs},k_{ys})r_o}$$

where $\phi(k_x, k_y) = k_x \sin\theta_o \cos\phi_o + k_y \left(\sin\theta_o \sin\phi_o + \frac{h_c}{r_o} \right) + \sqrt{k^2 - k_x^2 - k_y^2} \cos\theta_o$

2.5 *Pulse Propagation Across a Randomly Rough Knife Edge*

In this section, the frequency correlation of a pulsed waveform transmitted across a knife edge obstacle is examined. In turn, the frequency correlation will yield information about the average power in the transmitted pulse waveform. This will be accomplished using the two-frequency mutual coherence function as described in Ishimaru [1997].

In order to construct the response of the medium to a scattered pulse, the correlation of the output-scattered fields must be derived. Writing the input signal as

$$e_i(t) = \mathrm{Re}\left\{ E_i(t)\, e^{j\omega_0 t} \right\}$$

where $E_i(t)$ is the complex amplitude of the signal. If we write the incident pulse as an inverse Fourier transform, the complex amplitude, E(t), can be written

$$E_i(t) = \frac{1}{2\pi} \int_{-\infty}^{\infty} d\omega\, \tilde{E}_i(\omega)\, e^{j\omega t}$$

and the input spectrum becomes (for real signals)

$$\frac{1}{2}\left[\tilde{E}_i(\omega - \omega_0) + \tilde{E}_i^*(-\omega - \omega_0) \right] = \frac{1}{2}\left[\tilde{E}_i(\omega - \omega_0) + \tilde{E}_i(\omega + \omega_0) \right]$$

Then the transmitted pulse can be written as the time-domain, incident pulse convolved with the time and frequency dependent impulse response of the knife edge obstacle, or equivalently, in the frequency domain, the output signal becomes [Ishimaru, 1997],

$$E(t) = \frac{1}{2\pi}\int_{-\infty}^{\infty} d\omega \, H(\omega_0 + \omega)\tilde{E}_i(\omega)\, e^{j\omega t}$$

Here the Fourier transform of the complex amplitude, E, is written as $\tilde{E}$. A general expression for the correlation of the transmitted field, or the total power, is then found in the following time correlated signal,

$$\begin{aligned} C(t_1,t_2) &= \left\langle e(t_1)e^*(t_2)\right\rangle \\ &= \frac{1}{(2\pi)^2}\int_{-\infty}^{\infty} d\omega_1 \int_{-\infty}^{\infty} d\omega_2 \, \tilde{E}_i(\omega_1)\tilde{E}_i^*(\omega_2)\Gamma e^{j(\omega_1 t_1 - \omega_2 t_2)} \end{aligned}$$

Equation 2.5-1

where $\tilde{E}_i(\omega)$ is the complex envelope of the incident wave form at the time harmonic frequency ω and Γ is the *two-frequency mutual coherence function*.

The two-frequency mutual coherence function is the correlation of the time-varying, frequency domain transfer function, H(ω,t), at two different frequencies and two different times [Ishimaru, 1997]

$$\Gamma \equiv \Gamma(\omega_0 + \omega_1, \omega_0 + \omega_2; t_1, t_2) = \left\langle H(\omega_0 + \omega_1, t_1)H^*(\omega_0 + \omega_2, t_2)\right\rangle$$

Equation 2.5-2

Once the two-frequency mutual coherence is constructed, the scattered power density is found when $t_1 = t_2 = t$

$$P(t) = \int_{-\infty}^{\infty} d\omega_1 \int_{-\infty}^{\infty} d\omega_2 \tilde{E}_i(\omega_1)\tilde{E}_i^*(\omega_2)\Gamma(\omega_1, \omega_2)e^{j(\omega_1 - \omega_2)t}$$

Equation 2.5-3

2.5.1 *Two-Frequency Coherence Function for a smooth knife edge*

Since the expression for the rough knife edge is so complicated, the result for the smooth knife edge is a valuable check. Starting with the expression for the transmitted monochromatic field by a smooth knife edge,

$$
\begin{aligned}
P(t) &= \left\langle E(t)E^*(t)\right\rangle \\
&= \int_{-\infty}^{\infty} d\omega_1 \int_{-\infty}^{\infty} d\omega_2\, \vec{K}\cdot\vec{K}^*\, \tilde{E}_i(\omega_1)\tilde{E}_i^*(\omega_2)\, e^{-j(\omega_1-\omega_2)t} \int_{-h_c}^{\infty} du_1 \int_{-h_c}^{\infty} du_2 \\
&\quad\cdot \int_{-\infty}^{\infty} dx_1 \int_{-\infty}^{\infty} dx_2\, e^{-a_1 x_1^2}\, e^{-a_1 y_1^2} e^{-a_2^* x_2^2} e^{-a_2^* y_2^2}
\end{aligned}
$$

where the frequency dependent parameter, a, was previously defined as

$$
a_1 \equiv \left(\frac{1}{\alpha^2} + j\frac{k_1}{d}\right) = \left(\frac{1}{\alpha^2} + j\frac{\omega_{01}}{c_0\, d}\right);\; a_2 \equiv \left(\frac{1}{\alpha^2} - j\frac{k_2}{d}\right) = \left(\frac{1}{\alpha^2} - j\frac{\omega_{02}}{c_0\, d}\right)
$$

$$
\text{for } \omega_{01} = \omega_0 + \omega_1,\; \omega_{02} = \omega_0 + \omega_2
$$

Since all quantities are deterministic, no averaging is required and the spatial integrals are simply a product of separable integrations. Performing these spatial integrations

$$
\begin{aligned}
P(t) &= \left\langle E(t)E^*(t)\right\rangle \\
&= \int_{-\infty}^{\infty} d\omega_1 \int_{-\infty}^{\infty} d\omega_2\, \tilde{E}_i(\omega_1)\tilde{E}_i^*(\omega_2)\, \frac{\omega_{01}\omega_{02}\, e^{-j\frac{\omega_d}{c}(R_1+z_o)}}{2\pi c_0^2\, R_1\, z_o}\, e^{-j\omega_d t} \\
&\quad\cdot \frac{\pi}{4a_1 a_2^*}\, \mathrm{erfc}\left(-h_c\sqrt{a_1}\right) \mathrm{erfc}\left(-h_c\sqrt{a_2^*}\right)
\end{aligned}
$$

$$
\text{for } \omega_d \equiv \omega_{01} - \omega_{02} = \omega_1 - \omega_2
$$

Equation 2.5-4

Substituting for the frequency-dependent parameters

$$P(t) = \int_{-\infty}^{\infty} d\omega_1 \int_{-\infty}^{\infty} d\omega_2\, \tilde{E}_i(\omega_1)\tilde{E}_i^*(\omega_2)\, \frac{\omega_{01}\omega_{02}\, e^{-j\frac{\omega_d}{c}(R_1+z_o)}}{2\pi c^2 R_1 z_o} \frac{\pi e^{j\omega_d t}}{4\left(\frac{1}{\alpha^2}+j\frac{\omega_{01}}{c_0 d}\right)\left(\frac{1}{\alpha^2}-j\frac{\omega_{02}}{c_0 d}\right)}$$

$$\cdot\ \operatorname{erfc}\left(-h_c\sqrt{\left(\frac{1}{\alpha^2}+j\frac{\omega_{01}}{c_0 d}\right)}\right)\operatorname{erfc}\left(-h_c\sqrt{\left(\frac{1}{\alpha^2}-j\frac{\omega_{02}}{c_0 d}\right)}\right)$$

For a *narrow bandwidth* signal or a *large observation distance*, the complementary error function can be approximated by their values evaluated at the carrier frequency, leading to

$$P(t) \cong \int_{-\infty}^{\infty} d\omega_1 \int_{-\infty}^{\infty} d\omega_2\, \tilde{E}_i(\omega_1)\tilde{E}_i^*(\omega_2)\, \frac{\omega_{01}\omega_{02}\, e^{-j\frac{\omega_d}{c}(R_1+z_o)}}{(2\pi)^2 8 c_0^2 R_1 z_o} \frac{e^{j\omega_d t}}{\left(\frac{1}{\alpha^4}+\frac{\omega_{01}\omega_{02}}{c_0^2 d^2}+2j\frac{\omega_{01}-\omega_{02}}{\alpha^2 c_0 d}\right)}$$

$$\cdot\ \operatorname{erfc}\left(-h_c\sqrt{\left(\frac{1}{\alpha^2}+j\frac{\omega_0}{c_0 d}\right)}\right)\operatorname{erfc}\left(-h_c\sqrt{\left(\frac{1}{\alpha^2}-j\frac{\omega_0}{c_0 d}\right)}\right)$$

Changing the frequency integration to sum/difference coordinates

$$\omega_s = \frac{1}{2}(\omega_1+\omega_2), \quad \omega_d = (\omega_1-\omega_2)$$

$$d\omega_1 d\omega_2 = \left|\frac{\partial(\omega_1,\omega_2)}{\partial(\omega_s,\omega_d)}\right| d\omega_s d\omega_d = \begin{vmatrix} 1 & 0.5 \\ 1 & -0.5 \end{vmatrix} d\omega_s d\omega_d = -\, d\omega_s d\omega_d$$

$$\omega_{01} = \omega_0 + \omega_s + \frac{1}{2}\omega_d,\ \omega_{02} = \omega_0 + \omega_s - \frac{1}{2}\omega_d$$

the average power is approximately written for relatively small bandwidths, $\omega_d << \omega_0$, with the narrow band approximation

$$\omega_{01}\omega_{02} = \left[\omega_0^2 + 2\omega_0\omega_s + \omega_s^2 - \frac{1}{4}\omega_d^2\right] \cong \left[\omega_0^2 + 2\omega_0\omega_s\right]$$

$$P(t) \cong \operatorname{erfc}\left(-h_c\sqrt{\left(\frac{1}{\alpha^2}+j\frac{\omega_0}{c_0\,d}\right)}\right)\operatorname{erfc}\left(-h_c\sqrt{\left(\frac{1}{\alpha^2}-j\frac{\omega_0}{c_0\,d}\right)}\right)\int_{-\infty}^{\infty} d\omega_s \int_{-\infty}^{\infty} d\omega_d$$

$$\cdot\frac{1}{(2\pi)^2 8 c_0^2 R_1 z_o}\tilde{E}_i(\omega_s+\frac{1}{2}\omega_d)\tilde{E}_i^*(\omega_s-\frac{1}{2}\omega_d)\frac{\left[\omega_0^2+2\omega_0\omega_s\right]e^{j\omega_d t}\,e^{-j\frac{\omega_d}{c}(R_1+z_o)}}{\left(\frac{1}{\alpha^4}+\frac{\omega_0^2+2\omega_0\omega_s}{c_0^2 d^2}+2j\frac{\omega_d}{\alpha^2 c_0\,d}\right)}$$

Equation 2.5-5

If the incident pulse is assumed Gaussian (infinite in time), then the input signal and its spectrum are written

$$E_i(t)=E_0\;e^{-\frac{t^2}{2b^2}},\;\tilde{E}_i(\omega)=E_0\sqrt{2\pi}b\,e^{-\frac{\omega^2 b^2}{2}}$$

where b is the "pulse width"

Equation 2.5-6

Substituting and rearranging

$$P(t) \cong -\operatorname{erfc}\left(-h_c\sqrt{\left(\frac{1}{\alpha^2}+j\frac{\omega_0}{c_0\,d}\right)}\right)\operatorname{erfc}\left(-h_c\sqrt{\left(\frac{1}{\alpha^2}-j\frac{\omega_0}{c_0\,d}\right)}\right)\frac{E_0^2 b^2 d^2\pi}{8\,\omega_0\,R_1\,z_o}$$

$$\frac{1}{(2\pi)^2}\int_{-\infty}^{\infty} d\omega_d\,e^{-\frac{b^2}{2}\omega_d^2}\,e^{j\omega_d t}\,e^{-j\frac{\omega_d}{c}(R_1+z_o)}\int_{-\infty}^{\infty} d\omega_s\,\frac{e^{-b^2\omega_s^2}\;\left[\omega_0^2+2\omega_0\omega_s\right]}{\left(\omega_s+\frac{\omega_0}{2}+\frac{c_0^2\,d^2}{2\omega_0\alpha^4}+j\frac{\omega_d c_0\,d}{\omega_0\alpha^2}\right)}$$

Equation 2.5-7

The sum-frequency integration is easily accomplished using Laplace's Method (for the narrow band assumption)

$$P(t) \cong -\operatorname{erfc}\left(-h_c\sqrt{\left(\frac{1}{\alpha^2}+j\frac{\omega_0}{c_0\,d}\right)}\right)\operatorname{erfc}\left(-h_c\sqrt{\left(\frac{1}{\alpha^2}-j\frac{\omega_0}{c_0\,d}\right)}\right)\frac{E_0^2 b^2 d^2\,\pi}{8\omega_0\,R_1\,z_o}$$

$$\frac{1}{(2\pi)^2}\int_{-\infty}^{\infty} d\omega_d\,e^{-\frac{b^2}{2}\omega_d^2}\,e^{j\omega_d t}\,e^{-j\frac{\omega_d}{c}(R_1+z_o)}\frac{\omega_0^2}{\left(\frac{\omega_0}{2}+\frac{c_0^2\,d^2}{2\omega_0\alpha^4}+j\frac{\omega_d c_0\,d}{\omega_0\alpha^2}\right)}\frac{\sqrt{\pi}}{b}$$

Equation 2.5-8

This approximation has been checked for the values used in the examples for the LOS power calculations in Section 2.3 for pulse widths down to 10 nanoseconds for a 1 GHz carrier (or a 10% bandwidth in all cases 10MHz – 10GHz). Rearranging the difference-frequency integral,

$$P(t) \cong \mathrm{erfc}\left(-h_c \sqrt{\left(\frac{1}{\alpha^2} + j\frac{\omega_0}{c_0\, d} \right)} \right) \mathrm{erfc}\left(-h_c \sqrt{\left(\frac{1}{\alpha^2} - j\frac{\omega_0}{c_0\, d} \right)} \right) \frac{E_0^2\, \omega_0^2\, b\, d\alpha^2 \pi\sqrt{\pi}}{8 c_0\, R_1\, z_o (2\pi)^2}$$

$$\cdot \int_{-\infty}^{\infty} d\omega_d \frac{e^{-\frac{b^2}{2}\omega_d^2}\, e^{j\omega_d t}\, e^{-j\frac{\omega_d}{c}(R_1+z_o)}}{j\omega_d + \left(\frac{\omega_0^2\alpha^2}{2c_0\, d} + \frac{c_0\, d}{2\alpha^2} \right)}$$

Equation 2.5-9

If the convolutional operator is denoted, ⊗, then the integral is the inverse transform of a product (with a delay factor), which is a convolution of the corresponding time domain functions

$$P(t) \cong \mathrm{erfc}\left(-h_c \sqrt{\left(\frac{1}{\alpha^2} + j\frac{\omega_0}{c_0\, d} \right)} \right) \mathrm{erfc}\left(-h_c \sqrt{\left(\frac{1}{\alpha^2} - j\frac{\omega_0}{c_0\, d} \right)} \right) \frac{E_0^2\, \omega_0^2\, b\, d\alpha^2 \pi\sqrt{\pi}}{8(2\pi)^2\, c_0\, R_1\, z_o}$$

$$\cdot \left[e^{-\eta t}\, u(t) \right] \otimes \left[\frac{1}{b\sqrt{2\pi}} e^{-\frac{(t-t_o)^2}{2b^2}} \right]$$

Equation 2.5-10

$$\text{where } \eta = \left(\frac{\omega_0^2\alpha^2}{2c_0\, d} + \frac{c_0 d}{2\alpha^2} \right)$$

$$t_0 = \left(\frac{R_1 + z_o}{c_0} \right)$$

It is evident that as the factor, η, decreases, the pulse will distort for a smooth knife edge since the transmitted pulse is a convolution of the original with this decaying exponential.

Consequently, as the decay time of the exponential increases, the transmitted pulse width increases due to the convolution – pulse spread. Since η is very large, the exponential function is nearly a delta-function; this indicates that the pole due to the difference frequency could have been neglected. The constant delay term, t_0, is simply the time of passage, due to the finite speed of light, from the knife edge to the observation point.

2.5.2 *Two-Frequency Coherence Function for a Rough Knife Edge*

After a change of variables to bring the fluctuating portion of the knife edge roughness into the integral as was done in Section 2.2, the frequency correlation of the pulse transmitted across a rough knife edge is given by

$$
\begin{aligned}
P(t) &= \left\langle E(t) E^*(t) \right\rangle \\
&= \int_{-\infty}^{\infty} d\omega_1 \int_{-\infty}^{\infty} d\omega_2\, \vec{K}\cdot\vec{K}^*\, \tilde{E}_i(\omega_1)\tilde{E}_i^*(\omega_2)\, e^{-j(\omega_1-\omega_2)t} \int_{-h_c}^{\infty} du_1 \int_{-h_c}^{\infty} du_2 \\
&\quad \cdot \int_{-\infty}^{\infty} dx_1 \int_{-\infty}^{\infty} dx_2 \left\langle e^{-a_1\left(x_1^2+[u_1-\delta h_{c1}]^2\right)} e^{-a_2^*\left(x_2^2+[u_2-\delta h_{c2}]^2\right)} \right\rangle
\end{aligned}
$$

Equation 2.5-11

Through a comparison with Equation 2.5-3, the two-frequency mutual coherence function for the pulse propagation across the knife edge is seen to be

$$
\begin{aligned}
\Gamma(\omega_1,\omega_2) &= \left\langle H(\omega_1; x_o, y_o, z_0)\cdot H^*(\omega_2; x_o, y_o, z_0) \right\rangle \\
&= \frac{\omega_{01}\omega_{02}\, e^{-j\frac{\omega_d}{c}(R_1+z_o)}}{4\pi c^2 R_1 z_o} \int_{-\infty}^{\infty}\int_{-\infty}^{\infty}\int_{-\infty}^{\infty}\int_{-\infty}^{\infty}\int_{-h_c}^{\infty}\int_{-h_c}^{\infty} e^{-a_1\left(x_1^2+[u_1-\delta h_{c1}]^2\right)} \\
&\quad \cdot e^{-a_2^*\left(x_2^2+[u_2-\delta h_{c2}]^2\right)} p(\delta h_1, \delta h_{c2})\, du_1 du_2\, dx_1 dx_2\, d\delta h_{c1}\, d\delta h_{c2}
\end{aligned}
$$

given the joint pdf for the knife edge heights, $p(\delta h_1, \delta h_{c2})$. Again, assuming Gaussian statistics, and changing the x-integration into difference and sum coordinates,

$$x_s = \frac{1}{2}(x_1 + x_2), \quad x_d = (x_1 - x_2)$$

$$dx_1 dx_2 = \left|\frac{\partial(x_1, x_2)}{\partial(x_s, x_d)}\right| dx_s dx_d = \begin{vmatrix} 1 & 0.5 \\ 1 & -0.5 \end{vmatrix} dx_s dx_d = -dx_s dx_d$$

$$x_1 = x_s + \frac{1}{2}x_d, \; x_2 = x_s - \frac{1}{2}x_d$$

the indicated average may be accomplished in closed form, yielding the following unwieldy result, which includes the correlation function $C(x_d)$.

$$\Gamma(\omega_1, \omega_2) = \left\langle H(\omega_1; x_o, y_o, z_0) \cdot H^*(\omega_2; x_o, y_o, z_0)\right\rangle$$

$$= \frac{\omega_{01}\omega_{02}\, e^{-j\frac{\omega_d}{c}(R_1 + z_o)}}{4\pi c^2 R_1 z_o} \sqrt{\frac{\pi}{D(x_d)}} \int_{-\infty}^{\infty} dx_d \int_{-\infty}^{\infty} dx_s\, e^{-a_1\left(x_s + \frac{1}{2}x_d\right)^2} e^{-a_2^*\left(x_s - \frac{1}{2}x_d\right)^2}$$

$$\cdot \int_{-h_c}^{\infty} du_2 \int_{-h_c}^{\infty} du_1 \, \exp\left\{-\frac{1}{D(x_d)}\left(a_1 u_1^2\left(2\sigma^2 a_2^* + 1\right) + a_2^* u_1^2\left(2\sigma^2 a_1 + 1\right) - 4a_1 a_2^* C(x_d) u_1 u_2\right)\right\}$$

$$\text{where } D(x_d) \equiv 4\left(\sigma^4 - C^2(x_d)\right) a_1 a_2^* + 2\sigma^2\left(a_1 + a_2^*\right) + 1$$

Equation 2.5-12

performing the x_s integration,

$$\Gamma(\omega_1, \omega_2) = \frac{\omega_{01}\omega_{02}\, e^{-j\frac{\omega_d}{c}(R_1 + z_o)}}{4\pi c^2 R_1 z_o} \sqrt{\frac{\pi}{\left(a_1 + a_2^*\right) D(x_d)}} \int_{-\infty}^{\infty} dx_d \exp\left\{-\frac{1}{2}\frac{a_1 a_2^*}{\left(a_1 + a_2^*\right)} x_d^{\,2}\right\}$$

$$\cdot \int_{-h_c}^{\infty} du_2 \int_{-h_c}^{\infty} du_1 \, \exp\left\{-\frac{1}{D(x_d)}\left[a_1 u_1^2\left(2\sigma^2 a_2^* + 1\right) + a_2^* u_1^2\left(2\sigma^2 a_1 + 1\right) - 4a_1 a_2^* C(x_d) u_1 u_2\right]\right\}$$

Equation 2.5-13

Another change of variables in order to change the limits, $y_{1,2} = u_{1,2} + h_c$ yields

$$\Gamma(\omega_1,\omega_2) = \frac{\omega_{01}\omega_{02}\, e^{-j\frac{\omega_d}{c}(R_1+z_o)}}{4\pi c^2 R_1 z_o}$$

$$\cdot \int_{-\infty}^{\infty} dx_d \sqrt{\frac{\pi}{\left(a_1+a_2^*\right)\, D(x_d)}}\, \exp\left\{-\frac{1}{2}\frac{a_1 a_2^*}{\left(a_1+a_2^*\right)} x_d{}^2 - a_1\left(\frac{h_c^2\left(2\sigma^2 a_2^*+1\right)}{D(x_d)}\right)\right\}$$

$$\cdot \int_0^{\infty} dy_2 \exp\left\{-\frac{1}{D(x_d)}\left[a_2^*(y_2-h_c)^2\left(2\sigma^2 a_1+1\right) - 4a_1 a_2^* h_c C(x_d)(y_2-h_c)\right]\right\}$$

$$\cdot \int_0^{\infty} dy_1 \exp\left\{-\frac{1}{D(x_d)}\left[a_1 y_1^2\left(2\sigma^2 a_2^*+1\right) + y_1\left(2a_1 h_c\left(2\sigma^2 a_1+1\right) + 4a_1 a_2^* C(x_d)(y_2-h_c)\right)\right]\right\}$$

Equation 2.5-14

The y_1 integration may be evaluated to yield

$$\Gamma(\omega_1,\omega_2) = \frac{\omega_{01}\omega_{02}\, e^{-j\frac{\omega_d}{c}(R_1+z_o)}}{8\pi c^2 R_1 z_o} \int_{-\infty}^{\infty} dx_d \sqrt{\frac{\pi^2}{a_1\left(a_1+a_2^*\right)\left(2\sigma^2 a_2^*+1\right)}}\, \exp\left\{-\frac{1}{2}\frac{a_1 a_2^*}{\left(a_1+a_2^*\right)} x_d{}^2\right\}$$

$$\cdot \int_0^{\infty} dy_2 \exp\left\{-\frac{a_2^*}{\left(2\sigma^2 a_2^*+1\right)}(y_2-h_c)^2\right\} \operatorname{erfc}\left\{-\sqrt{a_1}\left[\frac{h_c\left(2\sigma^2 a_2^*+1\right) + 2a_2^* C(x_d)(y_2-h_c)}{\sqrt{\left(2\sigma^2 a_2^*+1\right) D(x_d)}}\right]\right\}$$

Equation 2.5-15

Assuming a Gaussian correlation function,

$$C(\Delta x) = \sigma^2\, e^{-\frac{\Delta x^2}{l_x^2}}$$

The approximation that the erfc(*) is relatively constant over the integration range remains true for large correlation lengths. Hence, the correlation function can be evaluated at $x_d = 0$ and the x_d integration can be performed, yielding

$$\Gamma(\omega_1,\omega_2) = \frac{\omega_{01}\omega_{02}\, e^{-j\frac{\omega_d}{c}(R_1+z_o)}}{8c^2 R_1 z_o a_1}\sqrt{\frac{2}{a_2^*\left(2\sigma^2 a_2^*+1\right)}}\int_0^{\infty} dy_2 \exp\left\{-\frac{a_2^*}{\left(2\sigma^2 a_2^*+1\right)}\,(y_2-h_c)^2\right\}$$

$$\cdot\operatorname{erfc}\left\{-\sqrt{a_1}\left[\frac{h_c\left(2\sigma^2 a_2^*+1\right)+2a_2^* C(0)(y_2-h_c)}{\sqrt{\left(2\sigma^2 a_2^*+1\right)\left(2\sigma^2\left(a_1+a_2^*\right)+1\right)}}\right]\right\}$$

Equation 2.5-16

Since the y_2 integration may not be evaluated at this point, we introduce the expression for the power density as a function of time (in sum and difference coordinates), and the pulse spectrum (Equation 2.5-6). Simplifying, using a narrow band approximation

$$P(t) = \left\langle E(t)E^*(t)\right\rangle$$

$$= \int_{-\infty}^{\infty} d\omega_d \int_{-\infty}^{\infty} d\omega_s\, 2\pi b^2 e^{-b^2\omega_s^2-\frac{b^2}{2}\omega_d^2}\ \frac{\left[\omega_0^2+2\omega_0\omega_s\right]e^{-j\frac{\omega_d}{c}(R_1+z_o)}}{8c^2 R_1 z_o a_0}\ e^{j\omega_d t}$$

$$\sqrt{\frac{2}{a_0^*\left(2\sigma^2 a_0^*+1\right)}}\int_0^{\infty} dy_2 \exp\left\{-\frac{a_0^*(y_2-h_c)^2}{\left(2\sigma^2 a_0^*+1\right)}\right\}$$

$$\cdot\operatorname{erfc}\left\{-\sqrt{a_0}\left[\frac{2\sigma^2 a_0^* y_2+h_c}{\sqrt{\left(2\sigma^2 a_0^*+1\right)\left(2\sigma^2\left(a_1+a_2^*\right)+1\right)}}\right]\right\}$$

Equation 2.5-17

$$a_0 \equiv \left(\frac{1}{\alpha^2}+j\frac{\omega_0}{c_0 d}\right)$$

where $\omega_d \equiv \omega_1-\omega_2 = \omega_{01}-\omega_{02}\,;\ \ \omega_s \equiv \frac{1}{2}(\omega_1+\omega_2)$

$$\omega_{01}\omega_{02} = \left[\omega_0^2+2\omega_0\omega_s+\omega_s^2-\frac{1}{4}\omega_d^2\right] \cong \left[\omega_0^2+2\omega_0\omega_s\right]$$

under the narrow band assumption, the sum-frequency integral is performed,

$$P(t) = \left\langle E(t)E^*(t) \right\rangle$$

$$= \frac{\pi b \omega_0^2}{4c^2 R_1 z_o a_0} \sqrt{\frac{2\pi}{a_0^*\left(2\sigma^2 a_0^* + 1\right)}} \int_{-\infty}^{\infty} d\omega_d \; e^{j\omega_d t} e^{-\frac{b^2}{2}\omega_d^2} e^{-j\frac{\omega_d}{c}(R_1 + z_o)}$$

$$\cdot \int_0^{\infty} dy_2 \exp\left\{ -\frac{a_0^* (y_2 - h_c)^2}{\left(2\sigma^2 a_0^* + 1\right)} \right\} \operatorname{erfc}\left\{ -\sqrt{a_0} \left[\frac{2\sigma^2 a_0^* y_2 + h_c}{\sqrt{\left(2\sigma^2 a_0^* + 1\right)\left(2\sigma^2\left(a_1 + a_2^*\right) + 1\right)}} \right] \right\}$$

Equation 2.5-18

Due to the limiting, narrow bandwidth approximation, the pulse response is the product of two independent integrals: one in the difference frequency and the other in the y_2 variable. The difference frequency integration yields a replica of pulsed waveform that is simply time-shifted. The y_2 integration has been derived previously in Section 2.2.2, when the continuous wave power was calculated.

$$P(t) = \left\langle E(t)E^*(t) \right\rangle$$

$$= \frac{\pi \omega_0^2}{4c^2 R_1 z_o a_0} \sqrt{\frac{1}{a_0^*\left(2\sigma^2 a_0^* + 1\right)}} \, e^{-\frac{(t - t_0)^2}{2b^2}}$$

$$\cdot \int_0^{\infty} dy_2 \exp\left\{ -\frac{a_0^* (y_2 - h_c)^2}{\left(2\sigma^2 a_0^* + 1\right)} \right\} \operatorname{erfc}\left\{ -\sqrt{a_0} \left[\frac{2\sigma^2 a_0^* y_2 + h_c}{\sqrt{\left(2\sigma^2 a_0^* + 1\right)\left(2\sigma^2\left(a_1 + a_2^*\right) + 1\right)}} \right] \right\}$$

Equation 2.5-19

where $\quad t_0 = \left(\frac{R_1 + z_o}{c_0} \right)$

Hence, the transmitted pulse, in the narrow-band approximation, is simply the time-delayed replica of the incident pulse weighted by the amplitude and phase effects of the rough knife edge. As an example, Figure 2.5-1 shows the received pulse shape for a transmitted Gaussian pulse incident on a rough edge (1 meter roughness) for different mean displacements of the knife edge from the LOS. The received pulse is simply an amplitude weighted replica of the incident pulse due to all the approximations (narrowband, etc.). The weights are identical to the curves found for the power received in Section 2.3.

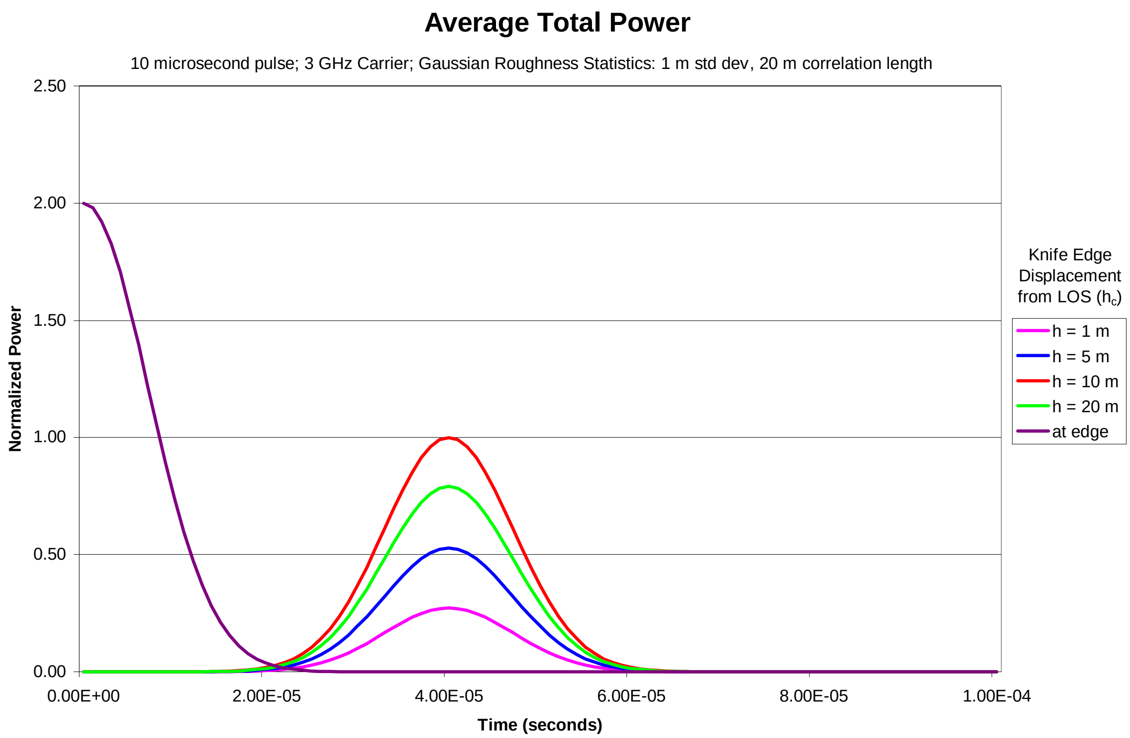

Figure 2.5-1: Received pulse shape for 1 meter roughness

Figure 2.5-2 shows a similar result as the previous figure, however, in this figure, the roughness is greater and therefore, the amplitudes are lower. Again, the weights of the curves are determined to be those found simply for the received power in Section 2.3.

When the pulse shape is considered to be the superposition of the direct and the scattered wave, one may expect that a significant dispersion effect will be present since the direct path can be much less than the path from the transmitter to knife edge to receiver. However, due to the narrow bandwidth assumption, dispersion will only become significant when the electrical path length is significant with respect to the pulse width. For a 20-meter separation from the LOS path to the edge, the dispersion effect will only become significant for pulse lengths on the order of nanoseconds, which have been discounted by the narrow band assumption. We may try to observe the dispersion effect as we move the edge farther from the LOS path. However, as the edge is removed away from the LOS path, the scattered wave becomes less significant, due to the beam taper; consequently, the dispersion effect will not be appreciable.

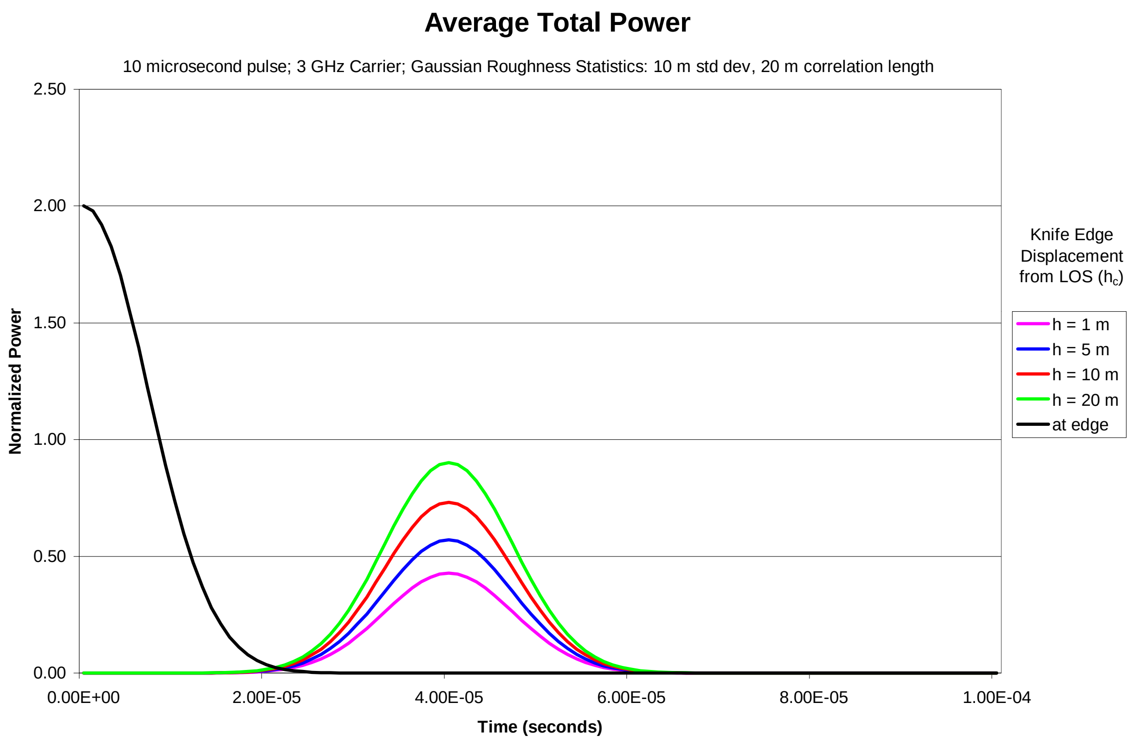

Figure 2.5-2: Received pulse shape for 10 meter roughness

2.6 Conclusions

We have presented a method for predicting the total field beyond a rough knife edge. Using a spectral approach in combination with the paraxial approximation and the Kirchhoff approximation, we can predict the field, total power and its coherent and incoherent components in the line-of-sight direction beyond the obstruction. In this chapter we have presented the particular case for a Gaussian roughness on the knife edge. The coherent field was given in terms of the complementary error function and the total power is given by an approximate expression; note that this expression was seen to be valid only for large, but practical, correlation lengths. The knife edge obstruction creates a total field that is a superposition of an incident field, $\vec{E}_i$, and the edge-diffracted field, $\vec{E}_d$. We note that the incident field is the field in the absence of the knife edge and the diffracted field can be separated into two components: a mean and a fluctuating portion,

$$\vec{E}_d = \langle \vec{E}_d \rangle + \delta \vec{E}_d$$

The mean diffraction field is a result of an effectively smooth knife edge; hence, this term is present even in the absence of roughness on the edge. The fluctuating portion results from the roughness on the knife edge. Hence, for small relative roughness, the diffracted field is equivalent to the mean diffracted field.

$$\vec{E}_d \approx \langle \vec{E}_d \rangle \text{ and } \delta \vec{E}_d \approx 0 \qquad \text{for } \frac{\sigma}{\lambda_0} << 1$$

We have seen this result for the Gaussian roughness; the smooth knife edge results in the conventional oscillatory behavior of the total field which is simply a manifestation of the interference between the incident and the diffracted fields. On the other hand, when the roughness on the edge increases, the edge diffracted-field becomes more incoherent and the phase interference consequently diminishes, leading to an attenuation of the oscillations in the coherent or mean total field.

$$\vec{E}_d \approx \delta \vec{E}_d \text{ and } \langle \vec{E}_d \rangle \approx 0 \qquad \text{for } \frac{\sigma}{\lambda_0} >> 1$$

Hence, as the roughness increases, we see in the figures that the interference pattern in the total field and total power decreases since the diffracted field becomes more incoherent. The model also predicts that the incoherent power is strongest near to the rough knife and is not generally appreciable when the point of observation of the diffracted field is far away from the edge. This, of course, is in complete agreement with our understanding that shadows, and hence the details of the shadow-causing boundary (knife edge), exist only a finite distance behind the boundary.

The wide angle scattering from a rough knife edge may be interpreted in a similar manner. The paraxial approach and the stationary phase result agree in magnitude under narrow (but reasonable) beamwidths and for large observation distances. This was a result of the assuming that the phase portion of the spectral integration dominates the result. However, under other circumstances, these large distance and smaller beamwidths may not be desirable. Hence, although an attempt at saddle point integration of the spectral integration has been performed, this task was interrupted by the difficulties encountered with the branch cuts emerging due to the spectral kernel and the branch cut from a Hankel function which enters the solution after reducing the problem by one dimension. This task can be completed using a transformation found in Banos [1966].

Finally a preliminary result has been presented for the propagation of a pulse past the rough knife edge. In reducing the problem to a usable form, it was found that a narrowband approximation was necessary. The received pulse, in both the smooth and rough edge result was found to be an amplitude-weighted replica of the transmitted pulse. The knife edge height and the roughness play the same role as previously recorded for LOS, continuous wave results: they change the amplitude of the pulse. Even with this approximation, the possibility of pulse spread was encountered under some extreme circumstances. In addition, due to the narrow band assumption, several integrals were dismissed as insignificant; however, as the bandwidth grows, these integrals will assume a greater role and consequently pulse distortion and dispersion may become an issue. As a future effort, the results presented in this dissertation should be generalized for larger bandwidths.

Chapter 3 Rough Surface Scattering

Rough surface scattering has become a well-established field. There have been many different approaches to the problem, ranging from the purely analytical to the purely numerical. However, in problems such as the foliage problem, few approaches go beyond the flat surface or the Kirchhoff models [Ulaby, 1990; Lang, 1993]. In this thesis scattering by the surface bounding a random medium will also be handled using the known techiques of impulse response [Brown, 1977] in section 3.3 and the Kirchhoff approximation in section 3.4.1. The Kirchhoff approximation is also rederived for a two-frequency which is applied to pulse scattering by a rough surface [Ishimaru, 1993] in section 3.4.2. Typically, in the numerical approaches, the integral equation plays a key role. The numerical solution is also examined in this thesis, first, by briefly reviewing a fast iterative method, the method of ordered multiple interactions (MOMI) in section 3.1 [Kapp, 1996]. This idea is then applied to a reformulation of scattering by dielectric surfaces in Section 3.2. In addition, the numerical (MOMI) approach is employed in **Chapter 8** in order to examine the interaction of an object above a rough surface.

3.1 Integral Equation Formulation of Rough Surface Scattering and the Method of Ordered Multiple Interactions

The integral equation governing both the TE and TM polarizations in the 2-D scalar problem has been derived in many sources including [Ishimaru, 1994], by many different techniques, such as equivalence and the use of Green's Identities. Green's second identity is given by

$$f(\vec{r}) = f^{i}(\vec{r}) + \int_{S+S_\infty} \left\{ f(\vec{r}') \frac{\partial G(\vec{r},\vec{r}')}{\partial n'} - G(\vec{r},\vec{r}') \frac{\partial f(\vec{r}')}{\partial n'} \right\} ds' , \qquad r \in V$$

Equation 3.1-1

In Equation 3.1-1, V represents a certain volume in space surrounded by the closed surface S and S_∞ as shown in Figure 3.1-1.

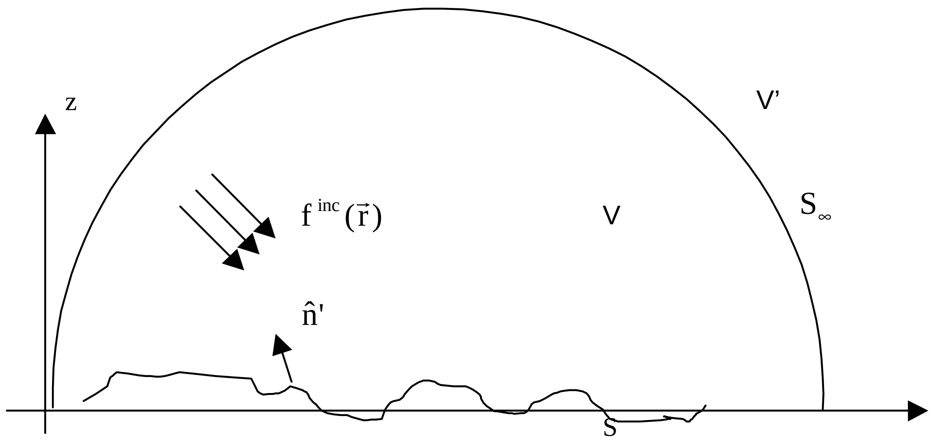

Figure 3.1-1: Problem Geometry for the Derivation of Boundary Integral Equations

Referring to Ishimaru [1994], an intermediate result derived by these methods is our starting point; we start with the following integral equation relating the total scalar field, $f(\vec{r})$, at the observation point, $\vec{r}$, to the incident field, $f^i(\vec{r})$ using Green's theorem:

$$f(\vec{r}) = 2f^i(\vec{r}) + \int_C \left\{ f(\vec{r}\,') \frac{\partial G(\vec{r},\vec{r}\,')}{\partial n'} - G(\vec{r},\vec{r}\,') \frac{\partial f(\vec{r}\,')}{\partial n'} \right\} dl', \quad \vec{r} \in C$$

where the contour integration is taken over a boundary enclosing the source and observation points consists of a hemisphere at infinity and a contour along the rough surface; see Figure 3.1-1.

The Green's function, $G(\vec{r},\vec{r}\,')$, and its normal derivative are chosen such that their contribution is zero at infinity; hence, only the integral over the surface remains. This integration over the surface is reduced in its support by limiting the illuminated region to only a portion of the surface by use of a tapered beam. A more detailed description of this process can be found in many sources including Kapp [1996].

For 1-D surfaces, the contour length may be projected onto the x-axis. This reduces the integration to an integral over one Cartesian coordinate. Hence, employing the transformation

$$dl' = \sqrt{1+\zeta_x^2(x')}\ dx'$$

Equation 3.1-2

we can construct the governing integral equations in rough surface scattering. First, the Electric Field Integral equation (EFIE), can be derived directly from Equation 3.1-1 by enforcing the following boundary condition on the perfectly conducting surface: $f(\vec{r}) = E_y(\vec{r}) = 0$. This results in the following first kind integral equation applicable for TE polarization.

$$E_y^i(\vec{r}) = \int_{-\infty}^{\infty} \frac{\partial E_y(\vec{r}')}{\partial n'} G(\vec{r},\vec{r}')\sqrt{1+\zeta_x^2(x')}\ dx'$$

Equation 3.1-3

In deriving the Magnetic Field Integral Equation (MFIE), the following boundary condition is enforced: the normal derivative of the tangential magnetic field, $\partial f(\vec{r}')/\partial n' = \partial H_y(\vec{r}')/\partial n'$, is zero on the surface. This results in the following second kind integral equation applicable for TM polarization.

$$H_y(\vec{r}) = 2H_y^i(\vec{r}) + 2\int_{-\infty}^{\infty} H_y(\vec{r}')\frac{\partial G(\vec{r},\vec{r}')}{\partial n'}\sqrt{1+\zeta_x^2(x')}dx'$$

Equation 3.1-4

In order to express the equation governing the TE polarization in the form similar to the MFIE, we take the normal derivative of both sides of Equation 3.1-4 along the unit normal $\hat{n}$ defined at the observation point $\vec{r}$. Then, we eliminate the weak singularity of the normal derivative of the Green's function through a limiting process [Ishimaru, 1994]. This yields the following second kind integral equation for the TE polarization

$$\frac{\partial E_y(\vec{r})}{\partial n} = 2\frac{\partial E_y^i(\vec{r})}{\partial n} - 2\int_{-\infty}^{\infty} \frac{\partial E_y(\vec{r})}{\partial n'}\frac{\partial G(\vec{r},\vec{r}')}{\partial n}\sqrt{1+\zeta_x^2(x')}dx'$$

Equation 3.1-5

The discretized versions of the above equations, when properly sampled, yield large, full matrices that scale as the number of unknowns squared. Scattering from a rough terrain, formulated with this integral equation approach typically was limited to small surfaces or narrow incident beams due to the matrix storage and inversion requirements of the conventional method of moments (MOM). Solving the integral equations numerically via the Method of Ordered Multiple Interactions (MOMI), however, has reduced this computation time and storage without approximation [Kapp, 1996]. Rewriting the above form of the second kind integral equations as

$$J(x) = J^i(x) + \int_D K(x,x')J(x')dx'$$

Equation 3.1-6

where $J(x)$ is the unknown surface current, $K(x,x')$ is the kernel or the propagator, and $J^i(x)$ is known, the Kirchhoff current. Although the domain of integration D is infinite by design, it can be made finite with the use of the appropriate tapered incident field. For the TE and TM cases, respectively

$$J^i(x) = 2\frac{\partial E_y^i(x,z)}{\partial n}\Big|_{z=\zeta(x)}, \quad J^i(x) = 2H_y^i(x,z)\Big|_{z=\zeta(x)}$$

$$J(x') = \frac{\partial E(x',z')}{\partial n'}\Big|_{z'=\zeta(x')}, \quad J(x') = H_y(x',z')\Big|_{z'=\zeta(x')}$$

$$K(x,x') = -2\frac{\partial G(x,x')}{\partial n}\sqrt{1+\zeta_x^2(x')}, \quad K(x,x') = 2\frac{\partial G(x,x')}{\partial n'}\sqrt{1+\zeta_x^2(x')}$$

Equation 3.1-7

After discretizing the resulting second kind equation and expressing it in a vector-matrix form

$$J = J^i + PJ$$

Equation 3.1-8

In Equation 3.1-8 both J (unknown) and J^i (known) are vectors and P is a square propagator matrix. The discretization is commonly carried out by taking values of surface height, current and propagator at the uniform grid $\{x_m\}$ of N discrete points separated by the spacing Δx. In this case, the m[th] element of each one of the above vectors and the (m,n)[th] element of the propagator matrix are given by

$$J_m = J(x_m)\,,\quad J^i_m = J^i(x_m) \quad \text{and} \quad P_{mn} = P(x_m, x_n)\Delta x$$

The off diagonal elements, P_{mn} with m≠n, of the discretized propagator matrix P are given by

$$P_{mn} = -2\frac{\partial G(x_m, x_n)}{\partial n_m}\sqrt{1+\zeta_x^2(x_n)}\,, \qquad P_{mn} = 2\frac{\partial G(x_m, x_n)}{\partial n'}\sqrt{1+\zeta_x^2(x_n)}$$

where $x_m = (2m-1)\Delta x - N\,\Delta x/2\,,\ m = 1,\ldots,N$ (observation point on the surface)

$x_n = (2n-1)\Delta x - N\,\Delta x/2\,,\ n = 1,\ldots,N$ (source point on the surface)

for the TE case and the TM case, respectively. The diagonal elements (usually called "self terms"), however, require special treatment and are given by, [Toporkov et. al, 1998],

$$P_{mm} = \pm\frac{\zeta_{xx}(x_m)}{2\pi\left[1+\zeta_x^2(x_m)\right]}\Delta x$$

The upper sign corresponds to the TM case and the lower sign to the TE case and $\zeta_{xx}(x_m)$ is the surface curvature at the point.

Direct matrix inversion becomes prohibitively large, requiring the storage of the NxN propagator matrix, where N is the number of unknowns. Furthermore, the computation time for LU decomposition scales as $N^3/3+N^2-5N/6$ [Kapp 1996]; here decomposing the original propagator matrix results in a lower triangular matrix, L and an upper triangular matrix, U. The MOMI approach to the scattering problem recasts the integral equation into a discretized form that is amenable to solution via simple forward elimination and back substitution without the enormous memory requirements of LU decomposition. After some manipulation, the discretized MFIE can be written in the following form

$$J = [I - U]^{-1}[I - L]^{-1}J^i + [I - U]^{-1}[I - L]^{-1}LUJ$$

Equation 3.1-9

Although it appears that matrix inversion is still needed to solve Equation 3.1-9, it can be shown that alternating forward and back substitution may solve this equation. The first term, $J_{B,}$ has been called the "new Born term". The following is a general iterative solution whose first term is J_B and the remaining terms are

$$J = \sum_{n=0}^{\infty} \left\{ [I - U]^{-1}[I - L]^{-1}LU \right\}^n [I - U]^{-1}[I - L]^{-1} J^i$$

Equation 3.1-10

The "new Born term" (n = 0) contains all orders of multiple scattering which are continuously forward scattered, continuously backward scattered, and those which are first forward scattered and then backward scattered. Numerical simulations have shown that the "new Born term" itself is adequate for most practical surfaces. For very rough perfectly conducting surfaces, a maximum of two MOMI iterations has typically proven to be sufficient.

3.2 The Development of a Numerical Impedance Boundary Conditions for Lossy Dielectric Interfaces

In considering scattering from the ocean, it is common practice to model the ocean surface as a perfect electric conductor (PEC). However, simulations that are more accurate require that the effects of the finite conductivity of seawater be included in the model. This is often achieved using an analytical impedance boundary condition (IBC). These models are adequate for many numerical simulations. The range of validity of such IBCs is somewhat unclear when considering low grazing angle (LGA) scattering from surfaces with significant spectral content at high frequencies.

A second important application of IBCs in the context of rough surface scattering is encountered in simulating propagation and scattering over natural terrain surfaces such as moist soil. The loss tangent of such materials at microwave frequencies is significantly smaller than the corresponding loss tangent of seawater. For this reason, analytical IBCs are less accurate for such surfaces. In addition, quantification of the error introduced with analytical IBCs is difficult.

Consequently, to address some of these concerns, a numerical IBC was developed for scattering from one-dimensional, lossy-dielectric interfaces. The numerical IBC is appears in the form of an integral equation for the surface magnetic fields in which the numerical IBC acts as a composite operator acting on the surface magnetic fields [Adams, 2000]. This is in contrast to the standard form of the integral equation for the magnetic field in which the correction term due to finite-loss effects appears as an operation on the tangential surface electric fields.

The integral equations for the surface fields in two-dimensions are written as a set of coupled integral equations. In addition, the more convenient operator form used by Adams [1998] is employed. These operators can be interpreted as in matrix form, once the problem is discretized using the method of moments (MOM). The equations are given as

$$\frac{1}{2}\psi(\rho)=\psi^{inc}(\rho)+\int_S\left[\psi(\rho)\frac{\partial G_1(\rho,\rho')}{\partial n'}-\frac{\partial\psi(\rho)}{\partial n'}G_1(\rho,\rho')\right]dS'$$
$$\frac{1}{2}\psi \quad =\psi^{inc}+P_1\psi - P_2\,\partial_n\psi$$

Equation 3.2-1

$$\frac{1}{2}\frac{\partial\psi(\rho)}{\partial n}=\frac{\partial\psi^{inc}(\rho)}{\partial n'}+\int_S\left[\psi(\rho')\frac{\partial^2 G_1(\rho,\rho')}{\partial n\partial n'}-\frac{\partial\psi(\rho)}{\partial n'}\frac{\partial G_1(\rho,\rho')}{\partial n}\right]dS'$$
$$\frac{1}{2}\partial_n\psi \quad =\partial_n\psi^{inc}+P_3\,\psi - P_4\,\partial_n\psi$$

Equation 3.2-2

where $\rho\in S$ and it is understood that a appropriate limiting procedure must be used to numerically treat the hypersingular kernel $\partial G_1/\partial n\partial n'$. It’s integral does not exist when the observation point is located on the surface.

The interior integral equations corresponding to these exterior equations are given below (and in the abbreviated, operator notation) in equations 3 and 4.

$$\frac{1}{2}\psi(\rho)=-\int_S\left[\psi(\rho)\frac{\partial G_2(\rho,\rho')}{\partial n'}-\frac{\partial\psi(\rho)}{\partial n'}G_2(\rho,\rho')\right]dS'$$
$$\frac{1}{2}\psi \quad =-\hat{P}_1\psi+\hat{P}_2\,\partial_n\psi$$

Equation 3.2-3

$$\frac{1}{2}\frac{\partial\psi(\rho)}{\partial n}\quad=-\int_S\left[\psi(\rho')\frac{\partial^2 G_2(\rho,\rho')}{\partial n\partial n'}-\frac{\partial\psi(\rho)}{\partial n'}\frac{\partial G_2(\rho,\rho')}{\partial n}\right]dS'$$
$$\frac{1}{2}\partial_n\psi \quad = \quad -\hat{P}_3\,\psi+\hat{P}_4\,\partial_n\psi$$

Equation 3.2-4

Here the definitions of the operators are apparent through a comparison with the equations. The following shorthand notation for the partial derivatives is also used:

$$\partial_n\psi=\frac{\partial\psi}{\partial n}$$

The operators with "hats" indicate the operators in the lower (dielectric) medium.

The integral equations Equation 3.4-2 and Equation 3.4-3 apply for both the TE and TM polarizations. For TE polarization, we make the substitution $\psi \to E_y$ while for TM polarization, $\psi \to H_y$. The relation of $\partial_n \psi$ to the field quantities is determined as follows. For TE polarization, $\vec{E} = \hat{y}\, E_y$, we have

$$\hat{n} \times \nabla \times \vec{E} = -\, j\omega\mu\, \hat{n} \times \vec{H}$$

which reduces to

$$-\,\hat{y}\, \frac{\partial E_y}{\partial n} = -\, j\omega\mu\, \hat{n} \times \vec{H}$$

Thus for TE polarization, the normal derivative of the electric field is related to the magnetic field through the relation

$$\frac{\partial E_y}{\partial n} = j\omega\mu\, H_{tan}$$

For TM polarization, we have the dual relation,

$$\frac{\partial H_y}{\partial n} = -\, j\omega\mu\, E_{tan}$$

Since the tangential electric and magnetic fields must be continuous across a material boundary which does not support a surface current, we have as the boundary condition between two media defined by the constitutive parameter pairs (ε_1, μ_1), (ε_2, μ_2)

$$\frac{1}{j\omega\mu_1} \frac{\partial E_{y1}}{\partial n} = \frac{1}{j\omega\mu_2} \frac{\partial E_{y2}}{\partial n}$$

for TE polarization and

$$\frac{1}{j\omega\varepsilon_1} \frac{\partial H_{y1}}{\partial n} = \frac{1}{j\omega\varepsilon_2} \frac{\partial H_{y2}}{\partial n}$$

for TM polarization. For a dielectric interface (no magnetic discontinuity), these can be rewritten as

$$\frac{\partial E_{y1}}{\partial n} = \frac{\partial E_{y2}}{\partial n}, \quad \frac{\partial H_{y1}}{\partial n} = \frac{\varepsilon_1}{\varepsilon_2}\frac{\partial H_{y2}}{\partial n}$$

If we consider a lossy dielectric interface, the above expression reflects the fact that the tangential H-field tends to a finite value while the tangential E-field tends to zero.

Consider scattering from a dielectric interface for TE polarization. Two of the four available integral equations in this case are

$$\frac{1}{2}\partial_n E \quad = \partial_n E^{inc} + P_3 E - P_4 \partial_n E$$

Equation 3.2-5

$$\frac{1}{2}E \quad = -\hat{P}_1 E + \hat{P}_2 \partial_n E$$

Equation 3.2-6

For a general dielectric constant, Equation 3.2-5 has two unknowns and must be supplemented by an integral equation from the lower medium. From Equation 3.2-6, we have

$$\left(\frac{1}{2} + \hat{P}_1\right)E \quad = \hat{P}_2 \partial_n E \;\Rightarrow\; E = \left(\frac{1}{2} + \hat{P}_1\right)^{-1}\hat{P}_2 \partial_n E$$

Equation 3.2-7

Using this result in Equation 3.2-5 gives an expression involving a single, unknown field quantity

$$\frac{1}{2}\partial_n E \quad = \partial_n E^{inc} + P_3\left(\frac{1}{2} + \hat{P}_1\right)^{-1}\hat{P}_2 \partial_n E - P_4 \partial_n E$$

Equation 3.2-8

The resulting integral equation is solved iteratively. The iteration count is reduced using an approximate factorization procedure (MOMI) that renormalizes the modified integral equation through the re-summation of the dominant multiple scattering interactions on the rough surface [Kapp, 1996]. Performing this renormalization, we arrive at the following matrix expression, written in the notation used by Kapp [1996].

$$\partial_n E = 2(I-U)^{-1}(I-L)^{-1}\partial_n E^{inc} + (I-U)^{-1}(I-L)^{-1} LU\,\partial_n E$$
$$+\,2(I-U)^{-1}(I-L)^{-1}P_3\left(\frac{1}{2}+\hat{P}_1\right)^{-1}\hat{P}_2\,\partial_n E$$

Equation 3.2-9

The number of iterations required to incorporate the effects of the finite loss of the lower medium increases as the loss tangent of the lower medium decreases. This behavior occurs because the numerical IBC is developed as a perturbation of the magnetic field integral equation for PECs. This may be seen in Equation 3.2-9. Comparing the result with that produced for a PEC surface, we immediately recognize the first two terms on the left-hand side correspond to the PEC surface. The last term accounts for the effects of the loss tangent of the lower medium. As the conductivity of the lower medium increases, this last term tends to zero. The first order approximation to scattering from the dielectric surface is thus the PEC result. The advantage over other techniques, however, is that this equation is exact and will reproduce the correct result even for surfaces with small curvature radii. One physically important problem where we can expect this to be important is the problem if grazing backscatter from ocean surfaces. For such problems, it is well known that the small wave structure produces the primary contribution to the backscattered field. When these contributions become important, the standard IBC fails and the present formulation will provide an advantage.

Unlike the analytical IBCs, the errors in the numerical IBC considered here can be reduced to an arbitrarily small level via iteration of the derived integral equation. The various factors affecting the convergence of the modified equation will be considered including loss tangent, surface roughness spectrum and angle of incidence. The inverse operation

$$\left(\frac{1}{2}+\hat{P}_1\right)^{-1}$$

is computed in O(N) operations due to the tightly banded nature (as conductivity approaches infinity) of $\hat{P}_2$. Thus, the computational cost associated with this term is negligible.

As an example of this technique, the scattered field from a wedge on a plane will be calculated. For this purpose, we use the following surface [Browe, 1999]. The surface height equations are given by

$$\begin{array}{ll} \frac{B}{\sqrt{2\alpha}}\exp\left\{-\alpha\left(x^2-\frac{1}{2\alpha}\right)\right\} & \frac{1}{\sqrt{2\alpha}} \le |x| \\ B\left[-\operatorname{sgn}(x)x+\frac{2}{\sqrt{2\alpha}}\right] & \delta \le |x| \le \frac{1}{\sqrt{2\alpha}} \\ B\left[\frac{2\delta}{\pi}\cos\left(\frac{\pi}{2\delta}\right)+\left(\frac{2}{\sqrt{2\alpha}}-\delta\right)\right] & |x| \le \delta \end{array}$$

where $\alpha=\dfrac{\frac{5}{2}-\ln(2)}{x_1{}^2}$, $B=\dfrac{\sqrt{2\alpha}\,h_{max}}{2}$, $\delta=\dfrac{B\pi\rho_c}{2}$.

The surface is specified completely by three parameters: the radius of curvature of the wedge tip measured at $x=0$ (ρ_c), the height of the surface from the plane to the wedge tip if $\rho_c=0$ (h_{max}), and the point on the x-axis where the height reaches $e^{-2}h_{max}$ (x_1). Although, the derivatives of the surface are required up through the third, the surface is constructed under the constraint of continuity up to the second derivative. The three parameters are shown graphically in Figure 3.2-1.

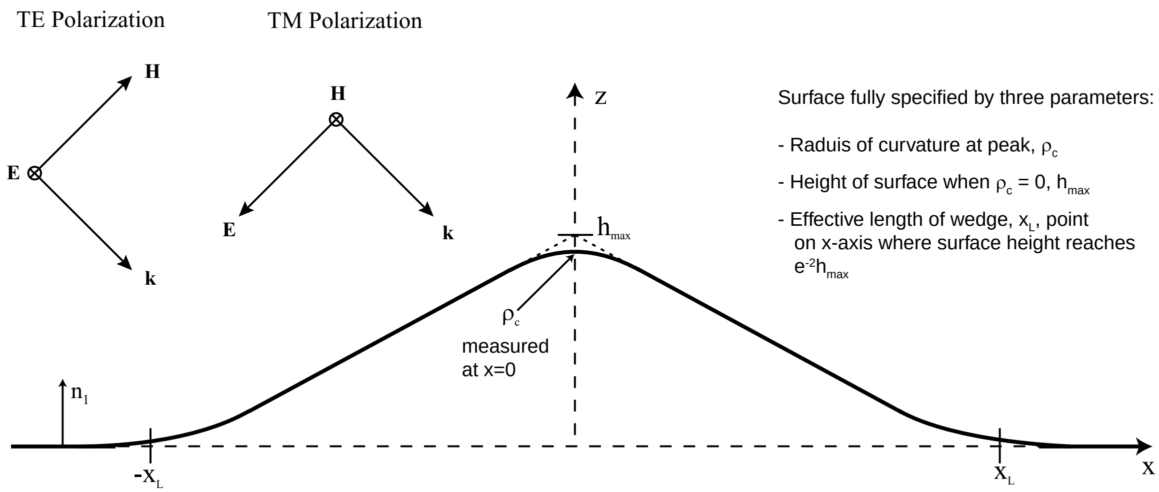

Figure 3.2-1: Surface geometry illustrating the three parameters needed to fully specify the surface. Also shown are the polarization definitions [Browe, 1999].

The wedge tip, in the region $|x| \leq \delta$, is represented by a cosine function. The radius of curvature at the wedge tip is measured at $x = 0$, the point where the second derivative of the cosine function is at its largest value. The faces of the wedge, in the region $\delta \leq |x| \leq \frac{1}{\sqrt{2\alpha}}$, are represented by straight-line segments. The faces of the wedge are smoothly joined to the planar surface by the Gaussian tails.

Figure 3.2-2 and Figure 3.2-3 show the scattered field for a beam incident to the surface at 75° for two different tip radii. These figures plot the magnitude of the far field as a function of the observation angle. The traces represent the different conductivities of the lower medium. The real part of the permitivity in lower medium is 2.0 and the conductivity of the medium varies from 0.1 to infinite (PEC) as noted in the legend. Figure 3.2-2 shows the result for an electrically small tip radius; consequently, we expect a large tip diffraction component.

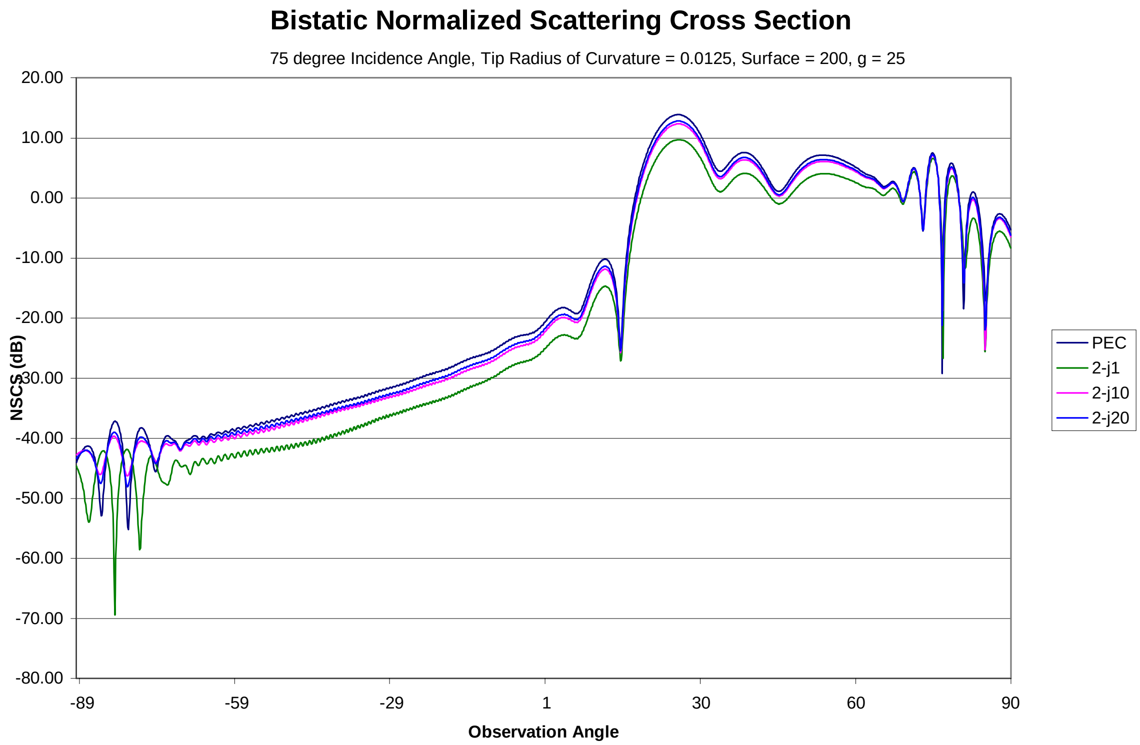

Figure 3.2-2: Scattering from wedge on a plane, small radius of curvature

First, we note that the agreement between the dielectric cases and in the specular direction (75°) is nearly perfect. This is due to the fact that we assume TE incidence and the Fresnel reflection coefficient for this polarizations at angles approaching grazing is one. Hence, we expect good agreement. Figure 3.2-3 demonstrates the scattering for a much larger tip radius of curvature. In this case, the tip diffraction is considerably smaller. This can be seen by comparing the backscatter regions of each plot. This region is governed by tip diffraction since there are no other physical features which would describe the backscattering. Note the 20 dB difference in computed cross section. The phase interference effects in the back scatter region is due to interference between direct tip diffraction and the tip diffracted energy which is reflected by the planar extension of the wedge in the backscatter region.

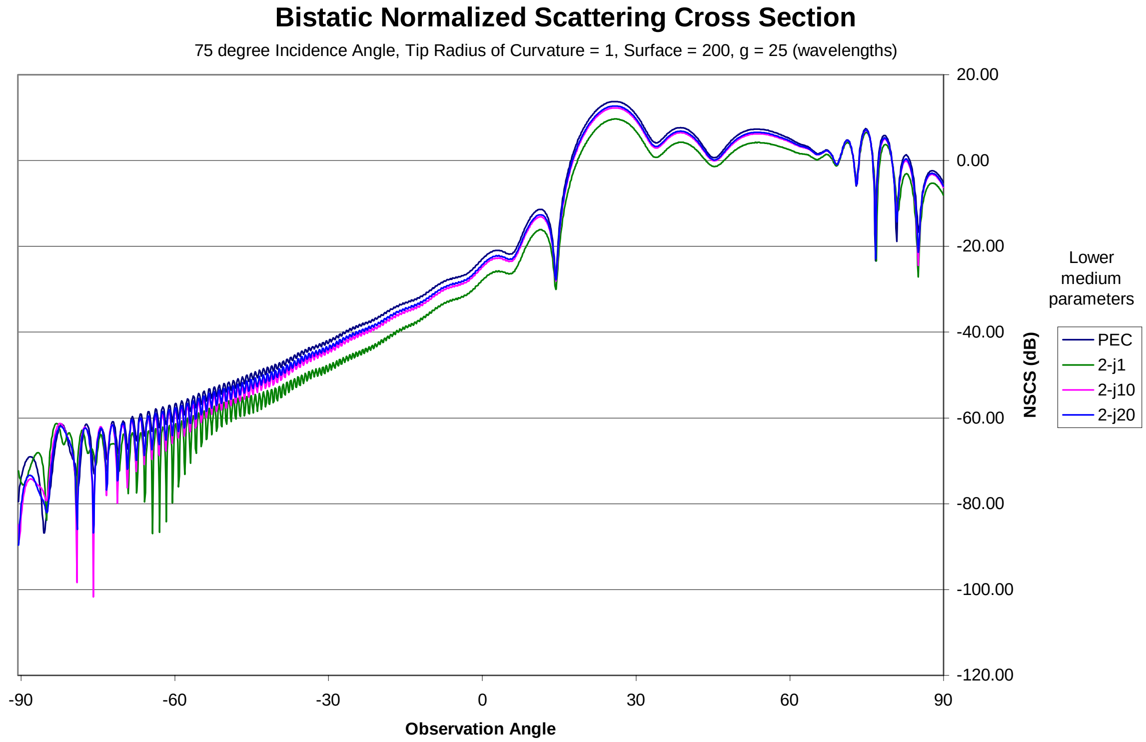

Figure 3.2-3: Scattering from wedge on a plane, larger radius of curvature

Each of the additional forward scatter features can be explained as well. A detailed explanation can be found in the thesis by Browe [1999]. Most notable are the largest peak due to specular reflection for the wedge face, and the interference between the waves reflected by the planar areas and the tip diffraction in the forward direction.

The final figure, Figure 3.2-4, shows the iteration count as the normalized residual error decreases (the iterative solution converges). Note that the convergence is shown for the tip radius of one wavelength and the range of permitivities (2-j50 to 2-j1). A solution for the permitivity of (2-j0.1) did not converge. From this plot, you can see that the convergence slows significantly, as the lower medium becomes less and less lossy. This is expected since the solution has been formulated as a perturbation series on the PEC solution. In addition, we have provided a trace for the smaller radius of curvature, 0.0125 wavelengths. Again, we can see that the smaller radius of curvature results in slower convergence; mostly likely this is due to multiple scattering within the lower medium at the wedge tip and penetration through the wedge tip.

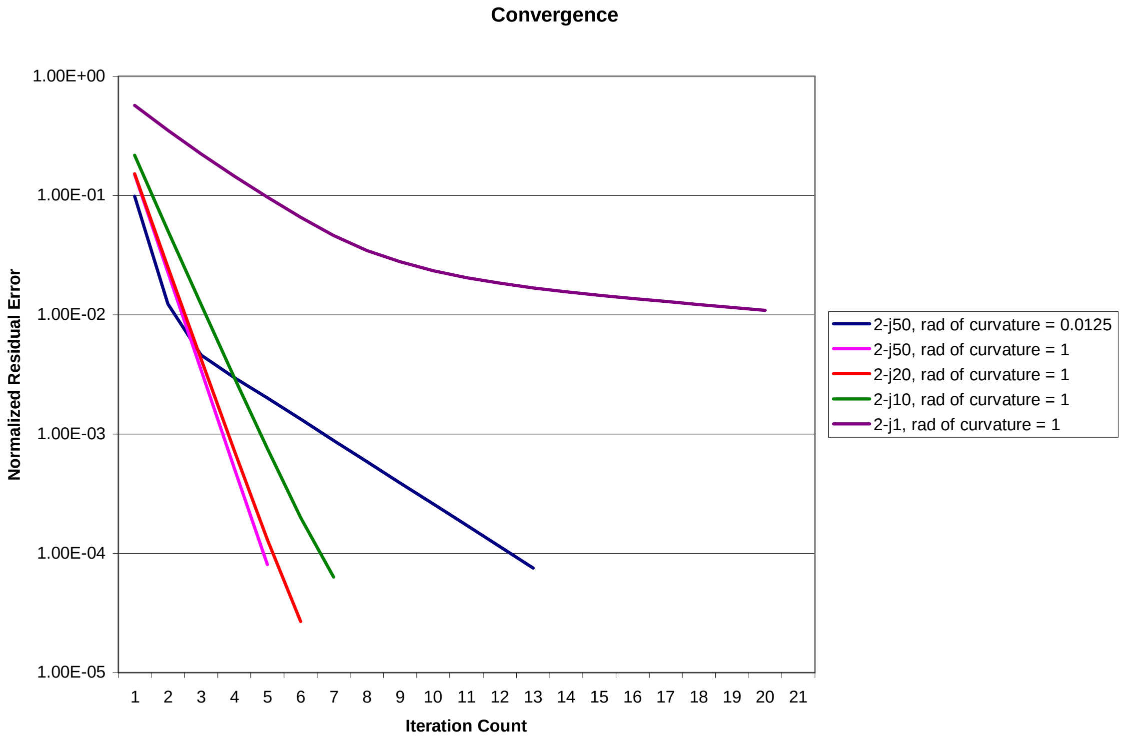

Figure 3.2-4: Convergence as a function of iteration count

Finally it is noted that this is a work in progress since the possibly more interesting TM case is not yet developed.

3.3 *The Incoherent Power via the Impulse Response Method*

The use of the impulse response method has been well established in literature for the calculation of the average incoherent power returned from the ocean surface under pulse illumination. One of the advantages of this approach is numerical: the average return power can be recast into a series of convolutions. The result, consequently, is found easily and efficiently using the Fast Fourier Transform, the FFT.

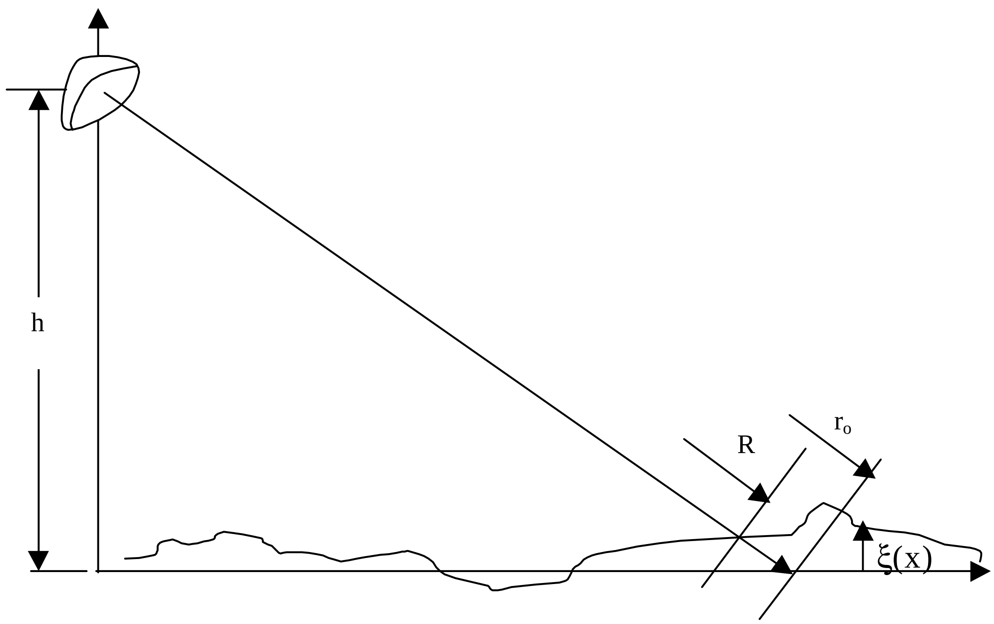

Figure 3.3-1: The Geometry for the Impulse Response Method

The power due to an incremental area with a given backscattering cross section is derived directly from the radar equation. Subsequently, extending this power to include the effects of the entire surface will lead to an expression for the returned power [Brown, 1977]. The average power returned from an element of area, dA, with a cross-section per unit area $\sigma^0(\theta,\phi)$ is given by the standard radar equation; see Figure 3.3-1.

$$dP_R(t) = \frac{P_T(t)\lambda^2 G^2(\theta,\phi)\sigma^o(\theta,\phi)}{(4\pi)^3 R^4} dA$$

Equation 3.3-1

where R = range from the radar to the elemental area, dA

$G(\theta,\phi)$ = antenna gain at the given angles

The average power returned from a distributed target, such as the terrain in this case, is calculated by a superposition of backscattered power from each elemental surface area, dA. A superposition of power is appropriate since the scattering surface is assumed to have a sufficiently random nature; there is no coherent return since the surface is uncorelated. The average backscattered power returned from the illuminated surface can be written as

$$P_R(t) = \frac{\lambda^2}{(4\pi)^3}\int_0^{\infty}\int_0^{2\pi}\frac{P_T\left(t-\frac{2\left(r_0-\xi(x,y)\sec\theta\right)}{c_0}\right)}{\left(r_0-\xi(x,y)\sec\theta\right)^4}G^2(\theta,\phi)\sigma^0(\theta,\phi)\,\rho\,d\phi\,d\rho$$

Equation 3.3-2

where the slant range to the terrain has been re-written: $R = r_0 - \xi(x,y)\sec\theta$. Since the integration is over the flat surface, cylindrical coordinates can be replaced with the radar coordinates ($r_0^2 = \rho^2 + h^2 \quad \Rightarrow \quad r_0\,dr_0 = \rho\,d\rho$), and the range to the surface can be approximated by the mean range for the evaluation of amplitude terms. Hence, the returned power can be re-written

$$P_R(t) \cong \frac{\lambda^2}{(4\pi)^3}\int_0^{\infty}\int_0^{2\pi}\frac{P_T\left(t-\frac{2\left(r_0-\xi(x,y)\sec\theta\right)}{c_0}\right)}{r_0^4}G^2(\theta,\phi)\sigma^0(\theta,\phi)\,r_0\,d\phi\,dr_0$$

Equation 3.3-3

The average power returned from the surface can then be found by evaluating the expectation with respect to the surface heights.

$$\left\langle P_R(t)\right\rangle \cong \int_{-\infty}^{\infty}\frac{\lambda^2}{(4\pi)^3}\int_0^{\infty}\int_0^{2\pi}\frac{P_T\left(t-\frac{2\left(r_0-\xi(x,y)\sec\theta\right)}{c_0}\right)}{r_0^4}G^2(\theta,\phi)\sigma^0(\theta,\phi)\,r_0\,d\phi\,dr_0\,p_\xi(\xi)\,d\xi$$

Equation 3.3-4

Introducing the change of variables,

$$\tilde{\xi}(x,y) = \frac{2\xi(x,y)\sec\theta}{c_0} \quad \Rightarrow \quad p_{\tilde{\xi}}(\tilde{\xi}) = \frac{c_0}{2\sec\theta} p_{\xi}\left(\frac{c_0}{2\sec\theta}\tilde{\xi}\right)$$

we express the average returned power as

$$\left\langle P_R(t)\right\rangle \cong \frac{\lambda^2}{(4\pi)^3}\int_0^{\infty}\int_0^{2\pi}\int_{-\infty}^{\infty}\frac{P_T\left(t-\frac{2r_0}{c_0}-\tilde{\xi}(x,y)\right)}{{r_0}^4} p_{\tilde{\xi}}(\tilde{\xi})\, d\tilde{\xi}\, G^2(\theta,\phi)\sigma^0(\theta,\phi)\; r_0\, d\phi\, dr_0$$

Equation 3.3-5

Recognizing the convolutional form in the random variable, $\tilde{\xi}$, we re-write the power received as

$$\left\langle P_R(t)\right\rangle \cong \frac{\lambda^2}{(4\pi)^3}\int_0^{\infty}\int_0^{2\pi}\frac{P_T\left(t-\frac{2r_0}{c_0}\right)\otimes p_{\tilde{\xi}}\left(t-\frac{2r_0}{c_0}\right)}{{r_0}^3} G^2(\theta,\phi)\sigma^0(\theta,\phi)d\phi\, dr_0$$

Equation 3.3-6

Substituting for the constant delay term,

$$t' = \frac{2r_0}{c_0}$$

Equation 3.3-7

and introducing the sifting properties of the Dirac Delta Function, the power received is written as follows

$$\left\langle P_R(t)\right\rangle \cong \int_{-\infty}^{\infty}\frac{\lambda^2}{(4\pi)^3}\int_0^{\infty}\int_0^{2\pi}\frac{P_T(t-t')\otimes p_{\tilde{\xi}}(t-t')}{{r_0}^3} G^2(\theta,\phi)\sigma^0(\theta,\phi)d\phi\, dr_0\, \delta\left(t'-\frac{2r_0}{c_0}\right)dt'$$

Equation 3.3-8

Hence, another convolution has appeared in the average return power integration. For that reason, the average scattered intensity from a rough surface can be recast as a series of convolutions

$$\langle P_r(t)\rangle = P_T(t) \otimes p_{\tilde{\xi}}(t) \otimes P_{FS}(t)$$

Equation 3.3-9

From equation in Equation 3.3-9, the last term represents the average backscattered power from a transmitted impulse function and has been called the "Flat Surface Impulse Response" (FSIR)

$$P_{FS}(t) = \frac{\lambda^2}{(4\pi)^3} \iint_{Surface} \frac{\delta\left(t - \frac{2r_0}{c}\right)}{r_0^{\ 4}} G^2(\theta,\phi)\sigma^o(\theta,\phi)dA$$

Equation 3.3-10

where: $\delta(*)$ = a Dirac delta function which accounts for the two way propagation delay

λ = wavelength of the carrier

$G(\theta, \phi)$ = radar antenna gain

$\sigma(\theta, \phi)$ = surface scattering cross section per unit area

dA = elemental surface area, $dA = r_0 dr_0 d\phi = \rho d\rho d\phi$

r_0 = slant range from the radar to the mean surface at dA

h = radar height above surface

This flat impulse response function is characterizes the average return from a surface with vanishingly small roughness which has been illuminated by a delta function pulse.

3.4 Pulse Scattering from Rough Surface

In this section, the Kirchhoff approximation for rough surface scattering is quickly reviewed, followed by an exposition, clarification and simplification of the work by Ishimaru [1995] on two-frequency rough surface scattering. It shall be proposed that this work will be used in conjunction with the two-frequency radiative transfer equation of Chapter 7 as a boundary condition. This is a work in progress.

3.4.1 The Kirchhoff approximation for rough surfaces

In this section, a brief account of the Kirchhoff approximation to scattering from a rough surface is given. The interest in this approximation, with respect to the more exact integral equation methods is the closed form, simple results. The Kirchhoff Approximation, also know as the tangent plane approximation, is a high frequency approximation. This implies that the surface is appears to be flat with respect to the incident wavelength. Loosely following the development of Ishimaru [1997], and assuming that the incident field, observed on the rough surface $(x', y', \zeta(x', y'))$, has the form,

$$\psi^{i}(\vec{r}') = \psi_0\, e^{-j\vec{k}_i \cdot \vec{r}'} = \psi_0\, e^{-jk_{ix}x' - jk_{iy}y' - jk_{iz}\zeta(x',y')}$$

Equation 3.4-1

then the scattered, or in this case reflected field, has the form,

$$\psi^{r}(\vec{r}') = \psi_0\, e^{-j\vec{k}_r \cdot \vec{r}'} = \psi_0\, e^{-jk_{rx}x' - jk_{ry}y' - jk_{rz}\zeta(x',y')} = R\psi^{i}(\vec{r}')$$

So that the *total* field at the rough surface observation coordinate can be written as

$$\psi^{total}(\vec{r}') \cong (1+R)\psi^{i}(\vec{r}')$$

hence, from Green’s theorem, the approximate substitution can be made,

$$\begin{aligned}\psi^{s}(\vec{r}_o) &= \int_{S'} \left[\psi^{total}(\vec{r}')\frac{\partial G(\vec{r}_o, \vec{r}')}{\partial n'} + \frac{\partial \psi^{total}(\vec{r}')}{\partial n'} G(\vec{r}_o, \vec{r}')\right] ds' \\ &\cong \int_{S'} \left[\left((1+R)\psi^{i}(\vec{r}')\right)\frac{\partial G(\vec{r}_o, \vec{r}')}{\partial n'} + (1+R)\, \hat{n}'\cdot\nabla\psi^{i}(\vec{r}')\, G(\vec{r}_o, \vec{r}')\right] ds'\end{aligned}$$

Equation 3.4-2

since, $\hat{n}' \cdot \vec{k}_r = -\hat{n}' \cdot \vec{k}_i$, assuming an incident plane wave and making the far field approximation for the Green’s function, the expression for the scattered field becomes

$$\psi^s(\vec{r}_o) \cong j\frac{\psi_o e^{-jkr_o}}{4\pi r_o}\int_{S'} (1+R)\left(\hat{n}'\cdot\vec{k}_s\right)e^{-j\left(\vec{k}_i-\vec{k}_s\right)\vec{r}'}$$

$$+\left(-\vec{k}_i\cdot\hat{n}'+R\,\vec{k}_i\cdot\hat{n}'\right)e^{-j\left(\vec{k}_i-\vec{k}_s\right)\vec{r}'}\,ds'$$

$$\cong j\frac{\psi_o e^{-jkr_o}}{4\pi r_o}\int_{S'}\left\{\hat{n}'\cdot\left(\vec{k}_s-\vec{k}_i\right)+\left(\vec{k}_s+\vec{k}_i\right)R\right\}e^{-j\left(\vec{k}_i-\vec{k}_s\right)\vec{r}'}\,ds'$$

Equation 3.4-3

Next, a substitution is made for the unit vector normal to the surface at the source point, and the source position vector.

$$\vec{r}' \equiv x'\hat{x}+y'\hat{y}+\zeta(x',y')\hat{z}$$
$$\equiv \vec{r}_t'+\zeta(x',y')\hat{z}$$

$$\hat{n}'=\frac{-\zeta_x(x',y')\,\hat{x}-\zeta_y(x',y')\,\hat{y}+\hat{z}}{\sqrt{1+\zeta_x^2(x',y')+\zeta_y^2(x',y')}}$$

In addition, the elemental surface area is projected onto the mean, flat surface at z = 0.

$$dS' = \sqrt{1+\zeta_x^2(x',y')+\zeta_y^2(x',y')}\,dx'\,dy'$$

Equation 3.4-4

$$\psi^s(\vec{r}_o) \cong j\frac{\psi_o e^{-jkr_o}}{4\pi r_o}\int_{S'}\left[\left(k_{sz}-k_{iz}\right)+R\left(k_{sz}+k_{iz}\right)\right]e^{-j\left(\vec{k}_{it}-\vec{k}_{st}\right)\vec{r}_t'+\left(\vec{k}_{iz}-\vec{k}_{sz}\right)\zeta'(x',y')}\,dx'\,dy'$$

$$-j\frac{\psi_o e^{-jkr_o}}{4\pi r_o}\int_{S'}\zeta_x(x',y')\left[\left(k_{sx}-k_{ix}\right)+R\left(k_{sx}+k_{ix}\right)\right]e^{-j\left(\vec{k}_{it}-\vec{k}_{st}\right)\vec{r}_t'+\left(\vec{k}_{iz}-\vec{k}_{sz}\right)\zeta'(x',y')}\,dx'\,dy'$$

$$-j\frac{\psi_o e^{-jkr_o}}{4\pi r_o}\int_{S'}\zeta_y(x',y')\left[\left(k_{sy}-k_{iy}\right)+R\left(k_{sy}+k_{iy}\right)\right]e^{-j\left(\vec{k}_{it}-\vec{k}_{st}\right)\vec{r}_t'+\left(\vec{k}_{iz}-\vec{k}_{sz}\right)\zeta'(x',y')}\,dx'\,dy'$$

Equation 3.4-5

In order to make this solution useful, the surface is assumed a perfect electric conductor (PEC), so that the reflection coefficient is negative one (-1) regardless of the incidence angle.

$$\psi^s(\vec{r}_o) \cong j\frac{\psi_o e^{-jkr_o}}{4\pi r_o}\int_{S'} [-2k_{iz}] e^{-j(\vec{k}_{it}-\vec{k}_{st})\cdot\vec{r}_t' + (\vec{k}_{iz}-\vec{k}_{sz})\cdot\zeta'(x',y')}\, dx'\,dy'$$
$$- j\frac{\psi_o e^{-jkr_o}}{4\pi r_o}\int_{S'} \zeta_x(x',y')[2k_{ix}] e^{-j(\vec{k}_{it}-\vec{k}_{st})\cdot\vec{r}_t' + (\vec{k}_{iz}-\vec{k}_{sz})\cdot\zeta'(x',y')}\, dx'\,dy'$$
$$- j\frac{\psi_o e^{-jkr_o}}{4\pi r_o}\int_{S'} \zeta_y(x',y')[2k_{iy}] e^{-j(\vec{k}_{it}-\vec{k}_{st})\cdot\vec{r}_t' + (\vec{k}_{iz}-\vec{k}_{sz})\cdot\zeta'(x',y')}\, dx'\,dy$$

Equation 3.4-6

Assuming that the surface is large (so that it is possible to exclude the edge contributions) and integrating Equation 3.4-6 by parts [Ishimaru, 1997], yields

$$\psi^s(\vec{r}_o) \cong j\frac{\psi_o e^{-jkr_o}}{4\pi r_o}\left[\frac{-2(k_{ix}\Delta k_x + k_{iy}\Delta k_y + k_{iz}\Delta k_z)}{\Delta k_z}\right]\int_{S'} e^{-j\Delta\vec{k}\cdot\vec{r}'}\, dx'\,dy'$$
$$\cong j\frac{\psi_o k e^{-jkr_o}}{2\pi r_o} F(\theta_i,\theta_s,\phi_s)\int_{S'} e^{-j\Delta\vec{k}\cdot\vec{r}'}\, dx'\,dy'$$

$$\text{for } F(\theta_i,\theta_s,\phi_s) = \left[\frac{1+\cos\theta_i\cos\theta_s - \sin\theta_i\sin\theta_s\cos\phi_s}{\cos\theta_i + \cos\theta_s}\right] \text{and} \quad \Delta k_x \equiv k_{sx} - k_{ix}, \text{ etc.}$$

Equation 3.4-7

The mean, average field can now be found as

$$\left\langle \psi^s(\vec{r}_o)\right\rangle \cong j\frac{\psi_o k e^{-jkr_o}}{2\pi r_o} F(\theta_i,\theta_s,\phi_s)\left\langle \int_{S'} e^{-j\Delta\vec{k}\cdot\vec{r}'}\, dx'\,dy'\right\rangle$$
$$\cong j\frac{\psi_o k e^{-jkr_o}}{2\pi r_o} F(\theta_i,\theta_s,\phi_s)\int_{S'} \left\langle e^{-j(k_{sz}-k_{iz})\cdot\zeta'}\right\rangle e^{-j(\vec{k}_{st}-\vec{k}_{it})\cdot\vec{r}'}\, dx'\,dy'$$

Equation 3.4-8

The average is recognized as the Fourier transform of the pdf, so that the bracketed quantity is simply the characteristic function. Assuming Gaussian distributed roughness, with a standard deviation of the heights, σ, defining the characteristic function of the Gaussian random variable, $\Phi(\Delta k_z)$, and recognizing the Dirac delta function

$$\left\langle \psi^s(\vec{r}_o)\right\rangle \cong j\frac{\psi_o k e^{-jkr_o}}{2\pi r_o}F(\theta_i,\theta_s,\phi_s)\Phi(\Delta k_z)\int_{S'} e^{-j(\vec{k}_{st}-\vec{k}_{it})\cdot\vec{r}'}\,dx'\,dy'$$

$$\cong j\frac{2\pi\psi_o k e^{-jkr_o}}{r_o}F(\theta_i,\theta_s,\phi_s)e^{-\left(\frac{\Delta k_z\sigma^2}{2}\right)}\delta(\vec{k}_{st}-\vec{k}_{it})$$

Equation 3.4-9

The mean field above shows that the scattering direction is in same x-y direction as the incident field. Hence, when the scattered z-direction is chosen to be the opposite of the incident field (k_{sz} = -k_{iz}) the coherent scattering corresponds to the reflected field, reduced by the exponential factor related to the surface heights; the randomly elevated plane [Brown, 1997].

3.4.2 Two-frequency rough surface scattering

Next the frequency correlation of the field is formed,

$$\left\langle \psi(\vec{r}_o,k_1)\psi^*(\vec{r}_o,k_2)\right\rangle \cong \frac{\psi_o^2 k_1k_2}{(2\pi)^2 r_o^2}F(\theta_i,\theta_s,\phi_s)F^*(\theta_i,\theta_s,\phi_s)$$
$$\cdot\int_{S'}\int_{S} e^{-j\Delta\vec{k}_1\cdot\vec{r}_1}\, e^{j\Delta\vec{k}_2\cdot\vec{r}_2}\,dx_1dy_1dx_2\,dy_2$$

$$\left\langle \psi(\vec{r}_o,k_1)\psi^*(\vec{r}_o,k_2)\right\rangle \cong \frac{\psi_o^2 k_1k_2}{(2\pi)^2 r_o^2}F(\theta_i,\theta_s,\phi_s)F^*(\theta_i,\theta_s,\phi_s)$$
$$\cdot\int_{S'}\int_{S} e^{-j(\Delta\vec{k}_{t,1}\cdot\vec{r}_{1t}-\Delta\vec{k}_{t,2}\cdot\vec{r}_{2t})}\left\langle e^{-j(\Delta k_{z,1}\zeta_1-\Delta k_{z,2}\zeta_2)}\right\rangle dx_1dy_1dx_2\,dy_2$$

Equation 3.4-10

The expression, $\vec{k}_{it,1}$, is vector of the x and y components of the wave number vector at frequency 1 and the difference of the incident and scattered wavenumber vectors is indicated

$$\Delta k_{1z}\equiv(k_{iz,1}-k_{sz,1});\quad \Delta k_{2z}=(k_{iz,2}-k_{sz,2})$$
$$\Delta\vec{k}_{1t}\equiv(\vec{k}_{it,1}-\vec{k}_{st,1});\quad \Delta\vec{k}_{2t}=(\vec{k}_{it,2}-\vec{k}_{st,2})$$

Performing the average using a joint Gaussian distribution for the heights (assuming the slopes are statistically independent)

$$\left\langle e^{-j\left(\Delta k_{z,1}\zeta_1-\Delta k_{z,2}\zeta_2\right)}\right\rangle = \int_{-\infty}^{\infty}\int_{-\infty}^{\infty} e^{-j\left(\Delta k_{z,1}\zeta_1-\Delta k_{z,2}\zeta_2\right)} \frac{e^{-\frac{\zeta_1^2+2C_n\zeta_1\zeta_2-\zeta_2^2}{2\sigma^2\left(1-C_n^2\left(\vec{r}_{dt}\right)\right)}}}{2\pi\sigma^2\sqrt{1-C_n^2\left(\vec{r}_{dt}\right)}} d\zeta_1 d\zeta_2$$

$$= e^{-\left(\Delta k_{z,1}^2+\Delta k_{z,2}^2\right)\frac{\sigma^2}{2}} e^{\Delta k_{z,1}\Delta k_{z,2}\sigma^2 C_n\left(\vec{r}_{dt}\right)}$$

Equation 3.4-11

Substituting, Equation 3.4-11, converting to sum and difference coordinates in Equation 3.4-10, (defining a sum and difference for each Cartesian coordinate)

$$\text{for} \quad x_s \equiv \frac{1}{2}\left(x_1+x_2\right);\ x_d \equiv \left(x_1-x_2\right)$$

$$\vec{r}_{st} \equiv \frac{1}{2}\left(\vec{r}_{1t}+\vec{r}_{2t}\right) = x_s\hat{x}+y_s\hat{y}; \quad \vec{r}_{dt} \equiv \left(\vec{r}_{1t}-\vec{r}_{2t}\right) = x_d\hat{x}+y_d\hat{y}$$

and the transverse (x-y) wavenumber vectors are also converted to sum and difference coordinates

$$\Delta\vec{k}_{1t} \equiv \left(\vec{k}_{it,1}-\vec{k}_{st,1}\right) \equiv \left(\Delta\vec{k}_{ct}+\frac{1}{2}\Delta\vec{k}_{dt}\right); \quad \Delta\vec{k}_{2t} = \left(\vec{k}_{it,2}-\vec{k}_{st,2}\right) \equiv \left(\Delta\vec{k}_{ct}-\frac{1}{2}\Delta\vec{k}_{dt}\right)$$

$$\text{for}\ \Delta\vec{k}_{ct} = \frac{1}{2}\left(\Delta\vec{k}_{1t}+\Delta\vec{k}_{2t}\right);\ \Delta\vec{k}_{dt} = \left(\Delta\vec{k}_{1t}-\Delta\vec{k}_{2t}\right)$$

results in the following expression for the total power (two-point, two-frequency correlation)

$$\left\langle \psi\left(\vec{r}_o,k_1\right)\psi^*\left(\vec{r}_o,k_2\right)\right\rangle \cong \frac{\psi_o^2\, k_1 k_2}{(2\pi)^2\, r_o^2}\left|F\left(\theta_i,\theta_s,\phi_s\right)\right|^2$$

$$\cdot \int_S\int_S e^{-j\left(\Delta\vec{k}_{ct}\cdot\vec{r}_{dt}-\Delta\vec{k}_{dt}\cdot\vec{r}_{st}\right)} e^{-\left(\Delta k_{1z}^2+\Delta k_{2z}^2\right)\frac{\sigma^2}{2}} e^{\Delta k_{1z}\Delta k_{2z}\sigma^2 C_n\left(\vec{r}_{dt}\right)} d\vec{r}_{dt} d\vec{r}_{st}$$

Equation 3.4-12

Next the mean power is subtracted from the total power in order to find the fluctuating power, $\left\langle |\delta\psi_s|^2 \right\rangle = \left\langle |\psi_s|^2 \right\rangle - |\langle \psi_s \rangle|^2$ and consequently, the two-frequency surface cross section is written as

$$\sigma_s^0(k_1,k_2) = \frac{4\pi r_o^2}{S\psi_o^2}\left\{ \left\langle \psi(\vec{r}_o,k_1)\psi^*(\vec{r}_o,k_2) \right\rangle \; - \langle \psi(\vec{r}_o,k_1)\rangle \langle \psi(\vec{r}_o,k_2)\rangle^* \right\}$$
$$\cong \frac{k_1k_2}{\pi}\left|F(\theta_i,\theta_s,\phi_s)\right|^2 \frac{1}{S}\int_S e^{j\Delta\vec{k}_{dt}\cdot\vec{r}_{st}}\, d\vec{r}_{st}$$
$$\cdot \int_S e^{-\left(\Delta k_{1z}^2+\Delta k_{2z}^2\right)\frac{\sigma^2}{2}}\left[e^{\Delta k_{1z}\Delta k_{2z}\sigma^2 C_n(\vec{r}_{dt})} - 1 \right] e^{-j\Delta\vec{k}_{ct}\cdot\vec{r}_{dt}}\, d\vec{r}_{dt}$$

Equation 3.4-13

This expression is equivalent to the two-frequency mutual coherence function of the rough surface in the Kirchhoff approximation. If we assume that the incident wave is a Gaussian tapered plane wave, the first integral in Equation 3.4-13 is evaluated

$$\frac{1}{S}\int_S e^{-\frac{\left(x_1^2+y_1^2\right)}{2b^2}} e^{-\frac{\left(x_2^2+y_2^2\right)}{2b^2}} e^{j\Delta\vec{k}_{dt}\cdot\vec{r}_{st}}\, d\vec{r}_{st} = \frac{1}{S}\int_S e^{-\frac{\left(x_s^2+y_s^2\right)}{b^2}} e^{j\Delta\vec{k}_{dt}\cdot\vec{r}_{st}}\, d\vec{r}_{st}$$
$$= \frac{1}{S}\int e^{-\frac{x_s^2}{b^2}} e^{j\Delta k_{dx}x_s}\, dx_s \int e^{-\frac{y_s^2}{b^2}} e^{j\Delta k_{dy}y_s}\, dy_s = \frac{\pi b^2}{S} e^{-\frac{\left(\Delta k_{dx}^2+\Delta k_{dy}^2\right)b^2}{4}}$$

Equation 3.4-14

The applicability of this is reviewed in Chapter 2 for pulse propagation across a randomly rough knife edge. There are two asymptotic limits where this integral may be evaluated: small height and large height. Considering only the large height approximation,

$$\left(\Delta k_{1z}^2 + \Delta k_{2z}^2\right)\frac{\sigma^2}{2} >> 1$$

the exponential function of the above argument will force the integrand to zero except near $\vec{r}_{st} \approx 0$ so that the correlation function can be expanded into a series about $\vec{r}_{st} \approx 0$ [Brown, 1997].

$$\sigma^2 C(\vec{r}_{dt}) \cong \sigma^2 - \left[\sigma_{\zeta_x}^2 \frac{x_d^2}{2} + \sigma_{\zeta_y}^2 \frac{y_d^2}{2} \right]$$

where the variance of the heights of the x and y surface slopes are given by $\sigma^2_{\zeta_x}, \sigma^2_{\zeta_y}$

$$\sigma_s^0(k_1,k_2) = \frac{4\pi r_o^2}{S}\left\{ \left\langle \psi(\vec{r}_o,k_1)\psi^*(\vec{r}_o,k_2)\right\rangle - \left\langle \psi(\vec{r}_o,k_1)\right\rangle\left\langle \psi(\vec{r}_o,k_2)\right\rangle^* \right\}$$

$$\cong \frac{k_1k_2}{\pi}\left|F(\theta_i,\theta_s,\phi_s)\right|^2 \frac{\pi b^2}{S} e^{-\frac{\left(\Delta k_{dx}^2+\Delta k_{dy}^2\right)b^2}{4}}$$

$$\cdot e^{-\frac{\sigma^2}{2}\left(\Delta k_{1z}^2+\Delta k_{2z}^2-2\Delta k_{1z}\Delta k_{2z}\right)} \int_S e^{-\Delta k_{1z}\Delta k_{2z}\left[\sigma^2_{\zeta_x}\frac{x_d^2}{2}+\sigma^2_{\zeta_y}\frac{y_d^2}{2}\right]} e^{-j\Delta\vec{k}_{ct}\cdot\vec{r}_{dt}}\, d\vec{r}_{dt}$$

Equation 3.4-15

Evaluating the remaining integral, the result for large heights is given by

$$\sigma_s^0(k_1,k_2) \cong \frac{k_1k_2\pi b^2}{2S\Delta k_{1z}\Delta k_{2z}\sigma_{\zeta_x}\sigma_{\zeta_y}}\left|F(\theta_i,\theta_s,\phi_s)\right|^2 e^{-\frac{\left(\Delta k_{dx}^2+\Delta k_{dy}^2\right)b^2}{4}}$$

$$\cdot e^{-\frac{\sigma^2}{2}(\Delta k_{1z}-\Delta k_{2z})^2} e^{-\frac{\Delta k_{cx}^2}{2\sigma^2_{\zeta_x}\Delta k_{1z}\Delta k_{2z}}-\frac{\Delta k_{cy}^2}{2\sigma^2_{\zeta_y}\Delta k_{1z}\Delta k_{2z}}}$$

Equation 3.4-16

Applying the definitions for the wavenumber vectors, the final exponential can be written as

$$\exp\left\{-\frac{\Delta k_{cx}^2}{2\sigma^2_{\zeta_x}\Delta k_{1z}\Delta k_{2z}}-\frac{\Delta k_{cy}^2}{2\sigma^2_{\zeta_y}\Delta k_{1z}\Delta k_{2z}}\right\} = \exp\left\{-\frac{(k_1+k_2)^2}{4k_1k_2}\tan^2\theta_i\left[\frac{\cos^2\phi_i}{\sigma^2_{\zeta_x}}+\frac{\sin^2\phi_i}{\sigma^2_{\zeta_y}}\right]\right\}$$

interpreting these as pdfs for the acceptable slopes of the “facets” which contribute to the backscattered power [Brown, 1997],

$$\sigma_s^0(k_1,k_2) \cong \frac{\pi b^2}{2S\cos^2\theta_i}\left|F(\theta_i,\theta_s,\phi_s)\right|^2 e^{-\frac{\left(\Delta k_{dx}^2+\Delta k_{dy}^2\right)b^2}{4}} e^{-\frac{\sigma^2}{2}(\Delta k_{1z}-\Delta k_{2z})^2}$$
$$\cdot p\left[\zeta_x = \frac{(k_1+k_2)}{2\sqrt{k_1k_2}}\tan\theta_i\cos\phi_i\right] p\left[\zeta_y = \frac{(k_1+k_2)}{2\sqrt{k_1k_2}}\tan\theta_i\sin\phi_i\right]$$

Equation 3.4-17

3.4.3 Future Work

A great deal of work is left undone in this rough surface scattering section. In the simulation of the scattering from dielectric surfaces, the TM polarization case needs to be completed. Once this step is taken, the numerical results can be compared with the available, and popular, Leontovich (Impedance) Boundary Conditions (IBC). These IBC's have not been evaluated for their accuracy in certain parameter spaces, most notably the low grazing angle region. Consequently, this is an avenue for further progress. In addition, other interesting results are possible when this formulation is extended to the TM polarization.

The two frequency surface scattering work, orignally developed by Ishimaru [1995] still has a great deal of room to grow; particularly in its application as a boundary condition. This effort will be more fully developed for use as a boundary condition for the two-frequency radiative transfer equation developed in Chapter 7 . The small height approximation to the above derivation may also be employed for greater applicability of the method. In addition, boundary perturbation theory for rough surface scattering may be used to derive a two-frequency rough surface scattering in the lower frequency limit in a similar manner. Finally, in combination with two-frequency radiative transfer equations, pulse propagation scattering simulations from a vegetated rough surface may be accomplished.

Chapter 4 The Impulse Response

In creating the convolutional model of this chapter, the radiative transfer equations are presented for time dependent, forward-backward scattering. The model developed assumes completely incoherent scattering and includes contributions from both the vegetation and the surface scattering along with a relatively simple accounting for their interaction. This model easily separates the three primary components of the scattering problem – the radar system, the geometry, and the environment, and then recombines them through a multiple convolution. The use of this simple model assumes that multiple interactions are insignificant and that only narrow-band signals and narrow-beamwidth antenna patterns are used.

Extending the basic model to volumes for which multiple scattering is important is accomplished with effective parameters. It is these effective parameters that are obtained by comparing the model with pulsed radar data at normal incidence, i.e., looking directly down through the foliage and onto the ground. Hence, the overall model is a hybrid approach wherein the basic physics are retained in the simple solution and are extended to a more complicated environment with effective parameters. By examining the model-based off-normal incidence, mean return waveforms, it is possible to estimate the degree of foliage penetration and subsequent surface scattering.

Alternate forms of this computationally efficient method for the determination of the scattered power density can be found in [Brown, 1977] for a rough surface and [Newkirk, 1996], [Adams, 1998] for a rough surface covering a penetrable volume. This approach creates a numerically efficient method since the incoherent return can be cast as a series of convolutions. Henceforth referred to as the Impulse Response approach, this method as applied to rough surfaces has been briefly reviewed in section 3.3. This idea has been extended to the volume response of vegetation over a rough surface.

4.1 Radiative Transfer

The geometry for the radiative transfer approach is given in Figure 4.1-1 below. In this figure, the first two boundaries' (enclosing the canopy) height statistics are described by the same random variable, $\xi(x)$ and the third (rough terrain) boundary's height statistics are described by the random variable, $\zeta(x)$. The mean heights of the layer boundaries, d_1 and d_2, are deterministic distances. Hence, we have implicitly assumed a zero mean surface with a layer of vegetation whose average thickness is d_1. This vegetative layer has mean height above ground equal to a constant, d_2.

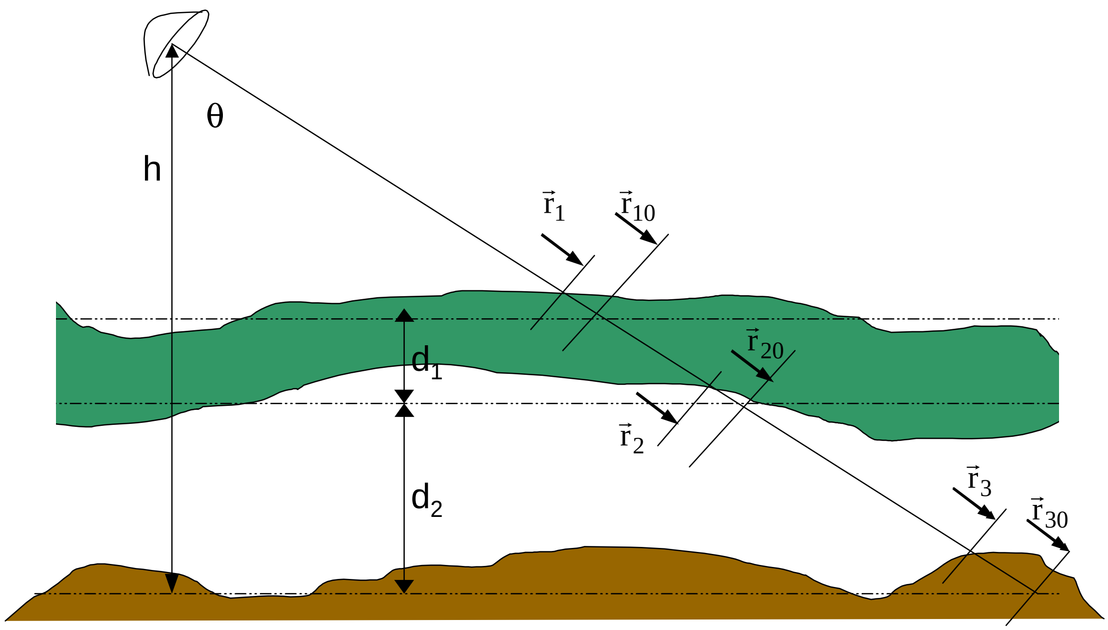

Figure 4.1-1: the geometry describing the volume and surface. Note that dotted lines indicate average levels for the associated boundary.

Beginning with a general form of the radiative transfer equation for the incoherent power density or the intensity in the medium, a simple form of the radiative transfer equation amenable to solution via convolution will be derived. The geometry for the general radiative transfer equation is given in Figure 5.1-1

Assuming that the scattering process is polarization insensitive, we will use the scalar radiative transfer equation, which relates the differential change in the power density over volume ds. This is written as (including the time dependent variation)

$$\frac{\partial I(\hat{s};\vec{r},t)}{\partial s} = -\rho\,\sigma_t I(\hat{s};\vec{r},t) + \frac{\rho\sigma_t}{4\pi}\iint_{4\pi} p(\hat{s},\hat{s}')I(\hat{s}';\vec{r},t)d\omega' + J_s(\hat{s};\vec{r}) - \frac{1}{c_s(\vec{r})}\frac{\partial}{\partial t}I(\hat{s};\vec{r},t)$$

Equation 4.1-1

where

- $I(\hat{s};\vec{r})$ is the power density in the $\hat{s}$ direction at the position: $\vec{r}$
- $\hat{s}$ is a direction of the power density
- ρ is the scatterer density
- $\sigma_t(\vec{r})$ is the scatterers total cross section which is the sum of the absorbing and scattering cross sections: $\sigma_t(\vec{r}) = \sigma_{abs}(\vec{r}) + \sigma_{sc}(\vec{r})$ and as written here, may be a function of position $\vec{r}$.
- $p(\hat{s},\hat{s}')$ is the scattering function of each scatterer; (prime denotes incident direction(s)) and is related to the amplitude of the field scattering function squared.
- $J_s(\hat{s};\vec{r})$ is the source function (emission sources)

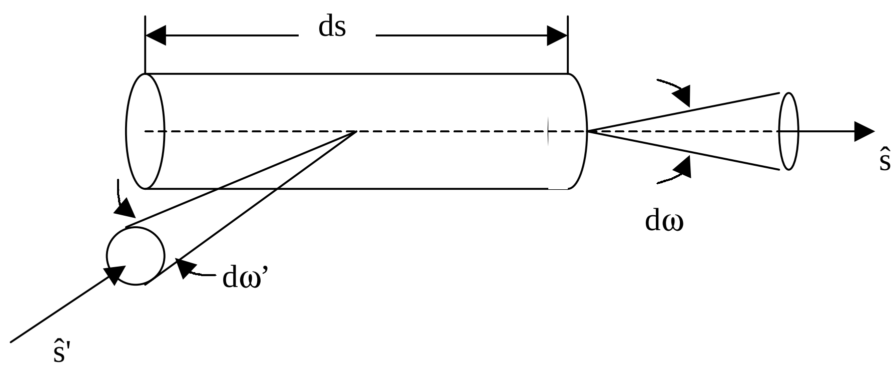

Figure 4.1-2: Scattering geometry for the intensity [Ishimaru, 1997]

Referring to Equation 4.1-1, the change in power in the $\hat{r}$ direction is proportional to the power incident on the differential volume element. This power is then depleted by absorption as well as scattering into other directions. On the other hand, the power, as it propagates through the differential volume, increases by an amount due to scattering into the $\hat{r}$ direction from other directions $\hat{r}'$ as well as energy emitted inside the differential volume:

We can now derive an impulse response representation by making the following assumption regarding the scattering function (or classically, the phase function), $p(\hat{r},\hat{r}')$. It will be assumed that each scatterer scatters energy in ***the forward and backward directions, exclusively***.

$$p(\hat{s},\hat{s}') = \frac{2}{\sigma_t}\left[\sigma_f \delta(\hat{s}'-\hat{s}) + \sigma_b \delta(\hat{s}'+\hat{s})\right]$$

where σ_f and σ_b are the position dependent forward and backward scattering cross section of each scatterer, respectively. These may be functions of depth into the medium, shown explicitly by the $\vec{r}$ dependence, as well as the scattering angle. In addition, we will assume that there are no emission sources present; consequently, the source term, $J_s(\hat{s};\vec{r})$, is zero. This is a good assumption for active sensing techniques [Ulaby, 1986].

With this scattering function assumed, the radiative transfer equation is recast into a greatly simplified form. Since the direction of power density propagation $\hat{s}$ has been limited to the radial direction, $\hat{r}$, the equation governing the power density can be written as a first order partial differential equation in two variables: time and distance. Implicitly assuming the $\vec{r}$ dependence in the cross section parameters, the simplified equation of transfer becomes

$$\frac{\partial I(\vec{r},\hat{r},t)}{\partial s} = -\rho_d\, \sigma_t I(\hat{r};\vec{r},t) + \rho\left[\sigma_f I(\hat{r};\vec{r},t) + \sigma_b I(-\hat{r};\vec{r},t)\right] - \frac{1}{c_s(\vec{r})}\frac{\partial I(\vec{r},\hat{r},t)}{\partial t}$$

$$\text{Initial Condition:} \quad I(\hat{r};\vec{r},t=t_0) = I(\vec{r},t_0)$$

Equation 4.1-2

In order to further simplify the equation of transfer, we split into it into two parts: downwelling, that power density which propagates in the forward hemisphere and upwelling, that power density which propagates in the backward hemisphere as defined by the direction of propagation, $\hat{r}$.

Let us first consider the downwelling intensity. In its solution, we will assume that the upwelling power density does not act as a source for the downwelling power density or $\sigma_b(r) = 0$. At this time, we consider this event to be second order scattering that may be neglected. Next, we define an effective extinction coefficient per unit volume $\tilde{k}_e(\vec{r}) = \rho\,\sigma_t(\vec{r}) - \rho\,\sigma_f(\vec{r})$. We then assume a medium that is radially distributed which results in the modified effective extinction coefficient: $\tilde{k}_e(r) = \rho\,\sigma_t(r) - \rho\,\sigma_f(r)$. Hence, implementing these assumptions, we find the greatly simplified equation

$$\frac{\partial\, I(\hat{r};\vec{r},t)}{\partial\, r} = -\,\tilde{k}_e(r)\, I(\hat{r}';\vec{r},t) - \frac{1}{c_s(\vec{r})}\frac{\partial\, I(\hat{r};\vec{r},t)}{\partial\, t}$$

Equation 4.1-3

Since it has been assumed that the upwelling power density does not contribute to the downwelling, there is no coupling of power from the upwelling into the downwelling. Consequently, given an initial power density at the upper foliage boundary with free space, $I_o(t - t')$ where t' is a range dependent delay, the solution for the downwelling power density is found in closed form.

The time-dependent nature of the radiative transfer equation has been removed using the method of characteristics. Rewriting the equation of transfer (for a single direction):

$$c_S(\vec{r})\frac{\partial\, I(r,t)}{\partial\, r} + \frac{\partial\, I(r,t)}{\partial\, t} = -\,c_S(\vec{r})\tilde{k}_e\, I(r,t)$$

$$\text{Initial Condition:} \quad I(r, t = t_0) = I(r, t_0)$$

Equation 4.1-4

Consequently, first parameterizing the variables along the characteristics $r = s;\ t = \tau$, we next solve the differential equations for the parameterized equations (assuming a constant speed of light for convenience)

$$\frac{dt(s,\tau)}{ds} = 1, \qquad \text{general solution: } t(s,\tau) = s + C_1$$

$$\text{with I.C.: } t(s = 0, \tau) = \tau \Rightarrow C_1 = \tau$$

$$\text{final solution: } t(s,\tau) = s + \tau$$

$$\frac{dr(s,\tau)}{ds} = c_0, \qquad \text{general solution: } r(s,\tau) = c_0 s + C_2$$

$$\text{with I.C.: } r(s=0,\tau) = (h-\zeta)\sec\theta \Rightarrow C_2 = (h-\zeta)\sec\theta$$

$$\text{final solution: } r(s,\tau) = c_0 s + (h-\zeta)\sec\theta$$

and solve for the characteristic variables:

$$s = \frac{r(s,\tau) - (h-\zeta)\sec\theta}{c_0},$$

$$\tau = t(s,\tau) - \frac{r(s,\tau) - (h-\zeta)\sec\theta}{c_0}$$

The equation of transfer is written

$$\frac{\partial I(r(s,\tau), t(s,\tau))}{\partial s} = \frac{\partial I(r(s,\tau), t(s,\tau))}{\partial r}\frac{\partial r}{\partial s} + \frac{\partial I(r(s,\tau), t(s,\tau))}{\partial t}\frac{\partial t}{\partial s} = -c_0 \tilde{k}_e I(r,t)$$

$$\text{Initial Condition: } \quad I(s_0,\tau) = I_0(\tau)$$

Equation 4.1-5

This has the solution

$$I(s,\tau) = I_0(\tau)\, e^{-c_0 \tilde{k}_e s}$$

Equation 4.1-6

The method of characteristics yields a time-shifted argument for the power density, while the distance dependence can be found by simple integration. For $r_1 = (r_{10} + \xi(x)\sec\theta)$, and a more general, depth-dependent wave propagation speed,

$$I(\hat{r}; r,\theta,\phi,t) = I_o\left(t - \frac{r_1}{c_0} - \int_{r_1}^{r} \frac{d\mu}{c_s(\mu)}\right)\exp\left\{-\int_{r_1}^{r} \tilde{k}_e(\mu)\, d\mu\right\}$$

Equation 4.1-7

where I_0 (t – t') is the time-delayed incident power envelope; the time delay is a function of the range in free space from the antenna to the canopy (r_1) and the range into the medium which may have a range dependent group velocity, $c_s(r)$. Note that the downwelling power density is directed in the $\hat{r}$ direction or along a radial path from the source antenna.

The differential equation governing the upwelling power density has a similar form; however, the downwelling power density acts as a source for the upwelling. In addition, the upwelling power density is directed in the $-\hat{r}$ direction or along a reverse radial path toward the source antenna. Consequently, the governing differential equation is the same with the exception of the coupling term relating the upwelling and the downwelling intensities. The differential equation governing the upwelling power density is expressed below.

$$\frac{\partial I(-\hat{r};\vec{r},t)}{\partial r} = -\tilde{k}_e(r)\, I(-\hat{r};\vec{r},t) - \frac{1}{c_s(\vec{r})}\frac{\partial I(-\hat{r},\hat{s},t)}{\partial t} + \sigma_b(r,\theta,\phi) I(\hat{r};r,t)$$

Equation 4.1-8

Subsequently, substituting the solution for the downwelling power density into Equation 4.1-8, the following differential equation is created governing the upwelling power density

$$\begin{aligned}\frac{\partial I(-\hat{r};\vec{r},t)}{\partial r} &= -\tilde{k}_e(r)\, I(-\hat{r};\vec{r},t) - \frac{1}{c_s(\vec{r})}\frac{\partial I(-\hat{r},\hat{s},t)}{\partial t} \\ &\quad + \sigma_b(r,\theta,\phi)\, I_o\left(t - \frac{r_1}{c_0} - \int_{r_1}^{r}\frac{d\mu}{c_s(\mu)}\right)\exp\left\{-\int_{r_1}^{r}\tilde{k}_e(\mu)\, d\mu\right\}\end{aligned}$$

Equation 4.1-9

The attenuated downwelling power density that passes through the foliage layer and is subsequently scattered by the underlying surface acts as a source for the upwelling power density at the foliage layer's lower boundary. In addition, the downwelling power density continuously contributes to the upwelling power density due to the coupling term. Note that this source was absent in the differential equation for the downwelling. Consequently, in formulating the solution, the upwelling power density has two independent sources: the power waveform backscattered by the surface and the backscattered downwelling power density from within the volume. Finally, the upwelling power density is evaluated at the top of the canopy ($r = r_1$). Again, invoking the method of characteristics as a solution method for the time dependence, the resulting solution of Equation 4.1-9 has two independent terms

$$I(-\hat{r}; r=r_1, \theta, \phi, t) = \sigma_s(\theta,\phi)\, I_o\left(t - \frac{r_1}{c_0} - 2\int_{r_1}^{r_3} \frac{d\mu}{c(\mu)} \right) \exp\left\{ -2\int_{r_1}^{r_3} \tilde{k}_e(\mu)\, d\mu \right\}$$
$$+ \int_{r_1}^{r_2} \sigma_b(\alpha)\, I_o\left(t - \frac{r_1}{c_0} - 2\int_{r_1}^{\alpha} \frac{d\mu}{c(\mu)} \right) \exp\left\{ -2\int_{r_1}^{\alpha} \tilde{k}_e(\mu)\, d\mu \right\} d\alpha$$

Equation 4.1-10

where

$\sigma_s(\theta,\phi) = \sigma_s^0(\theta,\phi)\, dA$, the surface's scattering cross section

$$r_1 = r_{10} + \xi(x)\sec\theta$$
$$r_2 = r_{10} + d_1 \sec\theta + \xi(x)\sec\theta$$
$$r_3 = r_{10} + (d_1 + d_2)\sec\theta + \zeta(x)\sec\theta$$

This expression shows a simple superposition of two terms; the first term is the rough surface return propagated back up through the foliage and the second term represents the foliage scattered return. In order to construct the average return power in the impulse response format, these two responses are averaged and manipulated to yield an impulse response term in each case. However, an additional assumption is necessary for a fully convolutional result similar to that given in the literature for a rough surface alone: the random variables, $\zeta(x)$ and $\xi(x)$, describing the canopy and the rough surface, respectively, must be assumed to be independent.

4.2 Incoherent Scattered Power: the Volume (Foliage) Return

In the formulation of the scattering from a rough surface with a vegetative cover, we have assumed that scattering occurs exclusively in the forward and backward directions; this implied that the power density in radial direction $\hat{r}$ does not interact with the power density in any other radial direction. This in turn has led to a closed form result for the downwelling intensity and consequently, an uncoupled relatively simple equation for the upwelling power density, Equation 4.1-10 in the previous section. The two terms of the solution in Equation 4.1-10 can be simplified independently. Each represents a different scattering phenomena, surface and volume scattering. In this section we examine the foliage or volume return.

We begin with the second term of Equation 4.1-10 for the upwelling power density, the volume response. After substitution for the slant range variables (r_1, r_2, …) with the associated distance and random variables as a function of antenna pointing angle, θ,

$$\begin{aligned} r_1 &= r_{10} + \xi(x)\sec\theta \\ r_2 &= r_{10} + d_1\sec\theta + \xi(x)\sec\theta \\ r_3 &= r_{10} + (d_1 + d_2)\sec\theta + \zeta(x)\sec\theta \end{aligned}$$

the power density is found to be approximated by the following

$$I(-\hat{r}; r, \theta, \phi, t) = \int_{r_{10}+\xi(x)\sec\theta}^{r_{10}+\xi(x)\sec\theta+d_1\sec\theta} \sigma_b(\alpha)\exp\left\{-2\int_{r_{10}+\xi(x)\sec\theta_1}^{\alpha} \tilde{k}_e(\mu)\,d\mu\right\}$$

$$\cdot\, I_o\left(t - \frac{(r_{10} + \xi(x)\sec\theta)}{c_0} - 2\int_{r_{10}+\xi(x)\sec\theta}^{\alpha} \frac{d\mu}{c(\mu)}\right) d\alpha$$

Equation 4.2-1

In general, following a slightly modified version of the method of Adams and Brown [1998a], and assuming a layered medium with parallel boundaries, the average power density can be expressed as

$$\left\langle I(-\hat{r}; r, \theta, \phi, t)\right\rangle = \int_{-\infty}^{\infty}\int_{r_{10}+\xi(x)\sec\theta}^{r_{10}+\xi(x)\sec\theta+d_1\sec\theta} \sigma_b(\alpha)\exp\left\{-2\int_{r_{10}+\xi(x)\sec\theta_1}^{\alpha} \tilde{k}_e(\mu)\,d\mu\right\}$$

$$\cdot\, I_o\left(t - \frac{(r_{10} + \xi(x)\sec\theta)}{c_0} - 2\int_{r_{10}+\xi(x)\sec\theta}^{\alpha} \frac{d\mu}{c(\mu)}\right) d\alpha\, p_{\xi}(\xi)\,d\xi$$

Equation 4.2-2

In order to create a convolutional form, the integration limits must be extended to infinity. The upper limit may be extended to infinity by *assuming that the extinction coefficient becomes very large once the range extends beyond the lower foliage* *boundary*; this will effectively eliminate the volume return after the lower foliage boundary is surpassed. The lower limit of integration, on the other hand, can be extended by the use of the unit step function, u(r - r_1). Consequently, the average power density can be rewritten in terms of integrals with infinite limits. Under the change of variables, $\mu' = \mu - [r_{10} + \xi(x)\sec\theta]$, the expression for the upwelling power density becomes

$$\langle I(-\hat{r};r,\theta,\phi,t)\rangle = \int_{-\infty}^{\infty}\int_{-\infty}^{\infty}\sigma_b(\alpha) I_o\left(t - \frac{(r_{10} + \xi(x)\sec\theta)}{c_0} - 2\int_0^{\alpha-[r_{10}+\xi(x)\sec\theta]}\frac{d\mu'}{c(\mu')} \right)$$

$$\cdot \exp\left\{-2\int_0^{\alpha-[r_{10}+\xi(x)\sec\theta]}\tilde{k}_e(\mu')d\mu'\right\} u(\alpha - [r_{10} + \xi(x)\sec\theta]) d\alpha\, p_\xi(\xi)\, d\xi$$

Equation 4.2-3

Assuming that there is no volume return from the atmosphere between the antenna and the foliage crown, the backscattering cross section, which is a function of distance, can also be shifted by the slant range. Defining two new functions

$$g(\gamma) = 2\int_0^{\gamma}\frac{d\mu'}{c(\mu')}$$

Equation 4.2-4

$$E(\gamma) = \sigma_b(\gamma)\exp\left\{ -2\int_0^{\gamma}\tilde{k}_e(\mu')d\mu' \right\} u(\gamma)$$

Equation 4.2-5

the average upwelling power density at the upper foliage layer can be rewritten

$$\langle I(-\hat{r};r,\theta,\phi,t)\rangle = \int_{-\infty}^{\infty}\int_{-\infty}^{\infty} I_o\left(t - \frac{r_1}{c_0} - g[\alpha - r_1]\right) E(\alpha - r_1) d\alpha\, p_\xi(\xi)\, d\xi$$

Equation 4.2-6

where it has been previously defined that $r_1 = (r_{10} + \xi(x)\sec\theta)$. Following the method of Adams and Brown, [1998a], the following definitions are constructed which transform distance into time

$$t' = g[\alpha - r_1] \qquad \Rightarrow \quad \alpha - r_1 = g^{-1}(t')$$

$$dt' = g'[\alpha - r_1]d\alpha = \quad g'(g^{-1}(t'))\, d\alpha$$

Substituting these expressions into the average upwelling power density of Equation 4.2-6, the average upwelling power density is reconstructed in the following form

$$\langle I(-\hat{r}; r, \theta, \phi, t)\rangle = \int_{-\infty}^{\infty}\int_{-\infty}^{\infty} I_o\left(t - \frac{r_1}{c_0} - t' \right)\frac{E(g^{-1}(t'))}{g'(g^{-1}(t'))} dt'\, p_\xi(\xi)\, d\xi$$

$$= \int_{-\infty}^{\infty}\int_{-\infty}^{\infty} I_o\left(t - \frac{r_1}{c_0} - t' \right)\tilde{E}(t')\, dt'\, p_\xi(\xi)\, d\xi$$

Equation 4.2-7

where a new function has been defined:

$$\tilde{E}(t) = \frac{E(g^{-1}(t))}{g'(g^{-1}(t))}$$

Noting that Equation 4.2-7 contains a convolution in the variable z, we perform the z integration, leaving the result in the form of a convolution (with convolution represented by the symbol: ⊗) shown in brackets below

$$\langle I(-\hat{r}; r = r_1, \theta, \phi, t)\rangle = \int_{-\infty}^{\infty} \left\{ I_o\left(t - \frac{r_1}{c_0} \right) \otimes \tilde{E}\left(t - \frac{r_1}{c_0} \right) \right\} p_\xi(\xi)\, d\xi$$

Equation 4.2-8

Substituting for the slant range in terms of the distance to the mean height and the random variable representing the distribution about the mean, i.e. $r_1 = (r_{10} + \xi(x)\sec\theta)$

$$\langle I(-\hat{r}; r = r_1, \theta, \phi, t)\rangle$$
$$= \int_{-\infty}^{\infty} \left\{ I_o\left(t - \frac{(r_{10} + \xi(x)\sec\theta)}{c_0} \right) \otimes \tilde{E}\left(t - \frac{(r_{10} + \xi(x)\sec\theta)}{c_0} \right) \right\} p_\xi(\xi)\, d\xi$$

Equation 4.2-9

First, we substitute for the constant delay term: we let

$$t_0 = \frac{r_{10}}{c_0}$$

Then we make a change of variables with respect to the random variable representing the crown height statistics; we form a new random variable and its associated probability density function

$$\tilde{\xi}(x) = \frac{\xi(x)\sec\theta}{c_0}$$

$$p_{\tilde{\xi}}(t) = \frac{c_0}{\sec\theta} p_{\xi}\left(\frac{c_0 t}{\sec\theta}\right)$$

Consequently, the average, upwelling power density becomes

$$\left\langle I(-\hat{r}; r = r_1, \theta, \phi, t)\right\rangle = \frac{c_0}{\sec\theta}\int_{-\infty}^{\infty}\left\{I_o\left(t - t_0 - \tilde{\xi}\right)\otimes\tilde{E}\left(t - t_0 - \tilde{\xi}\right)\right\}p_{\tilde{\xi}}(\tilde{\xi})\,d\tilde{\xi}$$

Equation 4.2-10

Again, the average, upwelling power density is re-expressed in the following convolutional form with respect to the modified surface height random variable

$$\left\langle I(-\hat{r}; r = r_1, \theta, \phi, t)\right\rangle = \frac{c_0}{\sec\theta} I_o\left(t - t_0\right)\otimes\tilde{E}\left(t - t_0\right)\otimes p_{\tilde{\xi}}(t - t_0)$$

Equation 4.2-11

Finally, in order to find the total power returning toward the radar, we integrate the power density over a surface. In this case, a convenient surface is the top of the canopy. Allowing for full penetration of the incident power density (i.e. no reflection from the boundary separating free space from the foliage), we substitute for the incident power density at the canopy (expressed in the { } brackets below) weighted by the antenna gain $G(\theta,\phi)$ in the direction (θ,ϕ),

$$I_0\left(\theta,\phi,t - t_0\right) = \frac{G(\theta,\phi)}{4\pi r_{10}^2} P_T\left(t - t_0\right)$$

Equation 4.2-12

Furthermore, we must assume a narrow beamwidth such that $\sec\theta \approx \sec\theta_0$ (boresight direction: θ_0). This is required since the integral to be performed over the radial coordinate implicitly contains θ dependence; otherwise, a convolutional form can not be obtained. For the power density traveling in the $\hat{r}$ direction:

$$\hat{r}\cdot d\bar{S} = \hat{r}\cdot\left(\nabla\xi - \hat{z}\right) r\,dr\,d\phi = \hat{r}\cdot\left(\nabla\xi - \hat{z}\right)\rho\,d\rho\,d\phi$$

Averaging over the slopes (assuming they are independent of the surface heights), we define the function:

$$t(\theta) = \left\langle \frac{\partial\xi}{\partial\rho}\sin\theta + \cos\theta \right\rangle_{\nabla\xi}$$

Allowing for the additional delay due to the transmission back to the antenna (an additional t_0) from the canopy and the receiving antenna's effective aperture, the following result is obtained

$$\begin{aligned}\left\langle P_R(t)\right\rangle = \int_0^{\infty}\int_0^{2\pi} \frac{c_0}{\sec\theta_0}\left\{\frac{G(\theta,\phi)}{4\pi r_{10}^2} t(\theta) P_T\left(t - 2t_0\right)\right\}\otimes\tilde{E}\left(t - 2t_0\right)\otimes p_{\tilde{\xi}}\left(t - 2t_0\right)\\ \cdot\frac{\lambda^2 G(\theta,\phi)}{(4\pi)^2 r_{10}^2}\, r_{10}\, d\phi\, dr_{10}\end{aligned}$$

Equation 4.2-13

substituting the original expression for t_0, we find

$$\begin{aligned}&\left\langle P_R(t)\right\rangle\\ &= \frac{c_0\, t(\theta_0)}{\sec\theta_0}\int_0^{\infty}\int_0^{2\pi}\left\{\frac{G(\theta,\phi)}{4\pi r_{10}^2} P_T\left(t - \frac{2r_{10}}{c_0}\right)\right\}\otimes\tilde{E}\left(t - \frac{2r_{10}}{c_0}\right)\otimes p_{\tilde{\xi}}\left(t - \frac{2r_{10}}{c_0}\right)\frac{\lambda^2 G(\theta,\phi)}{(4\pi)^2 r_{10}^2}\, r_{10}\, d\phi\, dr_{10}\\ &= \frac{\lambda^2}{(4\pi)^3}\frac{c_0 t(\theta_0)}{\sec\theta_0}\int_0^{\infty}\int_0^{2\pi}\left\{\frac{G^2(\theta,\phi)}{r_{10}^3} P_T\left(t - \frac{2r_{10}}{c_0}\right)\right\}\otimes\tilde{E}\left(t - \frac{2r_{10}}{c_0}\right)\otimes p_{\tilde{\xi}}\left(t - \frac{2r_{10}}{c_0}\right) d\phi\, dr_{10}\end{aligned}$$

Equation 4.2-14

Exploiting the shifting properties of the Dirac delta function and rearranging the resulting integrals yields

$$\langle P_R(t)\rangle = \frac{\lambda^2}{(4\pi)^3}\frac{c_0\, t(\theta_0)}{\sec\theta_0}\int_{-\infty}^{\infty} P_T(t-t')\otimes\tilde{E}(t-t')\otimes p_{\tilde{\xi}}(t-t')$$

$$\cdot\int_0^{\infty}\int_0^{2\pi}\frac{G^2(\theta,\phi)}{r_{10}^3}\,\delta\!\left(t'-\frac{2r_{10}}{c_0}\right)d\phi\, dr_{10}\, dt'$$

$$= \int_{-\infty}^{\infty}\left\{P_T(t-t')\otimes\tilde{E}(t-t')\otimes p_{\tilde{\xi}}(t-t')\right\}P_{FS'}(t')\, dt'$$

$$= P_T(t)\otimes\tilde{E}(t)\otimes p_{\tilde{\xi}}(t)\otimes P_{FS'}(t)$$

Equation 4.2-15

where the transmitted power waveform is given by $P_T(t)$ and the modified Flat Surface Impulse Response function is given by

$$P_{FS'}(t) = \frac{\lambda^2}{(4\pi)^3}\frac{c_0\, t(\theta_0)}{\sec\theta}\int_0^{\infty}\int_0^{2\pi}\frac{G^2(\theta,\phi)}{r_{10}^3}\,\delta\!\left(t-\frac{2r_{10}}{c_0}\right)d\phi\, dr_{10}$$

Equation 4.2-16

the modified probability density function for the crown height statistics is given by

$$p_{\tilde{\xi}}(t) = \frac{c_0}{\sec\theta_0}\, p_{\xi}\!\left(\frac{c_0 t}{\sec\theta_0}\right)$$

Equation 4.2-17

and $\tilde{E}(t)$ is a function relating decay to depth of penetration into the foliage layer

$$\tilde{E}(t) = \frac{E(g^{-1}(t))}{g'(g^{-1}(t))}$$

Equation 4.2-18

This general solution for the volume response can be modified to yield a simpler result. Assuming that the velocity is constant in each layer of the medium, the solution becomes more apparent. Here, we assume that medium 1 contains the leaves and branches (group velocity is c_{v1}) and medium 2 is the trunk region (group velocity c_{v2}).

The starting point for the upwelling power density due to the volume return (along a radial in the $\hat{r}$ direction) is then given by

$$I(-\hat{r}; r, \theta, \phi, t)$$
$$= \int_{r_{10}+\xi(x)\sec\theta_1}^{r_{10}+\xi(x)\sec\theta+d_1\sec\theta} I_o\left(t - \frac{2(r_{10}+\xi(x)\sec\theta)}{c_0} - \frac{2\left[\alpha - \left(r_{10}+\xi(x)\sec\theta\right)\right]}{c_{v1}} \right)$$
$$\cdot\, \sigma_b(\alpha) \exp\left\{ -2\int_{r_{10}+\xi(x)\sec\theta_1}^{\alpha} \tilde{k}_e(\mu)\, d\mu \right\} d\alpha$$

Equation 4.2-19

After following the previous procedure, the average power as a function of time, scattered from a volume with an irregular interface at the crown can be expressed in the convolutional form

$$\langle P(t) \rangle = P_T(t) \otimes P_{FS}(t) \otimes p_{\tilde{\xi}}(t) \otimes \tilde{E}(t)$$

Equation 4.2-20

where in this particular case,

$$t' = g(r') = \frac{2r'}{c} \;\Rightarrow\; r' = g^{-1}(t') = \frac{ct'}{2} \quad \text{and} \quad g'(r) = \frac{2}{c} = \text{constant}$$

Equation 4.2-21

Hence, for a group velocity in the volume given by c_v,

$$\tilde{E}(t) = \frac{E(g^{-1}(t))}{g'(g^{-1}(t))} = \frac{E\left(c_v t/2\right)}{2/c_v} = \frac{c_v}{2} \sigma_b \exp\left\{ -2\int_0^{c_v t/2} \tilde{k}_e(\mu')\, d\mu' \right\} u\left(c_v t/2\right)$$

Equation 4.2-22

Note that the unit step function u(t) “turns on” when t = 0.

4.3 Incoherent Scattered Power: the Rough Surface Return

We start with the expression for the power density attenuated by the foliage in its downward passage, scattered from the surface, and then attenuated by the foliage in its upward passage; this is the first term of Equation 4.1-10 in section 4.1. Note that the geometry of Figure 4.1-1 still applies

$$I(-\hat{r}; r = r_1, \theta, \phi, t) = \sigma_s(\theta,\phi)\, I_o\left(t - \frac{2r_1}{c_0} - 2\int_{r_1}^{r_3} \frac{d\mu}{c(\mu)} \right) \exp\left\{ -2\int_{r_1}^{r_3} \tilde{k}_e(\mu)\, d\mu \right\}$$

Equation 4.3-1

Substituting for the power density using the following relationship

$$I(r,\theta,\phi,t) = \frac{P_T(t)\, G(\theta,\phi)}{4\pi r^2}$$

Equation 4.3-2

where I is the power density (sometimes called intensity), P_T is the power waveform and the $\hat{r}$ direction is specified by the angles θ and ϕ. The average power returned from within the illuminated region can be evaluated by integrating over a surface encompassing the illuminated area. In this case, we choose to integrate over the area at the top of the canopy ($r = r_1$). Hence, substituting the power waveform for the incident power density in Equation 4.3-1 via the relationship in Equation 4.3-2 and performing the ensemble average over the random variables, the total average power *at the crown* is

$$\langle P(t) \rangle = \iint_{\substack{\text{surface at} \\ r\, =\, r_{10}}} \left\langle \sigma_s(\theta,\phi) \frac{G(\theta_a, \phi_a)}{4\pi r^2} P_T\left(t - \frac{r_1}{c_0} - 2\int_{r_1}^{r_3} \frac{d\mu}{c(\mu)} \right) \exp\left\{ -2\int_{r_1}^{r_3} \tilde{k}_e(\mu)\, d\mu \right\} \right\rangle dS$$

Equation 4.3-3

where the surface scattering cross section per unit area, $\sigma_s^0(\theta,\phi)$, has been included. The angles (θ,ϕ) are spherical coordinates centered at the antenna and can be related to the variables of integration. In addition, in this expression, the antenna gain has a boresight angle given by (θ_0, ϕ_0) and the angles (θ_a, ϕ_a) are spherical coordinates defined with respect to the antenna boresight direction, which may also be related to the variables of integration.

Although the solution procedure can proceed with a propagation speed, $c(\vec{r})$, and an effective extinction coefficient, $\tilde{k}_e(\vec{r})$ that vary with position as assumed in Equation

4.3-3, the following results are simplified since they are based on a constant group velocity and extinction coefficient in each layer.

- Free space, the group velocity is c_0
- Layer 1, the canopy region, the group velocity is c_{v1}, the effective extinction coefficient is $\tilde{k}_{e1},\ r \in (r_1, r_2)$
- Layer 2 the trunk region, the group velocity is c_{v2}, the effective extinction coefficient is $\tilde{k}_{e2},\ r \in (r_2, r_3)$

Hence, the integrals with respect to the radial distance within the argument of the transmitted power may be easily performed, yielding the average power *at the radar*

$$\langle P(t) \rangle = \iint\limits_{\substack{\text{surface at} \\ r = r_{10}}} \sigma_s^0(\theta,\phi) \cdot \left\langle \frac{\lambda^2 G^2(\theta_a,\phi_a)}{(4\pi)^3 r^4} P_T\left(t - \frac{2r_1}{c_0} - \frac{2(r_2 - r_1)}{c_{v1}} - \frac{2(r_3 - r_2)}{c_{v2}} \right) \exp\left\{ -2\int_{r_1}^{r_3} \tilde{k}_e(\mu)\, d\mu \right\} \right\rangle dS$$

Equation 4.3-4

The results will be cast in a convolutional form for the average returned power. After expanding the transmitted power waveform's delay time argument in terms of the random variables and constant terms,

$$\begin{aligned} r_1 &= r_{10} + \xi(x)\sec\theta \\ r_2 &= r_{10} + d_1 \sec\theta + \xi(x)\sec\theta \\ r_3 &= r_{10} + (d_1 + d_2)\sec\theta + \zeta(x)\sec\theta \end{aligned}$$

$$\begin{aligned} &\Rightarrow r_2 - r_1 = d_1 \sec\theta \\ &\Rightarrow r_3 - r_2 = d_2 \sec\theta + (\zeta(x) - \xi(x))\sec\theta \end{aligned}$$

and performing the integrations with respect to the extinction coefficients, the average return power as a function of time becomes

$$\left\langle P_R(t)\right\rangle = \iint\limits_{\substack{\text{Surface at}\\ r=r_{10}}} \frac{\lambda^2 G^2(\theta_a,\phi_a)}{(4\pi)^3 r^4}\sigma_s^0(\theta,\phi)$$

$$\cdot\int_{-\infty}^{\infty}\int_{-\infty}^{\infty} P_T\left(t-\frac{2r_{10}}{c_0}-\frac{2\xi(x)\sec\theta}{c_0}-\frac{2d_1\sec\theta}{c_{v1}}-\frac{2d_2\sec\theta}{c_{v2}}-\frac{2[\zeta(x)-\xi(x)]\sec\theta}{c_{v2}}\right)$$

$$\cdot\ \exp\left\{-2\tilde{k}_{e1}d_1\sec\theta-2\tilde{k}_{e2}(d_2+\zeta(x)-\xi(x))\sec\theta\right\}p_{\xi\zeta}(\xi,\zeta)d\xi d\zeta\, rdrd\phi$$

Equation 4.3-5

where $p_{\xi\zeta}(\xi,\zeta)$ is the joint probability density functions for the boundary heights of the foliage volume and the rough surface and for the power density traveling in the $\hat{r}$ direction:

$$\hat{r}\cdot d\bar{S}=\hat{r}\cdot(\nabla\xi-\hat{z})r\,dr\,d\phi=\hat{r}\cdot(\nabla\xi-\hat{z})\rho\,d\rho\,d\phi$$

Averaging over the slopes (assuming they are independent of the surface heights), we define the function:

$$t(\theta)=\left\langle\frac{\partial\xi}{\partial\rho}\sin\theta+\cos\theta\right\rangle_{\nabla\xi}$$

Equation 4.3-6

If the surface statistics are independent of the canopy height statistics, we write this as

$$\left\langle P_R(t)\right\rangle = \iint\limits_{\substack{\text{Surface at}\\ r=r_{10}}} \frac{\lambda^2 G^2(\theta_a,\phi_a)}{(4\pi)^3 r^4}\sigma_s^0(\theta,\phi)\,t(\theta)$$

$$\cdot\int_{-\infty}^{\infty}\int_{-\infty}^{\infty} P_T\left(t-\frac{2r_{10}}{c_0}-\frac{2\xi(x)\sec\theta}{c_0}-\frac{2d_1\sec\theta}{c_{v1}}-\frac{2d_2\sec\theta}{c_{v2}}-\frac{2[\zeta(x)-\xi(x)]\sec\theta}{c_{v2}}\right)$$

$$\cdot\ \exp\left\{-2\tilde{k}_{e1}d_1\sec\theta-2\tilde{k}_{e2}(d_2+\zeta(x)-\xi(x))\sec\theta\right\}p_{\xi}(\xi)p_{\zeta}(\zeta)\,d\xi d\zeta\, rdrd\phi$$

Equation 4.3-7

where $p_\xi(\xi)$ and $p_\zeta(\zeta)$ are the independent probability density functions for the boundary heights of the foliage volume and the rough surface, respectively. Rearranging and substituting for the constant terms, Equation 4.3-7 is rewritten

$$\left\langle P_R(t)\right\rangle = \iint_{\substack{\text{Surface at}\\ r=r_{10}}} \frac{\lambda^2 G^2(\theta_a,\phi_a)}{(4\pi)^3 r^4}\sigma_s^0(\theta,\phi)\, t(\theta)\exp\left\{-2\sec\theta\left(\tilde{k}_{e1}d_1+\tilde{k}_{e2}d_2\right)\right\}$$

$$\cdot\int_{-\infty}^{\infty}\int_{-\infty}^{\infty} P_T\left(t - t_0 - \frac{2\xi(x)\sec\theta}{c_a} - \frac{2\zeta(x)\sec\theta}{c_{v2}} \right)$$

$$\cdot\exp\left\{2\tilde{k}_{e2}\,\xi(x)\sec\theta\right\}p_\xi(\xi)d\xi\exp\left\{-2\tilde{k}_{e2}\zeta(x)\sec\theta\right\}p_\zeta(\zeta)\,d\zeta\, r\,dr\,d\phi$$

Equation 4.3-8

where $\tilde{k}_{e1}, \tilde{k}_{e2}$ are the effective extinction coefficients in medium 1 and 2, respectively ; and

$$t_0 = \frac{2r_{10}}{c_0} - \frac{2d_1\sec\theta}{c_{v1}} - \frac{2d_2\sec\theta}{c_{v2}}$$

$$\frac{1}{c_a} = \left(\frac{1}{c_0} - \frac{1}{c_{v2}}\right) \quad \text{or} \quad c_a = \frac{c_0\, c_{v2}}{c_{v2} - c_0}$$

Performing a change of variables which transform distance into time

$$t_1 = \frac{2\zeta(x)\sec\theta}{c_{v2}} \quad \Rightarrow \quad d\zeta = \frac{c_{v2}}{2\sec\theta}dt_1$$
$$t_2 = \frac{2\xi(x)\sec\theta}{c_a} \quad \Rightarrow \quad d\xi = \frac{c_a}{2\sec\theta}dt_2$$

and defining some new functions,

$$f_{t1}(t_1) = \exp\left\{-\tilde{k}_{e2}\, c_{v2}t_1\right\}p_{t1}(t_1)$$
$$f_{t2}(t_2) = \exp\left\{\tilde{k}_{e2}\, c_a t_2\right\}p_{t2}(t_2)$$

Noting that the probability density functions describing the boundaries must also be transformed,

$$p_{t1}(t_1) = \frac{c_{v2}}{2\sec\theta} p_\zeta\left(\frac{c_{v2}t_1}{2\sec\theta}\right)$$
$$p_{t2}(t_2) = \frac{c_a}{2\sec\theta} p_\xi\left(\frac{c_a t_2}{2\sec\theta}\right)$$

we find that the average returned power can be expressed as

$$\langle P_R(t)\rangle = \iint_{\substack{\text{Surface at}\\ r=r_{10}}} \frac{\lambda^2 G^2(\theta_a,\phi_a)}{(4\pi)^3 r_{10}^4} t(\theta)\sigma_s(\theta,\phi)\exp\left\{-2\sec\theta\left(\tilde{k}_{e1}d_1+\tilde{k}_{e2}d_2\right)\right\}$$
$$\frac{c_a c_{v2}}{4\sec^2\theta}\int_{-\infty}^{\infty}\int_{-\infty}^{\infty} P_T\left(t-t_0-t_1-t_2\right) f_{t1}(t_1)\,dt_1\, f_{t2}(t_2)\,dt_2\, r_{10}\,dr_{10}d\phi$$

Equation 4.3-9

Introducing a delta function and using its integration properties, we rewrite the above as

$$\langle P_R(t)\rangle = \iint_{\substack{\text{Surface at}\\ r=r_{10}}} \frac{\lambda^2 G^2(\theta_a,\phi_a)}{(4\pi)^3 r_{10}^4} t(\theta)\sigma_s(\theta,\phi)\exp\left\{-2\sec\theta\left(\tilde{k}_{e1}d_1+\tilde{k}_{e2}d_2\right)\right\}$$
$$\frac{c_a c_{v2}}{4\sec^2\theta}\int_{-\infty}^{\infty}\int_{-\infty}^{\infty} P_T\left(t-t_0-t_1-t_2\right) f_{t1}(t_1)\,dt_1\, f_{t2}(t_2)\,dt_2\, r_{10}\,dr_{10}d\phi$$

Equation 4.3-10

Performing the t_1 and the t_2 integrations and expressing the result in convolutional form, which is represented with the $\otimes$ symbol, we find

$$\langle P_r(t)\rangle = \iint_{\substack{\text{Surface at}\\ r=r_{10}}} \frac{c_a c_{v2}}{4\sec^2\theta}\frac{\lambda^2 G^2(\theta_a,\phi_a)}{(4\pi)^3 r_{10}^4} t(\theta)\sigma_s^0(\theta,\phi)\cdot\exp\left\{-2\sec\theta(\tilde{k}_{e1}d_1+\tilde{k}_{e2}d_2)\right\}$$
$$\cdot\left[P_T(t-t_0)\otimes f_{t1}(t-t_0)\otimes f_{t2}(t-t_0)\right] r_{10}\,dr_{10}\,d\phi$$

Equation 4.3-11

Integrating over the foliage upper surface, the returned power can be recast into the following convolutional form, following the methods outlined in previous section.

$$\langle P_r(t)\rangle = P_T(t)\otimes f_{t1}(t)\otimes f_{t2}(t)\otimes P_{FS'}(t)$$

Equation 4.3-12

where $f_{t1}(t)$ and $f_{t2}(t)$ are functions which depend on the probability density functions whose random variables are functions of the random variables representing the surface and canopy statistics, $\xi(x), \zeta(x)$ as well as the extinction coefficients, and the antenna boresight angle, θ. The flat surface impulse response function (FSIR), $P_{FS'}(t)$, is similar to the standard FSIR with the modifications (among others) that account for attenuation:

$$P_{FS'}(t) = \frac{\lambda^2 c_a c_{v2}}{4(4\pi)^3}\int_0^{\infty}\int_0^{2\pi}\frac{\delta\left(t-2r'/c\right)}{(r')^4}\frac{G^2(\theta_a,\phi_a)\,\sigma_s^0(\theta,\phi)}{\sec^2\theta}\,t(\theta)$$

$$\cdot\exp\left\{-2\sec\theta(\tilde{k}_{e1}d_1+\tilde{k}_{e2}d_2)\right\}r'\,dr'\,d\phi$$

Equation 4.3-13

Here the antenna gain is approximated by a circularly symmetric pattern with a pointing angle given by (θ_0,ϕ_0) and the angles (θ_a,ϕ_a) are spherical coordinates defined with respect to the antenna boresight direction. Consequently, the antenna gain can be represented by

$$G(\theta_a,\phi_a) = G_0(\theta_0,\phi_0)\exp\left\{-\frac{2}{\gamma}\sin^2\theta_a\right\}$$

Equation 4.3-14

This expression Equation 4.3-13 for the FSIR includes additional effective parameters related to the speeds in the different media, the incidence angle, and consequently, time or range:

$$h' = \frac{c_0}{c_{v1}} d_1 + \frac{c_0}{c_{v2}} d_2 + h$$

$$(r')^2 = (h')^2 + \rho^2$$

The integral for the FSIR can be simplified using the method presented in Brown [1977]; we begin by substituting the two-way incremental ranging time for the actual time: $\tau = t - {}^{2r'}\!/_{c}$. *Assuming that the beam is narrow* such that the surface incremental cross section is constant over the angular extent of interest and that $\sec\theta \cong \sec\theta_0$ (boresight) and the surface is locally flat, the FSIR is found in the following form

$$P_{FS'}(\tau) = \frac{\lambda^2 c_0 c_a c_{v2} (h')^2 G_0^2(\theta_0, \phi_0) \sigma_s^0(\theta_0, \phi_0)}{16\pi^3 (c_0\tau + 2h')^5} \exp\left\{ -\left(\frac{c_0\tau + 2h'}{h'} \right) (\tilde{k}_{e1} d_1 + \tilde{k}_{e2} d_2) \right\}$$

$$\cdot \int_0^{2\pi} \exp\left\{ -\frac{4}{\gamma} \sin^2 \theta_a \right\} d\phi$$

Equation 4.3-15

Note this expression can include an asymmetrical antenna pattern [Newkirk and Brown, 1992]. Summarizing, the final form of the solution to the average power returned due only to the rough surface could be expressed in the following convolutional form,

$$\langle P_r(t) \rangle = P_T(t) \otimes f_{t1}(t_1) \otimes f_{t2}(t_2) \otimes P_{FS'}(t)$$

Equation 4.3-16

where $f_{t1}(t_1)$ and $f_{t2}(t_2)$ are functions of time which depend on random variables which are functions of the surface and canopy statistics, $\xi(x), \zeta(x)$, as well as the extinction coefficients, and the pointing angle:

$$t_1 = \frac{2\zeta(x) \sec\theta}{c_{v2}} \quad \Rightarrow \quad p_{t1}(t_1) = \frac{c_{v2}}{2\sec\theta} p_\zeta\left(\frac{c_{v2} t_1}{2\sec\theta} \right)$$

$$t_2 = \frac{2\xi(x) \sec\theta}{c_a} \quad \Rightarrow \quad p_{t2}(t_2) = \frac{c_a}{2\sec\theta} p_\xi\left(\frac{c_a t_2}{2\sec\theta} \right)$$

$$f_{t1}(t_1) = \exp\left\{-\tilde{k}_{e2}\, c_{v2} t_1\right\} p_{t1}(t_1)$$
$$f_{t2}(t_2) = \exp\left\{\tilde{k}_{e2}\, c_a t_2\right\} p_{t2}(t_2)$$

Equation 4.3-17

The modified Flat Surface Impulse Response is given by

$$P_{FS'}(t) = \frac{\lambda^2 c_a c_{v2}}{4(4\pi)^3} \exp\left\{-2\sec\theta(\tilde{k}_{e1} d_1 + \tilde{k}_{e2} d_2)\right\}$$
$$\cdot \int_0^{\infty}\int_0^{2\pi} \frac{\delta\left(t - 2r'/c\right)}{(r')^4} \frac{G^2(\theta_a,\phi_a)\,\sigma_s^0(\theta,\phi)}{\sec^2\theta}\, t(\theta)\ \rho\, d\rho\, d\phi$$

Equation 4.3-18

for layered media with a constant velocity in each medium and where $\tilde{k}_{e1}$, $\tilde{k}_{e2}$ are the effective extinction coefficients in medium 1 (foliage region) and medium 2 (trunk region), respectively.

Computationally, for the specific case in which the propagation speed of the "trunk" region is equal to that of free space, one of the convolutions is no longer necessary and the average power returned takes the following form.

$$\langle P_R(t)\rangle = \iint_{\substack{\text{Surface at}\\ r = r_{10}}} \frac{\lambda^2 G^2(\theta_a,\phi_a)}{(4\pi)^3 r^4} \sigma_s^0(\theta,\phi) \exp\left\{-2\sec\theta\left(\tilde{k}_{e1} d_1 + \tilde{k}_{e2} d_2\right)\right\}$$
$$\cdot \int_{-\infty}^{\infty} \exp\left\{2\tilde{k}_{e2}\,\xi(x)\sec\theta\right\} p_\xi(\xi)\ d\xi$$
$$\cdot \int_{-\infty}^{\infty} P_T\left(t - t_0 - \frac{2\zeta(x)\sec\theta}{c_{v2}}\right) \exp\left\{-2\tilde{k}_{e2}\zeta(x)\sec\theta\right\} p_\zeta(\zeta)\, d\zeta\, r\, dr\, d\phi$$

Equation 4.3-19

The expectation over the canopy statistics may be performed analytically if a Gaussian distribution is assumed for the roughness.

$$\int_{-\infty}^{\infty} e^{2\tilde{k}_{e2}\,\xi(x)\sec\theta}\left[\frac{1}{\sqrt{2\pi}\sigma_{canopy}}\exp\left\{-\frac{\xi^2}{2\sigma_{canopy}^2}\right\}\right]d\xi = \exp\left\{2\tilde{k}_{e2}^2\,\sigma_{canopy}^2\sec^2\theta\right\}$$

Equation 4.3-20

and the power returned is rewritten in the following (computationally) simpler form

$$\langle P_r(t)\rangle = P_T(t)\otimes f_{t1}(t_1)\otimes P_{FS'}(t)$$

where the flat surface impulse response is now given by

$$P_{FS'}(t) = \frac{\lambda^2 c_{v2}}{2(4\pi)^3}G^2(\theta_a,\phi_a)\,\sigma_s^0(\theta,\phi) \cdot \int_0^{\infty}\int_0^{2\pi}\frac{\delta\left(t-2r'/c\right)}{(r')^4\sec(\theta)}\,e^{2\tilde{k}_{e2}^2\,\sigma_{canopy}^2\sec^2\theta}\,e^{-2\sec\theta(\tilde{k}_{e1}d_1+\tilde{k}_{e2}d_2)}\,\rho\,d\rho\,d\phi$$

Equation 4.3-21

with a change a variables $\left(r' = \tilde{r} + \frac{ct}{2}\right)$ and some properties of the delta function

$$\begin{aligned}P_{FS'}(t) &= \frac{\lambda^2 c_{v2}}{2(4\pi)^3}G^2(\theta_a,\phi_a)\,\sigma_s^0(\theta,\phi) \cdot \int_0^{\infty}\int_{-\frac{ct}{2}}^{2\pi}\frac{\delta(\tilde{r})}{(r')^4\sec(\theta)}\,e^{2\tilde{k}_{e2}^2\,\sigma_{canopy}^2\sec^2\theta}\,e^{-2\sec\theta(\tilde{k}_{e1}d_1+\tilde{k}_{e2}d_2)}\,\rho\,d\rho\,d\phi\\ &= \frac{\lambda^2 c_{v2}}{2(4\pi)^3}G^2(\theta_a,\phi_a)\,\sigma_s^0(\theta,\phi) \cdot \int_0^{\infty}\int_0^{2\pi}\frac{\delta\left(t-2r'/c\right)}{(r')^4\sec(\theta)}\,e^{2\tilde{k}_{e2}^2\,\sigma_{canopy}^2\sec^2\theta}\,e^{-2\sec\theta(\tilde{k}_{e1}d_1+\tilde{k}_{e2}d_2)}\,\rho\,d\rho\,d\phi\end{aligned}$$

Equation 4.3-22

4.4 Convolutional Model Results

Previously noted limitations of this radiative transfer result have included a limited scattering pattern for each volume scatterer. The chosen scattering pattern demands strictly forward scattering and backward scattering. This assumptions decreases the number of coupled differential equations from N (when N scattering directions are used in a quadrature approximation to the integral in the radiative transfer equation) down to two: coupled integral equations, one governing forward and one reverse scattering. Secondly, the upward propagating power density is assumed not to influence the downward propagating power density. This last assumption is key since it allows a closed form solution for the downward propagating power density. Otherwise, the solution would be in the form of two coupled differential equations. Finally, the antenna is assumed to have a narrow beamwidth and the transmitted pulse is narrowband.

As a simple example, a simulation for a layered medium with a constant propagation speed and constant extinction coefficient in each layer was performed. The results are shown in the following figures. The assumed parameters of the radar system are as follows:

- Radar: Matched Filter, 1 kW transmit power
- Waveform: Square Pulse with 5 ns pulse length
- Antenna: Gaussian pattern, 0.5 to 5 degree beamwidth, nadir pointed

The medium is assumed to have the following bulk propagation properties (arbitrary estimates since no data was available) and Gaussian statistics:

1. The foliage layer
   - 15 meter thickness
   - effective extinction coefficient as noted
   - group velocity; free space
   - Gaussian boundary statistics; variance of the heights: 1 m
   - backscatter to forward scatter cross-section, σ_f / σ_b : 500
   - absorption to total scattering cross-section, σ_a / σ_t : 0.9 (albedo)
2. The trunk layer
   - 5 meter thickness
   - effective extinction coefficient as noted
   - group velocity: free space
   - backscatter to forward scatter cross-section, σ_f / σ_b : 500
   - absorption to total scattering cross-section, σ_a / σ_t : 0.9

3. The ground layer
   - perfect electric conductor (PEC)
   - Gaussian statistics; variance of the heights: 0.3 m

The following results are based on derived data gathered from some measurements made by Ulaby [1988]. From these measurements, the parameters for the scattering amplitude described by Schwering were quantified. The Schwering amplitude scattering model is written as follows

$$p(\cos\theta) = (1-\alpha) + \alpha\, e^{-\left(\frac{\cos\theta}{2\cos\theta_0}\right)^2}$$

Equation 4.4-1

This model describes isotropic scattering in all directions with the exception of the forward direction, see Figure 4.4-1. In the forward direction, the amplitude is much larger and is described by a Gaussian beam. The parameter, α, is related to the ratio of the forward scattering lobe to the isotropic background. Since the convolutional model predicts only forward-backward scattering, α is considered to be

$$\alpha \quad = (1 - \text{forward-backward ratio}) = 1 - 1/500$$

So that given an extinction cross section, σ_e, and an albedo, W, the forward backward scattering cross sections can be derived.

$$\sigma_s = \sigma_f + \sigma_b = \sigma_f + (1-\alpha)\sigma_f = W\,\sigma_e$$

$$W = \text{albedo} = (\sigma_s/(\sigma_s + \sigma_a)) = 0.9$$

where σ_e, σ_s, σ_a = extinction scattering, absorption cross sections, respectively. Under high-moisture content conditions (referred to as “wet” in the following figures), Ulaby measured the ratio of the forward scattering lobe to the isotropic to be 500-to-1 and an extinction coefficient of 6 nepers per meter at 35 GHz. Other frequency parameters were scaled by the frequency to the three-quarters power.

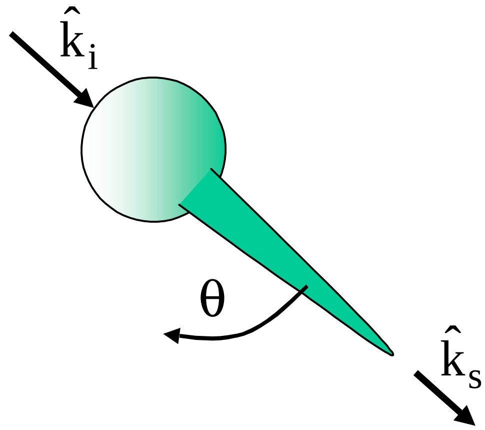

Figure 4.4-1: Schwering's scattering amplitude

Figure 4.4-2 shows the effect of canopy "roughness" on the return power waveform, the first "hump" in the waveform. Although the waveforms align at some portions, the leading edge of the return (the volume/foliage return) is "smeared" out by the roughness. Mathematically, this is a result of the convolution with the pdf of the air-canopy interface. When the standard deviation of the heights approaches zero, this convolution is with a delta function and the interface has no effect. However, the pdf "spreads out" as the roughness is made larger. Consequently, the return power waveform is more greatly affected, as the roughness becomes larger. The surface return behaves in a similar fashion. As the surface roughness is increased, the surface return "smears" as well. However, in this and the remaining simulations, the surface roughness is held constant. The surface return, average power waveform is the second "hump" in Figure 4.4-2.

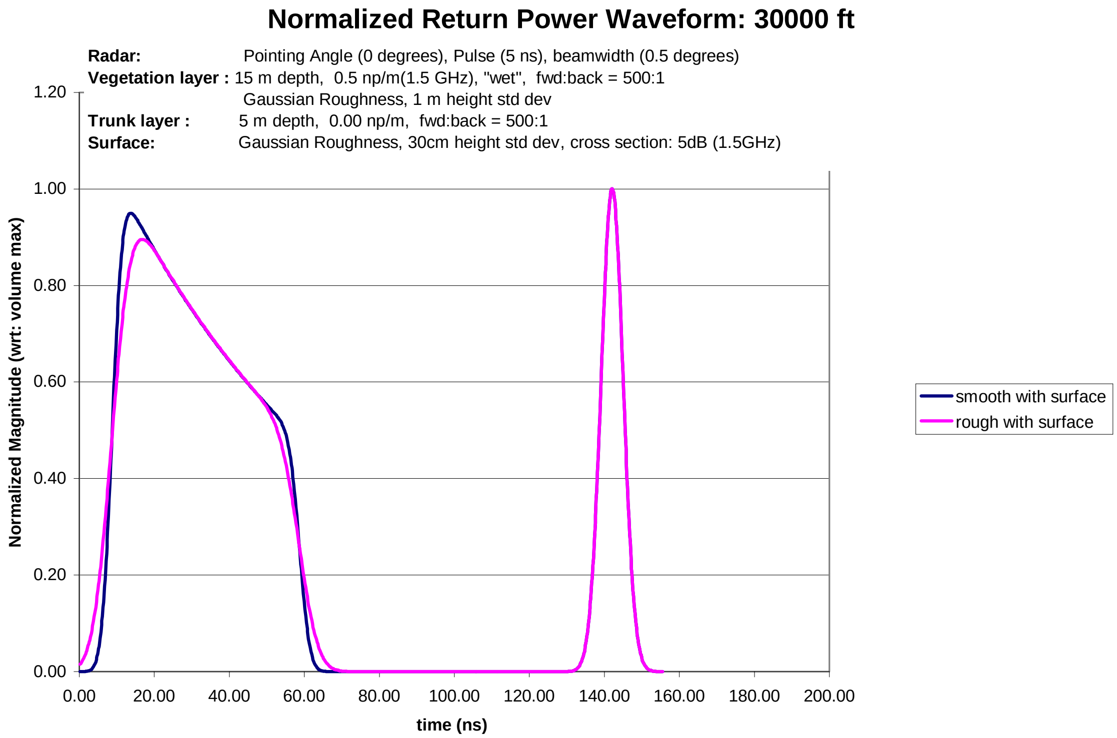

Figure 4.4-2: Air-canopy interface roughness effects on the return waveform

Ideally, the return waveform will have distinct features in the volume return and the surface return is distinct. The best case for discerning features will employ narrow beamwidth antennas, low altitudes and a nadir-pointing angle. In addition, a smaller extinction coefficient will result in a greater ability to penetrate the foliage. In addition to the volume return and the surface returns, a point target has been added to the model in a manner consistent with the formulation of the model. In other words, the return from the target is simply superimposed on the returns from the foliage-surface return. Consequently, there is an assumption that no multiple scattering occurs between the target and the surface or the foliage.

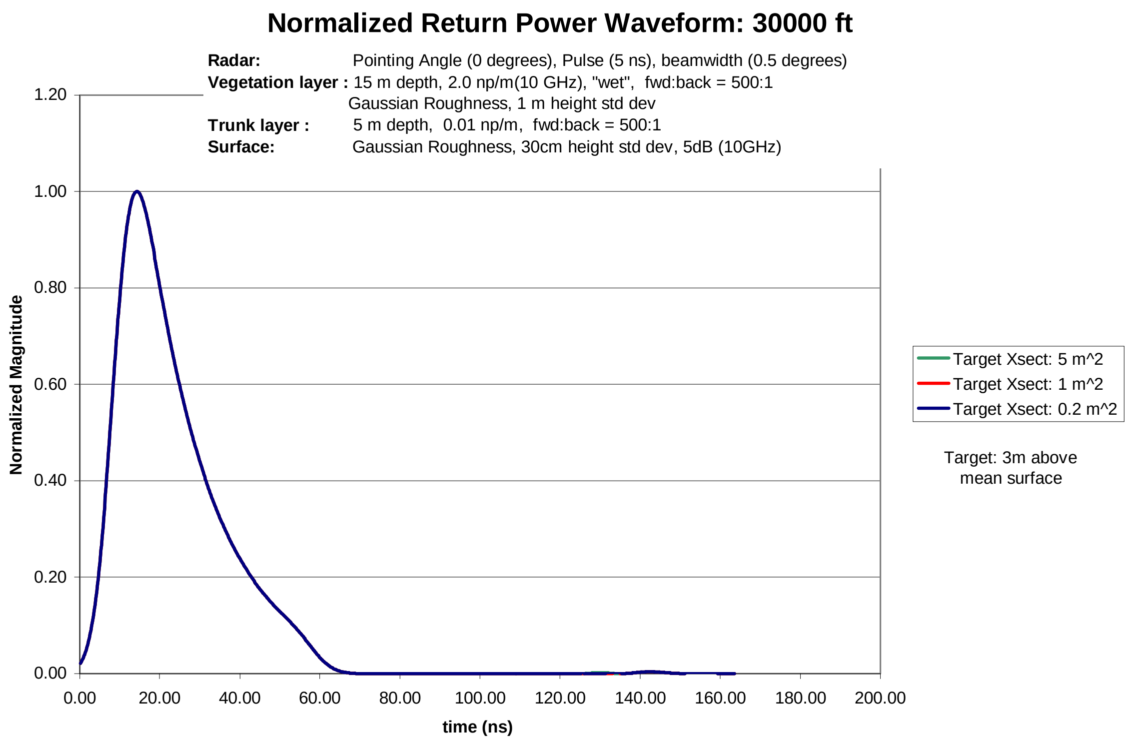

Figure 4.4-3: Average power returned from "wet" foliage at 10 GHz for different target cross sections.

In Figure 4.4-4 the extinction coefficient has been reduced in a manner consistent with the "dry" foliage conditions assumed in this chapter. Here we can see that the target has begun to emerge from the return waveforms attributed to the surface and the foliage.

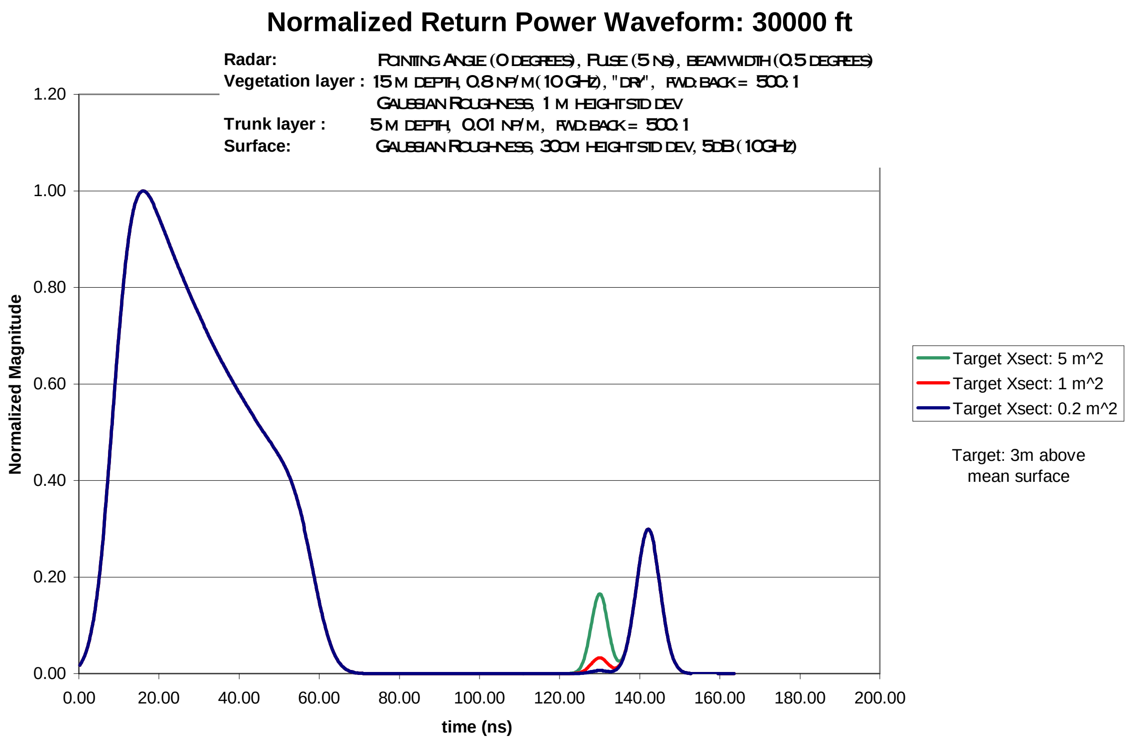

Figure 4.4-4: Average power returned from “dry” foliage at 10 GHz for different target cross sections.

Finally at 1.5 GHz, even in the wet foliage conditions, the target is visible and distinct from the surface and foliage average power waveforms in Figure 4.4-5. Figure 4.4-6 shows the target clearly visible at 1.5 GHz under the “dry” conditions.

The returned power waveform must also be compared to the noise power level. Given the power pattern of the antenna, $P(\theta,\phi)$, the antenna noise temperature due to an extended target with a temperature distribution, $T(\theta,\phi)$, such as the earth in remote sensing, is calculated as [Stutzman, 1998]

$$T_A = \frac{1}{\Omega_A}\int_0^{\pi}\int_0^{2\pi} T(\theta,\phi)P(\theta,\phi)\,d\Omega$$

Equation 4.4-2

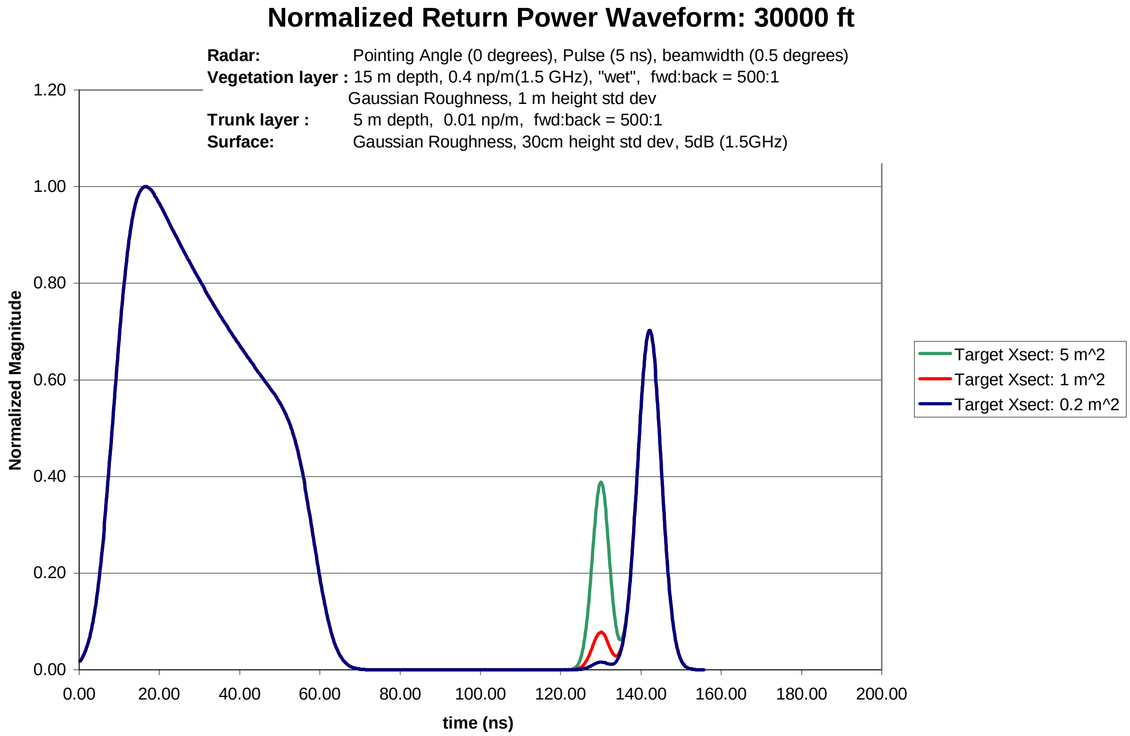

Figure 4.4-5: Average power returned from "wet" foliage at 1.5 GHz for different target cross sections.

For a constant temperature distribution, T_0, this simplifies considerably to

$$T_A = \frac{1}{\Omega_A} \int_0^{\pi} \int_0^{2\pi} T_0 \, P(\theta,\phi) d\Omega = \frac{T_0}{\Omega_A} \int_0^{\pi} \int_0^{2\pi} P(\theta,\phi) d\Omega = \frac{T_0}{\Omega_A} \Omega_A = T_0$$

Equation 4.4-3

Consequently, the noise power for a 35°C Earth and a 10 ns pulse length becomes

$$P_N = k\, T_{sys}\, B = 1.38 \times 10^{-23} (273 + 35) \left(\frac{1}{10^{-8}} \right) = 4.112 \times 10^{-13} \mathrm{W}$$

The signal-to-noise level at the matched filter receiver can now be determined. Figure 4.4-7 shows the signal-to-noise ratio under ideal conditions; "dry" foliage at 1.5 GHz.

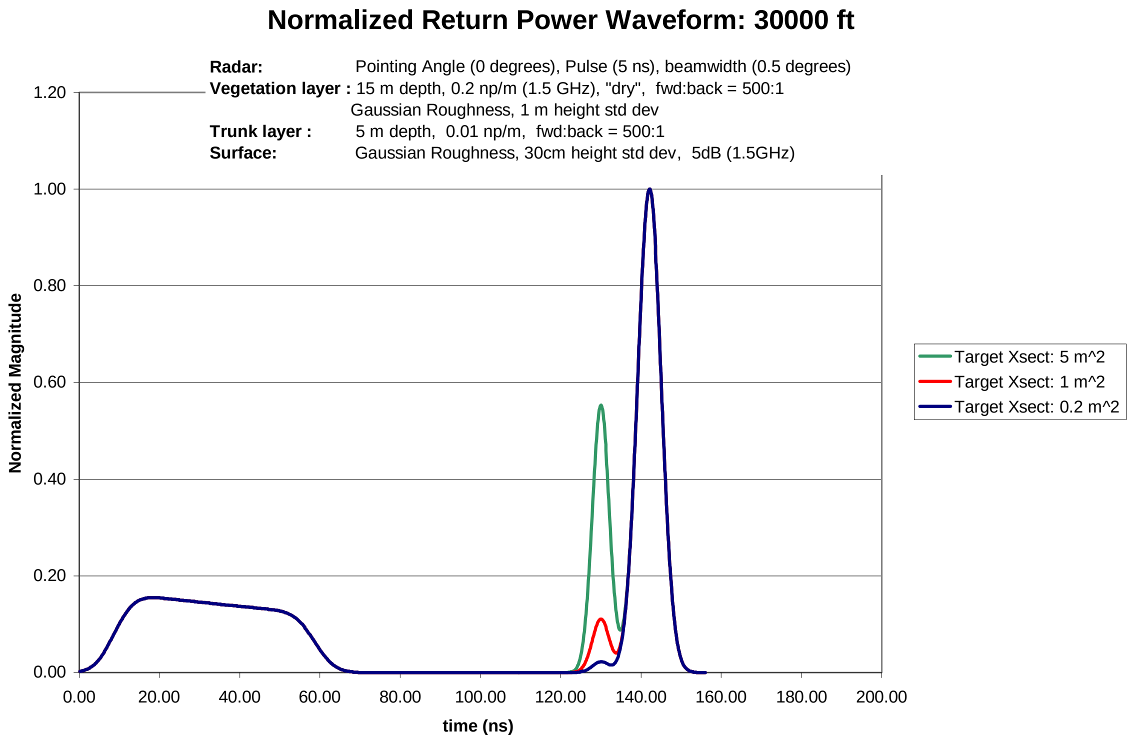

Figure 4.4-6: Average power returned from "dry" foliage at 1.5 GHz for different target cross sections.

Recall that each of these results given for the foliage penetration and subsequent target detection occurs with ideal radar parameters:

- the beamwidth is narrow, 0.5 degree
- the altitude is 30,000 ft
- the antenna is pointed directly downward (nadir),
- and the surface roughness is consistent with road surfaces.

As these parameters are varied, the foliage and surface returns will "smear," masking the target in their waveforms. These detrimental effects are confounded by the increase of the extinction through the foliage, and the target cross section.

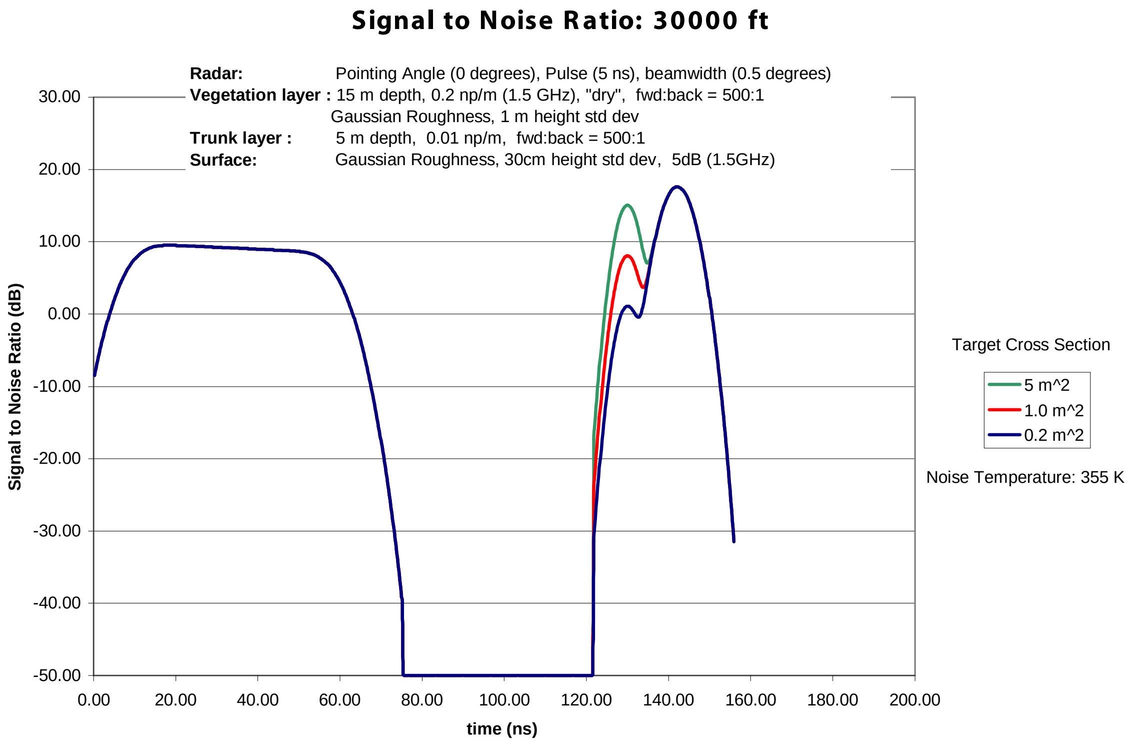

Figure 4.4-7: Signal-to-Noise ratio at 1.5 GHz under "dry conditions.

In the remaining figures, the effects of some of these factors are explored. Specifically, the radar platform altitude and the beamwidth are varied. In addition to the foliage and surface return waveforms, a point target has been included. This target has a 0.5 meter-squared cross section and lies 3 meters above the mean surface. Figure 4.4-8 again shows ideal conditions including "dry" foliage at 1.5 GHz. However, by the time the beamwidth reaches 5 degrees, the target is completely lost in the foliage return. In Figure 4.4-9 the effects of extinction have clearly decreased the target return so that it is only visible with the narrowest beamwidth. In addition, by the time the beamwidth reaches 5 degrees, the surface return is nearly lost to the volume return.

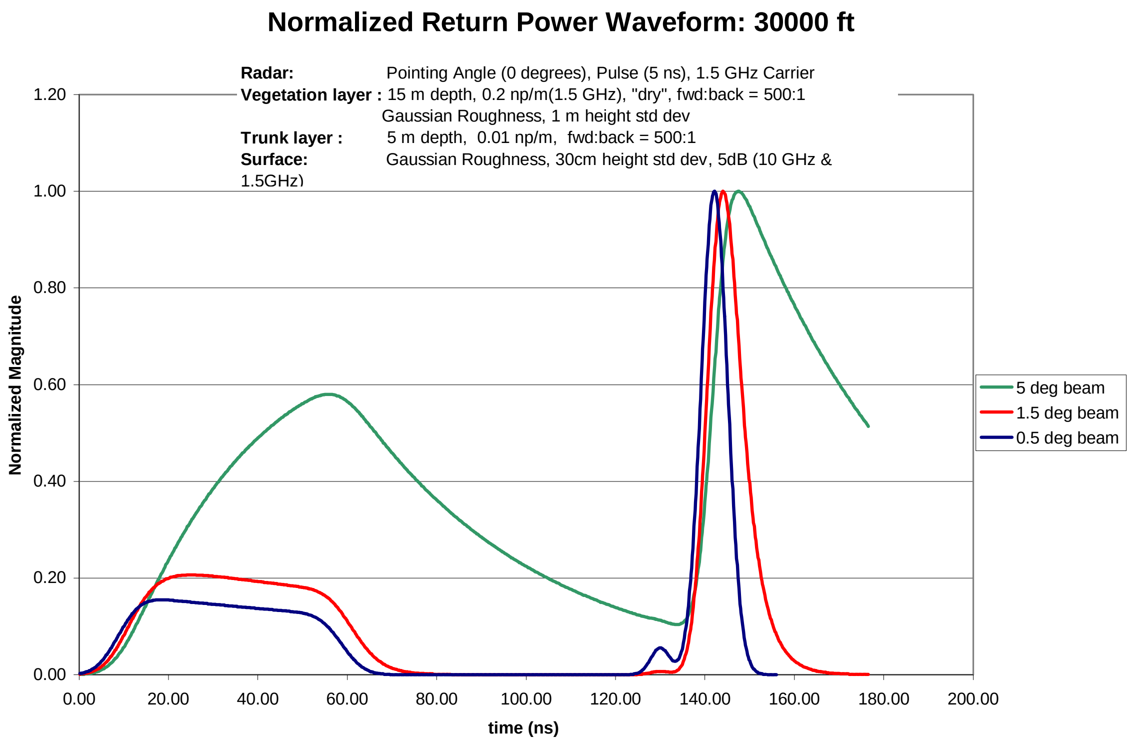

Figure 4.4-8: 1.5 GHz, dry foliage average power waveform with 0.5 m^2 target

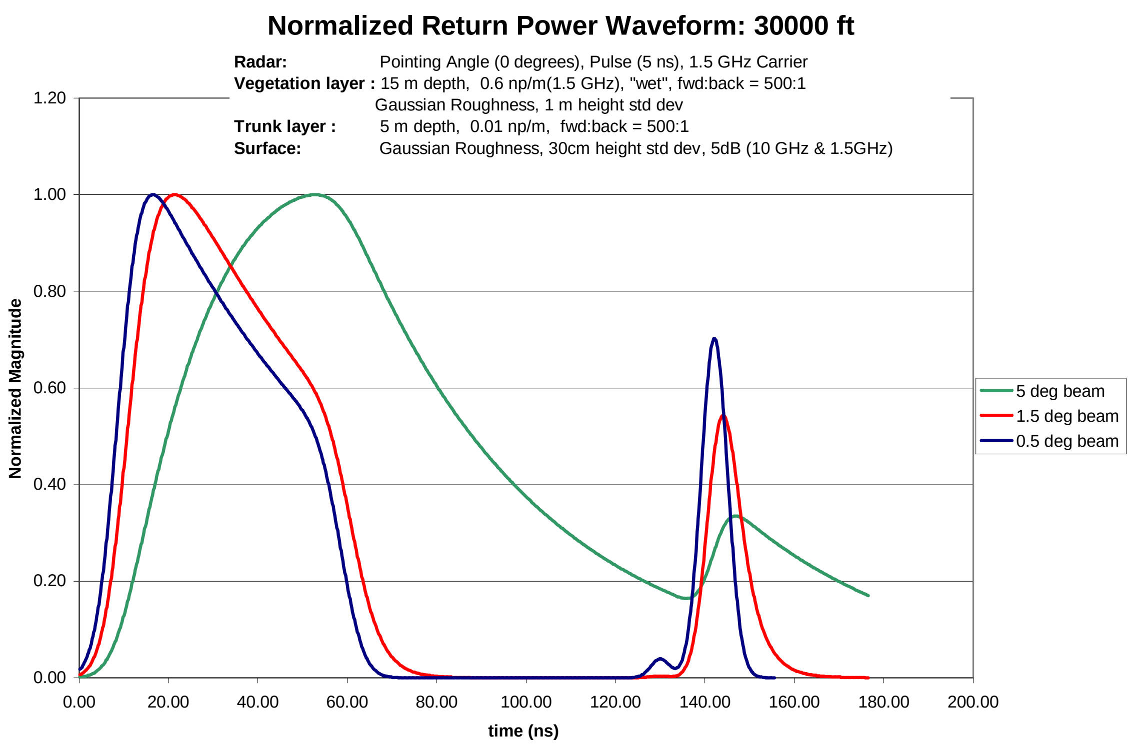

Figure 4.4-9: 1.5 GHz, wet foliage average power waveform with 0.5 m^2 target

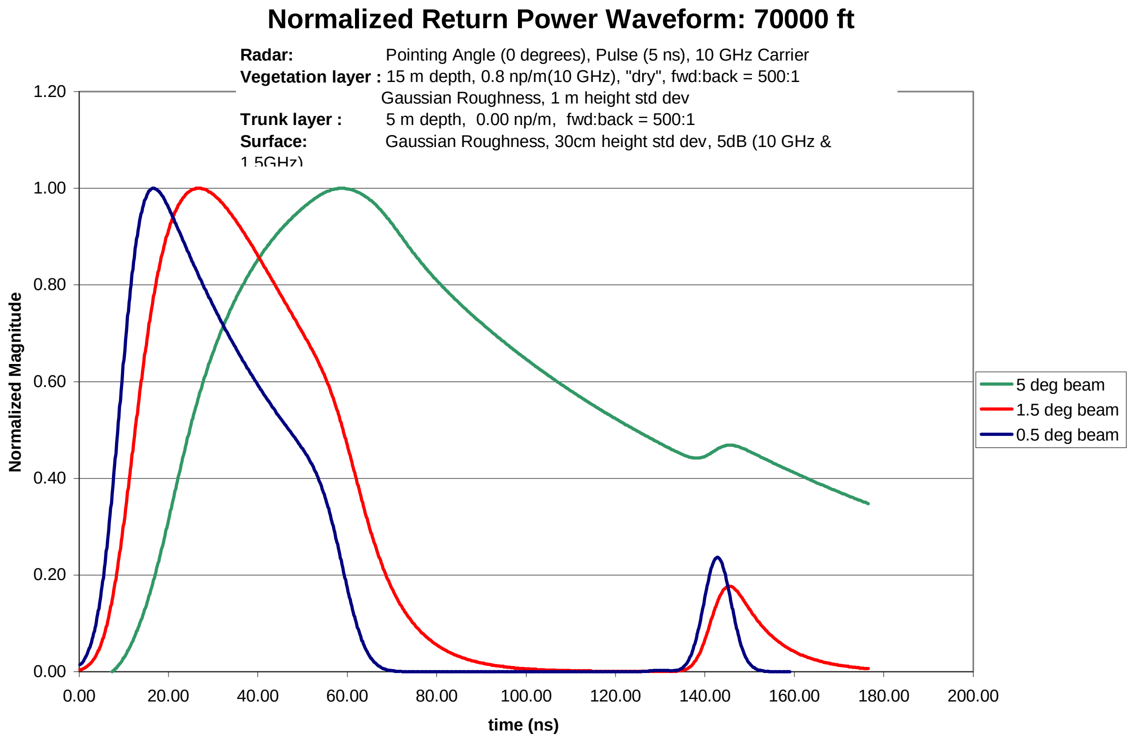

Figure 4.4-10: 10 GHz, dry foliage average power waveform with 0.5 m^2 target

The next two graphs show the average, return power waveforms for an altitude at 70,000 feet and 10 GHz. In Figure 4.4-10 the target is hidden and surface is nearly hidden as the beamwidth increases. Figure 4.4-11 shows that under wet conditions the surface is completely obscured as well as the target. Finally, Figure 4.4-12 shows that the increase in frequency to 35 GHz and the accompanying rise in extinction results average return power waveforms with no discernable features.

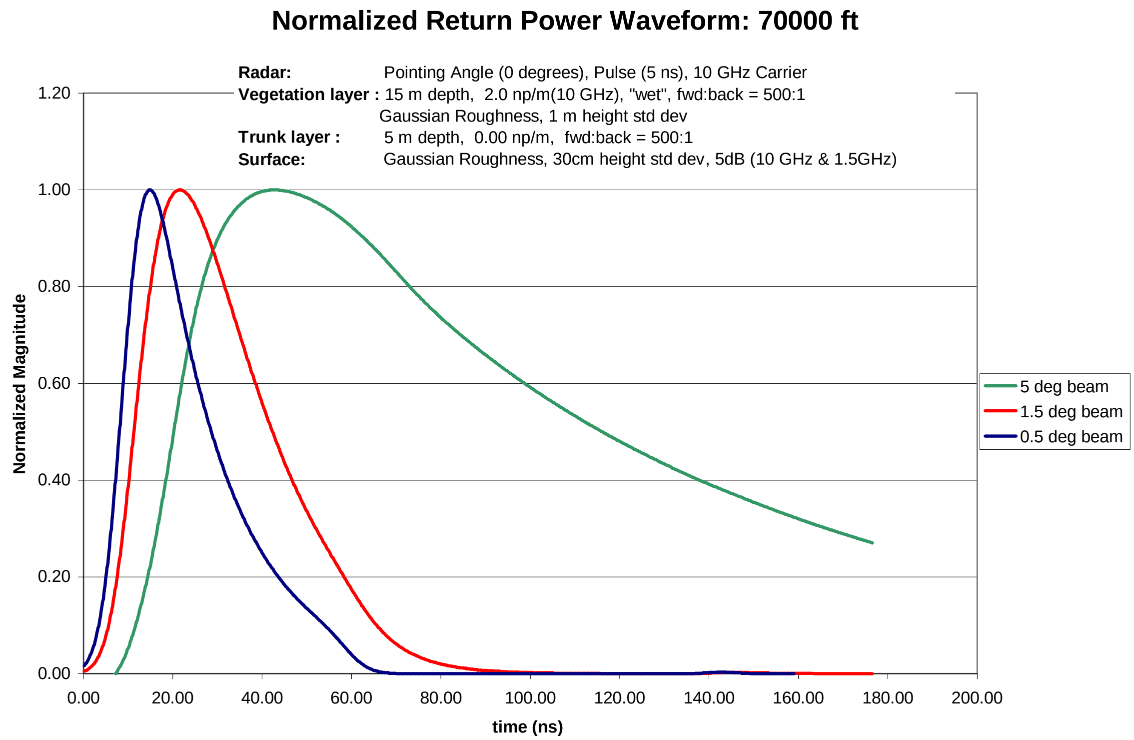

Figure 4.4-11: 10 GHz, wet foliage average power waveform with 0.5 m^2 target

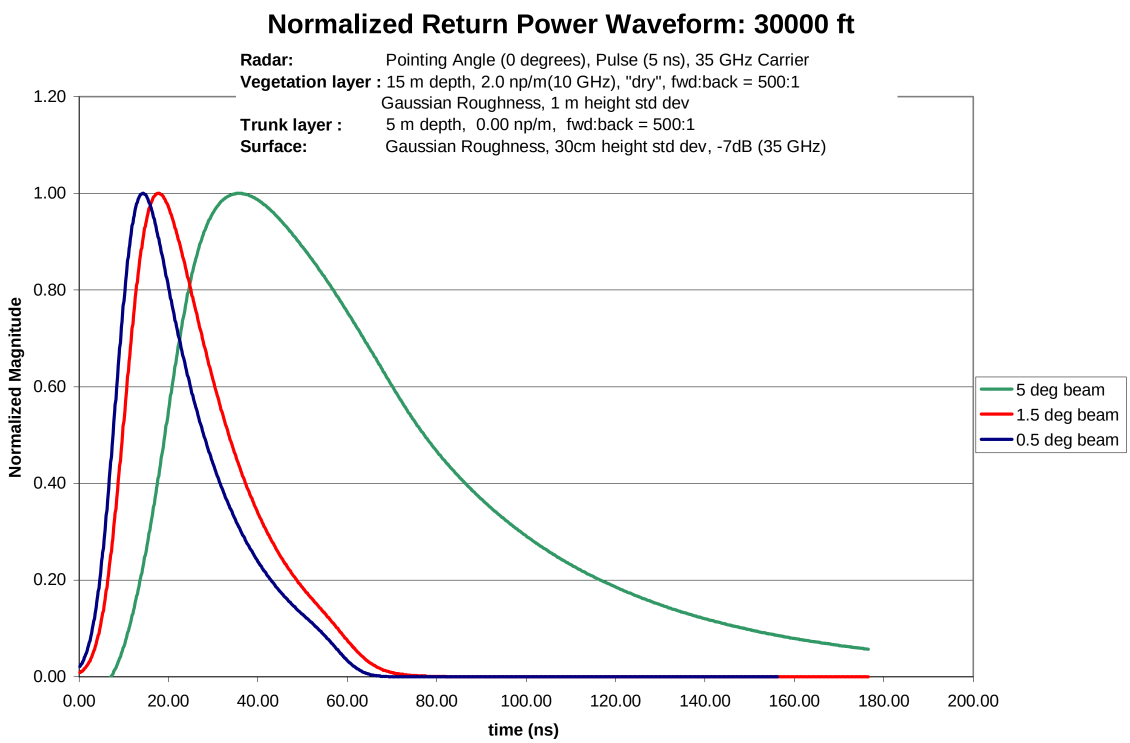

Figure 4.4-12: 35 GHz, dry foliage average power waveform with 0.5 m^2 target

Chapter 5 Beam Incidence in Radiative Transfer

In this study, the power scattered by a volume will be calculated using many different techniques including radiative transfer, single scattering and multiple scattering. In all cases, it is desired to manipulate the solution, making all the necessary assumptions, in order to create the “convolutional model” that was introduced in Chapter 4 . The necessary assumption is simply that the medium is strongly forward scattering. This chapter examines this aspect of the convolutional model: the assumption that multiple scattering is negligible outside the forward and backward directions. One measure of this assumption is beam broadening. In most literature, the beam wave case is treated using wave theory combined with the parabolic wave equation. This is a valid approach for forward scattering in a small angle in the forward direction. However, as seen in the studies by Schwering, the scattering of waves often has a component in other directions (see Section 4.4). In this chapter, the frame work for higher orders of multiple scattering for beam wave incidence are presented in the context of radiative transfer theory.

This chapter introduces the general radiative transfer solution. First, a forward-backward solution is obtained. With the exception of time-dependence, this solution is directly comparable to the convolutional result already developed. Subsequently, the forward-backward solution is compared to one other approximation and the full solution; the approximation includes scattering in all directions by the incident coherent power density, but no multiple scattering in the incoherent power density. Next the full solution to the radiative transfer equations for beam wave incidence is presented. Here, the general transfer equation is numerically evaluated for an incident beam; this solution includes multiple scattering as much as the classical radiative transfer equations allow.

5.1 Radiative Transfer Theory

The geometry for the development of the general radiative transfer equation is given in Figure 5.1-1

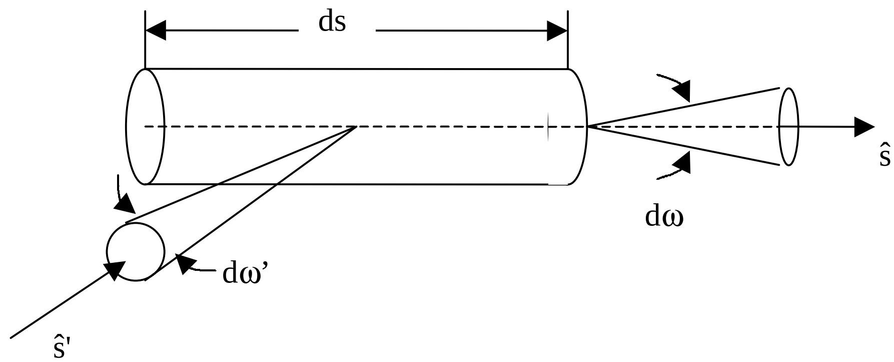

Figure 5.1-1: Scattering geometry for the intensity [Ishimaru, 1997]

Assuming that the scattering process is polarization insensitive, we will use the scalar radiative transfer equation, which relates the differential change in the power density over volume ds. This is written as

$$\frac{\partial I(\hat{s};\vec{r},t)}{\partial s} = -\rho\,\sigma_t I(\hat{s};\vec{r},t) + \frac{\rho\sigma_t}{4\pi}\iint_{4\pi} p(\hat{s},\hat{s}')I(\hat{s}';\vec{r},t)d\omega' + J_s(\hat{s};\vec{r})$$

Equation 5.1-1

where

- $I(\hat{s};\vec{r})$ is the power density in the $\hat{s}$ direction at the position: $\vec{r}$
- $\hat{s}$ is a direction of the power density
- ρ is the scatterer density
- $\sigma_t(\vec{r})$ is the scatterers total cross section which is the sum of the absorbing and scattering cross sections: $\sigma_t(\vec{r}) = \sigma_{abs}(\vec{r}) + \sigma_{sc}(\vec{r})$ and as written here, may be a function of position $\vec{r}$.
- $p(\hat{s},\hat{s}')$ is the scattering function of each scatterer; (prime denotes incident direction(s)) and is related to the amplitude of the field scattering function squared.

- $J_s(\hat{s};\vec{r})$ is the source function (emission sources)

Referring to Equation 5.1-1, the change in power in the $\hat{r}$ direction is proportional to the power incident on the differential volume element. This power is then depleted by absorption as well as scattering into other directions. On the other hand, the power, as it propagates through the differential volume, increases by an amount due to scattering into the $\hat{r}$ direction from other directions $\hat{r}'$ as well as energy emitted inside the differential volume.

5.2 *Radiative Transfer for Strictly Forward-Backward Scattering*

In this section, the radiative transfer solution for forward scatter only is presented. In some ways, this approach is a precursor and under some conditions, is directly comparable to the forthcoming convolutional solution.

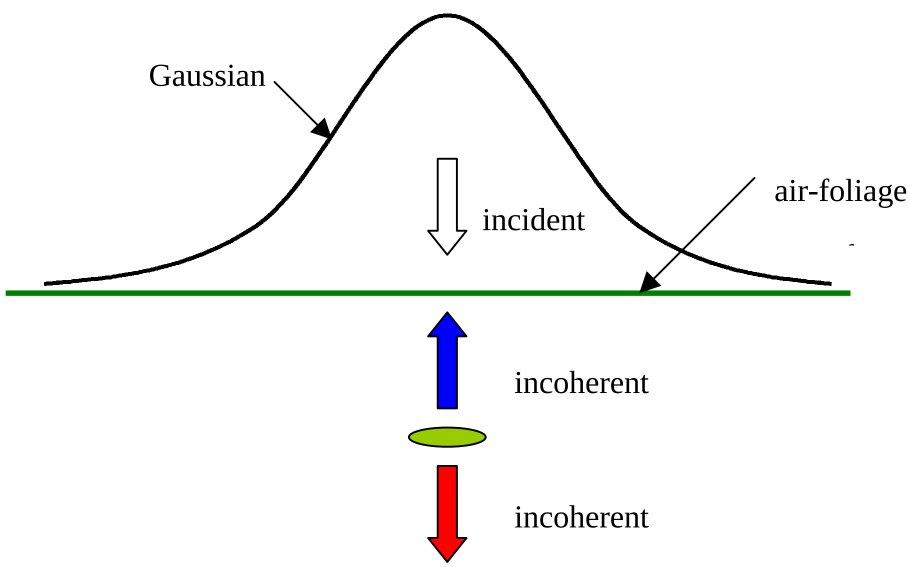

Figure 5.2-1: Single scattering for a single scatterer

Beginning with the classic, source-free radiative transfer equation, the integral over the solid angle is simplified.

$$\frac{d\,I(\vec{r},\hat{s})}{ds} = -\rho_d \sigma_t\, I(\vec{r},\hat{s}) + \frac{\rho_d \sigma_t}{4\pi} \iint_{4\pi} p(\hat{s},\hat{s}')I(\vec{r},\hat{s}')d\Omega'$$

This integral, which describes how the power density in one direction is scattered into another, will be approximated for scattering exclusively in the forward and backward directions. This simple solution can be obtained by assuming a very restrictive function for the scattering amplitude (sometimes referred to as the phase matrix) as follows

$$p(\hat{s},\hat{s}') = \frac{2}{\sigma_t}\left[\sigma_f\ \delta(\hat{s}'-\hat{s})\ +\sigma_b\ \delta(\hat{s}'+\hat{s})\ \right]$$

where the Dirac delta function, $\delta(*)$ has been introduced, as well as the forward and backscattered cross sections, σ_f and σ_b respectively. Note that this scattering function obeys the identity

$$\iint_{4\pi} p(\hat{s},\hat{s}')d\Omega = 4\pi\frac{\sigma_s}{\sigma_t} = 4\pi W_o$$

where W_o is the albedo of the scatterer. Hence the integral of the scattering function includes the loss due to scattering but excludes that due to absorption. Due to this selection for a scattering function, the radiative transfer equation becomes (splitting it into upward and downward directed power densities)

$$\frac{d\,I_d^+(\vec{r},\hat{s})}{ds} = -\rho_d\sigma_t\,I_d^+(\vec{r},\hat{s}) + \frac{\rho_d\sigma_t}{4\pi}\left[\frac{\sigma_f}{\sigma_t}I_d^+(\vec{r},\hat{s}) + \frac{\sigma_b}{\sigma_t}I_d^-(\vec{r},\hat{s})\right] + \frac{\rho_d\sigma_t}{4\pi}\frac{\sigma_f}{\sigma_t}I_{ri}(\vec{r},\mu_{inc})$$

$$-\frac{d\,I_d^-(\vec{r},\hat{s})}{ds} = -\rho_d\sigma_t\,I_d^-(\vec{r},\hat{s}) + \frac{\rho_d\sigma_t}{4\pi}\left[\frac{\sigma_b}{\sigma_t}I_d^+(\vec{r},\hat{s}) + \frac{\sigma_f}{\sigma_t}I_d^-(\vec{r},\hat{s})\right] + \frac{\rho_d\sigma_t}{4\pi}\frac{\sigma_b}{\sigma_t}I_{ri}(\vec{r},\mu_{inc})$$

Once again, converting (changing variables) to optical distance and rewriting this in matrix form, the following greatly simplified form is discovered

$$\frac{d}{d\tau}\begin{bmatrix} I_d^+(\vec{r},\hat{s}) \\ I_d^-(\vec{r},\hat{s}) \end{bmatrix} = \begin{bmatrix} -1+\dfrac{\sigma_f}{4\pi\sigma_t} & \dfrac{\sigma_b}{4\pi\sigma_t} \\ -\dfrac{\sigma_b}{4\pi\sigma_t} & 1-\dfrac{\sigma_f}{4\pi\sigma_t} \end{bmatrix}\begin{bmatrix} I_d^+(\vec{r},\hat{s}) \\ I_d^-(\vec{r},\hat{s}) \end{bmatrix} + \frac{1}{4\pi\sigma_t}\begin{bmatrix} \sigma_f \\ -\sigma_b \end{bmatrix} I_{ri}(\vec{r},\hat{s})$$

Using the previously determined, the coherent intensity is substituted into the above equation

$$\frac{d}{d\tau}\begin{bmatrix} I_d^+(\vec{r},\hat{s}) \\ I_d^-(\vec{r},\hat{s}) \end{bmatrix} = \begin{bmatrix} -1+\dfrac{\sigma_f}{4\pi\sigma_t} & \dfrac{\sigma_b}{4\pi\sigma_t} \\ -\dfrac{\sigma_b}{4\pi\sigma_t} & 1-\dfrac{\sigma_f}{4\pi\sigma_t} \end{bmatrix}\begin{bmatrix} I_d^+(\vec{r},\hat{s}) \\ I_d^-(\vec{r},\hat{s}) \end{bmatrix} + \begin{bmatrix} \dfrac{\sigma_f}{4\pi\sigma_t} \\ -\dfrac{\sigma_b}{4\pi\sigma_t} \end{bmatrix} A_0\, e^{-\frac{\rho^2}{2w^2}}\, e^{-\tau}$$

Equation 5.2-1

The solution to this problem can be found in several different ways; again, we may use the approach of Cole [1968] or Variations of Parameters [Boyce, 1977]. The initial conditions are stated as follows: the downward propagating incoherent power density at the top of the foliage layer is zero; the upward propagating incoherent power density at the bottom of the foliage layer is also zero. These conditions can be written as

$$\begin{bmatrix} I_d^+(\tau=0) \\ I_d^-(\tau=\tau_d) \end{bmatrix} = \begin{bmatrix} 0 \\ 0 \end{bmatrix}$$

Substituting for the matrix entries in Equation 5.2-1 for convenience and assuming that the incident beam is z-directed (normally incident), the differential equation is cast as

$$\frac{d}{d\tau}\begin{bmatrix} I_d^+ \\ I_d^- \end{bmatrix} = \begin{bmatrix} -\alpha & \beta \\ -\beta & \alpha \end{bmatrix}\begin{bmatrix} I_d^+ \\ I_d^- \end{bmatrix} + \begin{bmatrix} \dfrac{\sigma_f}{4\pi\sigma_t} \\ -\dfrac{\sigma_b}{4\pi\sigma_t} \end{bmatrix} s(\tau)$$

where the forcing function: $s(\tau) = A_0\, e^{-\frac{\rho^2}{2w^2}}\, e^{-\tau}$

Equation 5.2-2

the eigenvalues, $\lambda_{1,2}$, of the homogeneous system are found from the determinant of the matrix

$$\left(\lambda^2 - \alpha^2\right) + \beta^2 = 0 \quad \Rightarrow \quad \lambda_{1,2} = \pm\sqrt{\alpha^2 - \beta^2} = \pm\lambda$$

and the fundamental matrix (matrix of eigenvectors) and its complementary form which reduces to unity with the initial condition, can be written as

$$\overline{\overline{\psi}}(\tau) = \left[\overline{X}_1 e^{\lambda\tau} \ \overline{X}_2 e^{-\lambda\tau}\right] = \begin{bmatrix} \beta e^{\lambda\tau} & \beta e^{-\lambda\tau} \\ (\alpha+\lambda)e^{\lambda\tau} & (\alpha-\lambda)e^{-\lambda\tau} \end{bmatrix}$$

$$\overline{\overline{\Phi}}(\tau) = \frac{1}{2\lambda}\begin{bmatrix} \left[(\alpha+\lambda)e^{-\lambda\tau} - (\alpha-\lambda)e^{\lambda\tau}\right] & \beta\left(e^{\lambda\tau} - e^{-\lambda\tau}\right) \\ \beta\left(e^{-\lambda\tau} - e^{\lambda\tau}\right) & \left[(\alpha+\lambda)e^{\lambda\tau} - (\alpha-\lambda)e^{-\lambda\tau}\right] \end{bmatrix}$$

Equation 5.2-3

Note that the second fundamental matrix does display the desired property that $\overline{\overline{\Phi}}^{-1}(z) = \overline{\overline{\Phi}}(-z)$. Employing the boundary condition,

$$\overline{\overline{W}}^{[0]}\overline{I}_d(0) + \overline{\overline{W}}^{[\tau_d]}\overline{I}_d(\tau_d) = 0$$

where in this case, the matrices W are given as follows:

$$\overline{\overline{W}}^{[0]} = \begin{bmatrix} 1 & 0 \\ 0 & 0 \end{bmatrix}, \ \overline{\overline{W}}^{[\tau_d]} = \begin{bmatrix} 0 & 0 \\ 0 & 1 \end{bmatrix}$$

these values for the matrix indicate that there is no reflection at either boundary. If there were reflection at either boundary, then these matrices, W, will include the reflection coefficients; this case is demonstrated in Section 7.6. The solution of the differential equation is written simply as

$$\overline{I}(\tau) = \overline{\overline{\Phi}}(\tau)\int_0^\tau \overline{\overline{\Phi}}(-t)\overline{s}(t)dt - \overline{\overline{\Phi}}(\tau)\overline{\overline{D}}^{-1}\overline{\overline{W}}^{[\tau_d]}\overline{\overline{\Phi}}(\tau_d)\int_0^{\tau_d} \overline{\overline{\Phi}}(-t)\overline{s}(t)dt$$

Equation 5.2-4

This solution involves the fundamental matrix as well as the matrix, D, which incorporates the boundary conditions. D is given by [Cole, 1968]

$$\overline{\overline{D}} = \overline{\overline{W}}^{[0]}\overline{\overline{\Phi}}(\tau = 0) + \overline{\overline{W}}^{[\tau_d]}\overline{\overline{\Phi}}(\tau = \tau_d)$$

$$= \frac{1}{2\lambda}\begin{bmatrix} 2\lambda & 0 \\ \beta\left(e^{-\lambda\tau_d} - e^{\lambda\tau_d}\right) & \left[(\alpha+\lambda)e^{\lambda\tau_d} - (\alpha-\lambda)e^{-\lambda\tau_d}\right] \end{bmatrix}$$

and its inverse is given by

$$\overline{\overline{D}}^{-1} = \frac{1}{\left[(\alpha+\lambda)e^{\lambda\tau_d} - (\alpha-\lambda)e^{-\lambda\tau_d}\right]}\begin{bmatrix} \left[(\alpha+\lambda)e^{\lambda\tau_d} - (\alpha-\lambda)e^{-\lambda\tau_d}\right] & 0 \\ -\beta\left(e^{-\lambda\tau_d} - e^{\lambda\tau_d}\right) & 2\lambda \end{bmatrix}$$

Equation 5.2-5

The integrals in Equation 5.2-4 may be evaluated analytically. Substituting for the inverse of the fundamental matrix and the forcing function (coherent power density), the integrals are evaluated.

$$\int_0^\tau \overline{\overline{\Phi}}(-t)\bar{s}(t)dt$$

$$= \frac{A_0 e^{-\frac{\rho^2}{2w^2}}}{8\pi\lambda\sigma_t}\int_0^\tau \begin{bmatrix} \left[(\alpha+\lambda)e^{\lambda t} - (\alpha-\lambda)e^{-\lambda t}\right] & \beta\left(e^{-\lambda t} - e^{\lambda t}\right) \\ \beta\left(e^{\lambda t} - e^{-\lambda t}\right) & \left[(\alpha+\lambda)e^{-\lambda t} - (\alpha-\lambda)e^{\lambda t}\right] \end{bmatrix}\begin{bmatrix} \sigma_f \\ -\sigma_b \end{bmatrix} e^{-t}\, dt$$

$$= \frac{A_0 e^{-\frac{\rho^2}{2w^2}}}{8\pi\lambda\sigma_t}\int_0^\tau \begin{bmatrix} S_1 e^{-(1+\lambda)t} + S_2 e^{-(1-\lambda)t} \\ S_3 e^{-(1+\lambda)t} + S_4 e^{-(1-\lambda)t} \end{bmatrix} dt$$

$$= \frac{A_0 e^{-\frac{\rho^2}{2w^2}}}{8\pi\lambda\sigma_t}\begin{bmatrix} -\frac{S_1}{(1+\lambda)}\left(e^{-(1+\lambda)\tau} - 1\right) - \frac{S_2}{(1-\lambda)}\left(e^{-(1-\lambda)\tau} - 1\right) \\ -\frac{S_3}{(1+\lambda)}\left(e^{-(1+\lambda)\tau} - 1\right) - \frac{S_4}{(1-\lambda)}\left(e^{-(1-\lambda)\tau} - 1\right) \end{bmatrix}$$

Equation 5.2-6

where

$$
\begin{aligned}
S_1 &= \left[-(\alpha-\lambda)\sigma_f - \beta\sigma_b\right] \\
S_2 &= \left[(\alpha+\lambda)\sigma_f + \beta\sigma_b\right] \\
S_3 &= \left[-\beta\sigma_f - (\alpha+\lambda)\sigma_b\right] \\
S_4 &= \left[\beta\sigma_f + (\alpha-\lambda)\sigma_b\right]
\end{aligned}
$$

At this point, the solution to the strictly forward scattering solution can be found.

As an example, the propagation of a beam through a strongly forward scattering medium is given in Figure 5.2-2. The incoherent power density (diffuse power) behaves as expected. The diffuse energy grows as the coherent beam penetrates deeper into the medium. The coherent power constantly feeds the incoherent power; hence, the incoherent power is expected to grow as the coherent power penetrates the medium.

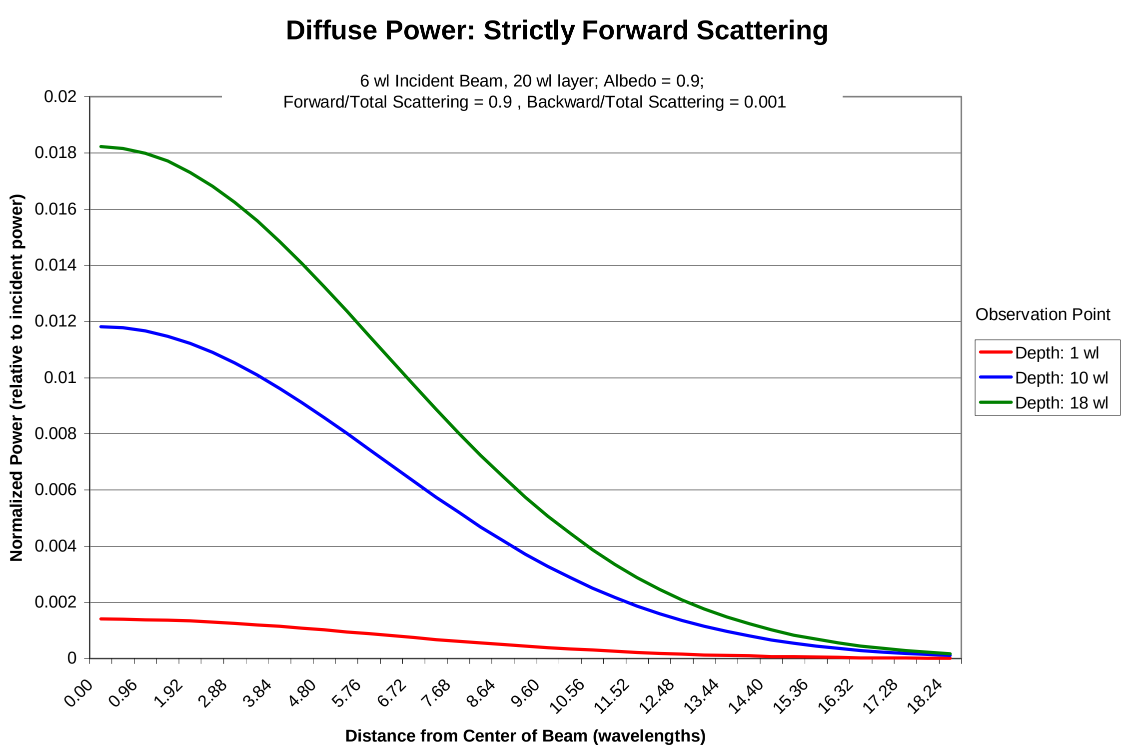

Figure 5.2-2: Strictly Forward Scatter, incoherent power density at several depths within the strongly forward scattering medium. Albedo = 0.9

At some point, the coherent energy will become negligible and consequently, the diffuse energy will no longer continue to grow. In fact due to absorption, the incoherent power begins diminishing due to scattering out of the path and absorption, both of which are defined as lost power in the strictly forward scatter model. Figure 5.2-3 displays similar results for a smaller particle albedo. For that reason, the diffuse power level is somewhat reduced with respect to the previous case, since a smaller albedo implies greater absorption. The general behavior, however, is consistent between the two results.

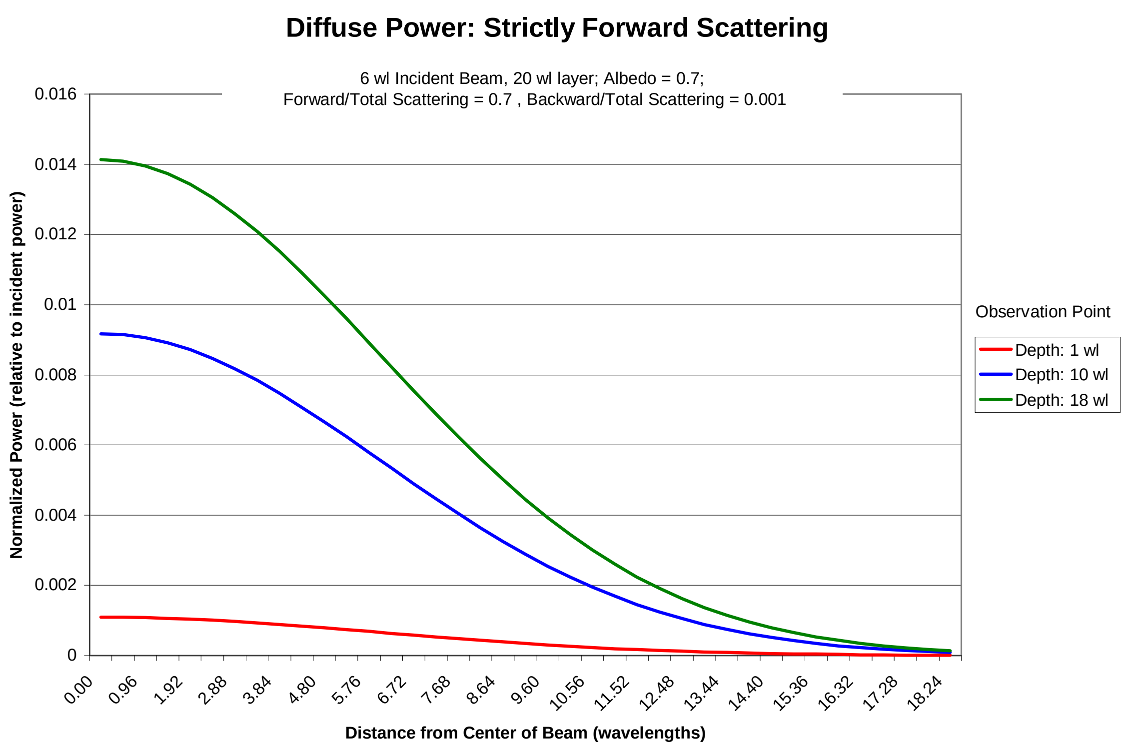

Figure 5.2-3: Strictly Forward Scatter, incoherent power density at several depths within the strongly forward scattering medium. Albedo = 0.7

5.3 Modified Forward Scatter Solution

In this section, a second, simplified beam-transfer solution is presented. There is, however, an added level of complexity: the coherent power is not restricted to scattering in only the forward and backward directions. As in the general case presented in the next section, the coherent power is scattered in directions as determined by the scattering amplitude. However, the incoherent power density still only scatters in the forward direction. Consequently, there is no coupling of incoherent power from one direction (ray path) into another; multiple scattering in all but the forward and backward directions is neglected. This solution will be used as a check case for the numerical simulation of the next, more complex section since the results are greatly simplified. Starting with the same integro-differential equation and assuming a normally incident beam (z-directed)

$$\cos(\theta)\frac{\partial I_d(\vec{r},\hat{s})}{\partial z}+\sin(\theta)\frac{\partial I_d(\vec{r},\hat{s})}{\partial \rho}=-\rho_d\sigma_t I_d(\vec{r},\hat{s})+\frac{\rho_d\sigma_t}{4\pi}\iint_{4\pi} p(\hat{s},\hat{s}')\left(I_d(\vec{r},\hat{s}')+I_{ri}(\vec{r},\hat{z})\right)d\Omega'$$

Equation 5.3-1

The primary approximation to be implemented is in the integral over the solid angle. For the diffuse power density, I_d, scattering can only occur in the forward direction. Hence, the only contribution to the power density in a given direction is that due to field scattered from coherent into the incoherent. In other words, the change in the incoherent power density in a given direction is reduced by the extinction, increased by the *forward* scatter of incoherent and increased by the coherent field scattered in that direction. This *incoherent power density* can now only continue to travel in its original direction (as indicated by the power scattering amplitudes below)

$$\begin{aligned}\frac{dI_d(\vec{r},\hat{s})}{ds}&=-\rho_d\sigma_t I_d(\vec{r},\hat{s})+\frac{\rho_d\sigma_t}{4\pi}p(\hat{s},\hat{s})I_d(\vec{r},\hat{s})+\frac{\rho_d\sigma_t}{4\pi}p(\hat{s},\hat{z})I_{ri}(\vec{r},\hat{z})\\&=-\rho_d\sigma_t I_d(\vec{r},\hat{s})+\frac{\rho_d\sigma_t}{4\pi}p(\hat{s},\hat{s})I_d(\vec{r},\hat{s})+\frac{\rho_d\sigma_t}{4\pi}p(\hat{s},\hat{z})A_0\,e^{-A_n s^2-B_n s-C_n}\end{aligned}$$

Equation 5.3-2

The exponential factors describing the incident, coherent power density are described in the appendix for this chapter. The first term on the left-hand side is the usual extinction: scattering loss (and absorption). The second term is the forward-scattered incoherent power density and the last term is the contribution of the coherent intensity into the incoherent power density. This idea is graphically illustrated in Figure 5.3-1; notice that incoherent power does not scatter into new directions; hence, multiple scattering is neglected to a great extent.

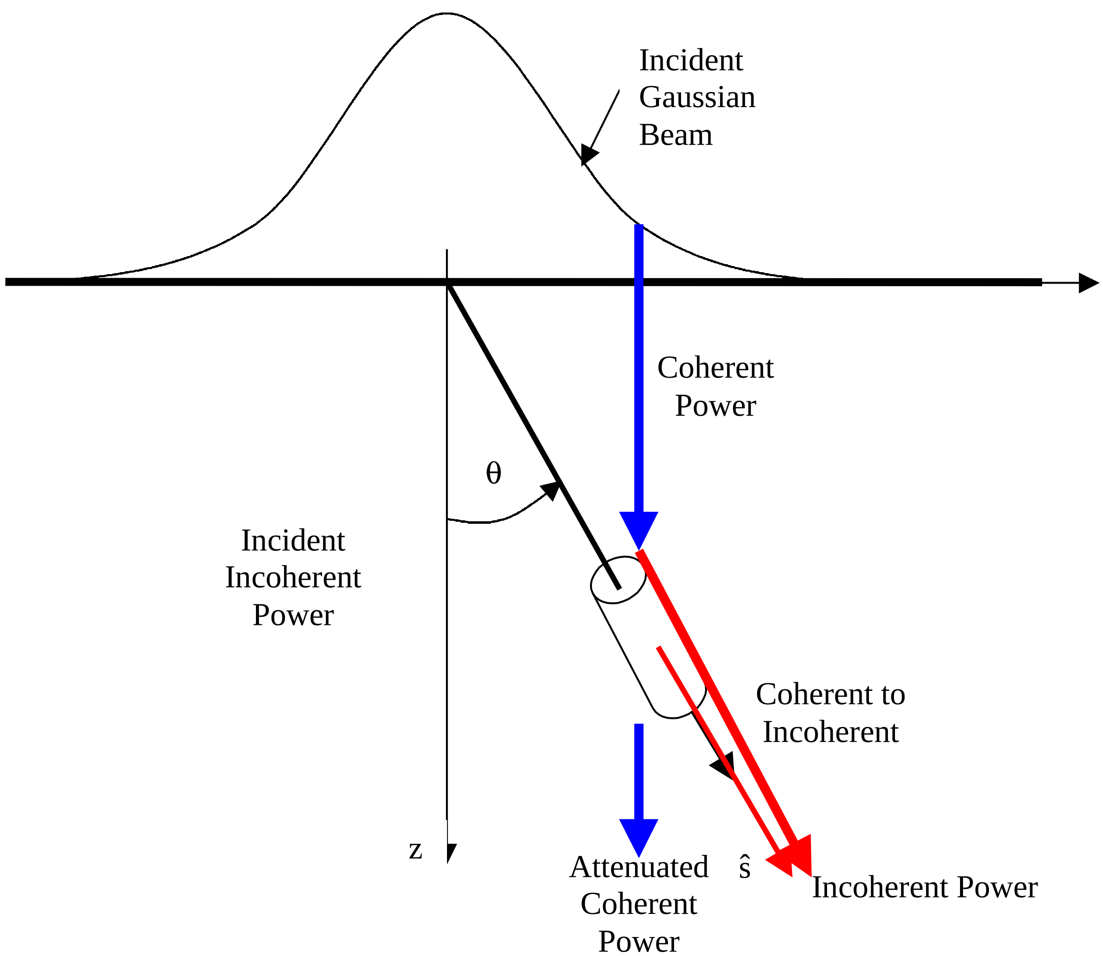

Figure 5.3-1: Modified forward scatter

Next, a change of variables is made, converting physical distance into the optical distance. This change is described by

$$\text{let}: \quad \tau \equiv \rho_d \sigma_t s, \;\; d\tau \equiv \rho_d \sigma_t ds; \;\; \text{Limits}: \quad s=0, \tau=0; s=s_o, \tau=\rho_d \sigma_t s_o$$

$$\text{arguments}: \quad a_n \equiv \frac{A_n}{(\rho_d \sigma_t)^2}, \;\; b_n \equiv \frac{B_n}{(\rho_d \sigma_t)}$$

The power scattering amplitude is modified to reflect only forward scattering:

$$p(\hat{s},\hat{s}) \equiv \frac{\sigma_f}{\sigma_t}, \quad \text{fractional forward scattering amplitude}$$

With these changes, the first-order, ordinary differential equation becomes

$$\frac{d\,I_d(\vec{r},\hat{s})}{d\tau} = -I_d(\vec{r},\hat{s}) + \frac{2\pi\sigma_f}{4\pi\sigma_t} I_d(\vec{r},\hat{s}) + \frac{1}{4\pi} p(\hat{s},\hat{z}) A_0\, e^{-a_n\tau^2 - b_n\tau - C_n}$$

A closed form solution may be obtained by first combining terms,

$$\frac{d\,I_d(\vec{r},\hat{s})}{d\tau} + \left(1 - \frac{2\pi\sigma_f}{4\pi\sigma_t}\right) I_d(\vec{r},\hat{s}) = \frac{1}{4\pi} p(\hat{s},\hat{z}) A_0\, e^{-a_n\tau^2 - b_n\tau - C_n}$$

Equation 5.3-3

Then, using an integrating factor, the differential equation evolves to a greatly simplified form

$$\frac{d\,I_d(\vec{r},\hat{s}) e^{k_e\tau}}{d\tau} + k_e I_d(\vec{r},\hat{s}) e^{k_e\tau} = \frac{1}{4\pi} p(\hat{s},\hat{z}) e^{k_e\tau} A_0\, e^{-a_n\tau^2 - b_n\tau - C_n}$$

$$\text{where } k_e \equiv \left(1 - \frac{\sigma_f}{4\pi\sigma_t}\right)$$

Equation 5.3-4

The left-hand side is further simplified by changing the variables in order to reduce the two-dimensional problem to one dimension,

$$\text{let}: \quad \zeta \equiv \tau\cos\theta \equiv \mu\tau = \mu\rho_d\sigma_t s, \;\; d\zeta \equiv \mu\rho_d\sigma_t ds$$

$$\text{when}: \tau=0, \zeta=0; \;\; \tau=\rho_d\sigma_t s_o \equiv \tau_o$$

This change of variables trnasforms the energy propagating in angles other than forward-backward to forward-backward. In addition, the coefficients in the exponential must take a modified form

$$\alpha_n \equiv \frac{A_n}{(\mu\rho_d\sigma_t)^2},\ \beta_n \equiv \frac{B_n}{(\mu\rho_d\sigma_t)},\ \tilde{k}_e \equiv \frac{k_e}{\mu}$$

yielding the simple equation

$$\frac{d}{d\zeta}\left[\ I_d(\vec{r},\hat{s})e^{\tilde{k}_e\zeta}\ \right] = \frac{1}{4\pi\mu}p(\hat{s},\hat{z})A_0\ e^{-\alpha_n\zeta^2-(\beta_n-\tilde{k}_e)\zeta-C_n}$$

Equation 5.3-5

A general solution is obtained by integrating, remembering to include an arbitrary constant, which is evaluated from the initial condition.

$$I_d(\vec{r}_o,\hat{s})e^{\tilde{k}_e\zeta} = \frac{1}{4\pi\mu}p(\hat{s},\hat{z})A_0\int_0^{\zeta} e^{-\alpha_n t^2-(\beta_n-\tilde{k}_e)t-C_n}dt + C$$

Equation 5.3-6

Rearranging and using an integral identity, the solution is rewritten in terms of the error function.

$$I_d(\vec{r},\hat{s}) = \frac{A_0 p(\hat{s},\hat{z})}{8\mu\sqrt{\pi\alpha_n}}\ e^{-\tilde{k}_e\zeta-C_n}\ e^{(\beta_n-\tilde{k}_e)^2/4\alpha_n}\left[\mathrm{erf}\left(\sqrt{\alpha_n}\zeta+\frac{(\beta_n-\tilde{k}_e)}{2\sqrt{\alpha_n}}\right)-\mathrm{erf}\left(\frac{(\beta_n-\tilde{k}_e)}{2\sqrt{\alpha_n}}\right)\right] + Ce^{-\tilde{k}_e\zeta}$$

Equation 5.3-7

Since the incoherent power density is zero at the top of the layer (the initial condition), the constant factor, C, evaluates to zero. The resulting solution for the incoherent power density in the chosen direction, specified by $\mu = \cos\theta$, is written

$$I_d(\vec{r},\hat{s}) = \frac{A_0 p(\hat{s},\hat{z})}{8\mu\sqrt{\pi\alpha_n}}\, e^{-\tilde{k}_e\zeta - C_n}\, e^{(\beta_n - \tilde{k}_e)^2/4\alpha_n}\left[\operatorname{erf}\left(\sqrt{\alpha_n}\,\zeta + \frac{(\beta_n - \tilde{k}_e)}{2\sqrt{\alpha_n}}\right) - \operatorname{erf}\left(\frac{(\beta_n - \tilde{k}_e)}{2\sqrt{\alpha_n}}\right)\right]$$

Equation 5.3-8

The length of the ray to the observation point is

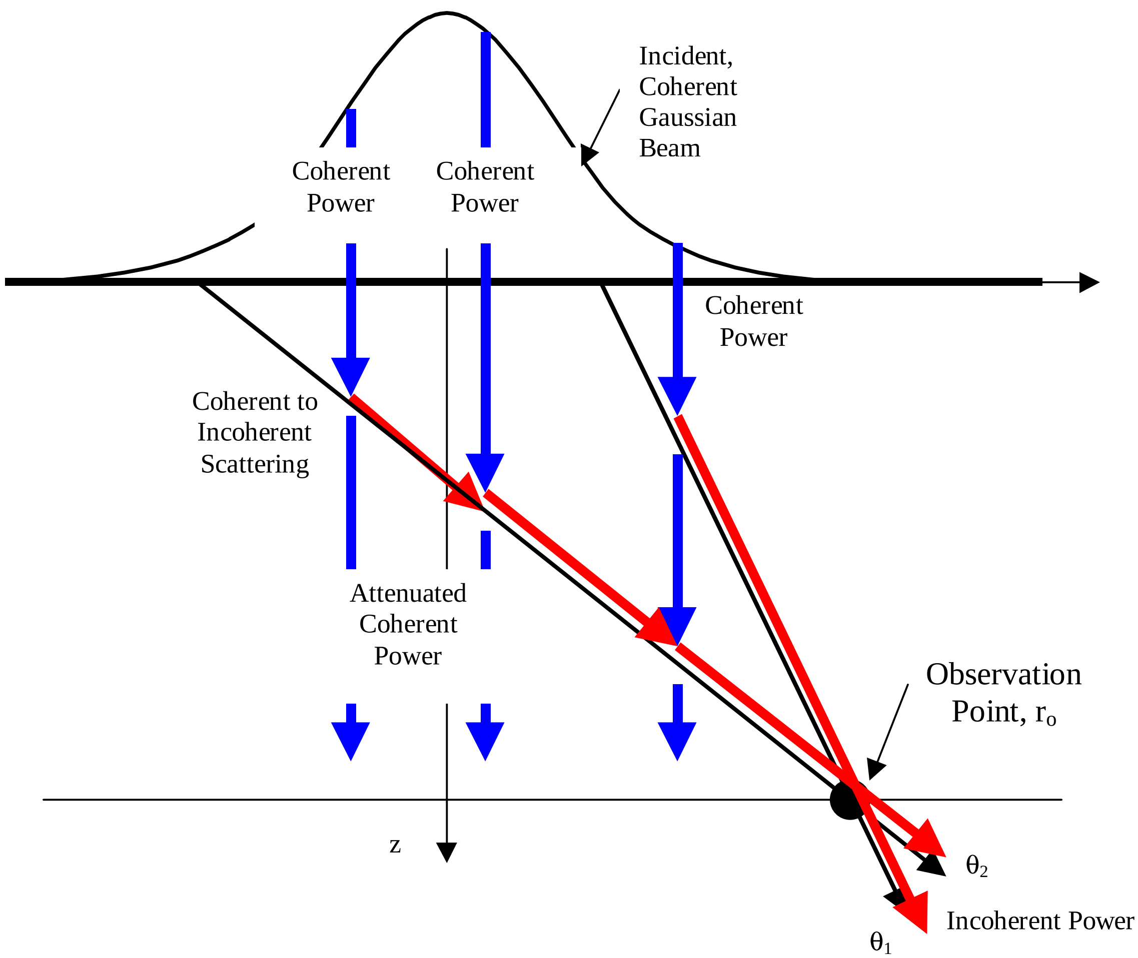

$$s_o = \frac{z_o}{\mu} \Rightarrow \tau_o = \rho_d\sigma_t\frac{z_o}{\mu} \text{ and } \zeta_o = \rho_d\sigma_t z_o$$

Figure 5.3-2: The incoherent power density, generated through the scattering by the coherent power density, for several different directions at a single observation point.

Hence, at the observation point, (ρ_o, z_o),

$$I_d(\vec{r}_o,\hat{s}) = \frac{A_0 p(\hat{s},\hat{z})}{8\mu\sqrt{\pi\alpha_n}} e^{-\tilde{k}_e\zeta_o - C_n} e^{(\beta_n - \tilde{k}_e)^2/4\alpha_n}\left[\operatorname{erf}\left(\sqrt{\alpha_n}\zeta_o + \frac{(\beta_n - \tilde{k}_e)}{2\sqrt{\alpha_n}}\right) - \operatorname{erf}\left(\frac{(\beta_n - \tilde{k}_e)}{2\sqrt{\alpha_n}}\right)\right]$$

Equation 5.3-9

This is the power density at a given observation point, $\vec{r}_o$, in the direction θ_1 or ($\hat{s}$ ~ cosθ). Figure 5.3-2 illustrates the variation of the incoherent power density assuming that the medium scatters the incident, coherent power density ***isotropically***.

Next, we consider the **incoherent** power density along the two paths: θ_1 and θ_2, Shown in Figure 5.3-2. The incoherent power propagating in the direction (θ_2) is generated by the incident **coherent** power density along the path shown. Since this path is longer with respect to the path for θ_1, and since the path θ_2 intercepts more of the incident power density, the path θ_2, will have a larger incoherent power density.

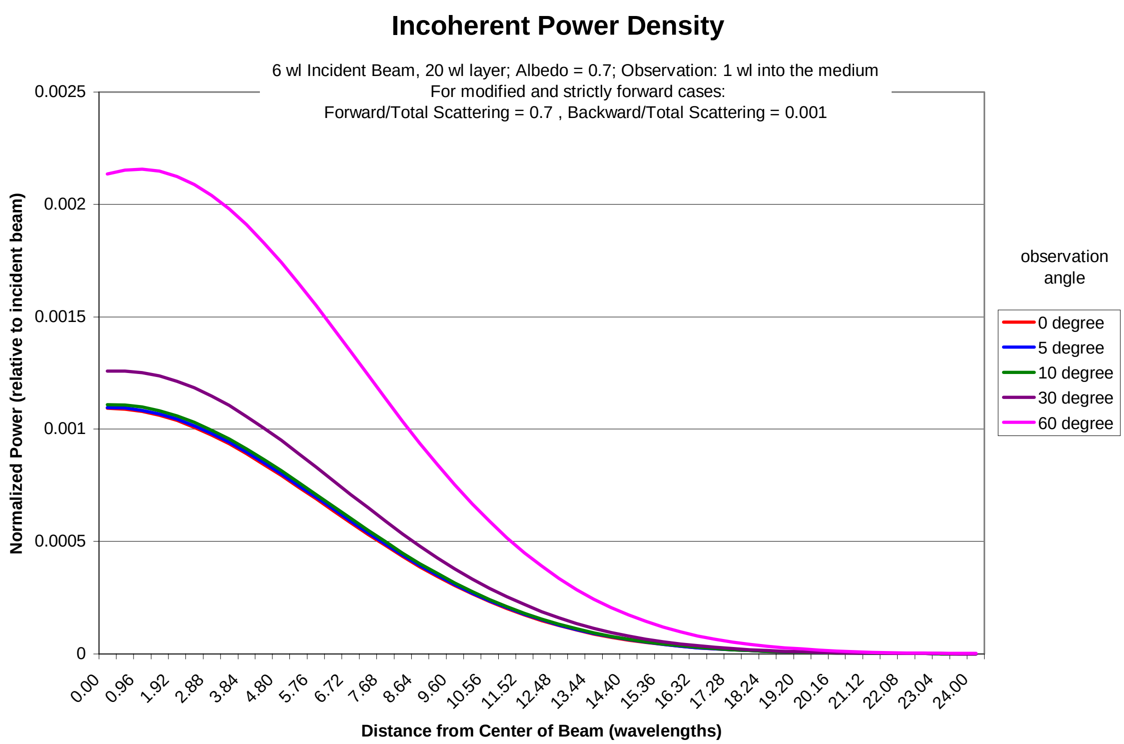

Figure 5.3-3: Incoherent power density scattered along the indicated angles as a funciton of the observation point at a depth of 1 wavelength.

This is the case if we ignore absorption. This effect can be seen in the numerical simulation of the modified forward scatter approximation of Figure 5.3-3. Note that as the angles become larger, the incoherent power density becomes larger.

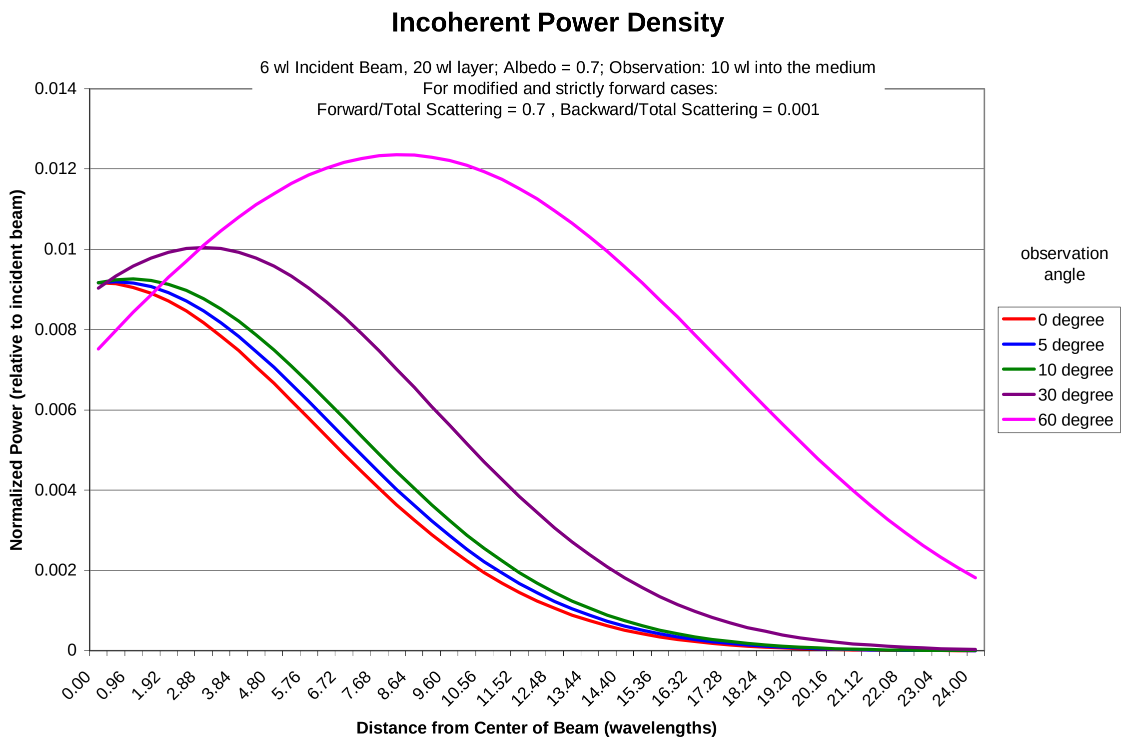

Figure 5.3-4: Incoherent power density scattered along the indicated angles as a function of the observation point at a depth of 10 wavelengths.

An observation point on the beam axis is expected to yield the largest incoherent power; however, when scattering loss and absorption are included, this expectation must be modified. In Figure 5.3-3 through Figure 5.3-5, the peak is shifting away from the beam axis. In these figures, the power density along different angles measured at a given observation point along a radial at three different depths are displayed as a function of the observation point. Note that at only one wavelength into the medium, the peak occurs near the beam axis. This is due to the negligible effects of absorption and scattering of the incident beam. However, as the depth is increased, the peak of the incoherent power density shifts away from the beam axis. Since the peak of the incident beam must travel a greater distance through the medium, as the observation depth is increased, a balance will be struck between the absorption/scattering loss and the observation point within the beam. Hence, the peak shifts. This effect is limited to the two-dimensional simulation developed in this chapter. Once three-dimensions are included, the peak shift will most likely disappear. The three dimensional case is a subject for future work.

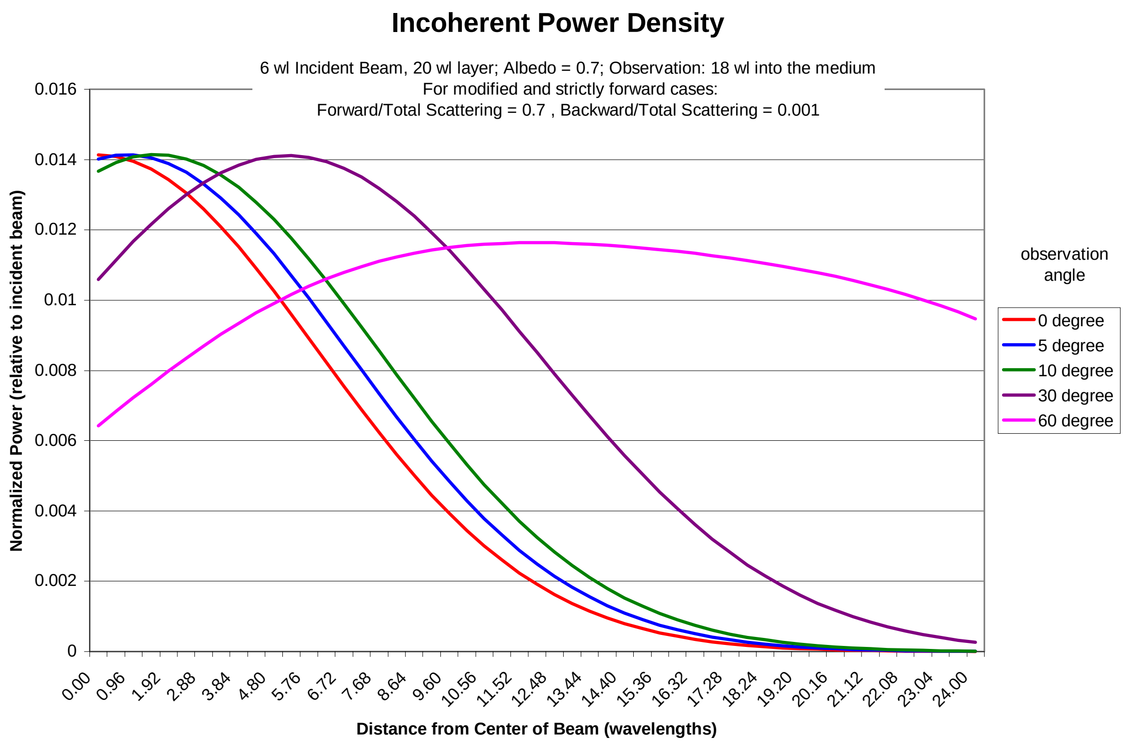

Figure 5.3-5: Incoherent power density scattered along the indicated angles as a function of the observation point at a depth of 18 wavelengths.

The total power can now be calculated at the observation point using Gaussian quadrature to integrate the contributions in every direction. First, the total intensity is expressed in the following integral relationship over the solid angle surrounding the observation point.

$$P_{total} = \iint_{4\pi} P_{density}\left(\vec{r}_o\right) d\Omega$$

Equation 5.3-10

Approximating the polar angle integral using Gaussian Quadrature, the total power is written as

$$P_{total} = \sum_{j=-N}^{N} y_j \int_0^{2\pi} I_d\left(\vec{r}_o, \mu_j\right) d\phi$$

Equation 5.3-11

Since the power density can be determined at the angles (quadrature points), μ_i, from the previous development and recalling that the power density has no ϕ-dependence

$$P_{total} = \sum_{j=-N}^{N} \int_0^{2\pi} y_j I_d\left(\vec{r}_d, \mu_j\right) d\phi = 2\pi \sum_{j=-N}^{N} y_j I_d\left(\vec{r}_o, \mu_j\right)$$

Equation 5.3-12

It is to be expected that the modified forward scatter solution will yield higher incoherent power densities than the corresponding strictly forward scatter solution. This is true since, given the same isotropic scatterers, the modified forward scatter solution captures some of the energy that is considered lost in the strictly forward scatter solution.

This is seen in Figure 5.3-6 in which the same isotropic scatterers are used to simulate ***total incoherent power*** in each of the strictly forward and modified forward cases. Only the 10-wavelength depth result for strictly forward scatter is given in this figure (indicated in the legend simply as “forward at 10 wl”), for reference. The strictly forward case includes power in only the forward direction; however, the modified forward is produced by summing the incoherent power in each of the forward directions as specified by a 5-point Gaussian Quadrature. At a one-wavelength depth, the beamwidth is consistent with the strictly forward/backward scattering solution, which will not show beam broadening. However, as the incoherent power is measured at larger depths, beam broadening becomes evident. This indicates that the strictly forward/backward scattering solution will not be sufficiently accurate for isotropic scatters in electrically “deep” media. Next, the full solution of the radiative transfer equations is derived for application with a numerical solution

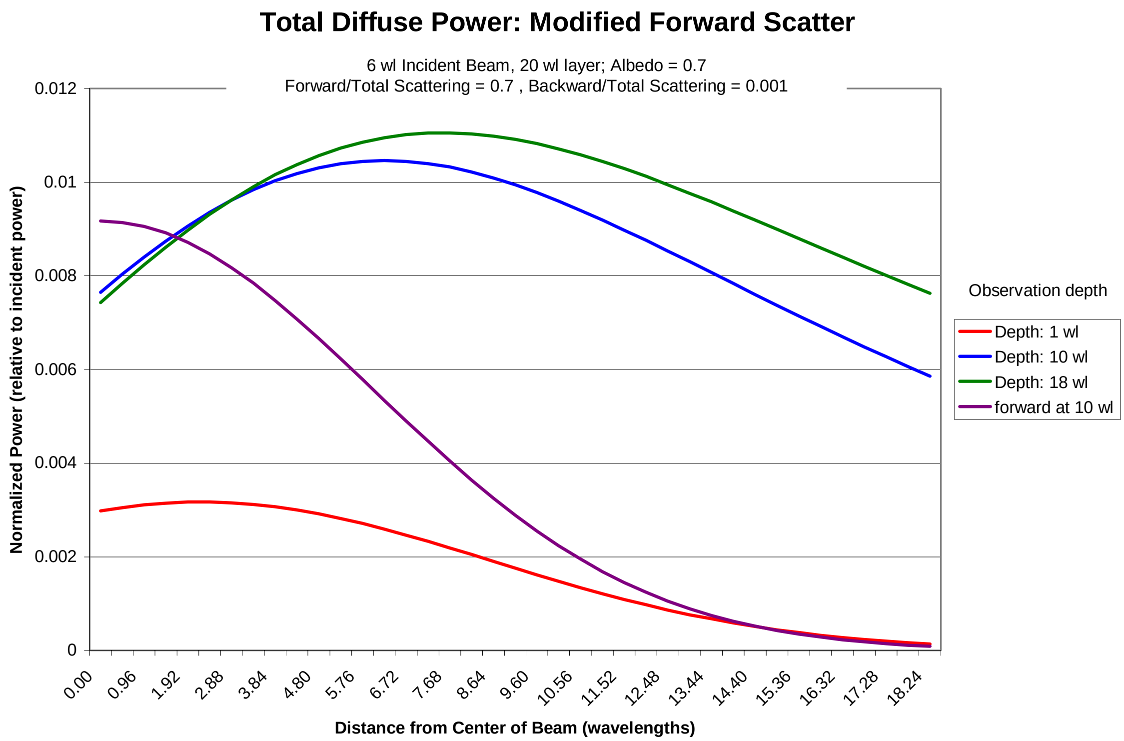

Figure 5.3-6: The total incoherent power at an observation point along the radial at a given depth (strictly forward scatter and modified forward scatter)

The beam bifurcation is an effect that is only expected in these two-dimensional simulations. Once the third dimension of the beam is included, this effect is expected to disappear. Note that only the axial point would be accurate, within a constant, in three dimensions since the problem is only symmetric at this point.

5.4 Beam Propagation using Radiative Transport Theory

An assumption employed in the derivation of the convolutional model, the subject of the next section, is that the scattering processes that are significant include only forward and backward scattering. This assumption implies that the illuminated volume contains the only scatterers that scattering energy back toward the radar. A solution of the radiative transfer equations has been presented for two cases now: strictly forward/backward (f-b) scattering, and a modified forward scatter. From the modified forward scatter solution, it is evident that isotropic scatterers can not be adequately modeled using the f-b solution. In this section, the general radiative transfer equations are developed and numerically solved for a beam-wave case. Again, it is seen that there will be significant beam broadening. Although it has been postulated that the f-b solution is inadequate for isotropic scattering, the full solution of the radiative transfer equations will yield the most accurate solution for beam wave propagation within the framework classical radiative transfer theory. Hence, this important result seems to be absent in literature with the exception of one case presented by Ishimaru [1993].

5.4.1 General Radiative Transfer for an Incident Beam Waveform

We begin the following illustration in Figure 5.4-1. From this figure, a heuristic derivation of the general transfer equation for beam incidence will be presented by following the more restrictive derivation by Ishimaru [1997].

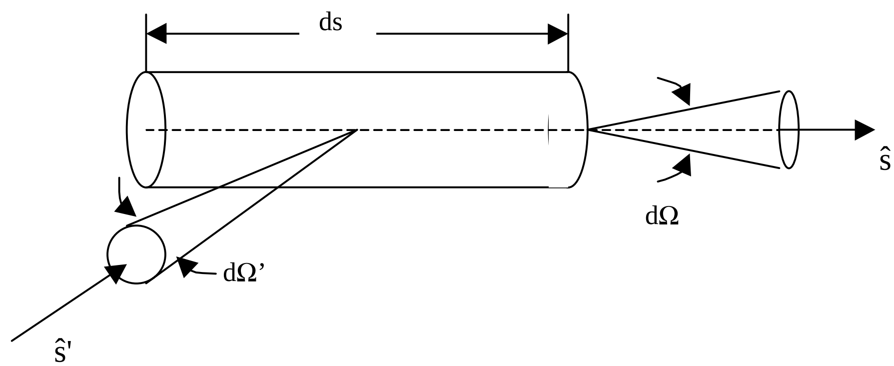

Figure 5.4-1: Scattering geometry for the intensity [Ishimaru, 1997]

The radiative transfer equation describes the evolution of the power density, $I(\vec{r},\hat{s})$, (sometimes called the total intensity) at the observation position, $\vec{r}$, in a characteristic direction, $\hat{s}$. Interpreting this equation in Cartesian coordinates, we find the ordinary differential equation in Equation 5.1-1 is interpreted as the following first-order partial differential equation,

$$\frac{d\,I(\vec{r},\hat{s})}{ds} = \frac{\partial z}{\partial s}\frac{\partial\,I(\vec{r},\hat{s})}{\partial z} + \frac{\partial \rho}{\partial s}\frac{\partial\,I(\vec{r},\hat{s})}{\partial \rho} = -\rho_d \sigma_t\,I(\vec{r},\hat{s}) + \frac{\rho_d \sigma_t}{4\pi}\iint_{4\pi} p(\hat{s},\hat{s}')I(\vec{r},\hat{s}')d\Omega'$$

Equation 5.4-1

The integral over the solid angle will be retained in this case. This integral represents the summation of incoherent and coherent energy that is traveling in other directions, $\hat{s}'$ that is scattered (according to the scattering amplitude, p(s,s')) into the direction of interest, $\hat{s}$. This is illustrated in the Figure 5.4-2.

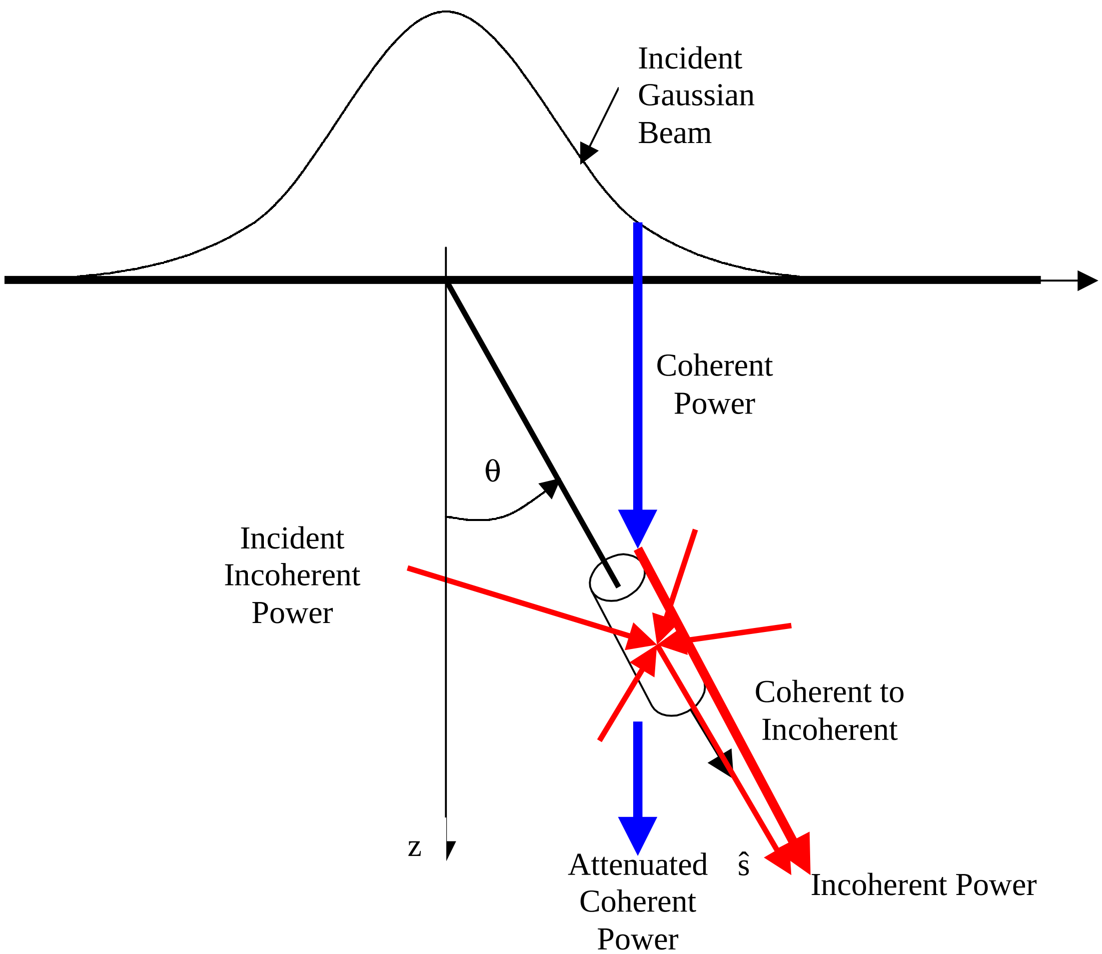

Figure 5.4-2: Illustration of scattering which includes multiple scattering

Evaluating the partial derivatives and splitting the total power density into coherent and incoherent portions, and $I(\vec{r},\hat{s})$, respectively,

$$\cos(\theta)\frac{\partial\left(I_d(\vec{r},\hat{s})+I_{ri}(\vec{r},\hat{s})\right)}{\partial z}+\sin(\theta)\frac{\partial\left(I_d(\vec{r},\hat{s})+I_{ri}(\vec{r},\hat{s})\right)}{\partial \rho}=$$

$$-\rho_d\sigma_t\left(I_d(\vec{r},\hat{s})+I_{ri}(\vec{r},\hat{s})\right)+\frac{\rho_d\sigma_t}{4\pi}\iint_{4\pi}p(\hat{s},\hat{s}')\left(I_d(\vec{r},\hat{s}')+I_{ri}(\vec{r},\hat{s}')\right)d\Omega'$$

Equation 5.4-2

Recalling that the scattering process is considered entirely incoherent, Equation 5.4-2 can be split into parts that govern the coherent and incoherent processes

$$\cos(\theta)\frac{\partial I_{ri}(\vec{r},\hat{s})}{\partial z}+\sin(\theta)\frac{\partial I_{ri}(\vec{r},\hat{s})}{\partial \rho}=-\rho_d\sigma_t I_{ri}(\vec{r},\hat{s})$$

Illustrates the coherent or “reduced” power density and

$$\cos(\theta)\frac{\partial I_d(\vec{r},\hat{s})}{\partial z}+\sin(\theta)\frac{\partial I_d(\vec{r},\hat{s})}{\partial \rho}=-\rho_d\sigma_t I_d(\vec{r},\hat{s})+\frac{\rho_d\sigma_t}{4\pi}\iint_{4\pi}p(\hat{s},\hat{s}')I_d(\vec{r},\hat{s})d\Omega'$$

is the incoherent or “diffuse’ power density. Each of these separate equations will be considered separately in the following sections. Note that the coherent power density acts as a source for the incoherent power density; consequently, a solution is attempted for the coherent power density first.

5.4.2 Characteristics Solution of the Coherent Power Density

The equation for the coherent power density (reduced intensity) was given in the previous subsection and is repeated here for convenience.

$$\cos(\theta)\frac{\partial I_{ri}(z,\rho,\theta)}{\partial z}+\sin(\theta)\frac{\partial I_{ri}(z,\rho,\theta)}{\partial \rho}=-\rho_d\sigma_t\,\partial\, I_{ri}(z,\rho,\theta)$$

Equation 5.4-3

The solution to this partial differential equation is most easily found using the method of characteristics. Consequently, first parameterizing the variables along the characteristics

$$\text{let } \rho = \eta \Rightarrow \phi_1(\eta) = \eta$$
$$z = 0 \Rightarrow \phi_2(\eta) = 0$$

We next solve the differential equations for the parameterized equations

1. $\dfrac{d\rho}{ds} = \sin(\theta), \qquad \text{general solution: } \rho = s\sin(\theta) + C_1$

   $\text{with I.C.: } \rho(\eta, s=0) = \eta \Rightarrow C_1 = \eta$

   $\text{final solution: } \rho = s\sin(\theta) + \eta$

2. $\dfrac{dz}{ds} = \cos(\theta), \qquad \text{general solution: } z = s\cos(\theta) + C_2$

   $\text{with I.C.: } z(\eta, s=0) = 0 \Rightarrow C_2 = 0$

   $\text{final solution: } z = s\cos(\theta)$

and solve for the characteristic variables

$$s = \frac{z}{\cos(\theta)}, \quad \eta = \rho - z\tan(\theta)$$

Hence, the characteristic equation for an incident Gaussian beam becomes

$$\frac{d\,I_{ri}(\vec{r},\hat{s})}{ds} = -\rho_d\sigma_t\, I_{ri}(\vec{r},\hat{s}) \Rightarrow I_{ri}(\vec{r},\hat{s}) = C_3\, e^{-\rho_d\sigma_t s}$$
$$\text{with IC: } I_{ri}(\rho(s,\eta), z(s,\eta), \theta) = A_0\, e^{-\frac{\eta^2}{2w^2}}$$

yields a solution to the characteristic equation incident beam.

$$I_{ri}(\vec{r},\hat{s}) = A_0\, e^{-\frac{\eta^2}{2w^2}}\, e^{-\rho_d\sigma_t s}$$
$$\text{or, } I_{ri}(z,\rho,\hat{s}) = A_0\, e^{-\frac{\rho^2}{2w^2}}\, e^{-\rho_d\sigma_t \frac{z}{\cos(\theta)}}$$

Note that the beamwidth is set by the symbol, w. Consequently, when a beam is normally incident ($\theta = 0°$), the beam shape for the reduced intensity within the random medium is a unchanged with the exception of the attenuation due to the extinction. This extinction is due to particle density and total cross-section and appears as a function of depth into the medium.

5.4.3 Solution for the Incoherent Power Density

The solution for the incoherent power density follows along the same procedure as that of the coherent power. However, the complexity of this problem requires a numerical solution, rather than the closed form solution for arbitrary scattering amplitudes. We begin with the radiative transfer equation governing the incoherent power density; restating the transfer equation

$$\cos(\theta)\frac{\partial I_d(\vec{r},\hat{s})}{\partial z}+\sin(\theta)\frac{\partial I_d(\vec{r},\hat{s})}{\partial \rho}=-\rho_d\sigma_t I_d(\vec{r},\hat{s})+\frac{\rho_d\sigma_t}{4\pi}\iint_{4\pi} p(\hat{s},\hat{s}')\left(I_d(\vec{r},\hat{s}')+I_{ri}(\vec{r},\hat{s}')\right)d\Omega'$$

Equation 5.4-4

This integro-differential equation cannot be solved for general amplitude-scattering function, p, and general boundary conditions. Consequently, the numerical solution of this equation is investigated. First invoking a change of variables from the polar angle to the cosine of this angle, we let $\mu = \cos(\theta)$ and redefine the amplitude scattering function as

$$p(\hat{s},\hat{s}') \Rightarrow p(\mu,\mu')$$

Next, we assume azimuthal symmetry within the random medium and integrate out the azimuthal dependence of the scattering function; this reduces the three dimensional problem down to two dimensions. This will only be valid for plane wave incidence and the beam axis for the beam wave incidence. Hence, the redefined amplitude scattering function is rewritten as [Ishimaru, 1997]

$$p_o(\mu,\mu') = \frac{1}{2\pi}\int_0^{2\pi} d\phi \frac{1}{2\pi}\int_0^{2\pi} d\phi' \, p(\mu,\phi;\mu',\phi')$$

Equation 5.4-5

Examples of this reduction are found in Ishimaru [1997]. For example, in terms of the cosines of the incident and scattering angles, μ and μ', respectively

$$\begin{aligned} \text{isotropic:} \quad & p_o(\mu,\mu') = W_o \equiv \text{albedo} \\ \text{Rayleigh:} \quad & p_o(\mu,\mu') = \frac{3}{4}\left[1+\mu^2\mu'^2 + \frac{1}{2}\left(1-\mu^2\right)\left(1-\mu'^2\right)\right] \end{aligned}$$

More general amplitude scattering functions may be derived in terms of Legendre polynomials as long as the scattering is symmetric about the direction of the incident wave [Ishimaru, 1997].

Consequently, after transforming the variable and the limits of integration, the transfer equation can be rewritten as follows (splitting the power density into diffuse and coherent portions as previously discussed).

$$\begin{aligned} \mu\frac{\partial I_d(\vec{r},\mu)}{\partial z} + \sqrt{1-\mu^2}\,\frac{\partial I_d(\vec{r},\mu)}{\partial \rho} &= -\rho_d\sigma_t I_d(\vec{r},\mu) + \frac{\rho_d\sigma_t}{4\pi}\int_{-1}^{1} p_o(\mu,\mu')\left(I_d(\vec{r},\mu') + I_{ri}(\vec{r},\mu')\right)d\mu' \\ &= -\rho_d\sigma_t I_d(\vec{r},\mu) + \frac{\rho_d\sigma_t}{2}\int_{-1}^{1} p_o(\mu,\mu') I_d(\vec{r},\mu')\,d\mu' + \frac{\rho_d\sigma_t}{4\pi} p_o(\mu,\mu_{inc}) I_{ri}(\vec{r},\mu_{inc}) \end{aligned}$$

Equation 5.4-6

Transforming back to the characteristics solution, we establish the following integro-differential equation

$$\frac{d I_d(\vec{r},\mu)}{ds} = -\rho_d\sigma_t I_d(\vec{r},\mu) + \frac{\rho_d\sigma_t}{2}\int_{-1}^{1} p_o(\mu,\mu') I_d(\vec{r},\mu')\,d\mu' + \frac{\rho_d\sigma_t}{4\pi} p_o(\mu,\mu_{inc}) I_{ri}(\vec{r},\mu_{inc})$$

The numerical solution of this equation has typically been performed using Gaussian Quadrature [Boyce, 1984]. First, we break the integral into a summation, weighted by the quadrature weights, y_j.

$$\frac{d\,I_d(\vec{r},\mu_i)}{ds} = -\rho_d\sigma_t\, I_d(\vec{r},\mu_i) + \frac{\rho_d\sigma_t}{2}\sum_{j=-N}^{N} y_j\, p_o(\mu_i,\mu_j) I_d(\vec{r},\mu_j) + \frac{\rho_d\sigma_t}{4\pi} p_o(\mu_i,\mu_{inc}) I_{ri}(\vec{r})$$

Now, the single, integro-differential equation with the summation over 2N quadrature points may now be rewritten as a system of 2N ordinary differential equations. Given an illumination which is ***normal*** to the boundary, the coherent power density incident to the elemental volume, ds, located at observation coordinates (ρ, z) is given by

$$I_{ri}\left(\rho, z; \hat{k}_i\right) = A_0\, e^{-\frac{\rho^2(s,\mu_i)}{2w^2}}\, e^{-\rho_d\,\sigma_t \frac{z}{\cos 0^o}} = A_0\, e^{-\frac{\rho^2(s,\mu_i)}{2w^2}}\, e^{-\rho_d\,\sigma_t\, z}$$

Where we recognize that the coordinates (ρ, z) must be translated into those appropriate for the characteristics solution. This conversion and the necessary geometry are given in the appendix to this chapter. From the results of this appendix, the incident coherent intensity to the elemental volume, ds, can be written in the following generic form;

$$I_{ri}\left(s,\mu_n;\hat{k}_i\right) = A_0\, e^{-\frac{\rho(s,\mu_i)^2}{2w^2}}\, e^{-\rho_d\,\sigma_t\, z} = A_0\, e^{-A_n s^2 - B_n s - C_n}$$

Consequently, the differential equation can be written as a system of ordinary, first order differential equations.

$$\frac{d}{ds}\begin{bmatrix} I_d(\rho_0,z_o,\mu_N) \\ \vdots \\ I_d(\rho_0,z_o,\mu_{-N}) \end{bmatrix} = -\rho_d\sigma_t \begin{bmatrix} I_d(\rho_0,z_o,\mu_N) \\ \vdots \\ I_d(\rho_0,z_o,\mu_{-N}) \end{bmatrix}$$
$$+\frac{\rho_d\sigma_t}{2}\begin{bmatrix} y_N p_0(\mu_N,\mu_N) & \cdots & y_N p_0(\mu_N,\mu_{-N}) \\ \vdots & \ddots & \vdots \\ y_{-N} p_0(\mu_{-N},\mu_N) & \cdots & y_{-N} p_0(\mu_{-N},\mu_{-N}) \end{bmatrix}\begin{bmatrix} I_d(\rho_0,z_o,\mu_N) \\ \vdots \\ I_d(\rho_0,z_o,\mu_{-N}) \end{bmatrix}$$
$$+\frac{\rho_d\sigma_t}{4\pi} A_0 \begin{bmatrix} p_0(\mu_N,1) e^{-A_N s^2 - B_N s - C_N} \\ \vdots \\ p_0(\mu_{-N},1) e^{-A_{-N} s^2 - B_{-N} s - C_{-N}} \end{bmatrix}\begin{bmatrix} I_d(\rho_0,z_o,\mu_N) \\ \vdots \\ I_d(\rho_0,z_o,\mu_{-N}) \end{bmatrix}$$

The “constants” A,B,C are functions of the angle, μ, and are defined in the Appendix. Employing another change of variables so that the optical distance, τ, is used

$$\text{let}: \quad \tau \equiv \rho_d \sigma_t s, \;\; d\tau \equiv \rho_d \sigma_t ds$$
$$a_n \equiv \frac{A_n}{(\rho_d \sigma_t)^2}, \;\; b_n \equiv \frac{B_n}{(\rho_d \sigma_t)}$$

we can then rewrite the matrix equation as

$$\frac{d}{d\tau}\begin{bmatrix} I_d(\rho_0, z_o, \mu_N) \\ \vdots \\ I_d(\rho_0, z_o, \mu_{-N}) \end{bmatrix} = -\begin{bmatrix} I_d(\rho_0, z_o, \mu_N) \\ \vdots \\ I_d(\rho_0, z_o, \mu_{-N}) \end{bmatrix}$$
$$+\frac{1}{2}\begin{bmatrix} y_N p_0(\mu_N, \mu_N) & \cdots & y_N p_0(\mu_N, \mu_{-N}) \\ \vdots & \ddots & \vdots \\ y_{-N} p_0(\mu_{-N}, \mu_N) & \cdots & y_{-N} p_0(\mu_{-N}, \mu_{-N}) \end{bmatrix}\begin{bmatrix} I_d(\rho_0, z_o, \mu_N) \\ \vdots \\ I_d(\rho_0, z_o, \mu_{-N}) \end{bmatrix}$$
$$+\frac{A_0}{4\pi}\begin{bmatrix} p_0(\mu_N, 1)e^{-a_N \tau^2 - b_N \tau - c_N} \\ \vdots \\ p_0(\mu_{-N}, 1)e^{-a_{-N} \tau^2 - b_{-N} \tau - c_{-N}} \end{bmatrix}\begin{bmatrix} I_d(\rho_0, z_o, \mu_N) \\ \vdots \\ I_d(\rho_0, z_o, \mu_{-N}) \end{bmatrix}$$

Equation 5.4-7

making a substitution for the constant matrix elements

$$\text{Let}: \;\; \bar{\bar{S}} \equiv -\bar{\bar{I}} + \frac{1}{2}\begin{bmatrix} y_N p_0(\mu_N, \mu_N) & \cdots & y_N p_0(\mu_N, \mu_{-N}) \\ \vdots & \ddots & \vdots \\ y_{-N} p_0(\mu_{-N}, \mu_N) & \cdots & y_{-N} p_0(\mu_{-N}, \mu_{-N}) \end{bmatrix}$$

Equation 5.4-8

where $\bar{\bar{I}}$ is the identity matrix. Using a short hand notation to denote the n^{th} quadrature value for the power density, $I_d(\rho_o, z_o, \mu_n) \Rightarrow I_{d,n}$ and the distances, d, the matrix equation can be rewritten as

$$\frac{d}{d\tau}\begin{bmatrix} I_{d,N} \\ \vdots \\ I_{d,-N} \end{bmatrix} = \overline{\overline{S}}\begin{bmatrix} I_{d,N} \\ \vdots \\ I_{d,-N} \end{bmatrix} + \frac{A_0}{4\pi}\begin{bmatrix} p_0(\mu_N,1)e^{-a_N\tau^2-b_N\tau-c_N} \\ \vdots \\ p_0(\mu_{-N},1)e^{-a_{-N}\tau^2-b_{-N}\tau-c_{-N}} \end{bmatrix}\begin{bmatrix} I_{d,N} \\ \vdots \\ I_{d,-N} \end{bmatrix}$$

Equation 5.4-9

Rather than an initial value problem, this a two-point boundary value problem. The boundary condition on the downward propagating and upward propagating power densities can be written in the following matrix form

$$\begin{bmatrix} I_{d,N} \\ \vdots \\ I_{d,1} \\ I_{d,-1} \\ \vdots \\ I_{d,-N} \end{bmatrix} = \begin{bmatrix} 0 \\ \vdots \\ 0 \\ 0 \\ \vdots \\ 0 \end{bmatrix}$$

Equation 5.4-10

This expression states that the downward propagating diffuse intensity is zero at the upper interface and that the upward propagating diffuse power density is zero at the lower interface. The solution of the nonhomogeneous boundary value problem can be obtained in the form of an integral transform.

In a homogeneous medium we may transform the optical depth into one dimension;

$$\text{let: } \zeta \equiv \mu\tau, \text{ such that } d\tau = \frac{d\zeta}{\mu}$$

$$\frac{d}{d\zeta}\begin{bmatrix} \mu_N I_{d,N} \\ \vdots \\ \mu_{-N} I_{d,-N} \end{bmatrix} = \overline{\overline{S}}\begin{bmatrix} I_{d,N} \\ \vdots \\ I_{d,-N} \end{bmatrix} + \frac{A_0}{4\pi}\begin{bmatrix} p_0(\mu_N,1)e^{-c_N} e^{-a_N\left(\frac{\zeta}{\mu_N}\right)^2 - b_N\left(\frac{\zeta}{\mu_N}\right)} \\ \vdots \\ p_0(\mu_{-N},1)e^{-c_{-N}} e^{-a_{-N}\left(\frac{\zeta}{\mu_{-N}}\right)^2 - b_{-N}\left(\frac{\zeta}{\mu_{-N}}\right)} \end{bmatrix}\begin{bmatrix} I_{d,N} \\ \vdots \\ I_{d,-N} \end{bmatrix}$$

Equation 5.4-11

since the cosines of the angles (quadrature values) are constant, they may be removed from the under the differential. Consequently, multiplying through by the inverse leads to the following matrix equation with some new definitions

$$\frac{d}{d\zeta}\begin{bmatrix} I_{d,N} \\ \vdots \\ I_{d,-N} \end{bmatrix} = \overline{\overline{P}}\begin{bmatrix} I_{d,N} \\ \vdots \\ I_{d,-N} \end{bmatrix} + \frac{A_0}{4\pi}\begin{bmatrix} \dfrac{p_0(\mu_N,1)}{\mu_N} e^{-c_N} e^{-a_N\left(\frac{\zeta}{\mu_N}\right)^2 - b_N\left(\frac{\zeta}{\mu_N}\right)} \\ \vdots \\ \dfrac{p_0(\mu_{-N},1)}{\mu_{-N}} e^{-c_N} e^{-a_{-N}\left(\frac{\zeta}{\mu_{-N}}\right)^2 - b_{-N}\left(\frac{\zeta}{\mu_{-N}}\right)} \end{bmatrix}\begin{bmatrix} I_{d,N} \\ \vdots \\ I_{d,-N} \end{bmatrix}$$

$$\text{where}: \quad \overline{\overline{P}} \equiv \begin{bmatrix} \dfrac{1}{\mu_N} & \cdots & 0 \\ \vdots & \ddots & \vdots \\ 0 & \cdots & \dfrac{1}{\mu_{-N}} \end{bmatrix}\overline{\overline{S}}$$

$$= \left\{-\begin{bmatrix} \dfrac{1}{\mu_N} & \cdots & 0 \\ \vdots & \ddots & \vdots \\ 0 & \cdots & \dfrac{1}{\mu_{-N}} \end{bmatrix} + \begin{bmatrix} \dfrac{y_N p_0(\mu_N,\mu_N)}{2\mu_N} & \cdots & \dfrac{y_N p_0(\mu_N,\mu_{-N})}{2\mu_N} \\ \vdots & \ddots & \vdots \\ \dfrac{y_{-N} p_0(\mu_{-N},\mu_N)}{2\mu_{-N}} & \cdots & \dfrac{y_{-N} p_0(\mu_{-N},\mu_{-N})}{2\mu_{-N}} \end{bmatrix}\right\}$$

Following the Green's Matrix solution in the book by [Cole, 1968], we start with the standard matrix equation

$$\frac{dI(\zeta)}{d\zeta} = \overline{\overline{P}}\, I(\zeta) + \bar{f}(\zeta)$$

Equation 5.4-12

where the matrix A is constant with respect to the modified optical distance, ζ, and the forcing function, f, physically represents the coherent incident power density "feeding" into the diffuse power density. The solution to Equation 5.4-12 can be cast as [Cole, 1968]

$$I(\zeta) = \overline{\overline{\psi}}(\zeta) \int_0^{\zeta} \overline{\overline{\psi}}^{-1}(t) f(t) dt - \overline{\overline{\psi}}(\zeta) \overline{\overline{D}}^{-1} \overline{\overline{W}}^{[\zeta_d]} \overline{\overline{\psi}}(\zeta_d) \int_0^{\zeta_d} \overline{\overline{\psi}}^{-1}(t) f(t) dt$$

$$\text{where} \quad \overline{\overline{D}} = \overline{\overline{W}}^{[0]} \overline{\overline{\psi}}(\zeta = 0) + \overline{\overline{W}}^{[\zeta_d]} \overline{\overline{\psi}}(\zeta = \zeta_d)$$

Equation 5.4-13

where the upper boundary of the random medium has been placed at an optical depth of zero ($\zeta = 0$) and the lower boundary of the medium occurs at ($\zeta = \zeta_d$), again in the modified optical depth coordinates. The matrix, ψ, is a particular fundamental matrix satisfying the homogeneous problem. Notice that the first integral must be re-evaluated with each time step, whereas the second integral is computed once.

The matrices, W, help describe the boundary conditions as follows

$$\overline{\overline{W}}^{[0]} I(0) + \overline{\overline{W}}^{[\zeta_d]} I(\zeta_d) = 0$$

Equation 5.4-14

where in this case, the matrices W are given as follows:

$$\overline{\overline{W}}^{[0]} = \begin{bmatrix} 1 & & 0 & 0 & & 0 \\ & \ddots & & & & \\ 0 & & 1 & 0 & & 0 \\ & & 0 & 0 & & 0 \\ & & & & \ddots & \\ 0 & & 0 & 0 & & 0 \end{bmatrix}, \quad \overline{\overline{W}}^{[\zeta_d]} = \begin{bmatrix} 0 & & 0 & 0 & & 0 \\ & \ddots & & & & \\ 0 & & 0 & 0 & & 0 \\ & & 0 & 1 & & 0 \\ & & & & \ddots & \\ 0 & & 0 & 0 & & 1 \end{bmatrix}$$

Equation 5.4-15

The solution to the homogeneous problem is found from an eigenvalue analysis. In this solution, we find the fundamental matrix, ψ, built up from the eigenvalues and eigenvectors of the homogeneous problem.

$$\psi(\zeta) = \begin{bmatrix} \beta_{1,1} \\ \vdots \\ \beta_{2N,1} \end{bmatrix} e^{\lambda_1 \zeta} + \begin{bmatrix} \beta_{1,2} \\ \vdots \\ \beta_{2N,2} \end{bmatrix} e^{\lambda_2 \zeta} + \cdots + \begin{bmatrix} \beta_{1,2N} \\ \vdots \\ \beta_{2N,2N} \end{bmatrix} e^{\lambda_{2N} \zeta}$$

Equation 5.4-16

From this solution, we construct the following fundamental solution matrix,

$$\overline{\overline{\Phi}}(\zeta) = \overline{\overline{\psi}}(\zeta)\overline{\overline{\psi}}^{-1}(0)$$

$$\overline{\overline{\Phi}}(\zeta) = \overline{\overline{\psi}}(\zeta)\overline{\overline{\psi}}(0) = \begin{bmatrix} \beta_{1,1}e^{\lambda_1\zeta} & & \beta_{1,2N}e^{\lambda_{2N}\zeta} \\ & \ddots & \\ \beta_{2N,1}e^{\lambda_1\zeta} & & \beta_{2N,2N}e^{\lambda_{2N}\zeta} \end{bmatrix} \begin{bmatrix} B_{1,1} & & B_{1,2N} \\ & \ddots & \\ B_{2N,1} & & B_{2N,2N} \end{bmatrix}$$

$$= \begin{bmatrix} \phi_{1,1}(\zeta) & \cdots & \phi_{1,2N}(\zeta) \\ \vdots & \ddots & \vdots \\ \phi_{2N,1}(\zeta) & \cdots & \phi_{2N,2N}(\zeta) \end{bmatrix}$$

$$\text{where:} \quad \phi_{i,j}(\zeta) = \sum_k \beta_{i,k} B_{k,j} e^{\lambda_k \zeta}$$

Equation 5.4-17

A useful property of this matrix is that its inverse is as follows

$$\overline{\overline{\Phi}}^{-1}(\zeta) = \overline{\overline{\Phi}}(-\zeta)$$

Now we are ready to compute a numerical solution to the general problem. First, we analytically evaluate the integrals in Equation 5.4-13 (as far as possible).

$$\int_0^{\zeta} \overline{\overline{\Phi}}^{-1}(t)\bar{f}(t) = \int_0^{\zeta} \overline{\overline{\Phi}}(-t)\bar{f}(t)$$

$$= \int_0^{\zeta} \begin{bmatrix} \phi_{1,1}(-t) & \cdots & \phi_{1,2N}(-t) \\ & \ddots & \\ \phi_{2N,1}(-t) & & \phi_{2N,2N}(-t) \end{bmatrix} \begin{bmatrix} \dfrac{A_0 p_0(\mu_1,1)}{4\pi\mu_1} e^{-c_N} e^{-a_1\left(\frac{t}{\mu_1}\right)^2 - b_1\left(\frac{t}{\mu_1}\right)} \\ \vdots \\ \dfrac{A_0 p_0(\mu_{2N},1)}{4\pi\mu_{2N}} e^{-c_{2N}} e^{-a_{2N}\left(\frac{t}{\mu_{2N}}\right)^2 - b_{2N}\left(\frac{t}{\mu_{2N}}\right)} \end{bmatrix}$$

where $\phi_{i,j}(-t) = \sum_k \beta_{i,k} B_{k,j} e^{-\lambda_k t}$

$$\int_0^{\zeta} \overline{\overline{\Phi}}(-t)f(t) = \int_0^{\zeta} \begin{bmatrix} \sum_{n=1}^{2N} \phi_{1,n} \dfrac{A_0 p_0(\mu_n,1)}{4\pi\mu_n} e^{-c_n} e^{-a_n\left(\frac{t}{\mu_n}\right)^2 - b_n\left(\frac{t}{\mu_n}\right)} \\ \vdots \\ \sum_{n=1}^{2N} \phi_{2N,n} \dfrac{A_0 p_0(\mu_n,1)}{4\pi\mu_n} e^{-c_n} e^{-a_n\left(\frac{t}{\mu_n}\right)^2 - b_n\left(\frac{t}{\mu_n}\right)} \end{bmatrix}$$

$$= \int_0^{\zeta} \begin{bmatrix} \sum_{n=1}^{2N} \sum_k \beta_{1,k} B_{k,n} e^{-\lambda_k t} \dfrac{A_0 p_0(\mu_n,1)}{4\pi\mu_n} e^{-c_n} e^{-a_n\left(\frac{t}{\mu_n}\right)^2 - b_n\left(\frac{t}{\mu_n}\right)} \\ \vdots \\ \sum_{n=1}^{2N} \sum_k \beta_{2N,k} B_{k,n} e^{-\lambda_k t} \dfrac{A_0 p_0(\mu_n,1)}{4\pi\mu_n} e^{-c_n} e^{-a_n\left(\frac{t}{\mu_n}\right)^2 - b_n\left(\frac{t}{\mu_n}\right)} \end{bmatrix}$$

moving the integrations inside the summations

$$\int_0^{\zeta} \overline{\overline{\Phi}}(-t)f(s) = \begin{bmatrix} \sum_{n=1}^{2N} \sum_{k=1}^{2N} \beta_{1,k} B_{k,n} \dfrac{A_0 p_0(\mu_n,1)}{4\pi\mu_n} e^{-c_n} \int_0^{\zeta} e^{-\left(\frac{a_n}{\mu_n^2}\right)t^2 - \left(\frac{b_n}{\mu_n} + \lambda_k\right)t} dt \\ \vdots \\ \sum_{n=1}^{2N} \sum_{k=1}^{2N} \beta_{2N,k} B_{k,n} \dfrac{A_0 p_0(\mu_n,1)}{4\pi\mu_n} e^{-c_n} \int_0^{\zeta} e^{-\left(\frac{a_n}{\mu_n^2}\right)t^2 - \left(\frac{b_n}{\mu_n} + \lambda_k\right)t} dt \end{bmatrix}$$

Equation 5.4-18

These integrations may be performed in closed form (in terms of the error function) using the integral relationship

$$\int_0^{\zeta} e^{-at^2-bt}dt = \frac{1}{2}\sqrt{\frac{\pi}{a}}\, e^{b^2/4a}\left[\operatorname{erf}\left(\sqrt{a}\zeta+\frac{b}{2\sqrt{a}}\right)-\operatorname{erf}\left(\frac{b}{2\sqrt{a}}\right)\right]$$

Equation 5.4-19

Substituting this result into Equation 5.4-18,

$$\int_0^{\zeta} \overline{\overline{\Phi}}(-t)f(s) = \begin{bmatrix} \sum_{n=1}^{2N}\sum_{k=1}^{2N}\beta_{1,k}B_{k,n}\frac{A_0p_0(\mu_n,1)}{4\pi\mu_n}e^{-c_n}I_{n,k} \\ \vdots \\ \sum_{n=1}^{2N}\sum_{k=1}^{2N}\beta_{2N,k}B_{k,n}\frac{A_0p_0(\mu_n,1)}{4\pi\mu_n}e^{-c_n}I_{n,k} \end{bmatrix}$$

Equation 5.4-20

$$\text{where}\quad I_{n,k} \equiv \int_0^{\zeta} e^{-\left(\frac{a_n}{\mu_n^2}\right)t^2-\left(\frac{b_n}{\mu_n}+\lambda_k\right)t}dt$$

$$= \frac{1}{2}\sqrt{\frac{\pi}{\left(\frac{a_n}{\mu_n^2}\right)}}\, e^{\left(\frac{b_n}{\mu_n}+\lambda_k\right)^2\Big/4\left(\frac{a_n}{\mu_n^2}\right)}\left[\operatorname{erf}\left(\sqrt{\left(\frac{a_n}{\mu_n^2}\right)}\zeta+\frac{\left(\frac{b_n}{\mu_n}+\lambda_k\right)}{2\sqrt{\left(\frac{a_n}{\mu_n^2}\right)}}\right)-\operatorname{erf}\left(\frac{\left(\frac{b_n}{\mu_n}+\lambda_k\right)}{2\sqrt{\left(\frac{a_n}{\mu_n^2}\right)}}\right)\right]$$

Equation 5.4-21

For further simplification in notation,

$$\text{let}:\quad \alpha_n \equiv \frac{a_n}{\mu_n^2} = \frac{A_n}{\mu_n^2(\rho_d\sigma_t)^2},\ \beta_n \equiv \frac{b_n}{\mu_n} = \frac{B_n}{\mu_n\rho_d\sigma_t}$$

then we can rewrite the above expression after the change of variables and rearranging the summations as

$$\int_0^{\zeta} \overline{\overline{\Phi}}(-t)f(s) = \begin{bmatrix} \sum_{n=1}^{2N} \frac{A_0 p_0(\mu_n,1)}{4\pi\mu_n} \frac{1}{2}\sqrt{\frac{\pi}{\alpha_n}}\, e^{-c_n} \sum_{k=1}^{2N} \beta_{1,k} B_{k,n} I_{n,k} \\ \vdots \\ \sum_{n=1}^{2N} \frac{A_0 p_0(\mu_n,1)}{4\pi\mu_n} \frac{1}{2}\sqrt{\frac{\pi}{\alpha_n}}\, e^{-c_n} \sum_{k=1}^{2N} \beta_{2N,k} B_{k,n} I_{n,k} \end{bmatrix}$$

Equation 5.4-22

$$\text{where} \quad I_{n,k} \equiv \int_0^{\zeta} e^{-\alpha_n t^2 - (\beta_n + \lambda_k)t} dt$$
$$= e^{(\beta_n+\lambda_k)^2/4\alpha_n} \left[\operatorname{erf}\left(\sqrt{\alpha_n}\,\zeta + \frac{(\beta_n + \lambda_k)}{2\sqrt{\alpha_n}} \right) - \operatorname{erf}\left(\frac{(\beta_n + \lambda_k)}{2\sqrt{\alpha_n}} \right) \right]$$

Consequently, we write the intensity in a given direction, using the new fundamental matrix, as

$$\bar{I}(\zeta) = \overline{\overline{\Phi}}(\zeta) \int_0^{\zeta} \overline{\overline{\Phi}}(-t)\bar{f}(t)dt \; - \overline{\overline{\Phi}}(\zeta)\overline{\overline{D}}^{-1}\overline{\overline{W}}^{[\zeta_d]}\overline{\overline{\Phi}}(\zeta_d) \int_0^{\zeta_d} \overline{\overline{\Phi}}(-t)\bar{f}(t)dt$$
$$\text{where} \quad \overline{\overline{D}} = \overline{\overline{W}}^{[0]}\overline{\overline{\Phi}}(\zeta = 0) + \overline{\overline{W}}^{[\zeta_d]}\overline{\overline{\Phi}}(\zeta = \zeta_d)$$

Equation 5.4-23

where all expressions are now known in closed form.

To find the total power at a location, $\vec{r}_o$, within the medium or at its boundary, we integrate the power density over the solid angle surrounding the observation point. First we express the total intensity as in the following integral relationship

$$P_{total} = \iint_{4\pi} P_{density}(\vec{r}_o) d\Omega$$

Equation 5.4-24

Approximating the polar angle integral using Gaussian Quadrature, we find

$$P_{total} = \sum_{j=-N}^{N} y_j \int_0^{2\pi} I_d(\vec{r}_o, \mu_j)\, d\phi$$

Equation 5.4-25

Since we can find the power density in the directions of the angles, μ_i, from the previous development, the solution for the total incoherent power can be reached. Recalling that the power density has no ϕ-dependence

$$P_{total} = \sum_{j=-N}^{N} \int_{0}^{2\pi} y_j \, I_d\left(\vec{r}_d, \mu_j\right) d\phi = 2\pi \sum_{j=-N}^{N} y_j \, I_d\left(\vec{r}_o, \mu_j\right)$$

Equation 5.4-26

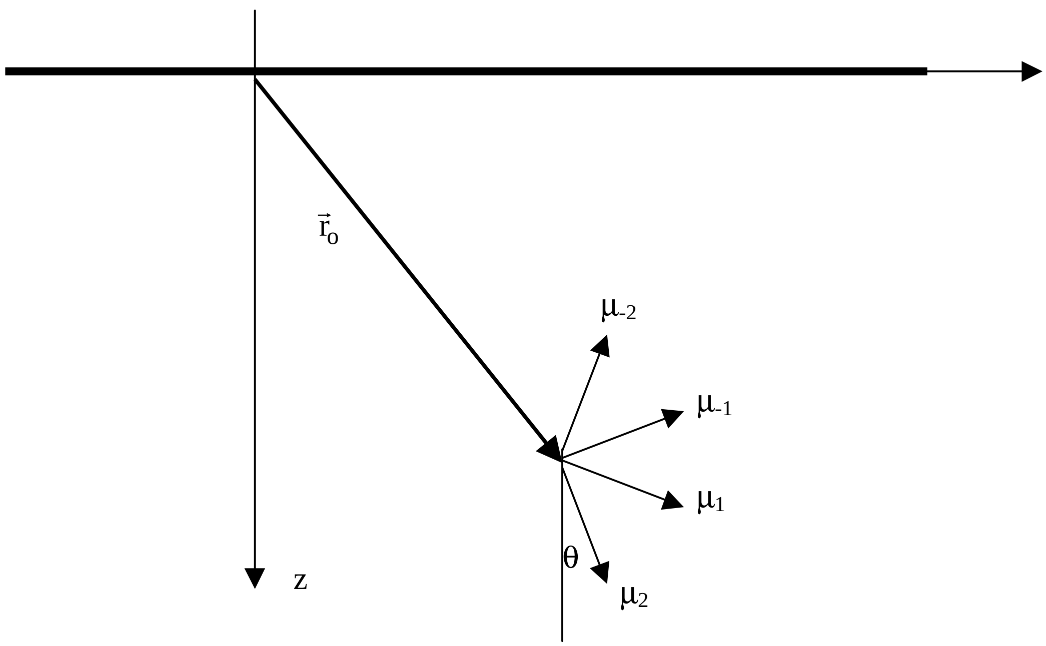

Figure 5.4-3: Illustration of the discrete angles in Gaussian quadrature

An example of this method is given in Figure 5.4-4. In this figure, the *total* incoherent power density is given for various depths. Significant beam broadening is evident as the incoherent power density is measured at deeper depths into the medium. In addition, some numerical problems are evident at the larger radii. Although larger beamwidths are expected, the one-wavelength depth curve does not seem to decay. This is due not only to the contribution of the backscattered energy but also to the following numerical problem. As the number of quadrature points is increased, the eigenvalues of the scattering matrix get larger and the solution becomes unstable. Hence, only five quadrature points were used to generate these curves. Comparison with ten quadrature points showed reasonable agreement out to a certain radius, then the solutions diverged. Comparison with the modified forward scatter solution (which does not suffer numerical instability) shows reasonable agreement out to a certain radius. This problem will require further refinement of this method and will be a topic of future efforts.

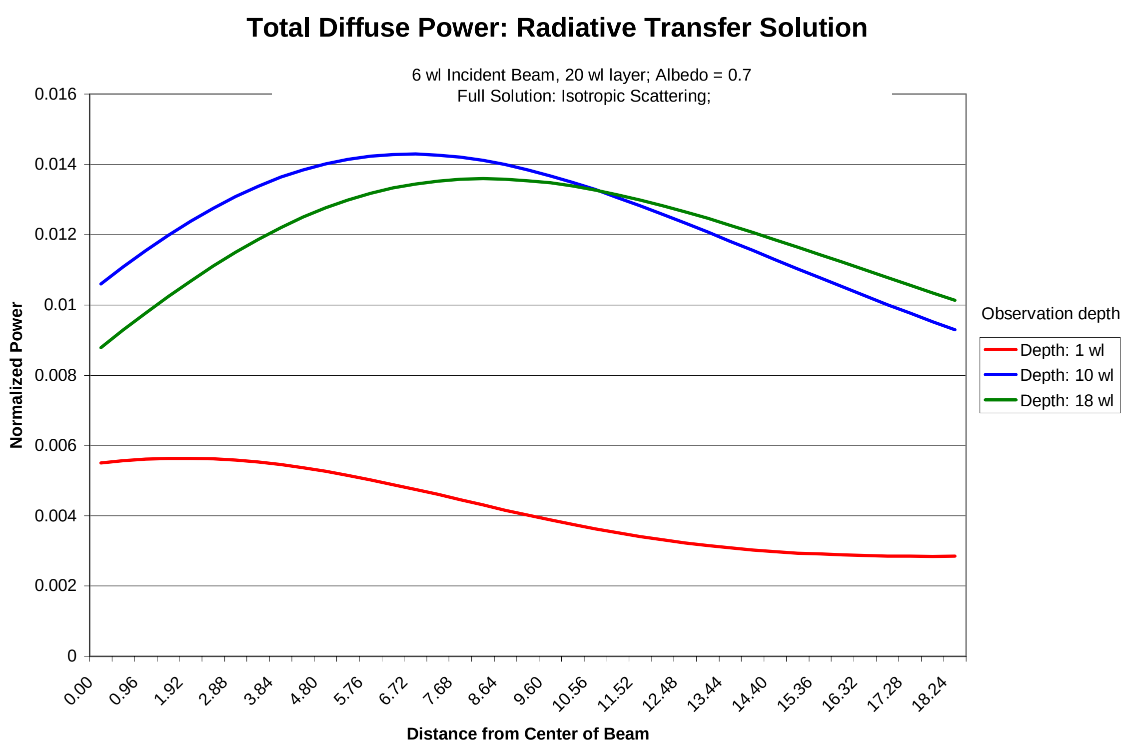

Figure 5.4-4: Incoherent power transmitted into the medium at varying depths using the full radiative transfer solution.

Figure 5.4-5 displays the total diffuse power at a depth of 10 wavelengths into the medium. In addition to the full radiative transfer solution, this figure also shows the results for the modified forward scatter result and the strictly forward/backward (f-b) solution. The beam broadening is very evident between the full solution and the f-b solution. Consequently, as seen with the modified forward scatter solution, isotropic scatterers may not be well represented in the f-b case for an electrical thick layer.

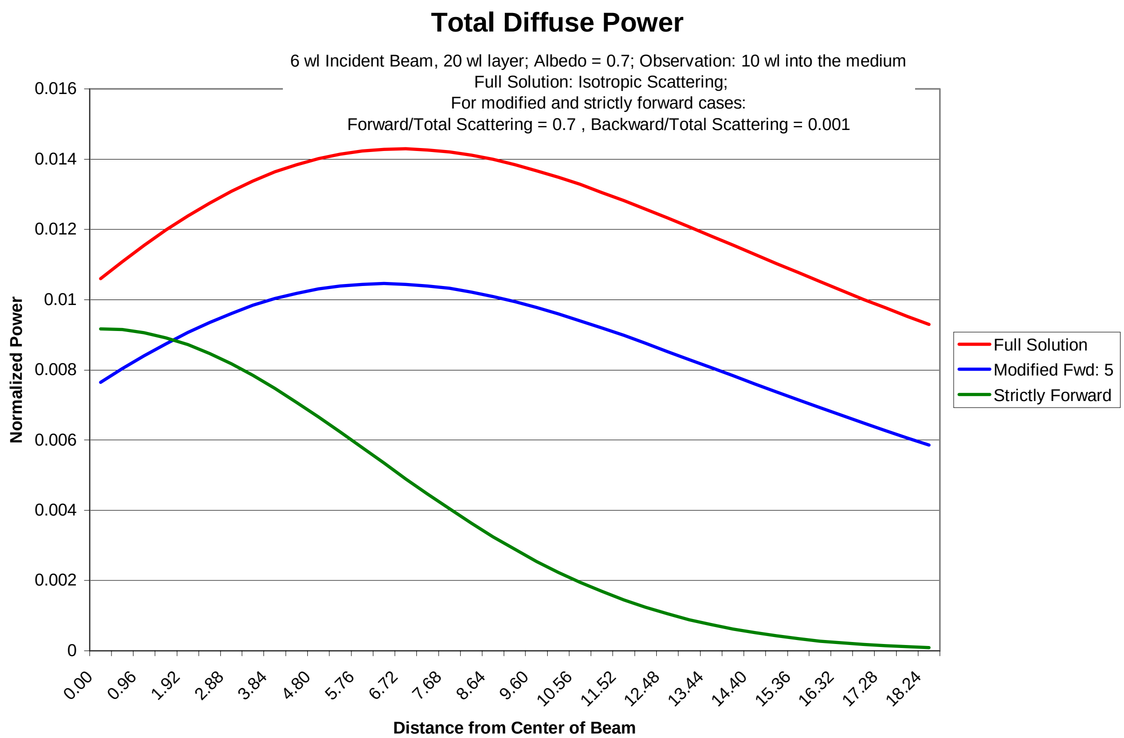

Figure 5.4-5: Comparison of the transmitted total incoherent power at a 10 wavelength depth into the medium for the f-b, modified forward and full solutions

Again, we note that the beam bifurcation is an effect that is only expected in these two-dimensional simulations. Once the third dimension of the beam is included, this effect is expected to disappear. Note that only the axial point would be accurate, within a constant, in three dimensions since the problem is only symmetric at this point.

5.5 Conclusions and Future Efforts

This chapter has outlined the development of a general interpretation of the radiative transfer equations. The beam wave solutions presented in this chapter have indicated that beam broadening will become significant when the discrete objects scatter isotropically or the medium is electrical deep. Isotropic scattering, however, is expected to yield a large beam spread. Hence, further examination of beam broadening for more general power scattering amplitudes, such as the one proposed by Schwering (see Section 4.4), is necessary. This is a work in progress; although the theory is developed, it has only been tested for forward-backward, isotropic scattering and two-dimensional beam broadening. The first step in the extension of this theory is the introduction of the third dimension. Subsequently, the introduction of the more complex scattering patterns will require further effort in the numerical implementation of the theory. In addition, there is still room for original work in extending the solutions to polarized waves and pulsed waves.

5.6 *Appendix: Geometrical Considerations*

In this solution, we must keep in mind that the directions are fixed by the quadrature points. Consequently, for a given angle (quadrature), μ_i, the observation coordinates (ρo, zo) must be calculated as in Figure 5.6-1. The problem is to find the radial distance in antenna coordinates in terms. In all cases, the observation point will be in the quadrant shown. Since a nadir pointed antenna pattern is symmetrical about the z-axis, only one quadrant of data needs to be calculated.

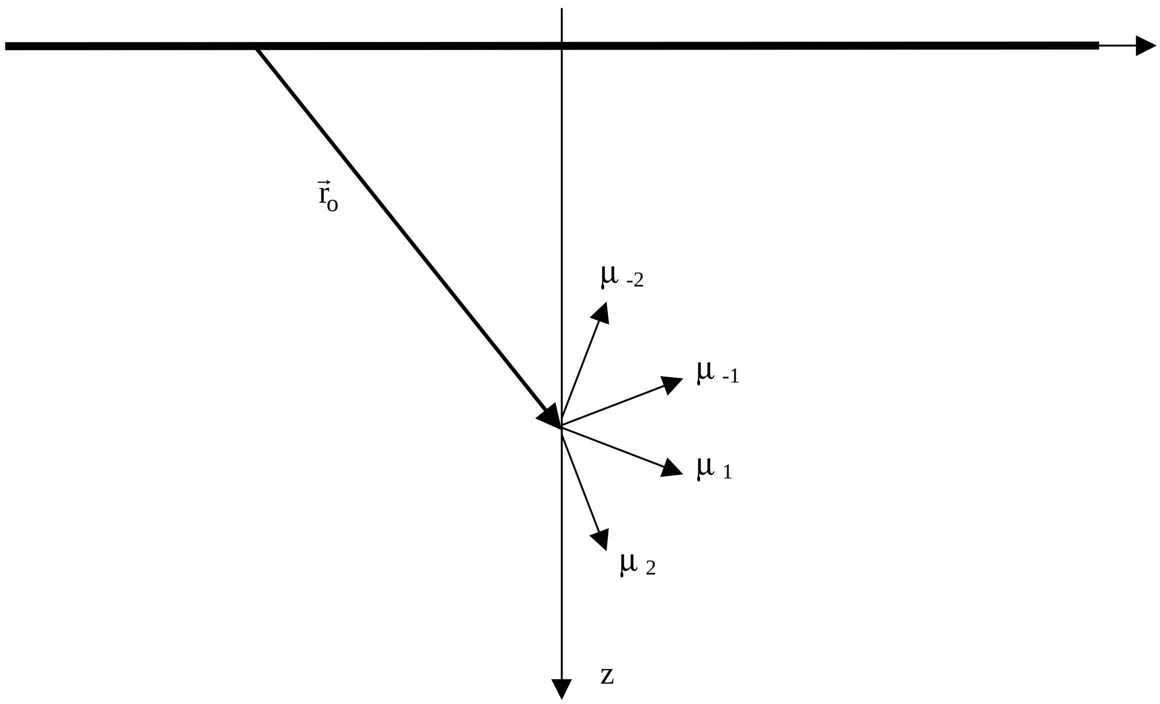

Figure 5.6-1: Gaussian Quadrature Illustration – fixed scattering angles

An expression is needed for the incient field in the characteristics coordinates. Starting with the expression for the incident Gaussian beam, with the corresponding loss into the medium

$$e^{-\frac{\rho^2}{2w^2}} e^{-\rho_d \sigma_t z}$$

the next sections develop the geometric expressions in the characteristic coordinates.

5.6.1 Case 1: Forward Scattering

$\left[0^o \leq \theta_i \leq 90^o\right]$

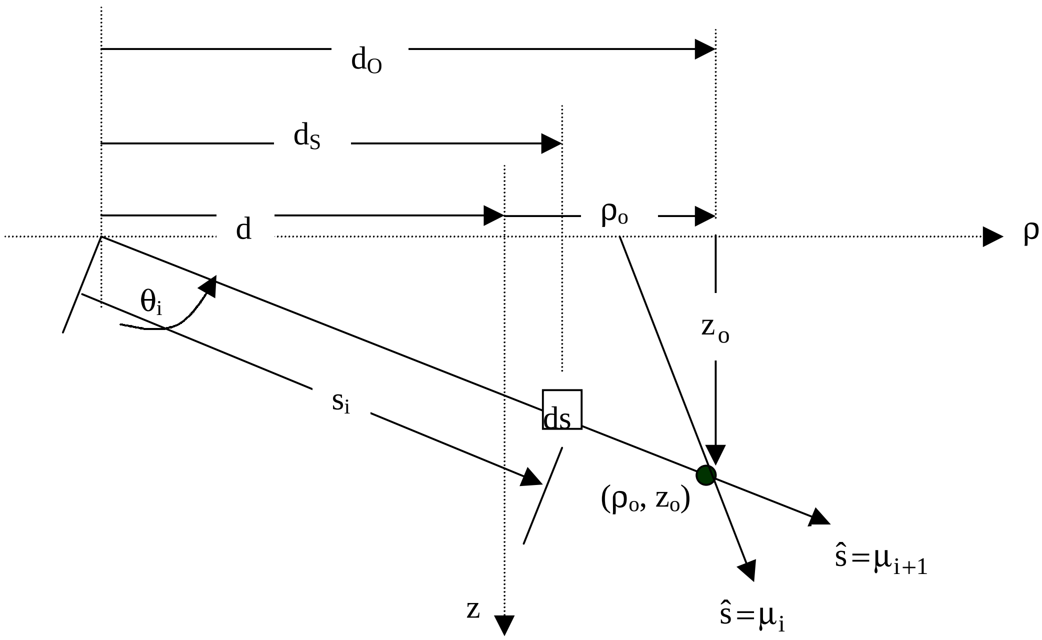

Figure 5.6-2: Translation of the Observation Coordinates into the Characteristics

$$d_o(\mu) = z_o \tan\theta = z_o \frac{\sqrt{1-\mu^2}}{\mu}$$

if $\left[d_o > \rho_o\right]$ - (e.g. μ_{i+1} in Figure 5.6-2) then the following evaluations hold

Integrate along characteristic from the upper boundary to the observation point so that:

Integration limits of s: $\int_0^{s_o} \cdots ds = \int_{(\rho=\rho_o - d_o, z=0)}^{(\rho=\rho_o, z=z_o)} \cdots ds$

$$\rho(s,\mu) = s\sin\theta - \left(d_o(\mu) - \rho_o\right) \quad \text{for } \left\{s\sin\theta \geq \left(d_o(\mu) - \rho_o\right)\right\}$$
$$\rho(s,\mu) = \left(d_o(\mu) - \rho_o\right) - s\sin\theta \quad \text{for } \left\{s\sin\theta < \left(d_o(\mu) - \rho_o\right)\right\}$$

so for each case, we arrive at the same expression for the square of the radial distance, ρ

$$
\begin{aligned}
\rho^2(s,\mu) = \left[s\sin\theta - (d_o(\mu) - \rho_o)\right]^2 &= \left[(d_o(\mu) - \rho_o) - s\sin\theta\right]^2 \\
&= s^2\sin^2\theta - 2s\left[d_o(\mu) - \rho_o\right]\sin\theta + \left[d_o(\mu) - \rho_o\right]^2 \\
&= s^2\sin^2\theta + 2s\left[\rho_o - d_o(\mu)\right]\sin\theta + \left[d_o(\mu) - \rho_o\right]^2
\end{aligned}
$$

if $\left[d_o \le \rho_o\right]$ - (e.g. μ_i in Figure 5.6-2) then the following evaluations hold

Integrate along characteristic from the upper boundary to the observation point so that:

Integration limits of s: $\int_0^{s_o} \cdots ds = \int_{(\rho=\rho_o - d_o, z=0)}^{(\rho=\rho_o, z=z_o)} \cdots ds$

$$
\begin{aligned}
\rho(s,\mu) &= \left[\rho_o - d_o(\mu) + s\sin\theta\right] \\
\rho^2(s,\mu) &= \left[\rho_o - d_o(\mu) + s\sin\theta\right]^2 \\
&= s^2\sin^2\theta + 2s\left[\rho_o - d_o(\mu)\right]\sin\theta + \left[\rho_o - d_o(\mu)\right]^2 \\
&= s^2\sin^2\theta + 2s\left[\rho_o - d_o(\mu)\right]\sin\theta + \left[d_o(\mu) - \rho_o\right]^2
\end{aligned}
$$

So in all cases the exponent for the incident coherent power density (***normal incidence, θ_{inc}=0***) is

with $z(s,\mu) = s\cos\theta = s\mu$

$$
\begin{aligned}
\therefore\ \frac{\rho^2(s,\mu)}{2w^2} + \rho_d\sigma_t\frac{z(s,\mu)}{\cos\theta_{inc}} &= \frac{\rho^2(s,\mu)}{2w^2} + \frac{\rho_d\sigma_t s\mu}{\cos(\theta_{inc} = 0^o)} \\
&= \left(\frac{1-\mu^2}{2w^2}\right)s^2 + \left(\frac{2\left[\rho_o - d_o(\mu)\right]\sqrt{1-\mu^2}}{2w^2} + \rho_d\sigma_t\mu\right)s + \left(\frac{(d_o(\mu) - \rho_o)^2}{2w^2}\right) \\
&= A s^2 + B s + C
\end{aligned}
$$

where the definitions of the “constants” A,B,C are obvious by comparison.

5.6.2 Case 2: Backward Scattering

$\left[90^o \le \theta_i \le 180^o\right]$

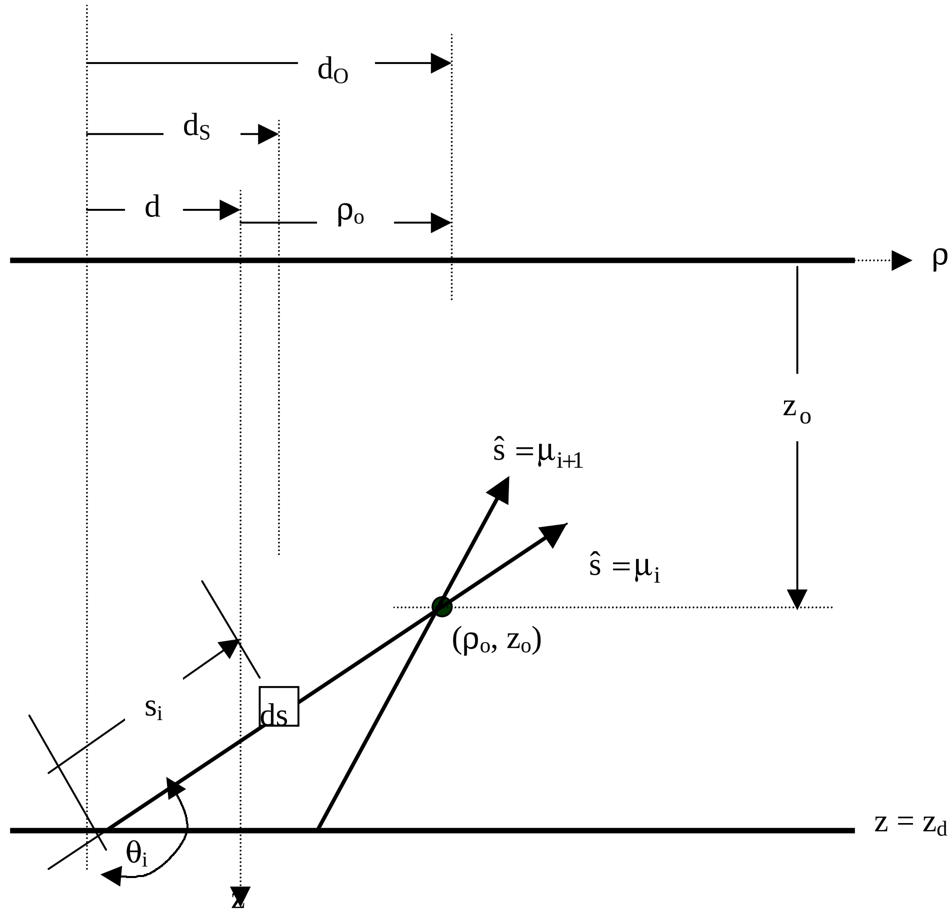

Figure 5.6-3: Translation of the Observation Coordinates into the Characteristics

$$d_o(\mu) = \frac{(z_d - z_o)}{\tan(\theta - \pi/2)} \; = -(z_d - z_o)\tan(\theta) = -(z_d - z_o)\frac{\sqrt{1-\mu^2}}{\mu}$$

- if $[d_o > \rho_o]$ - (e.g. μ_i in Figure 5.6-3) then the following evaluations hold

  Integrate along characteristic from the lower boundary to the observation point so that:

  Integration limits of s: $\int_0^{s_o} \cdots ds = \int_{(\rho=\rho_o - d_o, z=z_d)}^{(\rho=\rho_o, z=z_o)} \cdots \; ds$

$$
\begin{aligned}
\rho(s,\mu) &= \left[d_o(\mu) - \rho_o - s\cos(\theta - \pi/2)\right] \\
&= \left[d_o(\mu) - \rho_o - s\sin(\theta)\right], \qquad \text{for } \{s\sin(\theta) < d_o(\mu) - \rho_o\} \\
\rho(s,\mu) &= \left[s\cos(\theta - \pi/2) - (d_o(\mu) - \rho_o)\right] \\
&= \left[s\sin(\theta) - d_o(\mu) + \rho_o\right], \qquad \text{for } \{s\sin(\theta) \geq d_o(\mu) - \rho_o\}
\end{aligned}
$$

- if $[d_o < \rho_o]$ - (e.g. μ_{i+1} in Figure 5.6-3) then the following evaluations hold

Integrate along characteristic from the lower boundary to the observation point so that:

$$\text{Integration limits of s: } \int_0^{s_o} \cdots ds = \int_{(\rho=\rho_o - d_o, z=z_d)}^{(\rho=\rho_o, z=z_o)} \cdots \, ds$$

$$\rho(s,\mu) = \left[s\cos(\theta - \pi/2) - [d_0(\mu) - \rho_o]\right] = \left[s\sin\theta - [d_0(\mu) - \rho_o]\right]$$

- so for all values (and substituting in for $d(\mu)$)

$$
\begin{aligned}
\rho^2(s,\mu) &= \left[s\sin\theta - [d_0(\mu) - \rho_o]\right]^2 = \left(-\left[(d_0(\mu) - \rho_o) - s\sin\theta\right]\right)^2 \\
&= \left[s\sin\theta + [\rho_o - d_0(\mu)]\right]^2
\end{aligned}
$$

Hence, for this case, the exponent for the incident coherent power density (***normal incidence, θ_{inc}=0***) is

with $z(s,\mu) = z_d - s\sin(\theta - \pi/2) = z_d + s\cos\theta = z_d + s\mu$

$$
\begin{aligned}
\frac{\rho^2(s,\mu)}{2w^2} + \rho_d\sigma_t \frac{z(s,\mu)}{\cos\theta_{inc}} &= \frac{\left(s\sin(\theta) + [\rho_o - d_o(\mu)]\right)^2}{2w^2} + \rho_d\sigma_t \frac{(z_d + s\mu)}{\cos(\theta_{inc} = 0^o)} \\
&= \left(\frac{1-\mu^2}{2w^2}\right)s^2 + \left(\frac{2[\rho_o - d_o(\mu)]\sqrt{1-\mu^2}}{2w^2} + \rho_d\sigma_t\mu\right)s + \left(\frac{[\rho_o - d_o(\mu)]^2}{2w^2} + \rho_d\sigma_t z_d\right) \\
&= As^2 + Bs + C
\end{aligned}
$$

where the definitions of the “constants” A,B,C are obvious by comparison.

Chapter 6 Single Scattering and the Impulse Response

The simplest wave approach to scattering and propagation by a random medium is the single scatter approximation. Single scatter theory retains its simplicity by incorporating the assumption that the field incident to a random medium interacts with each scatterer only once and no multiple interactions occur among the scatterers that make up the random medium. This creates a scattered field, which is a summation of scattered *power* from each scatterer. The development of the convolutional model with single scatter theory is a first step in examining the limitations of the convolutional model. In addition, it is the first step in an extension of the convolutional model to more general scattering geometries using wave theory. Since the convolutional model incorporates several parameters that are determined by the physical environment, it has been proposed that these constants can be determined strictly through calibration by measured data. Given the results of the single scatter analysis, these constants may be interpreted in the context of a physical system. The multiple scattering approach in Chapter 7 will extend this idea that the constants in the convolutional model may be estimated, bounded and interpreted both before and after the model is calibrated with measured data.

In a previous section, the impulse response approach was introduced as an efficient means for computing the average power density from a rough surface. In this section, this impulse response technique is again derived from single scatter theory applied to a tenuous (sparse) random medium covering a rough surface. Like the radiative transfer extension, this method can use the convolutional approach; however, the equations are only developed into a form similar to the previous radiative transfer approach. The remainder of the development is presumed to be the same. Unlike the extension from the radiative transfer theory, the following method is derived for a more general case, which includes depolarization, strongly scattering- tenuous medium, and scattering which is more general than the forward-backward directions.

In addition, the single scatter derivation gives some insight into the pure phenomenological development of Chapter 4 . It is then simplified to match the convolutional approach, which only accounts for strictly forward scattering and backscattering. The single scatter approach also reduces to the common radar equation, which is briefly reviewed in the next section for future reference.

6.1 The Radar Equation

In the development of the single scatter theory in a random medium, the total received power, P, is written as a summation of the power scattered once by each particle. This simplification is due to the randomness of the scatterers in the medium: all interference effects are neglected. Consequently, summing up the power, P_R, returned to the radar from a continuum of scatterers in a random medium can be expressed using the standard radar equation

$$P_R = P_T \int_V \frac{\lambda^2 [G(\theta,\phi)]^2 \rho_d \, \sigma_b(\theta,\phi)}{(4\pi)^3 R^4} \, dV$$

Equation 6.1-1

where:
- λ = wavelength of the carrier
- $G(\theta, \phi)$ = radar antenna gain in the direction (θ,ϕ) or $\hat{k}_i$
- $\sigma_b(\theta, \phi)$ = particle backscattering cross section per unit area
- dV = elemental volume
- R = slant range from the radar to dV
- ρ_d = particle density per unit volume
- P_T = transmitted power

In this expression, the transmitted power is assumed to be a continuous wave signal. Consequently, the frequency dependence is monochromatic, since monochromatic dependence is implicit in the backscattering cross-section. This narrowband approximation is assumed in the transmitting and receiving subsystems as well as in the intervening medium. It will be shown that single scatter result does reduce to this form under the narrowband approximation. Next, the single scatter approximation is introduced. This will eventually lead to the radar equation and the convolutional result of Chapter 4 .

6.2 *The Single Scatter Approximation*

We begin by assuming a plane wave is incident on the scatterer; the incident field and the associated mean power density in free space are written as

$$\begin{aligned}
&\text{Incident Field} &&: \vec{E}_i(\vec{r}_s) = E_0\, e^{-j\vec{k}_i\cdot\vec{r}}\,\hat{e}_i\,, \\
&\text{Incident Power Density} &&: \vec{S}_i = \frac{1}{2}\left(\vec{E}_i(\vec{r}_s)\times\vec{H}_i^*(\vec{r}_s)\right) = \frac{1}{2\eta}\left|\vec{E}_i(\vec{r}_s)\right|^2\hat{e}_i
\end{aligned}$$

Equation 6.2-1

where the incidence direction is denoted by $\hat{k}_i$, the polarization is indicated by $\hat{e}_i$ (perpendicular to the incidence direction) and the impedance of background medium is given as (assumed to be non-magnetic)

$$\eta = \sqrt{\mu_0/\varepsilon}$$

In the development of the single scatter theory in a random medium, the total received power, P_R, is written as a summation of the power scattered once by each particle. This simplification is due to the randomness of the scatterers in the medium: all interference effects are neglected.

6.2.1 *The Scattered Field due to a Single Scatterer*

When the field scattered by a scatterer is examined, there are several regions in which the field's behavior is observed: the near field, Fresnel and far field regions. In the Fresnel and particularly the near field regions, the scattered waves display complicated phase and amplitude variations. Hence, for simplicity and as a common manner of practical convenience, we assume that the scattered field due to some incident field is to be observed only in the far field. Consequently when scatterers interact, they also are assumed to be in each other's far field. In acoustic wave propagation or when depolarization of an electromagnetic wave is expected to be negligible, a scatterer will scatter the incident field in all directions as weighted by scalar scattering amplitude.

Outside of the near field region, we may assume that the scattered field behaves as a spherical propagating wave, weighted by the scattering amplitude,

$$E_s = \frac{e^{-jkR}}{R} f(\hat{k}_s, \hat{k}_i) E_i$$

Equation 6.2-2

When the scatterer depolarizes the incident wave, the scattering amplitude will take on a more complex structure. In the matrix representation, the scattered field can be written in terms of the incident field. In the following matrix form, the incident and scattered fields are decomposed into their TE (⊥) and TM (||) components [Ishimaru, 1997]:

$$\begin{pmatrix} E_{s\perp} \\ E_{s\parallel} \end{pmatrix} = \frac{e^{-jkR}}{R} \begin{pmatrix} f_{11}(\hat{k}_s, \hat{k}_i) & f_{12}(\hat{k}_s, \hat{k}_i) \\ f_{21}(\hat{k}_s, \hat{k}_i) & f_{22}(\hat{k}_s, \hat{k}_i) \end{pmatrix} \begin{pmatrix} E_{i\perp} \\ E_{i\parallel} \end{pmatrix}$$

Equation 6.2-3

here the matrix $\overline{\overline{f}}(\hat{k}_s, \hat{k}_i)$ is the tensor scattering amplitude; the scattering direction is denoted by $\hat{k}_s$; and $R = |\vec{r}_o - \vec{r}_s|$ is the range from the scatterer to the observation point.

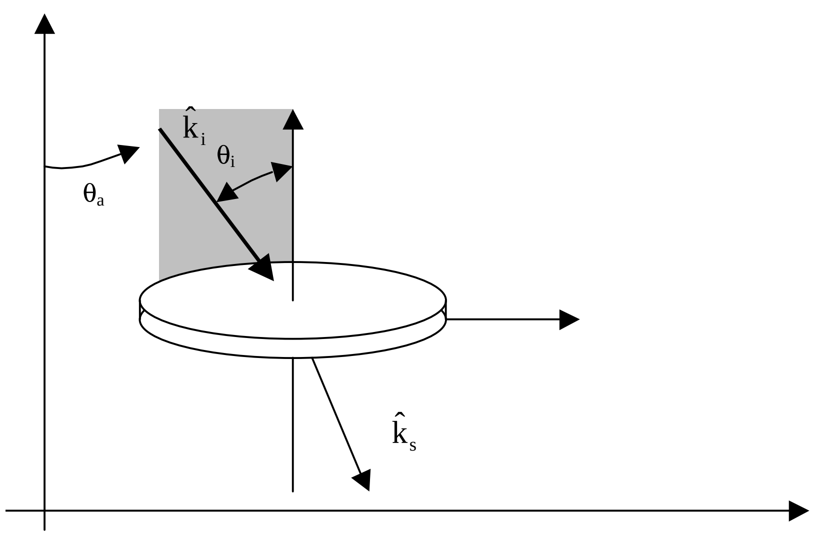

Figure 6.2-1: Scattering Polarization

Referring to Figure 6.2-1, we see that for a given incident field, the scattered field in the scattering plane can be determined. Then, both the incident and the scattered waves' polarizations are defined with respect to the "plane of scattering." This plane is created using the vector incidence and vector scattering direction. Consequently, the fields can be decomposed into TE and TM components (or perpendicular and parallel components) with respect to the plane of scattering. Hence, the scattered field vector, $\vec{E}_s(\vec{r})$, and scattered power density, $\vec{S}_s$, due to a single scatterer can be represented compactly as

$$\text{Scattered Field}: \ \vec{E}_S(\vec{r}_o) = \bar{\bar{f}}(\hat{k}_s, \hat{k}_i) \cdot \vec{E}_i(\vec{r}_s) \frac{e^{-jkR}}{R},$$
$$\text{Scattered Power}: S_s = \frac{1}{2}\left|\vec{E}_s(\vec{r}_o) \times \vec{H}_s^*(\vec{r}_o)\right| = \frac{1}{2\eta}\left|\vec{E}_s(\vec{r}_o)\right|^2$$

Equation 6.2-4

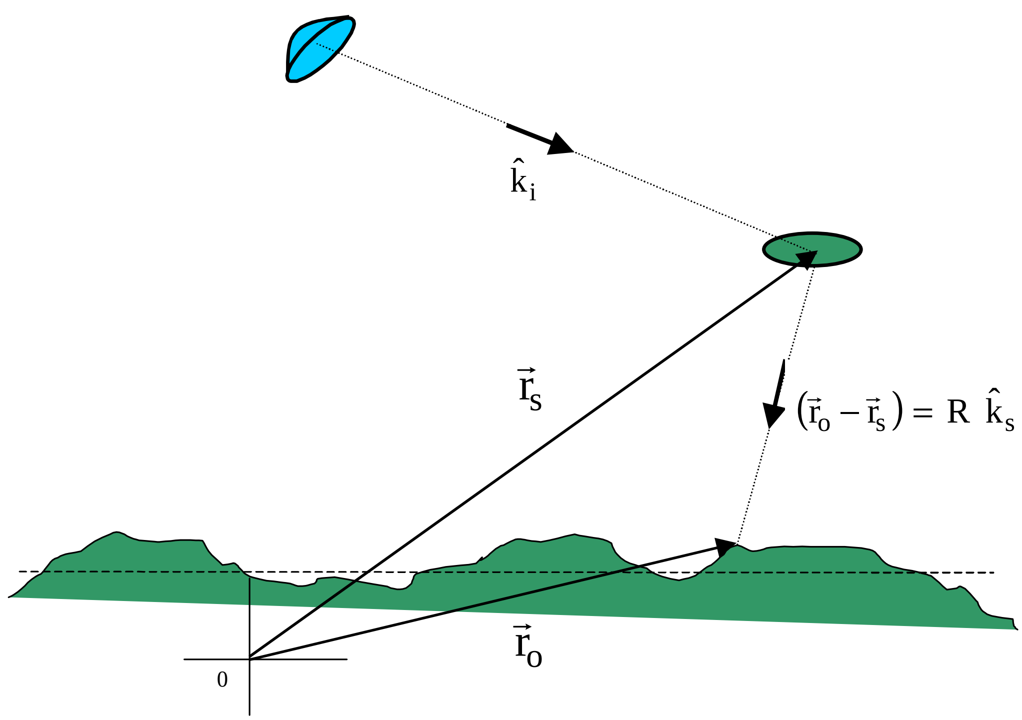

Figure 6.2-2: Scattering Geometry

The total field, the sum of the incident and the scattered fields, at the observation point can be written

$$\vec{E}(\vec{r}_a) = \vec{E}_i(\vec{r}_a) + \bar{\bar{f}}(\hat{k}_s, \hat{k}_i) \cdot \vec{E}_i(\vec{r}_s) \frac{e^{-jkR}}{R}$$

Equation 6.2-5

Scattering and depolarization by an ensemble of N scatterers can be accomplished using the single scatter approximation. Assuming that there is *no correlation between scatterers*, the total field at an observation point $\vec{r}_o$ can be written as the sum of the incident field (the field in the absence of scatterers) and the scattered field due to each of the scatterers.

$$\vec{E}(\vec{r}_a) = \vec{E}_i(\vec{r}_a) + \sum_{s=1}^{N} \bar{\bar{f}}(\hat{k}_s, \hat{k}_i) \cdot \vec{E}_i(\vec{r}_s) \frac{e^{-jkR}}{R}$$

Equation 6.2-6

When the incident field at scatterer, s, (under the summation) is simply given by the *free-space incident field evaluated at the position* $\vec{r}_s$, Equation 6.2-6 is the **single scatter** or **Born Approximation** (often, the Born approximation is attributed to an integral equation, not a summation). In other words, the incident field at each scatterer does not include the field incident due to scattering from other scatterers. Often the dyadic scattering matrix, above, is written as a product of the Fourier transform of the scattering operator and the remainder of the far-field form of the Green's function [Frisch, 1968]

$$\bar{\bar{f}}(\hat{k}_s, \hat{k}_i) = \tilde{S}(\hat{k}_s, \hat{k}_i) e^{-j(\vec{k}_i - \vec{k}_s)\cdot\vec{r}_s} = \frac{[\bar{\bar{I}} - \hat{k}_s\hat{k}_s]}{4\pi} \cdot \int \int e^{-j\vec{k}_s \cdot \vec{r}_a} S(\vec{r}_a, \vec{r}_s) e^{j\vec{k}_s \cdot \vec{r}_s} d\vec{r}_a d\vec{r}_s$$

Equation 6.2-7

This same form (Equation 6.2-6) can be extracted from the multiple scattering formalism found in Ishimaru [1997], attributed to Twersky [1962] by eliminating all but the first order terms; the zeroth order term is assigned to the incident field.

6.2.2 The Mean Field in the Single Scatter Approximation

Since the incident field is known and therefore deterministic, the mean field is easily written as

$$\left\langle \vec{E}(\vec{r}_a) \right\rangle = \vec{E}_i(\vec{r}_a) + \left\langle \sum_{s=1}^{N} \frac{e^{-jkR}}{R} \overline{\overline{f}}(\hat{k}_s, \hat{k}_i) \cdot \vec{E}_i(\vec{r}_s) \right\rangle$$

This average is performed over all random quantities. For a gas, this may only include position, while for foliage, it will include a host of characteristics including position, size, orientation, water content, shape, etc. In this paper we shall explicitly treat random position and the other quantities will be collected under a single random variable. In addition, we shall assume that random position and these other random quantities (such as orientation) are independent of the scatterer.

6.2.3 Statistical Description of the Random Medium

The probability of finding a scatterer within an incremental volume will be expressed as

$$p(\vec{r}_j)\, d\vec{r}_j = \frac{\rho(\vec{r}_j) dx_j dy_j dz_j}{N}$$

or the random number of scatterers within the unit volume divided by the total number of scatterers within the entire volume. The number density of the scatterers, $\rho(\vec{r}_s)$, is the number of scatterers within a unit volume. If we consider other aspects of the scatterer to be random, then the probability density function can be written as

$$p(\overline{\xi}_j) = \frac{P(\overline{\gamma}_j)\rho(\vec{r}_j)}{N}$$

where the vector random variable, $\overline{\gamma}$ represents the orientation, etc.

In order to describe the spatial distribution of the scatterers in addition to each scatterer's individual statistics, we construct the probability density function (pdf) of Equation 6.2-8. The joint distribution of any two scatterers written in a cluster expansion of centered random variables [Frisch, 1968]:

$$E\{\rho(\vec{r}_1),\rho(\vec{r}_2)\} = C(\vec{r}_1,\vec{r}_2); \quad E\{\rho(\vec{r}_1),\rho(\vec{r}_2),\rho(\vec{r}_3)\} = C(\vec{r}_1,\vec{r}_2,\vec{r}_3)$$

$$\begin{aligned} E\{\rho(\vec{r}_1),\rho(\vec{r}_2),\rho(\vec{r}_3),\rho(\vec{r}_4)\} = {} & C(\vec{r}_1,\vec{r}_2)C(\vec{r}_3,\vec{r}_4)+C(\vec{r}_1,\vec{r}_3)C(\vec{r}_2,\vec{r}_4) \\ & +C(\vec{r}_1,\vec{r}_4)C(\vec{r}_2,\vec{r}_3)+C(\vec{r}_1,\vec{r}_2,\vec{r}_3,\vec{r}_4) \end{aligned}$$

where E{*} indicates expected value

When Gaussian random variables are chosen, only the two-point correlation function exists. The use of these higher order statistics will prevent the absurdity that two scatterers can occupy the same space. Within the foliage, the correlation represents a spatial correlation and therefore, a finite correlation length is required. Hence, we construct the pdf with pair correlations. Another major assumption will also be included: the scatterer's individual properties (rotation, size, etc.) are statistically independent of the position statistics [Tsolakis, 1985].

$$p(\bar{\xi}_1,\bar{\xi}_2) = P(\bar{\gamma}_1)P(\bar{\gamma}_2)\left[\rho(\vec{r}_1)\rho(\vec{r}_2)+C(\vec{r}_1,\vec{r}_2)\right]$$

Equation 6.2-8

Here, the vector random variable, $\bar{\xi}$, represents a combination of the random variables for position, $\vec{r}$, and other scatterer properties, $\bar{\gamma}$. The function, $P(\bar{\gamma}_{1,2})$, is a joint pdf that describes the scatterer's size, rotation, etc. The density, $\rho(\vec{r})$, describes the scatterer's number density in the volume and finally the pair correlation between the scatterers is given by the correlation function $C(\vec{r},\vec{r}\,')$.

Recognizing that the incident field is deterministic in the single scatter approximation, the average field is rewritten

$$\left\langle \vec{E}(\vec{r}_a) \right\rangle = \vec{E}_i(\vec{r}_a) + \int_V d\vec{r} \sum_{s=1}^{N} \frac{e^{-jkR}}{R} \left\langle \bar{\bar{f}}(\hat{k}_s,\hat{k}_i) \right\rangle \cdot \vec{E}_i(\vec{r}_s) \frac{\rho(\vec{r}_s)}{N}$$

If the medium is uniform, the position probability density function is simply $\rho(\vec{r}_s)/N$ and the summation can be replaced by multiplication by N. Simplifying we find the mean field at an observation point $\vec{r}_a$.

$$\left\langle \vec{E}(\vec{r}_a) \right\rangle = \vec{E}_i(\vec{r}_a) + \int_V d\vec{r} \, \frac{e^{-jkR}}{R} \left\langle \bar{\bar{f}}(\hat{k}_s, \hat{k}_i) \right\rangle \cdot \vec{E}_i(\vec{r}_s) \rho(\vec{r}_s)$$

Equation 6.2-9

Here the configuration average $\langle \bullet \rangle$ is shown implicitly and the random positions are treated explicitly. In the notation of Tsolakis [1985], the average field is given by

$$\left\langle \vec{E}(\vec{r}_a) \right\rangle = \vec{E}_i(\vec{r}_a) + \int_V d\vec{r}_s \left\langle \left\langle \bar{\bar{u}}_s^a \right\rangle \right\rangle \cdot \vec{E}_i(\vec{r}_s) \rho(\vec{r}_s)$$

Equation 6.2-10

In this form the average over random quantities, excluding the position, is given by

$$\left\langle \left\langle \bar{\bar{u}}_j^a \right\rangle \right\rangle \equiv \left\langle \bar{\bar{u}}_j^a \right\rangle_{\gamma_j} = \int_V d\bar{\gamma}_j \, \bar{\bar{u}}_j^a \, p(\bar{\gamma}_j)$$

Equation 6.2-11

The double brackets indicate averaging over a specific vector of random variables, $\bar{\gamma}$, representing the orientation, etc. The scattering operator is given in this case (far field, tenuous medium) by

$$\bar{\bar{u}}_s^a \equiv \bar{\bar{f}}(\hat{k}_s, \hat{k}_i) \, \frac{e^{-jk\left|\vec{r}_a - \vec{r}_s\right|}}{\left|\vec{r}_a - \vec{r}_s\right|}$$

Equation 6.2-12

and represents a scattering characteristic of the individual scatterer. This notation will be used extensively in the next chapter which addresses multiple scattering.

6.2.4 The Mean Power in the Single Scatter Approximation

Next we consider the mean power transport through a random medium using the single scatter approximation. We begin by forming the two-point, two-frequency correlation of the field. Denoting the complex-conjugate transpose by the asterisk with an over-bar

$$\vec{E}(\vec{r}_a, k_1) \cdot \bar{\vec{E}}^*(\vec{r}_b, k_2) =$$

$$\left\{ \vec{E}_i(\vec{r}_a, k_1) + \sum_{j=1}^{N} \overset{=a}{u}_j(k_1) \cdot \vec{E}_i(\vec{r}_j, k_1) \right\} \cdot \left\{ \bar{\vec{E}}_i^*(\vec{r}_b, k_2) + \sum_{j=1}^{N} \left[\overset{=b}{u}_j(k_2) \cdot \vec{E}_i(\vec{r}_j, k_2) \right]^{\bar{*}} \right\}$$

Equation 6.2-13

expanding this expression

$$\begin{aligned}
\vec{E}(\vec{r}_a, k_1) \cdot \bar{\vec{E}}^*(\vec{r}_b, k_2) = {} & \vec{E}_i(\vec{r}_a, k_1) \cdot \bar{\vec{E}}_i^*(\vec{r}_b, k_2) \\
& + \sum_{j=1}^{N} \overset{=a}{u}_j(k_1) \cdot \vec{E}_i(\vec{r}_j, k_1) \cdot \bar{\vec{E}}_i^*(\vec{r}_b, k_2) \\
& + \sum_{j'=1}^{N} \vec{E}_i(\vec{r}_a, k_1) \cdot \bar{\vec{E}}_i^*(\vec{r}_{j'}, k_2) \cdot \left(\overset{=b}{u}_{j'}(k_2) \right)^{\bar{*}} \\
& + \sum_{j=1}^{N} \sum_{j'=1}^{N} \overset{=a}{u}_j(k_1) \cdot \vec{E}_i(\vec{r}_j, k_1) \cdot \bar{\vec{E}}_i^*(\vec{r}_{j'}, k_2) \cdot \left(\overset{=b}{u}_{j'}(k_2) \right)^{\bar{*}}
\end{aligned}$$

We next average the above equation to form the correlation of the fields at two points and two frequencies.

$$\begin{aligned}
\left\langle \vec{E}(\vec{r}_a, k_1) \cdot \bar{\vec{E}}^*(\vec{r}_b, k_2) \right\rangle = {} & \left\langle \vec{E}_i(\vec{r}_a, k_1) \cdot \bar{\vec{E}}_i^*(\vec{r}_b, k_2) \right\rangle \\
& + \left\langle \sum_{j=1}^{N} \overset{=a}{u}_j(k_1) \cdot \vec{E}_i(\vec{r}_j, k_1) \cdot \bar{\vec{E}}_i^*(\vec{r}_b, k_2) \right\rangle \\
& + \left\langle \sum_{j'=1}^{N} \vec{E}_i(\vec{r}_a, k_1) \cdot \bar{\vec{E}}_i^*(\vec{r}_{j'}, k_2) \cdot \left(\overset{=b}{u}_{j'}(k_2) \right)^{\bar{*}} \right\rangle \\
& + \left\langle \sum_{j=1}^{N} \sum_{j'=1}^{N} \overset{=a}{u}_j(k_1) \cdot \vec{E}_i(\vec{r}_j, k_1) \cdot \bar{\vec{E}}_i^*(\vec{r}_{j'}, k_2) \cdot \left(\overset{=b}{u}_{j'}(k_2) \right)^{\bar{*}} \right\rangle
\end{aligned}$$

Equation 6.2-14

The averaging operator commutes with the summations. In addition, we recognize that the incident field is deterministic, since the incident field is specified. After factoring the first three terms in Equation 6.2-14, it becomes

$$\left\langle \vec{E}(\vec{r}_a, k_1) \cdot \vec{E}^{\bar{*}}(\vec{r}_b, k_2) \right\rangle =$$

$$\left[\vec{E}_i(\vec{r}_a, k_1) + \sum_{j=1}^{N} \left\langle \overset{=a}{u}_j(k_1) \right\rangle \cdot \vec{E}_i(\vec{r}_j, k_1) \right] \cdot \left[\vec{E}_i^{\bar{*}}(\vec{r}_b, k_2) + \sum_{j'=1}^{N} \vec{E}_i^{\bar{*}}(\vec{r}_{j'}, k_2) \cdot \left\langle \overset{=b}{u}_{j'}(k_2)^{\bar{*}} \right\rangle \right]$$
$$+ \sum_{j=1}^{N} \sum_{j'=1}^{N} \left\langle \overset{=a}{u}_j(k_1) \cdot \vec{E}_i(\vec{r}_j, k_1) \cdot \vec{E}_i^{\bar{*}}(\vec{r}_{j'}, k_2) \cdot \overset{=b}{u}_{j'}(k_2)^{\bar{*}} \right\rangle$$

Equation 6.2-15

Finally, we note that the last average will require a joint probability density function. Consequently, we must include correlation between the position vectors, even if we desire delta correlation. Substituting for the pdf in the final term (assuming only correlations in position), we find

$$\left\langle \overset{=a}{u}_j(k_1) \cdot \vec{E}_i(\vec{r}_j, k_1) \cdot \vec{E}_i^{\bar{*}}(\vec{r}_{j'}, k_2) \cdot \left(\overset{=b}{u}_{j'}(k_2) \right)^{\bar{*}} \right\rangle$$
$$= \int_{-\infty}^{\infty} \int_{-\infty}^{\infty} \overset{=a}{u}_j(k_1) \cdot \vec{E}_i(\vec{r}_j, k_1) \cdot \vec{E}_i^{\bar{*}}(\vec{r}_{j'}, k_2) \cdot \left(\overset{=b}{u}_{j'}(k_2) \right)^{\bar{*}}$$
$$\cdot \left(P(\bar{\gamma}_1) P(\bar{\gamma}_2) \left[\rho(\vec{r}_1) \rho(\vec{r}_2) + C(\vec{r}_1, \vec{r}_2) \right] \right) d\bar{\xi} d\bar{\xi}_2$$

Equation 6.2-16

Recognizing the form for the average of the mean field in Equation 6.2-15, substituting Equation 6.2-16 and evaluating the average of the last term, the correlation is rewritten as

$$\left\langle \vec{E}(\vec{r}_a, k_1) \cdot \vec{E}^{\bar{*}}(\vec{r}_b, k_2) \right\rangle = \left\langle \vec{E}(\vec{r}_a, k_1) \right\rangle \cdot \left\langle \vec{E}^{\bar{*}}(\vec{r}_b, k_2) \right\rangle$$
$$+ \int_V d\xi_j \int_{V'} d\xi_{j'} \overset{=a}{u}_j(k_1) \cdot \vec{E}_i(\vec{r}_j, k_1) \cdot \vec{E}_i^{\bar{*}}(\vec{r}_{j'}, k_2) \cdot \left(\overset{=b}{u}_{j'}(k_2) \right)^{\bar{*}} P(\gamma_j) P(\gamma_{j'}) C(\vec{r}_j, \vec{r}_{j'})$$

Equation 6.2-17

If we assume that the positions are delta-correlated and substituting Equation 6.2-11 for the configuration averages (averages over orientation, etc.),

$$\left\langle \vec{E}(\vec{r}_a, k_1)\cdot \vec{E}^{*}(\vec{r}_b, k_2)\right\rangle = \left\langle \vec{E}(\vec{r}_a, k_1)\right\rangle \cdot \left\langle \vec{E}^{*}(\vec{r}_b, k_2)\right\rangle$$

$$+ \int_V d\vec{r}_j \left\langle\left\langle \bar{\bar{u}}_j^{a}(k_1)\right\rangle\right\rangle \cdot \vec{E}_i(\vec{r}_j, k_1)\cdot \vec{E}_i^{*}(\vec{r}_j, k_2)\cdot \left\langle\left\langle \bar{\bar{u}}_j^{b}(k_2)\right\rangle\right\rangle^{*}$$

Equation 6.2-18

This is the result for the single scatter approximation to the two-point, two-frequency correlation of the fields with delta correlated scatterers (in position). The left hand side is called the ***coherency matrix***, which is defined as [Goodman, 1985]

$$\bar{\bar{J}}\left(\vec{r}_a, k_1; \vec{r}_b, k_2\right) = \left\langle \vec{E}(\vec{r}_a, k_1)\cdot \vec{E}^{*}(\vec{r}_b, k_2)\right\rangle$$

$$= \begin{bmatrix} \left\langle E_\perp(\vec{r}_a, k_1) E_\perp^{*}(\vec{r}_b, k_2)\right\rangle & \left\langle E_\perp(\vec{r}_a, k_1) E_\parallel^{*}(\vec{r}_b, k_2)\right\rangle \\ \left\langle E_\parallel(\vec{r}_a, k_1) E_\perp^{*}(\vec{r}_b, k_2)\right\rangle & \left\langle E_\parallel(\vec{r}_a, k_1) E_\parallel^{*}(\vec{r}_b, k_2)\right\rangle \end{bmatrix}$$

Equation 6.2-19

at a common observation point, $\left(\vec{r}_a = \vec{r}_b\right)$, the trace gives the mean power density of the signal and the off-diagonal elements give the correlation between the power densities. The coherency matrix may be transformed into the more familiar Stokes parameters as follows

$$\bar{S} = \begin{bmatrix} s_0 \\ s_1 \\ s_2 \\ s_3 \end{bmatrix} = \begin{bmatrix} \left\langle E_\perp(\vec{r}_a, k_1) E_\perp^{*}(\vec{r}_b, k_2)\right\rangle + \left\langle E_\parallel(\vec{r}_a, k_1) E_\parallel^{*}(\vec{r}_b, k_2)\right\rangle \\ \left\langle E_\perp(\vec{r}_a, k_1) E_\perp^{*}(\vec{r}_b, k_2)\right\rangle - \left\langle E_\parallel(\vec{r}_a, k_1) E_\parallel^{*}(\vec{r}_b, k_2)\right\rangle \\ \left\langle E_\parallel(\vec{r}_a, k_1) E_\perp^{*}(\vec{r}_b, k_2)\right\rangle + \left\langle E_\perp(\vec{r}_a, k_1) E_\parallel^{*}(\vec{r}_b, k_2)\right\rangle \\ j\left(\left\langle E_\parallel(\vec{r}_a, k_1) E_\perp^{*}(\vec{r}_b, k_2)\right\rangle - \left\langle E_\perp(\vec{r}_a, k_1) E_\parallel^{*}(\vec{r}_b, k_2)\right\rangle \right) \end{bmatrix}$$

Equation 6.2-20

Once the configurationally averaged Green’s function is calculated for the medium (Equation 6.2-11), the coherency matrix is known; consequently, the Stokes parameters are known. Hence, since the incident field is deterministic at a given point, and once the pdf’s are assigned, all the parts of the problem have been determined and the vector problem can be solved, in the single scatter approximation.

6.3 Acoustic or Scalar Wave Propagation

In a one-dimensional case or an acoustic case, no depolarization will occur and the scattering amplitude is a scalar. Hence, the field can be written with the vector directions implicitly understood to be $\hat{k}_i$. The following solution can hold for a scalar field or *simply one of the components of the polarized fields* from the previous section. For weak cross-polarization, these components may then be recombined to form the Stokes parameters or the polarization sensitive result. For strong cross-polarization, there is an extra term in each of the following equations. In single scatter theory, this is would be a relatively simple addition. In scattering approximations beyond the single scatter, the solution would require the added complexity of a pair of coupled equations. Consequently, the simplicity of the following equations relies on the single scatter approximation.

6.3.1 The Coherent Field

If the individual scatterer characteristics (orientation, etc.) are statistically independent of position, the coherent or average field is simply an integration performed over the spatial extent of the random medium. If the orientation of the scatterer and the scatterer's position are independent, the average in assuming no depolarization can be written (assuming far field interactions)

$$\left\langle E(\vec{r}_a)\right\rangle = E_i(\vec{r}_a) + \int_V d\vec{r}_s \, \frac{e^{-jk\left|\vec{r}_a - \vec{r}_s\right|}}{\left|\vec{r}_a - \vec{r}_s\right|} \left\langle f(\hat{k}_s, \hat{k}_i)\right\rangle E_i(\vec{r}_s)\rho\left(\vec{r}_s\right)$$

Equation 6.3-1

6.3.2 The Correlation of the Field

The calculation of the average scattered power density, rather than the coherency matrix, begins with the calculation of the two-point correlation of the scattered field. We begin with the previous result for the single scattered field and multiply by its complex conjugate observed at a different location and at a different frequency.

$$E(\vec{r}_a, k_1)\, E^*(\vec{r}_b, k_2) =$$
$$\left\{ E_i(\vec{r}_a, k_1) + \sum_{j=1}^{N} u_j^a(k_1)\, E_i(\vec{r}_j, k_1) \right\} \left\{ E_i^*(\vec{r}_b, k_2) + \sum_{j=1}^{N} \left[u_j^b(k_2)\, E_i(\vec{r}_j, k_2) \right]^* \right\}$$

Equation 6.3-2

expanding this form, we obtain

$$\begin{aligned} E(\vec{r}_a, k_1)\, E^*(\vec{r}_b, k_2) = {} & E_i(\vec{r}_a, k_1) E_i^*(\vec{r}_b, k_2) + \sum_{j=1}^{N} u_j^a(k_1) E_i(\vec{r}_j, k_1)\, E_i^*(\vec{r}_b, k_2) \\ & + E_i(\vec{r}_a, k_1) \sum_{j=1}^{N} \left[u_j^b(k_2)\, E_i(\vec{r}_j, k_2) \right]^* \\ & + \sum_{j=1}^{N} u_j^a(k_1) E_i(\vec{r}_j, k_1) \sum_{j=1}^{N} \left[u_j^b(k_2)\, E_i(\vec{r}_j, k_2) \right]^* \end{aligned}$$

Equation 6.3-3

Hence, as previously derived in the polarization sensitive form, we arrive at the two-point, two-frequency correlation of the field. The average two-frequency correlation at an observation point, $\vec{r}_o$, takes the form (letting $\vec{r}_a = \vec{r}_b = \vec{r}_o$)

$$\begin{aligned} \left\langle E(\vec{r}_o, k_1)\, E^*(\vec{r}_o, k_2) \right\rangle = {} & \left\langle E(\vec{r}_o, k_1) \right\rangle \left\langle E^*(\vec{r}_o, k_2) \right\rangle \\ & + \int_V d\xi_1 \int_{V'} d\xi_2\;\; E_i(\vec{r}, k_1) E_i^*(\vec{r}\,', k_2)\, u_j^o(k_1) \left(u_{j'}^o(k_2) \right)^* P(\gamma_1) P(\gamma_2) C(\vec{r}, \vec{r}\,') \end{aligned}$$

Equation 6.3-4

Again, averaging over the configurations (size, orientation)

$$\begin{aligned} \left\langle E(\vec{r}_o, k_1)\; E^*(\vec{r}_o, k_2) \right\rangle = {} & \left\langle E(\vec{r}_o, k_1) \right\rangle \left\langle E^*(\vec{r}_o, k_2) \right\rangle \\ & + \int_V d\vec{r} \int_{V'} d\vec{r}\,'\;\; E_i(\vec{r}, k_1) E_i^*(\vec{r}\,', k_2) \left\langle \left\langle u_j^o(k_1) \right\rangle \right\rangle \left\langle \left\langle u_{j'}^o(k_2) \right\rangle \right\rangle^* C(\vec{r}, \vec{r}\,') \end{aligned}$$

Equation 6.3-5

Finally, we assume ***delta-correlated scatterers*** and the two-frequency correlation of the fields reduces to

$$\left\langle E(\vec{r}_o, k_1)\, E^*(\vec{r}_o, k_2)\right\rangle = \left\langle E(\vec{r}_o, k_1)\right\rangle \left\langle E^*(\vec{r}_o, k_2)\right\rangle$$
$$+ \int_V d\vec{r}_j \; E_i(\vec{r}_j, k_1) E_i^*(\vec{r}_j, k_2) \left\langle\left\langle u_j^o(k_1)\right\rangle\right\rangle \left\langle\left\langle u_j^o(k_2)\right\rangle\right\rangle^*$$

Equation 6.3-6

In an attempt to improve the single scatter formulation, the *first order multiple scattering* solution allows for exponential decay into the medium to the point at which the scattering occurs [Ishimaru, 1997]. Then an additional exponential decay term is introduced to account for the wave traveling from the scatterer to the observation point. This loss will be justified in the multiple scattering formulation and results from absorption and scattering. Once absorption by the scatterer is included, this lost energy, represented by the absorption cross section, σ_a, is added to the scattering cross section to form the total or extinction cross section, $\sigma_t = \sigma_a + \sigma_s$. Hence, as a coherent wave travels through an uncorrelated random medium, the coherent field is diminished by the total cross section of the scatterers encountered.

Therefore, referring to Figure 6.3-1, single scattering by a differential volume located at $\vec{r}_j$ inside a random medium can be written

$$\underset{(\text{loss in})}{e^{-\frac{\gamma_{eff}}{2} R_1}} \cdot \underset{(\text{scattering})}{\rho(\vec{r}_j) \frac{e^{-jk\left|\vec{r}_o - \vec{r}_j\right|}}{\left|\vec{r}_o - \vec{r}_j\right|} \left\langle f(\hat{k}_s, \hat{k}_i)\right\rangle} \cdot \underset{(\text{loss out})}{e^{-\frac{\gamma_{eff}}{2} R_2}}$$

here the power loss coefficient is given by $\gamma_{eff} R = \int_0^R \rho\langle\sigma_t\rangle dR$ and is derived from an average over the distribution of total scatterer cross sections where $\langle\sigma_t\rangle$ is the average total cross section. The first order multiple scattering form will be used in the next several sections.

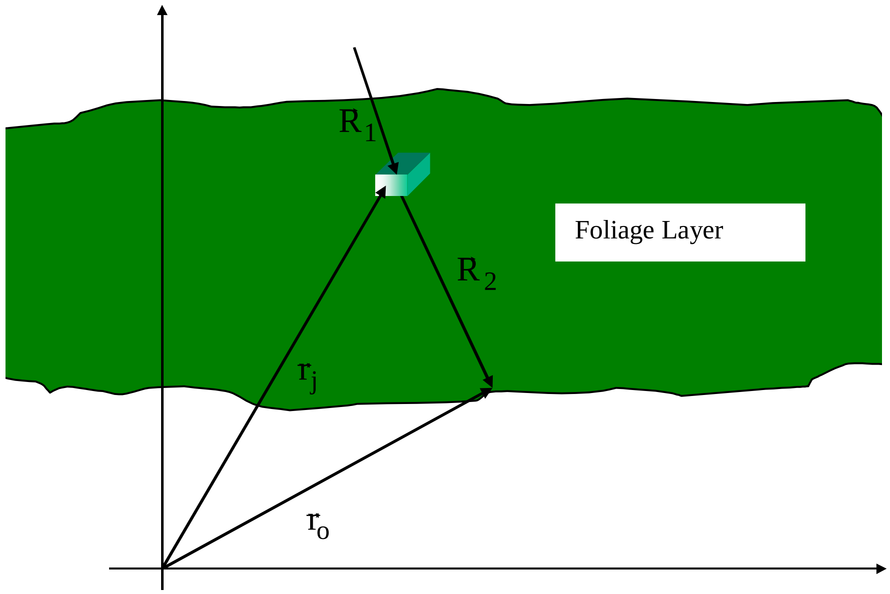

Figure 6.3-1: First order multiple scattering

6.3.3 Return Power Density

From the correlation of the output-scattered fields, we may construct pulse propagation results. Reviewing the development of Section 2.5.1, if we write the incident field as an inverse Fourier transform, the complex amplitude, E(t), of the input, scalar field can be written:

$$E_i(\vec{r}_j, t) = \int_{-\infty}^{\infty} d\omega \tilde{E}_i(\vec{r}_j, \omega) e^{-j\omega t}$$

Equation 6.3-7

The incident field is a function of position since it is weighted by the antenna pattern. The output field can be written as an inverse Fourier transform, employing a frequency domain transfer function approach (generalized to include time dependent behavior)

$$E(\vec{r}_j, t) = \int_{-\infty}^{\infty} d\omega \; H(\omega_0 + \omega, t) \tilde{E}_i(\vec{r}_j, \omega) e^{j\omega t}$$

Equation 6.3-8

Next, we find the position and time-dependent field correlation of the output field

$$\left\langle E\left(\vec{r}_a, t_1\right) E^*\left(\vec{r}_b, t_2\right)\right\rangle$$
$$= \left\langle \int_{-\infty}^{\infty} d\omega_1 \tilde{E}(\vec{r}_a, \omega_1) e^{-j\omega_1 t_1} \int_{-\infty}^{\infty} d\omega_2 \tilde{E}^*(\vec{r}_b, \omega_2)\ e^{j\omega_2 t_2} \right\rangle$$
$$= \int_{-\infty}^{\infty} d\omega_1 \int_{-\infty}^{\infty} d\omega_2 \left\langle \tilde{E}(\vec{r}_a, \omega_1) \cdot \tilde{E}^*(\vec{r}_b, \omega_2) \right\rangle e^{-j(\omega_1 t_1 - \omega_2 t_2)}$$

Equation 6.3-9

The two-position, two-frequency correlation in Equation 6.3-9 has been found in the previous section in terms of the incident field. Hence, from Equation 6.3-5, the frequency domain transfer function can be found. However, the coherent power density, is assumed negligible since it is dissipated by scattering and absorption. More importantly, the coherent power is not likely to be part of the backscattered energy since it is specularly reflected at the boundary(s). The coherent power will only be included in the backscattered waveform when the antenna is pointed at nadir. Using the previously derived two-frequency correlation

$$\left\langle \tilde{E}(\vec{r}_a, \omega_1) \tilde{E}^*(\vec{r}_b, \omega_2) \right\rangle = \iint \tilde{E}_i(\vec{r}, k_1) H(\omega_1) \tilde{E}_i^*(\vec{r}\,', k_2) H(\omega_2)\, p\left(\vec{r}, \vec{r}\,'\right) dV_j\, dV_{j'}$$
$$= \iint \tilde{E}_i(\vec{r}, k_1) \left\langle\left\langle u_j^a(k_1) \right\rangle\right\rangle \tilde{E}_i^*(\vec{r}\,', k_2) \left\langle\left\langle u_{j'}^b(k_2) \right\rangle\right\rangle^* C\left(\vec{r}, \vec{r}\,'\right) dV_j\, dV_{j'}$$

Equation 6.3-10

where we note that the joint pdf, $p\left(\vec{r}, \vec{r}\,'\right)$, has been replaced by the position correlation function since the other portions lead to the coherent field which has been neglected.

In first order multiple scattering theory, the transfer function at a single frequency can be simply derived from the transform of the spatial scattering function $f(\hat{k}_s, \hat{k}_i)$ modified by the loss in the medium and gain of the antenna at the given frequency. If we assume that the scatterers are *delta-correlated* and we let the observation points coincide, $\vec{r}_a = \vec{r}_b = \vec{r}_o$, the time independent transfer function is seen to be

$$H(\omega_1) = \left\langle\left\langle u_j^o(k_1)\right\rangle\right\rangle e^{-\frac{\gamma_{eff}}{2}R_1}\ e^{-\frac{\gamma_{eff}}{2}R_2}$$

$$= \frac{e^{-jk_2R_1}}{R_1}\ e^{-\frac{\gamma_{eff}}{2}R_1}\left\langle\left\langle f\left(\hat{k}_i, \hat{k}_s; \omega_0 + \omega_1\right)\right\rangle\right\rangle \frac{e^{-jk_1R_2}}{R_2}\ e^{-\frac{\gamma_{eff}}{2}R_2}$$

Equation 6.3-11

where R_1 refers to the penetration depth into the random medium to the scattering element at $\vec{r}_j$ and R_2 refers to the distance from the scattering center to the observation point $\vec{r}_o$. In addition, frequency dependence has been added to the scattering amplitude (ω_0 is the carrier radian frequency). Finally, as the number of scatterers approaches infinity, we begin to refer to scattering from a differential scattering volume. Hence, given the number density of the scatterers, the transfer function corresponding to scattering by a differential scattering element becomes

$$H(\omega_1) = \left\langle\left\langle u_j^o(k_1)\right\rangle\right\rangle e^{-\frac{\gamma_{eff}}{2}R_1}\ e^{-\frac{\gamma_{eff}}{2}R_2}\rho\left(\vec{r}_j\right)dV_j$$

One additional term will be introduced into the transfer function, the antenna pattern that weights the incident field. For simplicity, antenna gain at a given frequency for monostatic operation can be represented as follows

$$G_R(\theta, \phi; \omega) = G_T(\theta, \phi; \omega) = G(\omega)$$

Note the monostatic assumption: transmitting and receiving directions are identical. Next, we rewrite the gain of the transmit antenna as

$$G_T(\theta, \phi; \omega) = g_T(\omega) g_T^*(\omega)$$

Additionally, assume that the gain on transmit and the effective aperture area on receive are represented by

$$\frac{\lambda^2}{4\pi} G_R(\omega) = g_R(\omega)\, g_R^*(\omega)$$

Equation 6.3-12

Consequently, using only the frequency deviation, ω_1, from the carrier, ω_0, in place of the entire radian frequency $\omega_0+\omega_1$ (for brevity of notation) within the arguments, the transfer function is rewritten to include the antenna pattern's weighting

$$
\begin{aligned}
H(\omega_1) &= g_R(\omega_1) g_T(\omega_1) \left\langle\left\langle u_j^o(\omega_1) \right\rangle\right\rangle e^{-\frac{\gamma_{eff}}{2}R_1}\ e^{-\frac{\gamma_{eff}}{2}R_2} \rho(\vec{r}_j) dV_j \\
&= g_R(\omega_1) g_T(\omega_1) \frac{e^{-jk_2(R_1+R_2)}}{R_1 R_2}\ e^{-\frac{\gamma_{eff}}{2}(R_1+R_2)} \left\langle\left\langle f(\hat{k}_i, \hat{k}_s; \omega_1) \right\rangle\right\rangle \rho(\vec{r}_j) dV_j
\end{aligned}
$$

Equation 6.3-13

Consequently, after including the monostatic assumption ($R = R_1 = R_2$), we may move the antenna dependence from the incident field into the transfer function, so that

$$
\begin{aligned}
H(\omega_1)H^*(\omega_2) &= g_R(\omega_1) g_T(\omega_1) \left\langle\left\langle u_j^o(k_1) \right\rangle\right\rangle \left[g_R(\omega_2) g_T(\omega_2) \left\langle\left\langle u_j^o(k_2) \right\rangle\right\rangle \right]^* e^{-2\gamma_{eff} R} \rho(\vec{r}_j) dV_j \\
&= \frac{\lambda^2}{4\pi} G^2(\omega_0) \frac{\left\langle\left\langle f(\hat{k}_i, \hat{k}_s; \omega_1) \right\rangle\right\rangle \left\langle\left\langle f(\hat{k}_i, \hat{k}_s; \omega_2) \right\rangle\right\rangle^* e^{-j\frac{2(\omega_1-\omega_2)}{c}R}}{R^4} e^{-2\gamma_{eff} R} \rho(\vec{r}_j) dV_j
\end{aligned}
$$

Equation 6.3-14

and the average power becomes

$$
\left\langle P(t) \right\rangle = \int_{-\infty}^{\infty} d\omega_1 \int_{-\infty}^{\infty} d\omega_2 \tilde{E}_i(\omega_1) \tilde{E}_i^*(\omega_2) e^{-j(\omega_1-\omega_2)t} \int_V H(\omega_1) H^*(\omega_2) \rho_d(\vec{r}) d\vec{r}
$$

Equation 6.3-15

since the position dependence of the incident field has been moved to the transfer function. Next, we rewrite the two-frequency and position dependent integrand

$$
\begin{aligned}
\Gamma(\omega_0+\omega_1, \omega_0+\omega_2) &= \left\langle H(\omega_0+\omega_1) H^*(\omega_0+\omega_2) \right\rangle \\
&= \int_V \frac{\lambda^2}{4\pi} G^2(\omega_0) \frac{\left\langle\left\langle \tilde{f}(\hat{k}_i, \hat{k}_s; \omega_1) \right\rangle\right\rangle \left\langle\left\langle \tilde{f}(\hat{k}_i, \hat{k}_s; \omega_2) \right\rangle\right\rangle^* e^{-j\frac{2(\omega_1-\omega_2)}{c}R}}{R^4} e^{-2\gamma_{eff} R} \rho(\vec{r}_j) dV_j
\end{aligned}
$$

Equation 6.3-16

This quantity, Γ, is a simplified version of the ***two-frequency mutual coherence function*** [Ishimaru, 1997]. It has been simplified for the single scatter case. The two-frequency mutual coherence function is the correlation of the time-varying, frequency domain transfer function, H(ω,t), at two different frequencies and two different times (for time-varying medium) [Ishimaru, 1997]

$$\Gamma \equiv \Gamma(\omega_0 + \omega_1, \omega_0 + \omega_2; t_1, t_2) = \left\langle H(\omega_0 + \omega_1, t_1) H^*(\omega_0 + \omega_2, t_2) \right\rangle$$

Once the two-frequency mutual coherence is constructed, the scattered power density is found when $t_1 = t_2 = t$ [Ishimaru, 1997] from

$$\left\langle P(t) \right\rangle = \int_{-\infty}^{\infty} d\omega_1 \int_{-\infty}^{\infty} d\omega_2 \tilde{E}_i(\omega_1) \tilde{E}_i^*(\omega_2) e^{-j(\omega_1 - \omega_2)t}\, \Gamma(\omega_0 + \omega_1, \omega_0 + \omega_2)$$

When the bandwidth of the pulse is narrow with respect to the carrier frequency, the ***narrow-band approximation*** can also be made. In this case, the scattering function, as a function of frequency, is roughly constant and can be evaluated at the center, carrier frequency. Once this narrow-bandwidth approximation is made, the only frequency dependence in the two-frequency mutual coherence function appears in the Fourier kernel. A change of variables to the difference frequency $\omega_d = \omega_1 - \omega_2$ yields a simpler expression. The two frequency mutual function for a narrow band input signal becomes [Ishimaru, 1997]

$$\Gamma_0 \approx \left| \left\langle \left\langle \tilde{f}(\hat{k}_i, \hat{k}_s \omega_o) \right\rangle \right\rangle \right|^2 \frac{e^{-j\omega_d (R_1 + R_2)/c}}{R^4} e^{-2\gamma_{eff} R} \rho(\vec{r}_j) dV_j$$

Equation 6.3-17

Once the two-frequency mutual coherence function is constructed, the backscattered power density has been determined. When a finite number of discrete scatterers is present, in contrast to the formulation above, the volume integration over the density of scatterers will be replaced with a discrete summation.

For each scattering direction, $\hat{k}_s$, given the incident field direction, $\hat{k}_i$, the scattered field must be re-computed. Next, we make several definitions concerning the radar cross-section of this scatterer. First is the differential radar cross-section, σ_d for given incident and scattered field directions

$$\sigma_d\left(\hat{k}_i, \hat{k}_s\right) = \lim_{R\to\infty} \left\{ \frac{R^2 S_s}{S_i} \right\} = \left| \vec{f}(\hat{k}_i, \hat{k}_s) \right|^2$$

Equation 6.3-18

The bistatic cross-section will be denoted as σ_{bi} and is defined by the following:

$$\sigma_{bi} = 4\pi\sigma_d\left(\hat{k}_i, \hat{k}_s\right) = 4\pi\left|f\left(\hat{k}_i, \hat{k}_s\right)\right|^2$$

Equation 6.3-19

Another important cross-section in this work is the total observed cross-section (the scattering cross-section), σ_s. Denoting a differential unit of solid angle as dΩ, this cross-section is written

$$\sigma_s = \iint_{4\pi} \sigma_d \, d\Omega$$

Substituting Equation 6.3-19 into Equation 6.3-9, employing the narrow beamwidth and narrow band approximations, the inverse transforms are easily performed and the backscattered waveform reduces to

$$\begin{aligned} P(t) &= \iiint\limits_{\substack{\text{volume of}\\ \text{scatterers}}} \frac{\lambda^2 G^2(\theta,\phi)}{(4\pi)^3 R^4} \sigma_{bi}(\hat{k}_i, -\hat{k}_i)\, e^{-2\gamma_{eff} R} \rho(\vec{r}) \left| E_i\left(t - \frac{2R}{c}\right)\right|^2 dV \\ &= \iiint\limits_{\substack{\text{volume of}\\ \text{scatterers}}} \frac{\lambda^2 G^2(\theta,\phi)}{(4\pi)^3 R^4} \sigma_{bi}(\hat{k}_i, -\hat{k}_i)\, e^{-2\gamma_{eff} R} \rho(\vec{r})\, P_T\left(t - \frac{2R}{c}\right) dV \end{aligned}$$

Equation 6.3-20

Here, the free space, time delay to the scattering element at dV has been included. This time delay could be made more general by including a medium-dependent propagation speed.

Referring to Figure 6.3-2, the single scatter result is customized for application to the foliage problem with the rough interface. Breaking the volume integral into depth and surface integrations, we find a composite of a surface integration over the canopy and an integration along the depth coordinate along a given radial (ray-path). The return average power is given by

$$P_R(t;\theta,\phi) = \iint\limits_{\substack{\text{canopy}\\\text{crown}}} \int_{r_1}^{r_2} \frac{\lambda^2 G^2(\hat{r})}{(4\pi)^3 \left(r'+r_1\right)^4}\, \sigma_b(-\hat{r},\hat{r})\, e^{-2\gamma_{eff} r'} \rho(\vec{r}')\, P_T\!\left(t - \frac{2(r_1+r')}{c}\right) dr'\, dS$$

Equation 6.3-21

This returned power density is identical to the power density predicted by the convolutional radiative transfer result; however, the integrations have been re-arranged and time dependence is ignored up to this point.

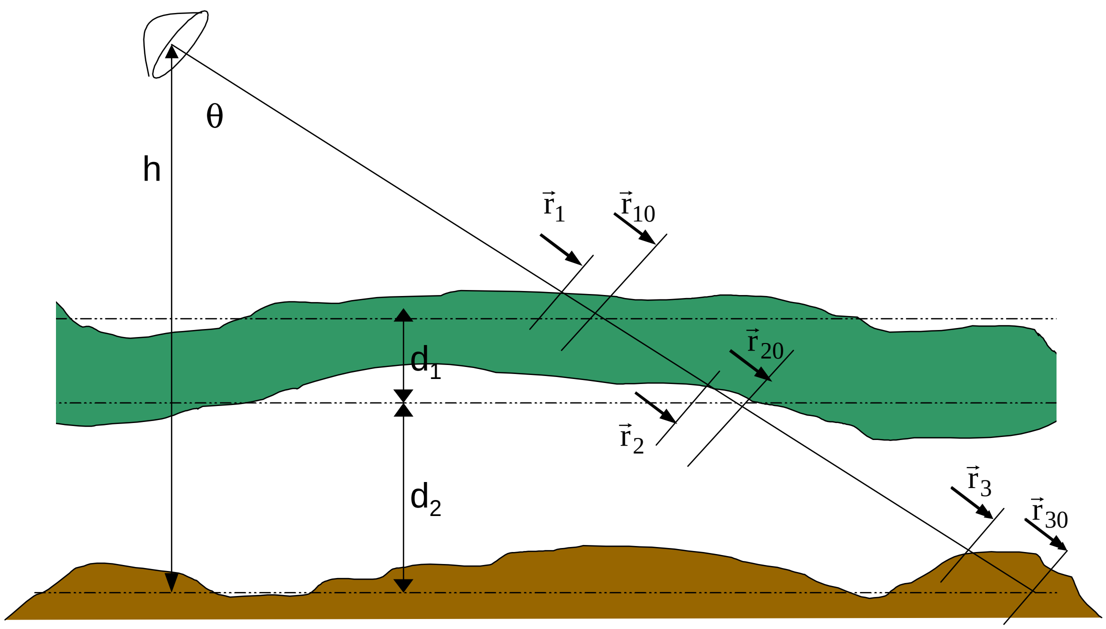

Figure 6.3-2: Problem geometry

Rearranging the order of integration, this is seen to be equivalent to the radiative transfer result derived in Chapter 4 . Assuming a the porpagation spped is the same everywhere, the radiative transfer approach of Chapter 4 yielded

$$I(-\hat{r}; r, \theta, \phi, t) = \int_a^b \sigma_b(\alpha) I_o\left(t - \frac{2\alpha}{c_0}\right)\exp\left\{-2\int_a^\alpha \tilde{k}_e(\mu)d\mu\right\} d\alpha$$

$$\text{where } a = r_{10} + \xi(x)\sec\theta_1$$

$$b = r_{10} + \xi(x)\sec\theta + d_1\sec\theta$$

When we integrate this radiative transfer result over the surface, substitute for the incident intensity, simplify the limits and compensate for the effective receiving area of the antenna, identical results are realized for the radiative transfer and the first order multiple scattering approaches.

$$P_R(t) = \int_0^\infty \int_0^{2\pi} \int_{r_1}^{r_2} \sigma_b(\alpha)\left\{\frac{\lambda^2 G^2(\theta,\phi)}{(4\pi)^3 R^4} P_T\left(t - \frac{2\alpha}{c_0}\right)\right\}\exp\left\{-2\int_{r_1}^\alpha \tilde{k}_e(\mu)\,d\mu\right\} d\alpha\,\rho d\phi d\rho$$

Equation 6.3-22

This, after the same manipulations found in Chapter 4 , can be written as

$$P_R(t) = \int_0^\infty \int_0^{2\pi} \int_{-\infty}^\infty \left[\int_{-\infty}^\infty P_T\left(t - \frac{r_1}{c_0} - t'\right)\tilde{E}(t')\,dt'\right] p_\xi(\xi)\,d\xi \;\; \rho d\phi d\rho$$

Equation 6.3-23

Hence, the inner, bracketed convolutional integral of Equation 6.3-8 is the one-dimensional average power received along the radial. Rewriting,

$$P_R(t) = \int_0^\infty \int_0^{2\pi} \int_{-\infty}^\infty \left[\int_{-\infty}^\infty P_T(t')G(t-t')\,dt'\right] p_\xi(\xi)\,d\xi \;\; \rho d\phi d\rho$$

Equation 6.3-24

the impulse response and the corresponding one-dimensional, two-frequency mutual coherence function can be identified as a Fourier transform pair:

$$G(t) = \int_{-\infty}^{\infty} \Gamma(\omega_d) e^{-j\omega_d t} \, d\omega_d$$

Equation 6.3-25

In general, for scattering in three-dimensions and for wide-band signals, the power density is written [Ishimaru, 1997]

$$I(t) = \iiint\limits_{\substack{\text{volume of} \\ \text{scatterers}}} \left[\int_{-\infty}^{\infty} A\left(\omega_1, t - \frac{2R}{c} \right) e^{j\omega_1 t} d\omega_1 \right] \left[\int_{-\infty}^{\infty} A\left(\omega_2, t - \frac{2R}{c} \right) e^{j\omega_2 t} d\omega_2 \right]^* \rho \, dV$$

Equation 6.3-26

where

$$A(t, \omega_n) = U_i(\omega_n) \tilde{F}(\omega_n; \hat{k}_s, \hat{k}_i) \, g_T(\omega) g_R(\omega) \frac{e^{-2jkR}}{R^2} e^{-2\int_0^R \rho \langle \sigma_t \rangle dR}$$

$\tilde{E}_i(\omega_n) =$ the complex envelope of the incident signal at the frequency, ω_n

and the asterisk signifies the complex conjugate. This analysis produced a simplified version of the impulse response for the *volume* return. Next, the surface return is briefly addressed.

First, this formulation does not account for the coherent and incoherent power transmitted through the foliage, scattered by the underlying rough surface, and transmitted back through the foliage to the radar. Under the single scatter approximation, the ground-scattered return does not interact with the volume return and consequently, is consistent with the results from the radiative transfer approach. The surface backscattered power due to the incident coherent field is given by

$$P_R(t; \theta, \phi) = \frac{\lambda^2 G^2(\hat{r})}{(4\pi)^3 r_3^2} \iint\limits_{\substack{\text{canopy} \\ \text{crown}}} \sigma_s^o(\theta, \phi) \, e^{-2\gamma_{eff} (r_3 - r_1)} P_T\left(t - \frac{2(r_3 - r_1)}{c} - \frac{2r_1}{c} \right) dS$$

Equation 6.3-27

The quantity, $\sigma_s^o(\theta, \phi)$, is the surface radar cross section per unit area. Here, the coherent field suffers an exponential decay as it propagates to the surface; it scatters incoherently (for non-nadir pointing); and consequently propagates back through the foliage. Since this integration is identical to the surface return found in the radiative transfer description, the remainder of this solution, like that of the foliage return, can be found in section 4.3, of Chapter 4 . In addition to the coherent power, an incoherent component will be incident to the surface due to scattering within the foliage. The incoherent power incident to the surface will assume a similar form. Consequently, there are two contributors to the power incident to the surface: incoherent power generated within the random medium and an attenuated coherent power. The surface will scatter each of these components *incoherently* back to the radar. At the receiver, under the narrowband and narrow beamwidth approximations, the received incoherent power due to surface scattering can be written

$$P_R(t) \cong \frac{\lambda^2 G_T(\hat{k}_i) G_R(\hat{k}_s)}{(4\pi)^3 r_3^2} \iint_{\substack{\text{canopy}\\ \text{crown}}} \sigma_s^o(\theta,\phi)\, e^{-2\gamma_{eff}(r_3 - r_1)} \cdot \int_{r_1}^{r_3} \sigma_{bi}(\hat{k}_i, \hat{k}_i)\, P_T\left(t - \frac{2r_1}{c} - \frac{r'}{c} - \frac{r_3 - r'}{c} - \frac{r_3 - r_1}{c}\right) \rho(\bar{r}')\, dr'\, dS$$

Equation 6.3-28

where the amplitude (1/r) dependence has been approximated.

6.4 Conclusions and Future Efforts

Like the convolution result, the first order multiple scattering result can accommodate a spatially varying velocity and may be re-cast into a convolutional, impulse response form when the narrow-band and narrow-beamwidth approximations are employed. More importantly, a further limitation of the convolutional approach has been identified: use of a narrow bandwidth approximation. This assumption is expected due to the use of constant forward and backscatter coefficients with respect to frequency in deriving the radiative transfer results. The use of the narrow beamwidth approximation has already been identified in the radiative transfer approach. However, using the full expression for two-frequency mutual coherence function, the impulse response approach may be extended to broader bandwidth pulses in addition to broader beamwidth antenna patterns while maintaining some convolutional aspects. In addition, it was demonstrated that the single scatter solution could be extended to include polarization effects. This effort looks feasible and should be attempted.

Concluding, finding the two-frequency mutual coherence function (or the impulse response) is key to determining the pulse propagation. Once this function is known, the pulse can be reconstructed. Next, a multiple scattering approach will be investigated in order to determine if a more general two-frequency mutual coherence function can be found. In addition, the multiple scattering approach will yield further insight into the extinction and effective medium parameters.

Chapter 7 Multiple Scattering Approach

In this chapter, the multiple scattering solution is developed in the Twersky approximation for both the mean field and its correlation. Like the exploration of the beam solution to the full radiative transfer equations, this step in the further development of the convolutional model is important in many regards. First the coefficients found in the convolutional model, such as extinction, and forward and backward scattering cross sections, are purely heuristic at this point. Although these values are expected to be calibrated by measured data, the number of free parameters in the convolutional model renders this calibration somewhat uncertain. In other words, a measured waveform may be reproduced using several different combinations of the free parameters found in the convolutional model. Consequently, if these parameters can be estimated or bounded at the outset, the calibration may be more accurate. Multiple scattering theory may be used to estimate these parameters. For example, as we see in the derivation of the mean field, multiple scattering theory predicts the decay of the wave as it propagates through a random medium. Hence, extinction coefficients may be estimated from these results and then fine-tuned using measured data rather than blindly fitting the data.

The first step executed in the multiple scattering approach is to calculate the mean field for a discrete random media with pair correlations. Using the Twersky expansion of the scattered fields, an equation for the mean Green's function is developed. Several different solution techniques are then explored including renormalization [Frisch, 1968] in Section 7.3.3 and stationary phase (for uncorrelated scatterers) in Section 7.3.2. This last approach is applicable to scalar version of the Distorted Wave Born Approximation (DWBA) proposed by Lang [1981]. The DWBA is then proposed as a viable alternative to the convolutional approach in Section 7.4.

In Section 7.5, the two-frequency radiative transfer equation is derived closely following the works of Barabanenkov [1971], Besieris [1981] and Tsolakis [1985]. Like Tsloakis, this is a development for discrete random media. The one variation, however, is that the discrete scatterers support only forward-backward scattering; they do not scatter isotropically, as assumed by Tsolakis [1985]. This leads to a simpler form for the two-frequency radiative transfer equations. A solution is presented in Section 7.6. Here it is proposed that the two-frequency rough surface scattering results of Section 3.4.2 should be used as the boundary condition. If, at this point, certain additional scattering mechanisms are ignored (as is done in the radiative transfer approach), the convolutional form may be recovered. Finally, the full development of the two-frequency radiative transfer equations is reviewed in the Appendix. Here it can be seen that the problem is reduced from the three-dimensional version for isotropic scattering down to a one-dimensional version when forward-backward scattering is assumed.

7.1 The Mean Field and the Dyson Equation

The single scattered field is defined as the incident field scattered by each of the N scatterers to the observation point, $\vec{r} = \vec{r}_a$, and is written as a simple summation over the scatterers that form the random medium. Equation 7.1-1 casts this as a vector equation that employs the dyadic notation that maintains the polarization.

$$\vec{E}(\vec{r}_a) = \vec{E}_i(\vec{r}_a) + \sum_{j=1}^{N} \overline{\overline{f}}(\hat{k}_s, \hat{k}_i) \cdot \vec{E}_i(\vec{r}_j) \frac{e^{-jkR}}{R}$$

Equation 7.1-1

or adopting the notation of Twersky [Ishimaru, 1997], this expression can be written more compactly as in Equation 7.1-2.

$$\vec{E}(\vec{r}_a) = \vec{E}_i(\vec{r}_a) + \sum_{j=1}^{N} \overline{\overline{u}}{}_j^a \cdot \vec{E}_i(\vec{r}_j)$$

Equation 7.1-2

where the *total* field at point $\vec{r} = \vec{r}_a$ is given by $\vec{E}_a$, and the incident field at position $\vec{r} = \vec{r}_a$ is denoted by $\vec{E}_i$ and the *operator* $\overline{\overline{u}}{}_n^a$ describes how the total field at the point $\vec{r} = \vec{r}_n$ scatters to the position, $\vec{r} = \vec{r}_a$. In a *tenuous* medium where each scatterer is in the far field of the others, this operator can be described by the product of the dyadic amplitude scattering function $\vec{f}(\hat{k}_s, \hat{k}_i)$ and the far field Green's function. We use the familiar form

$$\vec{E}_s(\vec{r}_a) = \frac{e^{-jk\left|\vec{r}_a - \vec{r}_j\right|}}{\left|\vec{r}_a - \vec{r}_j\right|} \vec{f}(\hat{k}_j, \hat{k}_i) \cdot \vec{E}_i(\vec{r}_j)$$

Equation 7.1-3

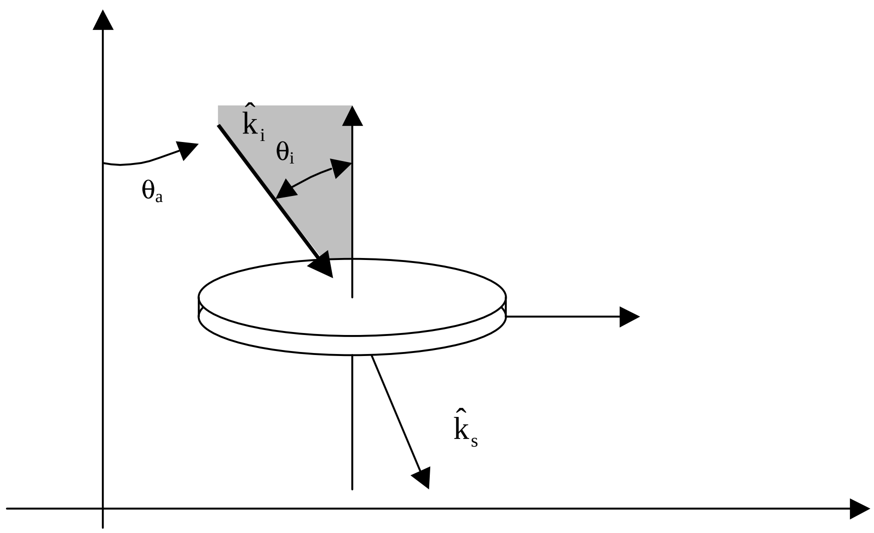

Figure 7.1-1: Local scattering coordinates

The vector directions are described in Figure 7.1-1. It is assumed that the incident wave is a plane wave and the scattered wave expands as a spherical wave. The assumption of the incident plane wave is reasonable as long as this scatterer is in the far field of either the source or another scatterer. In that case, the incident spherical wave is locally planar.

Consequently, the total field at an observation point $\vec{r} = \vec{r}_a$ is a summation of the double scattered fields (incident field scattered by each of the N scatterers to a different member of the N scatterers, then to the position $\vec{r} = \vec{r}_a$), the triple scattered fields, etc.

$$\vec{E}(\vec{r}_a) = \vec{E}_i(\vec{r}_a) + \sum_{j=1}^{N} \bar{\bar{u}}_j^{a} \cdot \vec{E}_i(\vec{r}_j) + \sum_{j=1}^{N} \sum_{k=1}^{N} \bar{\bar{u}}_j^{a} \cdot \bar{\bar{u}}_k^{j} \cdot \vec{E}_i(\vec{r}_k)$$
$$+ \sum_{j=1}^{N} \sum_{k=1}^{N} \sum_{m=1}^{N} \bar{\bar{u}}_j^{a} \cdot \bar{\bar{u}}_k^{j} \cdot \bar{\bar{u}}_m^{k} \, \vec{E}_i(\vec{r}_m) + \dots$$

Equation 7.1-4

Next, we address the Twersky approximation. If backscattering is not important, Twersky removed scattering paths that include the same scatterer twice (or more) in the above summations. He writes

$$\vec{E}(\vec{r}_a) = \vec{E}_i(\vec{r}_a) + \sum_{j=1}^{N} \bar{\bar{u}}_j^{a} \cdot \vec{E}_i(\vec{r}_j) + \sum_{j=1}^{N} \sum_{\substack{k=1, \\ k \neq j}}^{N} \bar{\bar{u}}_j^{a} \cdot \bar{\bar{u}}_k^{j} \cdot \vec{E}_i(\vec{r}_k)$$
$$+ \sum_{j=1}^{N} \sum_{\substack{k=1, \\ k \neq j}}^{N} \sum_{\substack{m=1, \\ m \neq j \\ m \neq k}}^{N} \bar{\bar{u}}_j^{a} \cdot \bar{\bar{u}}_k^{j} \cdot \bar{\bar{u}}_m^{k} \cdot \vec{E}_i(\vec{r}_m) + \dots$$

Equation 7.1-5

Equation 7.1-5 is an example of Twersky's "expanded form." Noting the limits on the summations, we see that in his formulation a number of events are ignored. These include ignoring triple scattering between two scatterers, ignoring quadruple scattering between three scatterers, etc.

7.2 Statistical Description of the Random Medium

If we consider the number density (number of scatterers per unit volume), then the probability density function can be written as

$$p(\omega_j) = \frac{P(\gamma_j)\rho(\vec{r}_j)}{N}$$

Equation 7.2-1

In order to describe the spatial distribution of the scatterers in addition to each scatterer's individual statistics, we construct the joint probability density function (pdf). The joint distribution of any two scatterers written in a cluster expansion of centered random variables [Frisch, 1968]:

$$
\begin{aligned}
&E\left\{\rho\left(\vec{r}_1\right),\rho\left(\vec{r}_2\right)\right\} = C\left(\vec{r}_1,\vec{r}_2\right); \\
&E\left\{\rho\left(\vec{r}_1\right),\rho\left(\vec{r}_2\right),\rho\left(\vec{r}_3\right)\right\} = C\left(\vec{r}_1,\vec{r}_2,\vec{r}_3\right) \\
&E\left\{\rho\left(\vec{r}_1\right),\rho\left(\vec{r}_2\right),\rho\left(\vec{r}_3\right),\rho\left(\vec{r}_4\right)\right\} = C\left(\vec{r}_1,\vec{r}_2\right)C\left(\vec{r}_3,\vec{r}_4\right)+C\left(\vec{r}_1,\vec{r}_3\right)C\left(\vec{r}_2,\vec{r}_4\right) \\
&\qquad\qquad +C\left(\vec{r}_1,\vec{r}_4\right)C\left(\vec{r}_2,\vec{r}_3\right)+C\left(\vec{r}_1,\vec{r}_2,\vec{r}_3,\vec{r}_4\right)
\end{aligned}
$$

where E{*} indicates expected value

When Gaussian random variables are chosen, only the two-point correlation function is non-zero. The use of these higher order statistics will prevent the absurdity that two scatterers can occupy the same space. Within the foliage, the correlation range represents a spatial correlation and is therefore presents a finite correlation length. Hence, we construct the pdf with pair correlations. Another assumption is to be made: the scatterer's individual properties (rotation, size, etc.) are statistically independent of the position statistics [Tsolakis, 1985].

$$
p\left(\bar{\xi}_1,\bar{\xi}_2\right) = P\left(\bar{\gamma}_1\right)P\left(\bar{\gamma}_2\right)\left[\rho\left(\vec{r}_1\right)\rho\left(\vec{r}_2\right)+C\left(\vec{r}_1,\vec{r}_2\right)\right]
$$

Equation 7.2-2

Where the vector random variable, $\bar{\xi}$, represents a combination of the random variables for position, $\vec{r}$, and other scatterer properties, $\bar{\gamma}$. The function, $P(\bar{\gamma}_{1,2})$, is a joint pdf that describes the scatterer's size, rotation, etc. The pdf, $\rho(\vec{r})$, describes the scatterer's number density in the volume and finally the spatial pair correlation between the scatterers is given by the correlation function $C(\vec{r},\vec{r}\,')$.

7.3 The Dyson Equation

We are now in a position to describe the characteristic moments of the field. The first moment, or the mean field, is described by the "Dyson" equation. We begin with

Equation 7.1-5, the equation for the total field at an observation point, $\vec{r}_a$. We then average, first with respect to the position [Tsolakis, 1985].

$$
\begin{aligned}
\left\langle \vec{E}(\vec{r}_a) \right\rangle = {} & \vec{E}_i(\vec{r}_a) + \int_V d\vec{r}_j \sum_{j=1}^{N} \overset{=a}{u_j} \cdot \vec{E}_i(\vec{r}_j) \frac{\rho(\vec{r}_j)}{N} \\
& + \int_V d\vec{r}_j \int_V d\vec{r}_k \sum_{j=1}^{N} \sum_{\substack{k=1,\\ k\neq j}}^{N} \overset{=a}{u_j} \cdot \overset{=j}{u_k} \cdot \vec{E}_i(\vec{r}_k) \frac{\left[\rho(\vec{r}_j)\rho(\vec{r}_k) + C(\vec{r}_j, \vec{r}_k)\right]}{N^2} \\
& + \int_V d\vec{r}_j \int_V d\vec{r}_k \int_V d\vec{r}_m \sum_{j=1}^{N} \sum_{\substack{k=1,\\ k\neq j}}^{N} \sum_{\substack{m=1,\\ m\neq j\\ m\neq k}}^{N} \overset{=a}{u_j} \cdot \overset{=j}{u_k} \cdot \overset{=k}{u_m} \cdot \vec{E}_i(\vec{r}_m)\, p\left(\vec{r}_j, \vec{r}_k, \vec{r}_m\right) + \ldots
\end{aligned}
$$

Equation 7.3-1

in the last integral, the symbolic form for the joint pdf of the three position vectors is given, instead of the explicit (much longer) form. Since the statistics of position do not depend on the specific scatterers, the summations can be performed resulting in

$$
\begin{aligned}
\left\langle \vec{E}(\vec{r}_a) \right\rangle_{\vec{r}} \cong {} & \vec{E}_i(\vec{r}_a) + N \int_V \overset{=a}{u_j} \cdot \vec{E}_i(\vec{r}_j) \frac{\rho(\vec{r}_j)}{N} d\vec{r}_j \\
& + N(N-1) \iint_V \overset{=a}{u_j} \cdot \overset{=j}{u_k} \cdot \vec{E}_i(\vec{r}_k) \frac{\left[\rho(\vec{r}_j)\rho(\vec{r}_k) + C(\vec{r}_j, \vec{r}_k)\right]}{N^2} d\vec{r}_k\, d\vec{r}_j \\
& + N(N-1)(N-2) \iiint_V \overset{=a}{u_j} \cdot \overset{=j}{u_k} \cdot \overset{=k}{u_m} \cdot \vec{E}_i(\vec{r}_m) \\
& \quad \cdot \frac{\left[\rho(\vec{r}_j)\rho(\vec{r}_k)\rho(\vec{r}_m) + \rho(\vec{r}_j)C(\vec{r}_k, \vec{r}_m) + \rho(\vec{r}_k)C(\vec{r}_m, \vec{r}_j) + \rho(\vec{r}_m)C(\vec{r}_j, \vec{r}_k)\right]}{N^3} d\vec{r}_k\, d\vec{r}_j\, d\vec{r}_m \\
& + \ldots
\end{aligned}
$$

Equation 7.3-2

As the number of scatterers becomes large, $N \rightarrow \infty$, the factors of N cancel and in the limit, the equation for the mean field reduces to

$$\left\langle \vec{E}(\vec{r}_a) \right\rangle_{\vec{r}} \cong \vec{E}_i(\vec{r}_a) + \int_V \overline{\overline{u}}{}^a_j \cdot \vec{E}_i(\vec{r}_j)\, \rho\left(\vec{r}_j\right) d\vec{r}_j$$

$$+ \iint_V \overline{\overline{u}}{}^a_j \cdot \overline{\overline{u}}{}^j_k \cdot \vec{E}_i(\vec{r}_k) \left[\rho\left(\vec{r}_j\right)\rho\left(\vec{r}_k\right) + C\left(\vec{r}_j, \vec{r}_k\right)\right] d\vec{r}_k\, d\vec{r}_j \; +$$

$$\iiint_V \overline{\overline{u}}{}^a_j \cdot \overline{\overline{u}}{}^j_k \cdot \overline{\overline{u}}{}^k_m \cdot \vec{E}_i(\vec{r}_m)$$
$$\cdot \left[\rho\left(\vec{r}_j\right)\rho\left(\vec{r}_k\right)\rho\left(\vec{r}_m\right) + \rho\left(\vec{r}_j\right)C\left(\vec{r}_k, \vec{r}_m\right) + \rho\left(\vec{r}_k\right)C\left(\vec{r}_m, \vec{r}_j\right) + \rho\left(\vec{r}_m\right)C\left(\vec{r}_j, \vec{r}_k\right)\right] d\vec{r}_k\, d\vec{r}_j\, d\vec{r}_m$$

$$+ \ldots$$

Equation 7.3-3

It can be seen, through Neumann expansion of the following integral equation, that the above “expanded” form for the mean field can be rewritten in the following compact integral equation form:

$$\left\langle \vec{E}(\vec{r}_a) \right\rangle = \vec{E}_i(\vec{r}_a) + \int_V d\vec{r}_j\, \overline{\overline{u}}{}^a_j \cdot \left\langle \vec{E}_i(\vec{r}_j) \right\rangle \rho(\vec{r}_j) + \int_V d\vec{r}_j \int_V d\vec{r}_k\, \overline{\overline{u}}{}^a_j \cdot \overline{\overline{U}}{}^j_k \cdot \left\langle \vec{E}_i(\vec{r}_k) \right\rangle C(\vec{r}_j, \vec{r}_k)$$

Equation 7.3-4

where the spatially averaged Twersky operator is given below

$$\overline{\overline{U}}{}^j_k = \overline{\overline{u}}{}^j_k + \int_V d\vec{r}_m\, \overline{\overline{u}}{}^j_m \cdot \overline{\overline{U}}{}^j_k\, \rho(\vec{r}_m) + \int_V d\vec{r}_m \int_V d\vec{r}_n\, \overline{\overline{u}}{}^j_m \cdot \overline{\overline{U}}{}^m_n \cdot \overline{\overline{U}}{}^n_k\, C(\vec{r}_m, \vec{r}_n)$$

$$\text{for } \overline{\overline{U}}{}^j_k \equiv \left\langle \overline{\overline{u}}{}^j_k \right\rangle$$

Equation 7.3-5

Since the Twersky operator contains the scattering amplitude as a parameter, we must also average over the orientation, size, etc. Following the notation used by Tsolakis [1985], we average the Twersky operator and its corresponding spatially averaged form over the configuration space,

$$\left\langle\left\langle \overset{=a}{u}_j \right\rangle\right\rangle \equiv \left\langle \overset{=a}{u}_j \right\rangle_{\gamma_j} = \int_V d\gamma_j\, \overset{=a}{u}_j\, P(\gamma_j)$$

$$\left\langle\left\langle \overset{=a}{U}_j \right\rangle\right\rangle \equiv \left\langle \overset{=a}{U}_j \right\rangle_{\gamma_j} = \int_V d\gamma_j\, \overset{=a}{U}_j\, P(\gamma_j)$$

Equation 7.3-6

Hence, we can rewrite the mean field and the mean Twersky operator equations as

$$\left\langle \vec{E}(\vec{r}_a)\right\rangle = \vec{E}_i(\vec{r}_a) + \int_V d\vec{r}_j \left\langle\left\langle \overset{=a}{u}_j \right\rangle\right\rangle \cdot \left\langle \vec{E}_i(\vec{r}_j)\right\rangle \rho(\vec{r}_j)$$
$$+ \int_V d\vec{r}_j \int_V d\vec{r}_k \left\langle\left\langle \overset{=a}{u}_j \right\rangle\right\rangle \cdot \left\langle\left\langle \overset{=j}{U}_k \right\rangle\right\rangle \cdot \left\langle \vec{E}_i(\vec{r}_k)\right\rangle C(\vec{r}_j, \vec{r}_k)$$

Equation 7.3-7

$$\left\langle\left\langle \overset{=j}{U}_k \right\rangle\right\rangle = \left\langle\left\langle \overset{=j}{u}_k \right\rangle\right\rangle + \int_V d\vec{r}_j \left\langle\left\langle \overset{=j}{u}_m \right\rangle\right\rangle \cdot \left\langle\left\langle \overset{=m}{U}_k \right\rangle\right\rangle \rho(\vec{r}_m)$$
$$+ \int_V d\vec{r}_m \int_V d\vec{r}_n \left\langle\left\langle \overset{=j}{u}_m \right\rangle\right\rangle \cdot \left\langle\left\langle \overset{=m}{U}_n \right\rangle\right\rangle \cdot \left\langle\left\langle \overset{=n}{U}_k \right\rangle\right\rangle C(\vec{r}_m, \vec{r}_n)$$

Equation 7.3-8

where the double brackets, $\langle\langle \bullet \rangle\rangle$, indicate configuration averaging with respect to the subscript index of the "Twersky operator."

In this chapter, we will only discuss the scalar wave propagation problem. In addition, since the expressions involving long summations are completed, the explicit arguments for the Green's function will be used in order to reduce confusion. Hence, we reduce the previous equations for the mean field and the mean Green's function to their scalar form (or component form of an uncoupled, polarized vector equation)

$$\left\langle E(\vec{r}_a)\right\rangle = E_i(\vec{r}_a) + \int_V d\vec{r}_j \left\langle\left\langle u_j^a \right\rangle\right\rangle \left\langle E_i(\vec{r}_j)\right\rangle \rho(\vec{r}_j)$$
$$+ \int_V d\vec{r}_j \int_V d\vec{r}_k \left\langle\left\langle u_j^a \right\rangle\right\rangle \left\langle\left\langle U_k^j \right\rangle\right\rangle \left\langle E_i(\vec{r}_k)\right\rangle C(\vec{r}_j, \vec{r}_k)$$

Equation 7.3-9

$$\left\langle\left\langle U_k^j \right\rangle\right\rangle = \left\langle\left\langle u_k^j \right\rangle\right\rangle + \int_V d\vec{r}_j \left\langle\left\langle u_m^j \right\rangle\right\rangle\left\langle\left\langle U_k^m \right\rangle\right\rangle \rho(\vec{r}_m)$$
$$+ \int_V d\vec{r}_m \int_V d\vec{r}_n \left\langle\left\langle u_m^j \right\rangle\right\rangle\left\langle\left\langle U_n^m \right\rangle\right\rangle\left\langle\left\langle U_k^n \right\rangle\right\rangle C(\vec{r}_m, \vec{r}_n)$$

Equation 7.3-10

7.3.1 "Perfect Gas" Solution of the Dyson Equation

The solution to the "perfect gas" problem, i.e. zero correlation case, has been derived in Ishimaru [1997]. Starting with the Foldy-Twersky integral equation for the scalar coherent field,

$$\left\langle \vec{E}(\vec{r}_a) \right\rangle = \vec{E}_i(\vec{r}_a) + \int_V d\vec{r}_j\, u_j^a \left\langle \vec{E}_i(\vec{r}_j) \right\rangle \rho(\vec{r}_j)$$

Equation 7.3-11

we explicitly include the far-field expression for the scattering operator (assumes tenuous medium).

$$\left\langle \vec{E}(\vec{r}_a) \right\rangle = \vec{E}_i(\vec{r}_a) + \int_V d\vec{r}_j\, f\left(\hat{k}_s, \hat{k}_i\right) \frac{e^{-jk\left|\vec{r}_a - \vec{r}_j\right|}}{4\pi\left|\vec{r}_a - \vec{r}_j\right|} \left\langle \vec{E}_i(\vec{r}_j) \right\rangle \rho(\vec{r}_j)$$

Equation 7.3-12

A simple case occurs when the incident field is a normally incident plane wave and the medium is homogeneous with a depth, d.

$$\left\langle \vec{E}(\vec{r}_a) \right\rangle = \vec{E}_i(\vec{r}_a) + \int_0^d dz \int_{-\infty}^{\infty} dy \int_{-\infty}^{\infty} dx\ f\left(\hat{k}_s, \hat{k}_i\right) \frac{e^{-jk\left|\vec{r}_a - \vec{r}_j\right|}}{4\pi\left|\vec{r}_a - \vec{r}_j\right|} \left\langle \vec{E}_i(\vec{r}_j) \right\rangle \rho(\vec{r}_j)$$

Equation 7.3-13

Under these assumptions, the effects of the medium are not significant in the direction transverse to the propagation direction. Therefore, we expect the mean field to be invariant in the x and y directions for a z-directed incident plane wave [Ishimaru, 1997].

Consequently, the integral over the volume of scatterers can be written. We find that the stationary point in transverse directions occurs when [Ishimaru, 1997]

$$\frac{\partial\left(k\left|\vec{r}_a - \vec{r}_j\right|\right)}{\partial x_j} = \frac{\partial\left(k\sqrt{\left(x_a - x_j\right)^2 + \left(y_a - y_j\right)^2 + \left(z_a - z_j\right)^2}\right)}{\partial x_a} = 0$$
$$= k\frac{\left(x_a - x_j\right)}{\left|\vec{r}_a - \vec{r}_j\right|} = 0$$

in the x-coordinate and the following

$$\text{and} \quad \frac{\partial\left(k\left|\vec{r}_a - \vec{r}_j\right|\right)}{\partial y_j} = \frac{\partial\left(k\sqrt{\left(x_a - x_j\right)^2 + \left(y_a - y_j\right)^2 + \left(z_a - z_j\right)^2}\right)}{\partial y_a} = 0$$
$$= k\frac{\left(y_a - y_j\right)}{\left|\vec{r}_a - \vec{r}_j\right|} = 0$$

in the y-coordinate. Hence, this yields the stationary points $(x_S = x, y_S = y)$, where (x_s, y_s) is the stationary point. In the evaluation of the integral by stationary phase, the second order partial derivatives are needed,

$$\frac{\partial^2\left(k\left|\vec{r}_a - \vec{r}_j\right|\right)}{\partial x_a^2} = \frac{\partial^2\left(k\sqrt{\left(x_a - x_j\right)^2 + \left(y_a - y_j\right)^2 + \left(z_a - z_j\right)^2}\right)}{\partial x_a^2}$$
$$= k\left(\frac{1}{\left|\vec{r}_a - \vec{r}_j\right|} - \frac{\left(x_a - x_j\right)^2}{\left|\vec{r}_a - \vec{r}_j\right|^3}\right)$$

$$\frac{\partial^2\left(k\left|\vec{r}_a-\vec{r}_j\right|\right)}{\partial y_a^2}=\frac{\partial^2\left(k\sqrt{\left(x_a-x_j\right)^2+\left(y_a-y_j\right)^2+\left(z_a-z_j\right)^2}\right)}{\partial y_a^2}$$

$$=k\left(\frac{1}{\left|\vec{r}_a-\vec{r}_j\right|}-\frac{\left(y_a-y_j\right)^2}{\left|\vec{r}_a-\vec{r}_j\right|^3}\right)$$

and finally,

$$\frac{\partial^2\left(k\left|\vec{r}_a-\vec{r}_j\right|\right)}{\partial x_a \partial y_a}=\frac{-k\left(x_a-x_j\right)\left(y_a-y_j\right)}{\left|\vec{r}_a-\vec{r}_j\right|^3}$$

Hence, the stationary phase evaluation of the double integral in the x and y coordinates is given by

$$\int_{-\infty}^{\infty} dy \int_{-\infty}^{\infty} dx\ f\left(\hat{k}_s,\hat{k}_i\right)\frac{e^{-jk\left|\vec{r}_a-\vec{r}_j\right|}}{4\pi\left|\vec{r}_a-\vec{r}_j\right|}\cong\begin{Bmatrix}\dfrac{2\pi j}{k} f\left(\hat{k}_i,\hat{k}_i\right)\exp\{-jk(z-z_a)\},\ \text{for } z_a<z \\ \dfrac{2\pi j}{k} f\left(-\hat{k}_i,\hat{k}_i\right)\exp\{-jk(z_a-z)\},\ \text{for } z_a>z\end{Bmatrix}$$

Equation 7.3-14

Hence, this analysis has lead to a medium that scatters in the forward and backward directions; all other scattering is cancelled, on average. If the backscattered field is neglected with respect to the forward-scattered field, the resulting integral equation for the mean field is then given by

$$\left\langle\vec{E}(\vec{r}_a)\right\rangle=\vec{E}_i(\vec{r}_a)+\int_0^d dz\,\frac{2\pi j}{k} f\left(\hat{k}_i,\hat{k}_i\right)\exp\{-jk(z-z_a)\}\left\langle\vec{E}_i(\vec{r}_j)\right\rangle\rho(\vec{r}_j)$$

Equation 7.3-15

This equation is solved exactly if the form of the solution is taken to be

$$\left\langle \vec{E}(\vec{r}) \right\rangle = C\, e^{-jKz}$$

The solution and the effective medium wavenumber, K, for incident plane wave is then found to be

$$\left\langle \vec{E}(\vec{r}_a) \right\rangle = \vec{E}_0 \exp\left\{ -j\left(k + \frac{2\pi f\left(\hat{k}_i, \hat{k}_i\right)}{k} \rho \right) z \right\} = \vec{E}_0 \exp\{-jKz\}$$

Equation 7.3-16

The uniform scatterer density is given by ρ. Assuming lossless scatterers, we may employ the optical theorem in order to obtain the damping of the field.

$$\left\langle \vec{E}(\vec{r}_a) \right\rangle = \vec{E}_0 \exp\left\{ -j\left(k + \frac{2\pi f\left(\hat{k}_i, \hat{k}_i\right)}{k} \rho - j\frac{\rho\, \sigma_{sc}}{2} \right) z \right\}$$

Equation 7.3-17

Absorption loss may be added phenomenologically.

7.3.2 Dyson Equation for the "Perfect Gas Medium"

The equation for the mean Green's function in the perfect gas approximation (i.e. no correlation among scatterers) is given by

$$\left\langle G(\vec{r}_j, \vec{r}_k) \right\rangle = f\left(\hat{k}_s, \hat{k}_i\right) G(\vec{r}_j, \vec{r}_k) + \int_V d\vec{r}_m\, f\left(\hat{k}_s, \hat{k}_i\right) G(\vec{r}_j, \vec{r}_m) \left\langle G(\vec{r}_m, \vec{r}_k) \right\rangle \rho(\vec{r}_m)$$

Equation 7.3-18

noting the explicit substitution for the Twersky scattering operator by its far field approximation. Next, we assume that the scattering function is independent of the observation direction. So that

$$f\left(\hat{k}_s, \hat{k}_i; \omega\right) = f\left(\hat{k}_i; \omega\right)$$

where the frequency dependence has been explicitly included in the argument list. Hence we have scatterers that are strongly forward or backward scattering or that are isotropic. Hence, the scattering amplitude is no longer a function of the observation coordinate, $\vec{r}_j$ and may be removed from the integral. The equation for the mean Green's function is now written (with the frequency dependence assumed in both the Green's function itself and the scattering amplitude)

$$\left\langle G(\vec{r}_j,\vec{r}_k)\right\rangle = f\left(\hat{k}_i\right)G(\vec{r}_j,\vec{r}_k) + f\left(\hat{k}_i\right)\int_V d\vec{r}_m\ G(\vec{r}_j,\vec{r}_m)\left\langle G(\vec{r}_m,\vec{r}_k)\right\rangle\rho(\vec{r}_m)$$

Equation 7.3-19

Operating on Equation 7.3-11 with the $\left(\nabla^2+k^2\right)$ and recalling that this operates on the observation coordinate $\vec{r}_j$ only

$$\begin{aligned}\left(\nabla^2+k^2\right)\left\langle G(\vec{r}_j,\vec{r}_k)\right\rangle &= \left(\nabla^2+k^2\right)f\left(\hat{k}_i\right)G(\vec{r}_j,\vec{r}_k)\\ &\quad+\left(\nabla^2+k^2\right)f\left(\hat{k}_i\right)\int_V d\vec{r}_m\ G(\vec{r}_j,\vec{r}_m)\left\langle G(\vec{r}_m,\vec{r}_k)\right\rangle\rho(\vec{r}_m)\end{aligned}$$

Equation 7.3-20

by definition of the Green's function, operation on the first term on the left hand side and the operation on the Green's function within the integration result in Dirac delta functions.

$$\begin{aligned}\left(\nabla^2+k^2\right)\left\langle G(\vec{r}_j,\vec{r}_k)\right\rangle &= -f\left(\hat{k}_i\right)\delta\left(\vec{r}_j-\vec{r}_k\right) - f\left(\hat{k}_i\right)\int_V d\vec{r}_m\ \delta\left(\vec{r}_j-\vec{r}_m\right)\left\langle G(\vec{r}_m,\vec{r}_k)\right\rangle\rho(\vec{r}_m)\\ &= -f\left(\hat{k}_i\right)\delta\left(\vec{r}_j-\vec{r}_k\right) - \left\langle G(\vec{r}_j,\vec{r}_k)\right\rangle f\left(\hat{k}_i\right)\rho(\vec{r}_j)\end{aligned}$$

Equation 7.3-21

Hence, the Dyson equation for the mean Green's function is written as

$$\left[\nabla^2+k^2+f\left(\hat{k}_i\right)\rho(\vec{r}_j)\right]\left\langle G(\vec{r}_j,\vec{r}_k)\right\rangle = -f\left(\hat{k}_i\right)\delta\left(\vec{r}_j-\vec{r}_k\right)$$

Equation 7.3-22

In the strictly forward/backward scattering medium, the scattering occurs in one direction only. Recognizing that the propagation is only in this one direction, that of the incident direction, there is no loss of generality to assume that the propagation direction is z-directed. Consequently, the Laplacian reduces to a one-dimensional form, and *under the assumption that the solution takes the form of a plane wave*, the equation for the mean Green's function becomes

$$\left[\frac{d^2}{dz^2} + k^2 + f\left(\hat{k}_i\right)\rho(\vec{r}_j)\right] \left\langle G(\vec{r}_j, \vec{r}_k)\right\rangle = -f\left(\hat{k}_i\right)\delta\left(\vec{r}_j - \vec{r}_k\right)$$

Equation 7.3-23

Of course, an arbitrary incident field may be written as a superposition of plane waves. Performing a Fourier transform, the mean Green's function is given by

$$\left\langle \tilde{G}(\vec{r}_j, \vec{r}_k, u)\right\rangle = \frac{\tilde{f}\left(\pm \hat{k}_i, \hat{k}_i\right)}{\left[u^2 - \left(k^2 + \tilde{f}\left(\pm \hat{k}_i, \hat{k}_i\right)\rho(\vec{r}_j)\right)\right]} = \frac{\tilde{f}\left(\pm \hat{k}_i, \hat{k}_i\right)}{\left[u^2 - k_{eff}^2\right]}$$

Equation 7.3-24

and the poles of the system, k_{eff}, are given by

$$\begin{aligned} k_{eff} &= \pm\sqrt{k^2 + f\left(\pm \hat{k}_i, \hat{k}_i\right)\rho(\vec{r}_j)} \\ &\cong k + \frac{f\left(\pm \hat{k}_i, \hat{k}_i\right)\rho(\vec{r}_j)}{2k} \end{aligned}$$

Equation 7.3-25

the approximate equality (via the binomial expansion) holds when the medium perturbation to the wavenumber is much less than the free space wavenumber. This form results in a solution for the effective medium Green's function

$$\left\langle G\left(\vec{r}_a\right)\right\rangle = \frac{e^{-jk_{eff}\left|\vec{r}_a - \vec{r}'\right|}}{4\pi\left|\vec{r}_a - \vec{r}'\right|}$$

Equation 7.3-26

which is identical to the plane wave result for stationary phase, Equation 7.3-16. Hence, in the perfect gas assumption, the effect of the medium is a ‘renormalization of the wavenumber, which is replaced by an effective wave number, having generally an imaginary part” (see Equation 7.3-17) [Frisch, 1965].

7.3.3 The Dyson Equation for a Medium with Pair Correlations

In general, the perfect gas assumption does not hold and the mean Green’s function takes on a more complicated form [Frisch, 1968]:

$$\left\langle G(\vec{r},\vec{r}\,';\omega)\right\rangle = G(\vec{r},\vec{r}\,';\omega) + G(\vec{r},\vec{r}\,';\omega)\hat{M}(\vec{r},\vec{r}\,';\omega)\left\langle G(\vec{r},\vec{r}\,';\omega)\right\rangle$$

Equation 7.3-27

Here the “Mass Operator”, $\hat{M}$, encompasses averaging over the range of correlations among the different scatterers and is most easily understood from the diagram technique [Frisch, 1968]. In the restrictive case of this chapter, however, the averaging is limited to pair correlations and the equation for the mean Green’s function reduces to the following form (assuming only far field interactions)

$$\begin{aligned}
\left\langle G(\vec{r}_j,\vec{r}_k)\right\rangle &= f\left(\hat{k}_i,\hat{k}_s\right)G(\vec{r}_j,\vec{r}_k) + \int_V d\vec{r}_j\, f\left(\hat{k}_i,\hat{k}_s\right)G(\vec{r}_j,\vec{r}_m)\left\langle G(\vec{r}_m,\vec{r}_k)\right\rangle \rho(\vec{r}_m) \\
&\quad + \int_V d\vec{r}_m \int_V d\vec{r}_n\, f\left(\hat{k}_i,\hat{k}_s\right)G(\vec{r}_j,\vec{r}_m)\left\langle G(\vec{r}_m,\vec{r}_n)\right\rangle\left\langle G(\vec{r}_n,\vec{r}_k)\right\rangle C(\vec{r}_m,\vec{r}_n) \\
&= f\left(\hat{k}_i,\hat{k}_s\right)G(\vec{r}_j,\vec{r}_k) + \int_V d\vec{r}_j\, f\left(\hat{k}_i,\hat{k}_s\right)G(\vec{r}_j,\vec{r}_m)\left\langle G(\vec{r}_m,\vec{r}_k)\right\rangle \rho(\vec{r}_m) \\
&\quad + \int_V d\vec{r}_m \int_V d\vec{r}_n\, f\left(\hat{k}_i,\hat{k}_s\right)G(\vec{r}_j,\vec{r}_m)M(\vec{r}_m,\vec{r}_n)\left\langle G(\vec{r}_n,\vec{r}_k)\right\rangle
\end{aligned}$$

Equation 7.3-28

where the kernel of the reduced Mass operator is denoted by $M(\vec{r}_m,\vec{r}_n)$. The mass operator is already in a reduced form since we’ve only considered pair correlations.

Next, the operator, $\left(\nabla^2 + k^2\right)$, is applied to the above equation. This operator is applied to all functions of the observation coordinate, including the scattering amplitude. The result of this operation will result in a simpler form if the scattering amplitude can be excluded from this operation. The scattering amplitude is *independent of the observation direction* in only two circumstances:

- **Isotropic Scattering** (treated by Tsolakis)
- **Forward or Backward Scattering** directions relative to the incident direction

Then, the scattering amplitude is a function of frequency and the incidence direction only. Isotropic scattering was not only used by Tsolakis, but also by Frisch in deriving the Foldy Approximation [Frisch, 1965].

After applying the operator when the scattering amplitude is independent of the observation direction, the equation for the mean Green's function becomes

$$\begin{aligned}\left(\nabla^2+k^2\right)\left\langle G(\vec{r}_j,\vec{r}_k)\right\rangle = &-f\left(\hat{k}_i\right)\delta\left(\vec{r}_j-\vec{r}_k\right)-f\left(\hat{k}_i\right)\int_V d\vec{r}_m\,\delta\left(\vec{r}_j-\vec{r}_m\right)\left\langle G(\vec{r}_m,\vec{r}_k)\right\rangle\rho(\vec{r}_m)\\ &-f\left(\hat{k}_i\right)\int_V d\vec{r}_m\int_V d\vec{r}_n\,\delta\left(\vec{r}_j-\vec{r}_m\right)M(\vec{r}_m,\vec{r}_n)\left\langle G(\vec{r}_n,\vec{r}_k)\right\rangle\\ = &-f\left(\hat{k}_i\right)\delta\left(\vec{r}_j-\vec{r}_k\right)-f\left(\hat{k}_i\right)\left\langle G(\vec{r}_j,\vec{r}_k)\right\rangle\rho(\vec{r}_j)\\ &-f\left(\hat{k}_i\right)\int_V d\vec{r}_n\,M(\vec{r}_j,\vec{r}_n)\left\langle G(\vec{r}_n,\vec{r}_k)\right\rangle\end{aligned}$$

Equation 7.3-29

Above, the scattering amplitude is shown as a function of the incident direction only. This result can be interpreted for either the isotropic or the forward/backward case.

In a homogeneous random medium, both the mass operator kernel and the Green's function are functions of the distance coordinate. Hence, the equation for the mean Green's function finally assumes the form

$$\begin{aligned}\left(\nabla^2+k^2+f\left(\hat{k}_i\right)\rho(\vec{r}_j)\right)\left\langle G(\vec{r}_j,\vec{r}_k)\right\rangle = &-f\left(\hat{k}_i\right)\delta\left(\vec{r}_j-\vec{r}_k\right)\\ &-f\left(\hat{k}_i\right)\int_V d\vec{r}_n\,G(\vec{r}_j,\vec{r}_n)\,C(\vec{r}_j-\vec{r}_n)\left\langle G(\vec{r}_n,\vec{r}_k)\right\rangle\\ = &-f\left(\hat{k}_i\right)\delta\left(\vec{r}_j-\vec{r}_k\right)\\ &-f\left(\hat{k}_i\right)\int_V d\vec{r}_n\,M(\vec{r}_j-\vec{r}_n)\left\langle G(\vec{r}_n,\vec{r}_k)\right\rangle\end{aligned}$$

Equation 7.3-30

Again, solving by Fourier transform techniques, noting the convolutional integral,

$$\left\langle \tilde{G}(u,\vec{r}_k) \right\rangle = \frac{\tilde{f}\left(\hat{k}_i\right)}{\left(u^2 - k^2 - \tilde{f}\left(\hat{k}_i\right)\rho(\vec{r}_j) - \tilde{f}\left(\hat{k}_i\right) \tilde{M}(\vec{r}_j - \vec{r}_n)\right)}$$

Equation 7.3-31

The effective wavenumber in this Fourier space is found from the dispersion relation

$$\left(u^2 - k^2 - \tilde{f}\left(\hat{k}_i\right)\rho(\vec{r}_j) - \tilde{f}\left(\hat{k}_i\right) \tilde{M}(\vec{r}_j - \vec{r}_n)\right) = 0$$

Equation 7.3-32

A more manageable solution can be found if we apply the ***first-order smoothing approximation*** to the mass operator [Frisch, 1968]. In this approximation, the kernel of the Mass operator, $M(\vec{r}_m, \vec{r}_n)$, in the double integral, is replaced by the approximation

$$\begin{aligned} &\int_V d\vec{r}_m \int_V d\vec{r}_n\, f\left(\hat{k}_i, \hat{k}_s\right) G(\vec{r}_j, \vec{r}_m) \left[M(\vec{r}_m, \vec{r}_n)\right] \left\langle G(\vec{r}_n, \vec{r}_k) \right\rangle \\ &\qquad \cong \int_V d\vec{r}_m \int_V d\vec{r}_n\, f\left(\hat{k}_i, \hat{k}_s\right) G(\vec{r}_j, \vec{r}_m) \left[G(\vec{r}_m, \vec{r}_n) C(\vec{r}_m, \vec{r}_n)\right] \left\langle G(\vec{r}_n, \vec{r}_k) \right\rangle \end{aligned}$$

Equation 7.3-33

7.3.4 Low Frequency Approximation for the Mean Green's function

An alternate solution for the mean Green's function can be found by making certain limiting assumptions. When the discrete scatterers are large with respect to the wavelength, the scattering is primarily forward scattering; this approximation is the primary focus of this thesis. However, when the scatterers are small with respect to the wavelength, they begin to scatter more isotropically. In addition, the measured scattering amplitude matches the prediction of Schwering. Here the scattering pattern is a strong forward scatterer superimposed on a much weaker isotropic background. Hence, the isotropic solution is of some interest.

Frisch used the isotropic scattering approximation to derive the mean Green's function for small scatterers [Frisch, 1968] and eventually produced the Foldy

Approximation and a further extension to correlated, isotropic scatterers. Starting with the equation for the mean Green's function in the first-order smoothing approximation,

$$\begin{aligned}\left\langle G(\vec{r}_j,\vec{r}_k)\right\rangle = {} & f\left(\hat{k}_i,\hat{k}_s\right)G(\vec{r}_j,\vec{r}_k) + \int_V d\vec{r}_j\, f\left(\hat{k}_i,\hat{k}_s\right)G(\vec{r}_j,\vec{r}_m)\left\langle G(\vec{r}_m,\vec{r}_k)\right\rangle\rho(\vec{r}_m) \\ & + \int_V d\vec{r}_m \int_V d\vec{r}_n\, f\left(\hat{k}_i,\hat{k}_s\right)G(\vec{r}_j,\vec{r}_m)M(\vec{r}_m,\vec{r}_n)\left\langle G(\vec{r}_n,\vec{r}_k)\right\rangle \\ = {} & f\left(\hat{k}_i,\hat{k}_s\right)G(\vec{r}_j,\vec{r}_k) + \int_V d\vec{r}_j\, f\left(\hat{k}_i,\hat{k}_s\right)G(\vec{r}_j,\vec{r}_m)\left\langle G(\vec{r}_m,\vec{r}_k)\right\rangle\rho(\vec{r}_m) \\ & + \int_V d\vec{r}_m \int_V d\vec{r}_n\, f\left(\hat{k}_i,\hat{k}_s\right)G(\vec{r}_j,\vec{r}_m)G(\vec{r}_m,\vec{r}_n)\left\langle G(\vec{r}_n,\vec{r}_k)\right\rangle C(\vec{r}_m,\vec{r}_n)\end{aligned}$$

Equation 7.3-34

we operate on it with the Helmholtz operator $\left(\nabla^2+k^2\right)$ and recall that the operator u_k^j is related to the free space Green's function. Consequently,

$$\begin{aligned}\left(\nabla^2+k^2\right)\left\langle G(\vec{r}_j,\vec{r}_k)\right\rangle = {} & -\delta(\vec{r}_j,\vec{r}_k) - f\left(\hat{k}_i,\hat{k}_s\right)\left\langle G(\vec{r}_j,\vec{r}_k)\right\rangle\rho(\vec{r}_k) \\ & - \int_V d\vec{r}_n\, f\left(\hat{k}_i,\hat{k}_s\right)G(\vec{r}_j,\vec{r}_n)C(\vec{r}_j,\vec{r}_n)\left\langle G(\vec{r}_n,\vec{r}_k)\right\rangle\rho(\vec{r}_n)\end{aligned}$$

Equation 7.3-35

If we consider small, discrete scatterers, the correlation function becomes localized. Hence, the correlation function is very peaked at the scatterer location $\vec{r}_n$ and the slowly varying mean Green's function may be removed from the integration.

$$\begin{aligned}\left(\nabla^2+k^2\right)\left\langle G(\vec{r}_j,\vec{r}_k)\right\rangle \cong {} & -\delta(\vec{r}_j,\vec{r}_k) - 4\pi f\left(\hat{k}_i,\hat{k}_s\right)\left\langle G(\vec{r}_j,\vec{r}_k)\right\rangle\rho(\vec{r}_k) \\ & - \left\langle G(\vec{r}_n,\vec{r}_k)\right\rangle\rho(\vec{r}_n)\int_V d\vec{r}_n\, f\left(\hat{k}_i,\hat{k}_s\right)G(\vec{r}_j,\vec{r}_n)C(\vec{r}_j,\vec{r}_n)\end{aligned}$$

taking into account the isotropic scattering pattern, this can be rewritten

$$\left(\begin{array}{l}\nabla^2 + k^2 + 4\pi f(k)\rho(\vec{r}_n) \\ \quad + 4\pi\rho(\vec{r}_n) f(k)\int_V d\vec{r}_n \; G(\vec{r}_j, \vec{r}_n) C(\vec{r}_j, \vec{r}_n)\end{array}\right)\left\langle G(\vec{r}_j, \vec{r}_k)\right\rangle \cong -\delta(\vec{r}_j, \vec{r}_k)$$

$$\left(\nabla^2 + k_{Foldy}^2 + 4\pi\rho(\vec{r}_n) f(k)\int_V d\vec{r}_n \; G(\vec{r}_j, \vec{r}_n) C(\vec{r}_j, \vec{r}_n)\right)\left\langle G(\vec{r}_j, \vec{r}_k)\right\rangle \cong -\delta(\vec{r}_j, \vec{r}_k)$$

in this form, we see by the definition of the Green's function that the wavenumber has been modified.

The finite size scatterers are expected to produce spatial correlation functions that are essentially unit step functions. Finally approximating the correlation function with [Frisch, 1965]

$$\varepsilon^2 \, e^{-\frac{|r-r'|}{a}}$$

where a is the dimension of the scatterer (or the correlation length in a continuous random medium. Since ($a/\lambda << 1$), the effective wavenumber reduces to

$$k_{eff}^2 \cong k_{Foldy}^2 + 4\pi\rho(\vec{r}_n) f(k)\varepsilon^2 a^2 \left(1 + j2k_{Foldy}a\right)$$

$$k_{eff} \cong k_{Foldy}\sqrt{1 + 4\pi\rho(\vec{r}_n) f(k)\varepsilon^2 a^2 \left(1 + j2k_{Foldy}a\right)}$$

Hence the effect of the random medium is another renormalization, shows a double renormalization of the wavenumber [Frisch, 1965]. This shows that the correlation in the random medium has introduced an additional exponential loss term attributable to multiple scattering in the effective medium, as the wave propagates into the medium.

7.4 The Distorted Born Approximation

In the previous chapter concerning the single scatter approach, we saw that the mean power could be derived using this simple theory. In the last chapter, single scatter theory, we found the average power is given by

$$
\begin{aligned}
P(t) &= \left\langle E\left(\vec{r}_a, t_1\right) E^*\left(\vec{r}_b, t_2\right)\right\rangle \\
&= \left\langle \int_{-\infty}^{\infty} d\omega_1 E(\vec{r}_a, \omega_1)\, e^{-j\omega_1 t_1} \int_{-\infty}^{\infty} d\omega_2 E^*(\vec{r}_b, \omega_2)\, e^{-j\omega_2 t_2} \right\rangle \\
&= \int_{-\infty}^{\infty} d\omega_1 \int_{-\infty}^{\infty} d\omega_2 \left\langle E(\vec{r}_a, \omega_1) \cdot E^*(\vec{r}_b, \omega_2) \right\rangle e^{-j\left(\omega_1 t_1 - \omega_2 t_2\right)}
\end{aligned}
$$

Equation 7.4-1

in the case of co-located observation points $\vec{r}_a = \vec{r}_b$. In the single scatter, scalar wave propagation, we found that the two-frequency mutual coherence function could be rewritten as

$$
\begin{aligned}
&\left\langle E(\vec{r}_a, \omega_1) E^*(\vec{r}_b, \omega_2) \right\rangle \\
&\quad = \int_{-\infty}^{\infty} d\omega_1 \int_{-\infty}^{\infty} d\omega_2 \int_V d\vec{r} \int_{V'} d\vec{r}\,'\, E_i(\vec{r}, k_1) E_i^*(\vec{r}\,', k_2) \left\langle \left\langle u_j^a(k_1) \right\rangle \right\rangle \left\langle \left\langle u_{j'}^b(k_2) \right\rangle \right\rangle^* C\left(\vec{r}, \vec{r}\,'\right) dV_j\, dV_{j'}
\end{aligned}
$$

Equation 7.4-2

where the incident field is known (deterministic). In the single scattering approach, the configurationally averaged Twersky operators were replaced by the single scatter result; in the Distorted Born Approximation, however, the mean Green's function, found through multiple scattering approach, is used. The result will be similar to the single scattering approach, except for the substitution of the effective wave number for the free space wavenumber. In addition, the artificial introduction of the loss term found in the single scatter development is no longer necessary since will enter the complex form of the effective wavenumber. The average power was finally given as

$$
\begin{aligned}
\left\langle P(t) \right\rangle = \int_{-\infty}^{\infty} d\omega_1 \int_{-\infty}^{\infty} d\omega_2 E_i\left(\omega_1\right) E_i^*\left(\omega_2\right) e^{-j\left(\omega_1 - \omega_2\right)t} \\
\cdot \int_V H(\omega_o + \omega_1) H^*(\omega_o + \omega_2)\, \rho_d\left(\vec{r}\right) d\vec{r}
\end{aligned}
$$

Equation 7.4-3

And the two-frequency mutual coherence function is given by

$$\Gamma(\omega_0+\omega_1,\omega_0+\omega_2) = \left\langle H(\omega_0+\omega_1)H^*(\omega_0+\omega_2)\right\rangle$$

$$= \int_V \frac{\lambda^2}{4\pi} G^2(\omega_0) \frac{\left\langle\left\langle f\left(\hat{k}_i,\hat{k}_s;\omega_1\right)\right\rangle\right\rangle \left\langle\left\langle f\left(\hat{k}_i,\hat{k}_s;\omega_2\right)\right\rangle\right\rangle^* e^{-j(k_{eff}(\omega_1)-k_{eff}(\omega_2))R}}{R^4} \rho\left(\vec{r}_j\right) dV_j$$

Equation 7.4-4

Consequently, the convolutional model could also be derived in the DWBA. Starting from Equation 7.4-4, the scattering amplitude would be replaced with the forward-backward solution. Then, upon making the assumptions and following the steps of Section 4.2, the DWBA could be reduced to the convolutional-DWBA result. This of course, would be a limited form of the DWBA compared with the above result and with the vector result of Lang [1981].

7.5 Two Frequency Radiative Transfer Equation

The solution using single scatter theory is greatly enhanced through the introduction of the Distorted Wave Born Approximation (DWBA). Although based in multiple scattering theory for the mean field, the DWBA still neglects the effects of multiple scattering its formulation of the propagation of the power density. In this section, the wave based approach to power propagation is extended to include multiple scattering though the development of a two-frequency radiative transfer equation. This development closely follows that of Tsolakis [1985] and Besieris [1981]. These papers, in turn, are based on a previous, pioneering work by Barabanenkov [1971].

The coherency matrix is formed by forming the following product

$$\vec{E}(\vec{r}_a, k_1) \cdot \overline{\vec{E}}^*(\vec{r}_b, k_2) =$$

$$\left\{ \begin{array}{l} \vec{E}_i(\vec{r}_a, k_1) + \sum\limits_{j=1}^{N} \overline{\overline{u}}_j^{a}(k_1) \cdot \vec{E}_i(\vec{r}_j, k_1) \\ + \sum\limits_{j=1}^{N} \sum\limits_{\substack{k=1, \\ k \neq j}}^{N} \overline{\overline{u}}_j^{a}(k_1) \cdot \overline{\overline{u}}_k^{j}(k_1) \cdot \vec{E}_i(\vec{r}_k, k_1) \\ + \sum\limits_{j=1}^{N} \sum\limits_{\substack{k=1, \\ k \neq j}}^{N} \sum\limits_{\substack{m=1, \\ m \neq k \\ m \neq j}}^{N} \left[\begin{array}{r} \overline{\overline{u}}_j^{b}(k_1) \cdot \overline{\overline{u}}_k^{j}(k_1) \cdot \overline{\overline{u}}_m^{k}(k_1) \\ \cdot \vec{E}_i(\vec{r}_m, k_1) \end{array} \right] \\ + \quad \ldots \end{array} \right\} \cdot \left\{ \begin{array}{l} \overline{\vec{E}}_i^*(\vec{r}_b, k_2) + \sum\limits_{j=1}^{N} \overline{\left[\overline{\overline{u}}_j^{b}(k_2) \cdot \vec{E}_i(\vec{r}_j, k_2) \right]}^* \\ + \sum\limits_{j=1}^{N} \sum\limits_{\substack{k=1, \\ k \neq j}}^{N} \overline{\left[\overline{\overline{u}}_j^{b}(k_2) \cdot \overline{\overline{u}}_k^{j}(k_2) \cdot \vec{E}_i(\vec{r}_k, k_2) \right]}^* \\ \sum\limits_{j=1}^{N} \sum\limits_{\substack{k=1, \\ k \neq j}}^{N} \sum\limits_{\substack{m=1, \\ m \neq k \\ m \neq j}}^{N} \overline{\left[\begin{array}{r} \overline{\overline{u}}_j^{b}(k_1) \cdot \overline{\overline{u}}_k^{j}(k_1) \cdot \overline{\overline{u}}_m^{k}(k_1) \\ \cdot \vec{E}_i(\vec{r}_m, k_1) \end{array} \right]}^* \\ + \quad \ldots \end{array} \right\}$$

Equation 7.5-1

Using the Twersky approximation, the **two frequency, two-point correlation** can be written in a convenient, closed form [Tsolakis, 1985]. At this point rather than pursuing a case with depolarization, we will concentrate on ***scalar wave propagation***. Referring to the Appendix, assuming no depolarization, each component of the coherency matrix can be written

$$\begin{aligned} \left\langle E(\vec{r}_a, k_1) E^*(\vec{r}_b, k_2) \right\rangle &= \left\langle E(\vec{r}_a, k_1) \right\rangle \left\langle E^*(\vec{r}_b, k_2) \right\rangle \\ &+ \int_V d\vec{r}_j \left\langle \left\langle U(\vec{r}_a, \vec{r}_j; k_1) \right\rangle \right\rangle \left\langle E(\vec{r}_j, k_1) E^*(\vec{r}_j, k_2) \right\rangle \left\langle \left\langle U(\vec{r}_b, \vec{r}_j; k_2) \right\rangle \right\rangle^* \rho(\vec{r}_j) \\ &+ \int_V d\vec{r}_j \int_V d\vec{r}_k \left\langle \left\langle U(\vec{r}_a, \vec{r}_j; k_1) \right\rangle \right\rangle \left\langle E(\vec{r}_j, k_1) E^*(\vec{r}_k, k_2) \right\rangle \left\langle \left\langle U(\vec{r}_b, \vec{r}_k; k_2) \right\rangle \right\rangle^* C(\vec{r}_j, \vec{r}_k) \end{aligned}$$

Equation 7.5-2

Note that when this operator is applied to an incident field, it yields zero. In addition, this expression explicitly shows the frequency dependence in the Green's function as well as the field quantities.

Defining the two-point, two-frequency coherence function

$$\Gamma'(\vec{r}_a, \vec{r}_b, k_1, k_2) \equiv \left\langle E(\vec{r}_a, k_1) E^*(\vec{r}_b, k_2) \right\rangle$$

We apply the operator twice; once with respect to the observation coordinate at $\vec{r}_a$ and then with respect to the observation coordinate at $\vec{r}_b$; forming the difference

$$\left(\nabla^2_{\vec{r}_a} + k_1^2\right)\Gamma'(\vec{r}_a,\vec{r}_b,k_1,k_2) - \left(\nabla^2_{\vec{r}_b} + k_2^2\right)\Gamma'(\vec{r}_a,\vec{r}_b,k_1,k_2)$$

Equation 7.5-3

and using the result for the mean field, we find

$$\left[\left(\nabla^2_{\vec{r}_a} - \nabla^2_{\vec{r}_b}\right) + \left(k_1^2 - k_2^2\right) + \left\{f\left(\hat{k}_i,k_1\right)\rho(\vec{r}_a) - f^*\left(\hat{k}_i,k_2\right)\rho(\vec{r}_b)\right\}\right]\Gamma'(\vec{r}_a,\vec{r}_b,k_1,k_2)$$

$$\begin{aligned}
= &- f\left(\hat{k}_i,k_1\right)\Gamma'(\vec{r}_a,\vec{r}_a,k_1,k_2)\left\langle\left\langle U^*(\vec{r}_b,\vec{r}_a;k_2)\right\rangle\right\rangle\rho\left(\vec{r}_a\right) \\
&+ \left\langle\left\langle U(\vec{r}_a,\vec{r}_b;k_1)\right\rangle\right\rangle\Gamma'(\vec{r}_b,\vec{r}_b,k_1,k_2)\ f^*\left(\hat{k}_i,k_2\right)\rho\left(\vec{r}_b\right) \\
&- \int_V d\vec{r}_k\left[f\left(\hat{k}_i,k_1\right)C\left(\vec{r}_a,\vec{r}_k\right) - f^*\left(\hat{k}_i,k_2\right)C(\vec{r}_j,\vec{r}_b)\right] \\
&\quad\cdot\left[\left\langle\left\langle U(\vec{r}_a,\vec{r}_j;k_1)\right\rangle\right\rangle\Gamma'(\vec{r}_j,\vec{r}_b,k_1,k_2) + \left\langle\left\langle U^*(\vec{r}_b,\vec{r}_j;k_2)\right\rangle\right\rangle\Gamma'(\vec{r}_a,\vec{r}_j,k_1,k_2)\right]
\end{aligned}$$

Equation 7.5-4

This closed equation is the desired form of the scalar-valued Bethe-Salpeter equation found in the papers by both Besieris [1981] and Tsolakis [1985]. The difference is in the form of the scattering amplitude function. Rather than assuming isotropic scattering as was done in the paper by Tsolakis [1985], a forward/backward scattering approximation is assumed for the scattering amplitude. Hence, rather than dipole-like scatterers in which the scatterer is small with respect to the wavelength, we have assumed that the scatterer is large with respect to the wavelength. We next follow in the footsteps of Besieris and Tsolakis in order to derive the two-frequency radiative transfer model.

Recall that under one of the propagation conditions assumed in this chapter, the waves are scattered in the forward direction only. Since the incident wave is assumed to be propagating in the z-direction, the Laplacian, the field quantities and the green's function reduce to a z-variation only, and the wave equation will reduce to a one-dimensional form. For example, Equation 7.5-4 becomes

$$\left[\left(\frac{d^2}{dz_a^2}-\frac{d^2}{dz_b^2}\right)+\left(k_1^2-k_2^2\right)+\left\{f\left(\hat{k}_i,k_1\right)\rho(z_a)-f^*\left(\hat{k}_i,k_2\right)\rho(z_b)\right\}\right]\Gamma'(z_a,z_b,k_1,k_2)$$

$$\begin{aligned}
= & -f\left(\hat{k}_i,k_1\right)\Gamma'(z_a,z_a,k_1,k_2)\left\langle\left\langle U^*(z_b,z_a;k_2)\right\rangle\right\rangle\rho\left(z_a\right) \\
& +\left\langle\left\langle U(z_a,z_b;k_1)\right\rangle\right\rangle\Gamma'(z,z_b,k_1,k_2)\, f^*\left(\hat{k}_i,k_2\right)\rho\left(z_b\right) \\
& -\int_V dz_k\left[f\left(\hat{k}_i,k_1\right)C\left(z_a,z_k\right)-f^*\left(\hat{k}_i,k_2\right)C(z_j,z_b)\right] \\
& \quad\cdot\left[\left\langle\left\langle U(z_a,z_j;k_1)\right\rangle\right\rangle\Gamma'(z_j,z_b,k_1,k_2)+\left\langle\left\langle U^*(z_b,z_j;k_2)\right\rangle\right\rangle\Gamma'(z_a,z_j,k_1,k_2)\right]
\end{aligned}$$

Equation 7.5-5

the following steps, however, will reflect the more general, three-dimensional result. The three dimensional problem is more general and will apply to both the isotropic and the forward/backward cases (within a constant).

The next step in deriving the transfer model is a transformation to center of mass coordinates. With this in mind, we substitute

$$\vec{R}\equiv\frac{1}{2}(\vec{r}_a+\vec{r}_b)\ \text{ and }\ \vec{r}\equiv(\vec{r}_a-\vec{r}_b)$$

$$k_s\equiv\frac{1}{2}(k_1+k_2)\ \text{ and }\ k_d\equiv(k_1-k_2)$$

We define a new set of functions: mutual coherence function, the scatterer correlation, the mass operator kernel, and the mean Green's function

$$\begin{aligned}
&\Gamma'(\vec{r}_a,\vec{r}_b,k_1,k_2)=\Gamma\left(\vec{R},\vec{r},k_s,k_d\right)\\
&C\left(\vec{r}_a,\vec{r}_b\right)=B\left(\vec{R},\vec{r}\right)\\
&f\left(k_1\right)C\left(\vec{r}_a,\vec{r}_b\right)\left\langle\left\langle U(\vec{r}_a,\vec{r}_b;k_1)\right\rangle\right\rangle=M\left(\vec{R},\vec{r};k_s+\frac{1}{2}k_d\right)\\
&\left\langle\left\langle U(\vec{r}_a,\vec{r}_b;k_1)\right\rangle\right\rangle\equiv\left\langle\left\langle G\left(\vec{R},\vec{r};k_s+\frac{1}{2}k_d\right)\right\rangle\right\rangle
\end{aligned}$$

Considering a "smoothly inhomogeneous" medium, we may simplify the expressions by assuming that these quantities vary rapidly with the difference variable and slowly with the sum variables. Expanding these functions in a Taylor series, substituting into the equation for the two-frequency mutual coherence function and truncating after the first term, we arrive at a simpler form.

A Fourier transform with respect to the fast (difference) variable changes our solution space to "phase space" [Besieris, 1981]. This particular transform, the Wigner Transform, is accomplished for the two-frequency coherence function as follows

$$W(\vec{R},\vec{u},k_s,k_d)=\frac{1}{2\pi}\int d\vec{r}\,\Gamma\left(\vec{R},\vec{r},k_s,k_d\right)e^{-j\vec{u}\cdot\vec{r}}$$

The result, W, will be referred to as the ***two-frequency Wigner distribution function***. where the transform variable has been identified as the vector, $\vec{u}$. The other quantities of interest transform as follows [Tsolakis, 1985],

$$\begin{aligned}
\phi(\vec{R},\vec{u}) &= \frac{1}{(2\pi)^3}\int d\vec{r}\,B\left(\vec{R},\vec{r}\right)e^{-j\vec{u}\cdot\vec{r}}\\
\tilde{M}(\vec{R},\vec{u},\ldots) &= \frac{1}{(2\pi)^3}\int d\vec{r}\,M\left(\vec{R},\vec{r},\ldots\right)e^{-j\vec{u}\cdot\vec{r}}\\
\left\langle\left\langle\tilde{G}(\vec{R},\vec{u},\ldots)\right\rangle\right\rangle &= \frac{1}{(2\pi)^3}\int d\vec{r}\left\langle\left\langle G(\vec{R},\vec{r},\ldots)\right\rangle\right\rangle e^{-j\vec{u}\cdot\vec{r}}
\end{aligned}$$

Equation 7.5-6

The ellipsis in Equation 7.5-6 has been added to indicate placeholders for additional (dummy) variables.

The configurationally averaged Wigner-transformed Green's function is found from the Dyson equation of Equation 7.3-30 (suitably transformed to center of mass coordinates)

$$\left(\nabla_{\vec{r}}^2+k^2+f(k_s)\rho(\vec{r})\right)\left\langle\left\langle G(\vec{R},\vec{r})\right\rangle\right\rangle = -f\left(\hat{k}_i\right)\delta(\vec{r}) - f\left(\hat{k}_i\right)\int_V d\vec{r}'\,M(\vec{r}-\vec{r}')\left\langle\left\langle G(\vec{R},\vec{r}')\right\rangle\right\rangle$$

Equation 7.5-7

and the solution via Fourier transform yields

$$\left\langle\left\langle \tilde{G}(\vec{R},\vec{r},k)\right\rangle\right\rangle = f\left(k_s\right)\left[2\,H(\vec{R},\vec{u},k_s)\right]^{-1} = \frac{1}{2} f\left(k_s\right)\left[\, H_R(\vec{R},\vec{u},k_s) + jH_I(\vec{R},\vec{u},k_s)\,\right]^{-1}$$

Equation 7.5-8

The quantity $H(\vec{R},\vec{u},k_s)$ is the “complex Hamiltonian” of the effective medium, as defined in the paper by Besieris [1981].

In this expression, the imaginary portion of the transformed mass operator kernel accounts for scattering loss. Like Besieris and Tsolakis, we assume that the regular and scattering loss terms are small, but not negligible. Hence, a constant energy surface is defined by setting the Hamiltonian equal to zero

$$\begin{aligned} &H_R(\vec{R},\vec{u},k_s) + jH_I(\vec{R},\vec{u},k_s) = 0 \\ &\cong H_R(\vec{R},\vec{u},k_s) = 0 \end{aligned}$$

This equation defines the surface in the (R, u) coordinate space where the wavenumber is equal to the effective wavenumber. This is directly reminiscent of the definition for the effective wavenumber from Equation 7.3-32.

The remainder of the development is similar to that found in ray optics. Hence, the these results are comparable to the ray equation result [Marcuse, 1982]

$$n\frac{d\vec{r}}{dl} = \nabla S$$

where the function S defines the constant phase surface, n is the refractive index and the vector $\vec{r}$ points from a fixed origin to all points on the light ray. However, in the development of this chapter, the surfaces of constant energy and constant phase may not coincide. We can see that an effective index of refraction may be defined as follows

$$n_{eff}\left(\vec{R},\vec{u},k_s\right) = \left|\nabla_{\vec{u}} H_R\left(\vec{R},\vec{u},k_s\right)\right|_{u=k_{eff}}$$

Later, this form will be slightly modified in order to comply with the definitions given by Tsolakis [1985].

In order to derive an equation of transfer that is similar to that given in literature, the coherent power must be separated from the incoherent power. This is a requirement since the standard radiative transfer equations are based primarily on the propagation of incoherent power. The first step in producing a radiative transfer formulation will be to split the two-frequency Wigner distribution into a coherent, W_C, and an incoherent, W_I, portion.

$$\begin{aligned} W(\vec{R},\vec{u},k_s,k_d) &= \frac{1}{2\pi}\int d\vec{r}\,\Gamma\left(\vec{R},\vec{u},k_s,k_d\right)e^{-j\vec{u}\cdot\vec{r}} \\ &= W_C(\vec{R},\vec{u},k_s,k_d) + W_I(\vec{R},\vec{u},k_s,k_d) \end{aligned}$$

the coherent portion obeys a generalized transport equation derived by Tsolakis [1985],

$$\begin{aligned} &\left|\nabla_{\vec{u}} H_R\left(\vec{R},\vec{u},k_s\right)\right| \frac{dW_C(\vec{R},\vec{u},k_s,k_d)}{dl} + \left[f_I\left(k_s\right)\rho(\vec{R}) + \tilde{M}_I\left(\vec{R},\vec{u}',k_s\right)\right] W_C(\vec{R},\vec{u},k_s,k_d) \\ &- jk_d\left[\frac{k_s}{4} + \frac{1}{2}\frac{df_R\left(k_s\right)}{dk_s}\rho(\vec{R}) + \frac{1}{2}\frac{d\tilde{M}_R\left(\vec{R},\vec{u}',k_s\right)}{dk_s}\right] W_C(\vec{R},\vec{u},k_s,k_d) \ = \ 0 \end{aligned}$$

Equation 7.5-9

Notice that this equation behaves just as expected. The form is the same as the overall transport equation with the exception of the scattering integral. Hence, as proposed in previous chapters concerning classical radiative transfer formulation, the coherent power propagates, losing power but no power is scattered back into its path. There are differences with the radiative transfer formulation that will be acknowledged in an upcoming discussion. The incoherent portion of the two-frequency Wigner distribution is chosen as follows [Tsolakis, 1985].

$$W_I\left(\vec{R},\vec{u},k_s,k_d\right) = k_s \frac{\left|\nabla_{\vec{u}} H_R\left(\vec{R},\vec{u},k_s\right)\right|}{\left|\nabla_{\vec{u}} H_R\left(\vec{R},\vec{u},k_s\right)\right|^3}\,\delta\left\{\left[H_R(\vec{R},\vec{u};\ k_s)\ \right]^{-1}\right\} I\left(\vec{R},\vec{s},k_s,k_d\right)$$

Equation 7.5-10

This is the ***two-frequency incoherent power density*** at a point $\vec{R}$ propagating in the direction, $\vec{s} = \vec{u}/u$. Adopting the effective wavenumber, k_{eff}, as the value of u for which $H_R(\vec{R}, u\vec{s}, k_s) = 0$, the definition for

$$n_{eff}(\vec{R}, \vec{s}, k_s) = \left[\frac{\left| \nabla_{\vec{u}} H_R(\vec{R}, u\vec{s}, k_s) \right|}{k_s} \right]_{u=k_{eff}(\vec{R}, \vec{s}, k_s)}$$

Equation 7.5-11

In an anisotropic medium, the phase velocity and the group velocity are not in the same direction. This case has been derived for the isotropic scatterers by Tsolakis [1985] but will not be addressed here. In the case of isotropic pair correlations, the quantities, $\tilde{M}_R(\vec{R}, \vec{u}, k_s), \tilde{M}_I(\vec{R}, \vec{u}, k_s)$ and $\phi(\vec{R}, \vec{u} - \vec{u}')$, no longer depend on a vector, u, only on its magnitude. Consequently, the two-frequency radiative transfer equation reduces to [Tsolakis, 1985]

$$\begin{aligned} n_{eff}^2(\vec{R}, k_s) \frac{d}{dl} \left[I(\vec{R}, \vec{s}, k_s, k_d) n_{eff}^{-2}(\vec{R}, k_s) \right] &= -\alpha(\vec{R}, \vec{s}, k_s) I(\vec{R}, \vec{s}, k_s, k_d) \\ &+ j \frac{k_d}{k_s n_{eff}(\vec{R}, k_s)} \left[\frac{k_s}{4} + 2\pi \frac{d}{dk_s} \left[\rho(\vec{R}) f_R(k_s) + \tilde{M}'(\vec{R}, k_{eff}(\vec{R}, k_s) \vec{s}, k_s) \right] \right] I(\vec{R}, \vec{s}, k_s, k_d) \\ &+ \iint_{\substack{\text{solid} \\ \text{angle}}} d\Omega(\vec{s}') p(\vec{R}, \vec{s}, \vec{s}', k_s) I(\vec{R}, \vec{s}, k_s, k_d) \\ &+ \iint_{\substack{\text{solid} \\ \text{angle}}} d\Omega(\vec{s}') p(\vec{R}, \vec{s}, \vec{s}', k_s) W_C(\vec{R}, \vec{s}, k_s, k_d) \end{aligned}$$

Equation 7.5-12

Equation 7.5-12 looks like the classical radiative transfer equation. The extinction coefficient is given by

$$\alpha(\vec{R}, \vec{s}, k_s) = \frac{1}{k_s n_{eff}(\vec{R}, k_s)} \left[f_I(k_s) \rho(\vec{R}) + \tilde{M}_I(\vec{R}, \vec{u}', k_s) \right]$$

Equation 7.5-13

The first term represents the true absorption and the second term is the loss due to scattering. There is an extra factor, which accounts for frequency offset effects.

$$j\frac{k_d}{k_s n_{eff}\left(\vec{R},k_s\right)}\left[\frac{k_s}{4}+\frac{1}{2}\frac{d}{dk_s}\left[\rho\left(\vec{R}\right)f_R\left(k_s\right)+\tilde{M}'\left(\vec{R},k_{eff}\left(\vec{R},k_s\right)\vec{s},k_s\right)\right]\right]$$

Equation 7.5-14

Recall, however, that the frequency dependence of this solution is limited due to a narrowband assumption. The “power” scattering amplitude (or “phase matrix” from radiometry) is given by

$$p\left(\vec{R},\vec{s},\vec{s}',k_s\right)=\frac{2\left|f\left(k_s\right)\right|^2 k_{eff}^2\left(\vec{R},k_s\right)}{k_s^2\,n_{eff}^2\left(\vec{R},k_s\right)}\left[\phi\left(\vec{R},\vec{u}-\vec{u}',k_{eff}\left(\vec{R},k_s\right)\right)+\rho(\vec{R})\right]$$

Equation 7.5-15

An obvious difference from the classical transfer formulation is the extinction. When the difference frequency is zero, the extinction coefficient is real as expected; on the other hand, a non-zero difference frequency yields a complex extinction coefficient.

7.6 Solution of the two-frequency radiative transfer equation for a forward-backward scattering medium

The derivation of the two-frequency radiative transfer equation for discrete scatterers has been shown to reduce to a one-dimensional transfer equation when the scattering amplitude of the particles has strongly forward and backward patterns only. In general, the two-frequency radiative transfer equation is given as

$$n_{eff}^2(\vec{R},k_s)\frac{d}{dl}\left[I(\vec{R},\vec{s},k_s,k_d)n_{eff}^{-2}(\vec{R},k_s)\right] = -\kappa(\vec{R},\vec{s},k_s)I(\vec{R},\vec{s},k_s,k_d)$$

$$+ j\frac{k_d}{k_s n_{eff}(\vec{R},k_s)}\left[\frac{k_s}{4}+2\pi\frac{d}{dk_s}\left[\rho(\vec{R})f_R(k_s)+\tilde{M}'(\vec{R},k_{eff}(\vec{R},k_s)\vec{s},k_s)\right]\right]I(\vec{R},\vec{s},k_s,k_d)$$

$$+ \iint_{\substack{\text{solid}\\ \text{angle}}} d\Omega(\vec{s}')p(\vec{R},\vec{s},\vec{s}',k_s)I(\vec{R},\vec{s},k_s,k_d)$$

$$+ \iint_{\substack{\text{solid}\\ \text{angle}}} d\Omega(\vec{s}')p(\vec{R},\vec{s},\vec{s}',k_s)W_C(\vec{R},\vec{s},k_s,k_d)$$

Equation 7.6-1

Assuming the incident field is z-directed and if we assume strictly forward-backward scatterers, the two-frequency radiative transfer equation simplifies to a linear, nonhomogeneous set of ordinary differential equations.

$$n_{eff}^2(\vec{R},k_s)\frac{d}{dl}\left[I(\vec{R},\hat{z},k_s,k_d)n_{eff}^{-2}(\vec{R},k_s)\right] = -\tilde{\kappa}(\vec{R},\hat{z},k_s)I(\vec{R},\hat{z},k_s,k_d)$$
$$+ \iint_{\substack{\text{solid}\\ \text{angle}}} d\Omega(\vec{s}')p(\vec{R},\vec{s},\vec{s}',k_s)I(\vec{R},\hat{z},k_s,k_d)$$
$$+ \iint_{\substack{\text{solid}\\ \text{angle}}} d\Omega(\vec{s}')p(\vec{R},\vec{s},\vec{s}',k_s)W_C(\vec{R},\hat{z},k_s,k_d)$$

Equation 7.6-2

For simplicity in notation, the difference frequency component has been absorbed into a new, modified extinction coefficient, $\tilde{\kappa}$. However, both the coherent and the incoherent power densities travel in only one direction, z. Therefore, both of these terms are accompanied by delta functions which reduce the integral over the solid angle to simple forward or backward scattering. If the incident power is normal to the boundary (foliage-air interface), a new power density (intensity) dependent variable can be defined that only depends on the depth coordinate, Z.

$$I_d(Z,\hat{z},k_s,k_d) \equiv I(Z,\hat{z},k_s,k_d)n_{eff}^{-2}(Z,k_s)$$

in turn, this can be split into forward and backward propagating power density components

$$\bar{I}_d(Z,\hat{z},k_s,k_d) \equiv \begin{Bmatrix} I_d^+(Z,\hat{z},k_s,k_d), & \text{for downward / forward propagation} \\ \\ I_d^-(Z,\hat{z},k_s,k_d), & \text{for upward / backward propagation} \end{Bmatrix}$$

Consequently, the selection of this forward-backward scattering function has produced the following simplified, coupled radiative transfer equations.

$$\begin{aligned}\frac{d\,I_d^+(Z,k_s,k_d)}{dZ} = -\tilde{\kappa}(Z,k_s)I_d^+(Z,k_s,k_d) + {} & \left[\sigma_f I_d^+(Z,k_s,k_d) + \sigma_b I_d^-(Z,k_s,k_d)\right] \\ & +\sigma_f\, W_C(Z,k_s,k_d)\end{aligned}$$

$$\begin{aligned}-\frac{d\,I_d^-(Z,k_s,k_d)}{dZ} = -\tilde{\kappa}(Z,k_s)I_d^-(Z,k_s,k_d) + {} & \left[\sigma_b I_d^+(Z,k_s,k_d) + \sigma_f I_d^-(Z,k_s,k_d)\right] \\ & +\sigma_b W_C(Z,k_s,k_d)\end{aligned}$$

Equation 7.6-3

Additionally, we consider the problem to be bounded above by the air-foliage interface and below by the rough surface. Assuming no reflection from the air-foliage boundary, the foliage surface boundary causes the only reflection. The two-point boundary value problem will then have the following boundary condition (in matrix form)

$$\begin{bmatrix} 1 & 0 \\ 0 & 0 \end{bmatrix}\begin{bmatrix} I_d^+(Z=0) \\ I_d^-(Z=0) \end{bmatrix} + \begin{bmatrix} 0 & 0 \\ -\Gamma & 1 \end{bmatrix}\begin{bmatrix} I_d^+(Z=Z_d) \\ I_d^-(Z=Z_d) \end{bmatrix} = \begin{bmatrix} 0 \\ 0 \end{bmatrix}$$

Equation 7.6-4

From this representation, given a surface with a complex reflection coefficient, Γ, the downward propagating wave and the upward propagating reflected wave cancel by construction. Consequently, converting (changing variables) to optical distance and rewriting this in matrix form, and

$$\frac{d}{dZ}\begin{bmatrix} I_d^+(Z,k_s,k_d) \\ I_d^-(Z,k_s,k_d) \end{bmatrix} = \begin{bmatrix} -\tilde{\kappa}(Z,k_s)+\sigma_f & \sigma_b \\ -\sigma_b & \tilde{\kappa}(Z,k_s)-\sigma_f \end{bmatrix}\begin{bmatrix} I_d^+(Z,k_s,k_d) \\ I_d^-(Z,k_s,k_d) \end{bmatrix} + \begin{bmatrix} \sigma_f \\ -\sigma_b \end{bmatrix} W_C(Z,k_s,k_d)$$

Equation 7.6-5

Substituting for the elements of the matrix and dropping the arguments of the coherent and incoherent power densities, the above "Schuster" equations can be rewritten in the familiar form [Schuster, 1905],

$$\frac{d}{dZ}\begin{bmatrix} I_d^+ \\ I_d^- \end{bmatrix} = \begin{bmatrix} -\alpha & \beta \\ -\beta & \alpha \end{bmatrix}\begin{bmatrix} I_d^+ \\ I_d^- \end{bmatrix} + \begin{bmatrix} \sigma_f \\ -\sigma_b \end{bmatrix} W_C(Z)$$

Equation 7.6-6

the eigenvalues, $\lambda_{1,2}$, of the homogeneous system are found from the determinant of the matrix

$$\left(\lambda^2 - \alpha^2\right) + \beta^2 = 0 \quad \Rightarrow \quad \lambda_{1,2} = \pm\sqrt{\alpha^2 - \beta^2} = \pm\lambda$$

and the fundamental matrix (matrix of eigenvectors),

$$\psi(Z) = \left[\overline{X}_1 e^{\lambda Z} \ \ \overline{X}_2 e^{-\lambda Z}\right] = \begin{bmatrix} \beta e^{\lambda Z} & \beta e^{-\lambda Z} \\ (\alpha+\lambda)e^{\lambda Z} & (\alpha-\lambda)e^{-\lambda Z} \end{bmatrix}$$

and its more convenient form,

$$\begin{aligned} \overline{\overline{\Phi}}(\tau) &= \frac{1}{2\lambda\beta}\begin{bmatrix} \beta\left[(\alpha+\lambda)e^{-\lambda\tau} - (\alpha-\lambda)e^{\lambda\tau}\right] & \beta^2\left(e^{\lambda\tau} - e^{-\lambda\tau}\right) \\ \left(\alpha^2-\lambda^2\right)\left(e^{\lambda\tau} - e^{-\lambda\tau}\right) & \beta\left[(\alpha+\lambda)e^{\lambda\tau} - (\alpha-\lambda)e^{-\lambda\tau}\right] \end{bmatrix} \\ &= \frac{1}{2\lambda}\begin{bmatrix} \left[(\alpha+\lambda)e^{-\lambda\tau} - (\alpha-\lambda)e^{\lambda\tau}\right] & \beta\left(e^{\lambda\tau} - e^{-\lambda\tau}\right) \\ \beta\left(e^{-\lambda\tau} - e^{\lambda\tau}\right) & \left[(\alpha+\lambda)e^{\lambda\tau} - (\alpha-\lambda)e^{-\lambda\tau}\right] \end{bmatrix} \end{aligned}$$

Note that the second fundamental matrix does display the desired property that

$$\overline{\overline{\Phi}}^{-1}(z) = \overline{\overline{\Phi}}(-z)$$

Consequently, for the boundary condition

$$\overline{\overline{W}}^{[0]}\bar{I}_d(0) + \overline{\overline{W}}^{[Z_d]}\bar{I}_d(Z_d) = 0$$

where in this case, the matrices W are found from Equation 7.6-6:

$$\overline{\overline{W}}^{[0]} = \begin{bmatrix} 1 & 0 \\ 0 & 0 \end{bmatrix}, \ \overline{\overline{W}}^{[Z_d]} = \begin{bmatrix} 0 & 0 \\ -\Gamma & 1 \end{bmatrix}$$

Although the solution method outlined previously can be used, the general is found by the variation of parameters this time:

$$\bar{I}_d(Z) = \overline{\overline{\Phi}}(Z)\bar{u}_o + \overline{\overline{\Phi}}(Z)\int_0^Z \overline{\overline{\Phi}}^{-1}(t)\begin{bmatrix} \sigma_f \\ -\sigma_b \end{bmatrix}\overline{W_C}(t)dt$$

Equation 7.6-7

The solution for the "initial value matrix is formed by evaluating the boundary condition as follows:

at $Z = 0,$

$$[1 \quad 0]\bar{I}_d = [1 \quad 0]\begin{bmatrix} I_d^+(Z=0) \\ I_d^-(Z=0) \end{bmatrix} = \begin{bmatrix} 0 \\ 0 \end{bmatrix}$$

$$\Rightarrow [1 \quad 0]\left(\overline{\overline{\Phi}}(0)\bar{u}_o + \overline{\overline{\Phi}}(0)\int_0^0 \overline{\overline{\Phi}}^{-1}(t)\begin{bmatrix} \sigma_f \\ -\sigma_b \end{bmatrix}W_C(t)dt\right) = \begin{bmatrix} 0 \\ 0 \end{bmatrix}$$

$$\Rightarrow [1 \quad 0]\left(\overline{\overline{\Phi}}(0)\bar{u}_o\right) = \begin{bmatrix} 0 \\ 0 \end{bmatrix}$$

at $Z = Z_d$,

$$[-\Gamma \quad 1]\bar{I}_d(Z_d) = [1 \quad 0]\begin{bmatrix} I_d^+(Z=0) \\ I_d^-(Z=0) \end{bmatrix} = \begin{bmatrix} 0 \\ 0 \end{bmatrix}$$

$$\Rightarrow [-\Gamma \quad 1]\left(\overline{\overline{\Phi}}(Z_d)\bar{u}_o + \overline{\overline{\Phi}}(Z_d) \int_0^{Z_d} \overline{\overline{\Phi}}^{-1}(t) \begin{bmatrix} \sigma_f \\ -\sigma_b \end{bmatrix} W_C(t)dt \right) = \begin{bmatrix} 0 \\ 0 \end{bmatrix}$$

so that the solution for the initial vector is found from

$$\begin{bmatrix} [1 \quad 0]\left(\overline{\overline{\Phi}}(0) \right) \\ [-\Gamma \quad 1]\left(\overline{\overline{\Phi}}(Z_d)\bar{u}_o + \int_0^{Z_d} \overline{\overline{\Phi}}(Z_d - t) \begin{bmatrix} \sigma_f \\ -\sigma_b \end{bmatrix} W_C(t)dt \right) \end{bmatrix} = \begin{bmatrix} 0 \\ 0 \end{bmatrix}$$

$$\begin{bmatrix} [1 \quad 0]\overline{\overline{\Phi}}(0) \\ [-\Gamma \quad 1]\overline{\overline{\Phi}}(Z_d) \end{bmatrix}\bar{u}_o = \begin{bmatrix} 0 \\ [\Gamma \quad -1] \int_0^{Z_d} \overline{\overline{\Phi}}(Z_d - t)\begin{bmatrix} \sigma_f \\ -\sigma_b \end{bmatrix} W_C(t)dt \end{bmatrix}$$

Equation 7.6-8

and

$$\bar{u}_o = \begin{bmatrix} [1 \quad 0]\overline{\overline{\Phi}}(0) \\ [-\Gamma \quad 1]\overline{\overline{\Phi}}(Z_d) \end{bmatrix}^{-1} \begin{bmatrix} 0 \\ [\Gamma \quad -1] \int_0^{Z_d} \overline{\overline{\Phi}}(Z_d - t)\begin{bmatrix} \sigma_f \\ -\sigma_b \end{bmatrix} W_C(t)dt \end{bmatrix}$$

$$= \begin{bmatrix} [1 \quad 0]\overline{\overline{\Phi}}(0) \\ [-\Gamma \quad 1]\overline{\overline{\Phi}}(Z_d) \end{bmatrix}^{-1} \begin{bmatrix} 0 \\ [\Gamma \quad -1] \int_0^{Z_d} \overline{\overline{\Phi}}(Z_d - t)\begin{bmatrix} \sigma_f \\ -\sigma_b \end{bmatrix} W_C(t)dt \end{bmatrix}$$

$$\text{where}: \ \overline{\overline{\Phi}}(Z_d - t) = \frac{1}{2\lambda}\begin{bmatrix} [(\alpha+\lambda)e^{-\lambda(Z_d - t)} - (\alpha-\lambda)e^{\lambda(Z_d - t)}] & \beta\left(e^{\lambda(Z_d - t)} - e^{-\lambda(Z_d - t)}\right) \\ \beta\left(e^{-\lambda(Z_d - t)} - e^{\lambda(Z_d - t)}\right) & [(\alpha+\lambda)e^{\lambda(Z_d - t)} - (\alpha-\lambda)e^{-\lambda(Z_d - t)}] \end{bmatrix}$$

the solution is found to be as follows

$$\bar{u}_o = \begin{bmatrix} 0 \\ S_1(k_s, k_d)\left(1 - e^{\lambda Z_d}\right) + S_2(k_s, k_d)\left(1 - e^{-\lambda Z_d}\right) \end{bmatrix}$$

Equation 7.6-9

Where,

$$S_1(k_s,k_d)=\frac{1}{\lambda}\frac{\Gamma(\sigma_b+\sigma_f\,[\alpha-\lambda])-\sigma_b(\alpha+\lambda)-\sigma_f\,\beta}{\Gamma\beta\left(e^{-\lambda Z_d}+e^{\lambda Z_d}\right)-(\alpha-\lambda)e^{-\lambda Z_d}+(\alpha+\lambda)e^{\lambda Z_d}}$$
$$S_2(k_s,k_d)=\frac{1}{\lambda}\frac{\Gamma(\sigma_b-\sigma_f\,[\alpha+\lambda])-\sigma_b(\beta+\lambda-\alpha)+\sigma_f\,\beta}{\Gamma\beta\left(e^{-\lambda Z_d}+e^{\lambda Z_d}\right)-(\alpha-\lambda)e^{-\lambda Z_d}+(\alpha+\lambda)e^{\lambda Z_d}}$$

Let the frequency dependent ratio of backward to forward scattering cross-section be denoted $\chi(k_d)$. Then assuming *a narrowband signal* so that the forward scattering cross section is constant with frequency, the backward scattering cross section is written in terms of the forward scattering cross section, $\sigma_b(k_s)=\sigma_f(k_s)\chi(k_s)$. Reintroducing the frequency dependence of the scattering cross section, Γ, into Equation 7.6-9, and

$$S_1(k_s,k_d)=\frac{1}{\lambda}\frac{\Gamma\sigma_f\;[\chi+\alpha(1-\chi)+\lambda(1+\chi)-\beta\,]}{\Gamma\beta\left(e^{-\lambda Z_d}+e^{\lambda Z_d}\right)-(\alpha-\lambda)e^{-\lambda Z_d}+(\alpha+\lambda)e^{\lambda Z_d}}$$
$$S_2(k_s,k_d)=\frac{1}{\lambda}\frac{\Gamma(\sigma_b-\sigma_f\,[\alpha+\lambda])-\sigma_b(\beta+\lambda-\alpha)+\sigma_f\,\beta}{\Gamma\beta\left(e^{-\lambda Z_d}+e^{\lambda Z_d}\right)-(\alpha-\lambda)e^{-\lambda Z_d}+(\alpha+\lambda)e^{\lambda Z_d}}$$

Applying the two-frequency reflection coefficient previously derived from the Kirchhoff approximation above to the solution (see Section 3.4.2), the incoherent intensity will be determined. The only missing information is the source term, the coherent power density. This will be found in a manner similar to the above solution. Therefore, all quantities have been found in Equation 7.6-7. With this information, we may find the two-frequency mutual coherence function and finally weight the result by the spectrum of the transmitted pulse. Performing the necessary inverse Fourier transforms completes the recovery of the time domain solution.

7.7 Conclusions and Future Efforts

The multiple scattering approach has yielded two useful results with respect to the convolutional model of Chapter 4 : the Distorted Wave Born Approximation (DWBA), and the two-frequency radiative transfer equation. From the calculation of the mean

Green’s function, the DWBA will provide an avenue to calculate the scattered power. More specifically, however, using the mean Green’s function in the convolutional result from the single scatter development of Section 6.3.3 will yield a more predictable and interpretable convolutional model. In this development, the simple far field form of the Green’s function in combination with the scattering amplitude would be replaced by the mean Green’s function, see Section 7.3. Finally, the two-frequency radiative transfer equation was reduced to a forward-backward result. Hence, if the upward propagating power density can not scatter into the downward propagating power density, then this two-frequency radiative transfer result can be manipulated into the convolutional form, following the steps in Section 4.2. Consequently, the result will be a more general, physically interpretable form of the convolutional model.

This section of the dissertation has created a host of possible avenues to explore. First, the DWBA should be implemented, first for uncorrelated scatterers and then with pair correlated scatterers. This result will lend some physical interpretation to the convolutional solution. Then the solution of Section 7.6 must be implemented (along with the two-frequency rough surface result) and compared with the simple convolutional result. Not only will this provide further insight into the physical mechanisms, but it will also add some new dimensions to the analysis – frequency dependence. Obviously, implementing this solution will add complexity to the simple convolutional result, in the form of some difficult inverse Fourier transforms.

7.8 Appendix: Two Frequency Radiative Transfer Equation

The solution using single scatter theory is greatly enhanced through the introduction of the Distorted Wave Born Approximation (DWBA). Although based in multiple scattering theory for the mean field, the DWBA still neglects the effects of multiple scattering its formulation of the propagation of the power density. In this section and the following sections, the wave based approach to power propagation is extended to include multiple scattering though the development of a two-frequency radiative transfer equation. This development closely follows that of Tsolakis [1985] and Besieris [1981]. These papers, in turn, are based on a previous, pioneering work by Barabanenkov [1971].

7.8.1 *Two Frequency, Two Point Coherency Matrix*

The coherency matrix is formed by forming the following product

$$
\begin{aligned}
&\vec{E}(\vec{r}_a,k_1)\cdot\vec{E}^{\overline{*}}(\vec{r}_b,k_2) = \\
&\left\{\begin{aligned}
&\vec{E}_i(\vec{r}_a,k_1) + \sum_{j=1}^{N}\overset{=a}{u}_j(k_1)\cdot\vec{E}_i(\vec{r}_j,k_1)\\
&+\sum_{j=1}^{N}\sum_{\substack{k=1,\\k\neq j}}^{N}\overset{=a}{u}_j(k_1)\cdot\overset{=j}{u}_k(k_1)\cdot\vec{E}_i(\vec{r}_k,k_1)\\
&+\sum_{j=1}^{N}\sum_{\substack{k=1,\\k\neq j}}^{N}\sum_{\substack{m=1,\\m\neq k\\m\neq j}}^{N}\left[\begin{aligned}&\overset{=b}{u}_j(k_1)\cdot\overset{=j}{u}_k(k_1)\cdot\overset{=k}{u}_m(k_1)\\&\qquad\cdot\vec{E}_i(\vec{r}_m,k_1)\end{aligned}\right]\\
&+\quad\ldots
\end{aligned}\right\}\cdot
\left\{\begin{aligned}
&\vec{E}_i^{\overline{*}}(\vec{r}_b,k_2) + \sum_{j=1}^{N}\left[\overset{=b}{u}_j(k_2)\cdot\vec{E}_i(\vec{r}_j,k_2)\right]^{\overline{*}}\\
&+\sum_{j=1}^{N}\sum_{\substack{k=1,\\k\neq j}}^{N}\left[\overset{=b}{u}_j(k_2)\cdot\overset{=j}{u}_k(k_2)\cdot\vec{E}_i(\vec{r}_k,k_2)\right]^{\overline{*}}\\
&\sum_{j=1}^{N}\sum_{\substack{k=1,\\k\neq j}}^{N}\sum_{\substack{m=1,\\m\neq k\\m\neq j}}^{N}\left[\begin{aligned}&\overset{=b}{u}_j(k_1)\cdot\overset{=j}{u}_k(k_1)\cdot\overset{=k}{u}_m(k_1)\\&\qquad\cdot\vec{E}_i(\vec{r}_m,k_1)\end{aligned}\right]^{\overline{*}}\\
&+\quad\ldots
\end{aligned}\right\}
\end{aligned}
$$

Equation 7.8-1

Next, we expand this form up through third order summations

$$
\begin{aligned}
\vec{E}(\vec{r}_a,k_1)\cdot\vec{E}^{\overline{*}}(\vec{r}_b,k_2) &= \vec{E}_i(\vec{r}_a,k_1)\cdot\vec{E}_i^{\overline{*}}(\vec{r}_b,k_2)\\
&+\sum_{j=1}^{N}\overset{=a}{u}_j(k_1)\cdot\vec{E}_i(\vec{r}_j,k_1)\cdot\vec{E}_i^{\overline{*}}(\vec{r}_b,k_2) + \vec{E}_i(\vec{r}_a,k_1)\cdot\sum_{j=1}^{N}\left[\overset{=b}{u}_j(k_2)\cdot\vec{E}_i(\vec{r}_j,k_2)\right]^{\overline{*}}\\
&+\sum_{j=1}^{N}\overset{=a}{u}_j(k_1)\cdot\vec{E}_i(\vec{r}_j,k_1)\cdot\sum_{k=1}^{N}\left[\overset{=b}{u}_k(k_2)\cdot\vec{E}_i(\vec{r}_k,k_2)\right]^{\overline{*}}\\
&+\vec{E}_i(\vec{r}_a,k_1)\cdot\sum_{j=1}^{N}\sum_{\substack{k=1,\\k\neq j}}^{N}\left[\overset{=b}{u}_j(k_2)\cdot\overset{=j}{u}_k(k_2)\cdot\vec{E}_i(\vec{r}_k,k_2)\right]^{\overline{*}}
\end{aligned}
$$

$$+\sum_{j=1}^{N}\sum_{\substack{k=1,\\k\neq j}}^{N}\bar{\bar{u}}_{j}^{a}(k_1)\cdot\bar{\bar{u}}_{k}^{j}(k_1)\cdot\vec{E}_{i}(\vec{r}_{k},k_1)\cdot\vec{E}_{i}^{\bar{*}}(\vec{r}_{b},k_2)$$

$$+\sum_{j=1}^{N}\bar{\bar{u}}_{j}^{a}(k_1)\cdot\vec{E}_{i}(\vec{r}_{j},k_1)\cdot\sum_{j=1}^{N}\sum_{\substack{k=1,\\k\neq j}}^{N}\left[\bar{\bar{u}}_{j}^{b}(k_2)\cdot\bar{\bar{u}}_{k}^{j}(k_2)\cdot\vec{E}_{i}(\vec{r}_{k},k_2)\right]^{\bar{*}}$$

$$+\sum_{j=1}^{N}\sum_{\substack{k=1,\\k\neq j}}^{N}\bar{\bar{u}}_{j}^{a}(k_1)\cdot\bar{\bar{u}}_{k}^{j}(k_1)\cdot\vec{E}_{i}(\vec{r}_{k},k_1)\cdot\sum_{j=1}^{N}\left[\bar{\bar{u}}_{j}^{b}(k_2)\cdot\vec{E}_{i}(\vec{r}_{j},k_2)\right]^{\bar{*}}$$

$$+\vec{E}_{i}(\vec{r}_{a},k_1)\cdot\sum_{j=1}^{N}\sum_{\substack{k=1,\\k\neq j}}^{N}\sum_{\substack{m=1,\\m\neq k\\m\neq j}}^{N}\left[\bar{\bar{u}}_{j}^{b}(k_2)\cdot\bar{\bar{u}}_{k}^{j}(k_2)\cdot\bar{\bar{u}}_{m}^{k}(k_2)\cdot\vec{E}_{i}(\vec{r}_{m},k_2)\right]^{\bar{*}}$$

$$+\sum_{j=1}^{N}\sum_{\substack{k=1,\\k\neq j}}^{N}\sum_{\substack{m=1,\\m\neq k\\m\neq j}}^{N}\bar{\bar{u}}_{j}^{b}(k_1)\cdot\bar{\bar{u}}_{k}^{j}(k_1)\cdot\bar{\bar{u}}_{m}^{k}(k_1)\cdot\vec{E}_{i}(\vec{r}_{m},k_1)\cdot\vec{E}_{i}^{\bar{*}}(\vec{r}_{b},k_2)$$

$$+\ \ldots$$

Equation 7.8-2

Averaging over position only, replacing the summations by simple multiplication, and noting the form

$$\sum_{j=1}^{N}\left[\bar{\bar{u}}_{j}^{b}(k_2)\cdot\vec{E}_{i}(\vec{r}_{j},k_2)\right]^{\bar{*}}=\sum_{j=1}^{N}\vec{E}_{i}^{\bar{*}}(\vec{r}_{j},k_2)\cdot\left(\bar{\bar{u}}_{j}^{b}(k_2)\right)^{\bar{*}}$$

Equation 7.8-3

Equation 7.8-2 becomes, as we let letting the number of scatterers, N, go to infinity,

$$
\begin{aligned}
\left\langle \vec{E}(\vec{r}_a,k_1)\cdot \vec{E}^{\bar{*}}(\vec{r}_b,k_2)\right\rangle &= \vec{E}_i(\vec{r}_a,k_1)\cdot \vec{E}_i^{\bar{*}}(\vec{r}_b,k_2) \\
&+ \int_V d\vec{r}_j\, \overset{=a}{u}_j(k_1)\cdot \vec{E}_i(\vec{r}_j,k_1)\cdot \vec{E}_i^{\bar{*}}(\vec{r}_b,k_2)\, P(\gamma_j)\rho(\vec{r}_j) \\
&+ \int_V d\vec{r}_j\, \vec{E}_i(\vec{r}_a,k_1)\cdot \vec{E}_i^{\bar{*}}(\vec{r}_j,k_2)\cdot \left[\overset{=b}{u}_j(k_2)\right]^{\bar{*}} P(\gamma_j)\rho(\vec{r}_j) \\
&+ \int_V d\vec{r}_j \int_V d\vec{r}_k\, \overset{=a}{u}_j(k_1)\cdot \vec{E}_i(\vec{r}_j,k_1)\cdot \vec{E}_i^{\bar{*}}(\vec{r}_k,k_2)\cdot \left[\overset{=b}{u}_k(k_2)\right]^{\bar{*}} \left[\rho(\vec{r}_j)\rho(\vec{r}_k)+C(\vec{r}_j,\vec{r}_k)\right] \\
&+ \int_V d\vec{r}_j \int_V d\vec{r}_k\, \vec{E}_i(\vec{r}_a,k_1)\cdot \vec{E}_i^{\bar{*}}(\vec{r}_k,k_2)\cdot \left[\overset{=j}{u}_k(k_2)\right]^{\bar{*}}\cdot \left[\overset{=b}{u}_j(k_2)\right]^{\bar{*}} \left[\rho(\vec{r}_j)\rho(\vec{r}_k)+C(\vec{r}_j,\vec{r}_k)\right] \\
&+ \int_V d\vec{r}_j \int_V d\vec{r}_k\, \overset{=a}{u}_j(k_1)\cdot \overset{=j}{u}_k(k_1)\cdot \vec{E}_i(\vec{r}_k,k_1)\cdot \vec{E}_i^{\bar{*}}(\vec{r}_b,k_2) \left[\rho(\vec{r}_j)\rho(\vec{r}_k)+C(\vec{r}_j,\vec{r}_k)\right] \\
&+ \int_V d\vec{r}_j \int_V d\vec{r}_k \int_V d\vec{r}_m\, \overset{=a}{u}_j(k_1)\cdot \vec{E}_i(\vec{r}_j,k_1)\cdot \vec{E}_i^{\bar{*}}(\vec{r}_m,k_2)\cdot \left(\overset{=k}{u}_m(k_2)\right)^{\bar{*}}\cdot \left(\overset{=b}{u}_k(k_2)\right)^{\bar{*}} \\
&\qquad \cdot \left[\rho(\vec{r}_j)\,\rho(\vec{r}_k)\rho(\vec{r}_m)+\rho(\vec{r}_m)C(\vec{r}_j,\vec{r}_k)+\rho(\vec{r}_j)C(\vec{r}_k,\vec{r}_m)+\rho(\vec{r}_k)C(\vec{r}_j,\vec{r}_m)\right] \\
&+ \int_V d\vec{r}_j \int_V d\vec{r}_k \int_V d\vec{r}_m\, \overset{=a}{u}_j(k_1)\cdot \overset{=j}{u}_k(k_1)\cdot \vec{E}_i(\vec{r}_k,k_1)\cdot \vec{E}_i^{\bar{*}}(\vec{r}_m,k_2)\cdot \left[\overset{=b}{u}_m(k_2)\right]^{\bar{*}} \\
&\qquad \cdot \left[\rho(\vec{r}_j)\rho(\vec{r}_k)\rho(\vec{r}_m)+\rho(\vec{r}_m)C(\vec{r}_j,\vec{r}_k)+\rho(\vec{r}_j)C(\vec{r}_k,\vec{r}_m)+\rho(\vec{r}_k)C(\vec{r}_j,\vec{r}_m)\right] \\
&+ \int_V d\vec{r}_j \int_V d\vec{r}_k \int_V d\vec{r}_m\, \vec{E}_i(\vec{r}_a,k_1)\cdot \vec{E}_i^{\bar{*}}(\vec{r}_m,k_2)\cdot \left(\overset{=k}{u}_m(k_2)\right)^{\bar{*}}\cdot \left(\overset{=j}{u}_k(k_2)\right)^{\bar{*}}\cdot \left(\overset{=b}{u}_j(k_2)\right)^{\bar{*}} \\
&\qquad \cdot \left[\rho(\vec{r}_j)\,\rho(\vec{r}_k)\rho(\vec{r}_m)+\rho(\vec{r}_m)C(\vec{r}_j,\vec{r}_k)+\rho(\vec{r}_j)C(\vec{r}_k,\vec{r}_m)+\rho(\vec{r}_k)C(\vec{r}_j,\vec{r}_m)\right] \\
&+ \int_V d\vec{r}_j \int_V d\vec{r}_k \int_V d\vec{r}_m\, \overset{=b}{u}_j(k_1)\cdot \overset{=j}{u}_k(k_1)\cdot \overset{=k}{u}_m(k_1)\cdot \vec{E}_i(\vec{r}_m,k_1)\cdot \vec{E}_i^{\bar{*}}(\vec{r}_b,k_2) \\
&\qquad \cdot \left[\rho(\vec{r}_j)\,\rho(\vec{r}_k)\,\rho(\vec{r}_m)+\rho(\vec{r}_m)C(\vec{r}_j,\vec{r}_k)+\rho(\vec{r}_j)C(\vec{r}_k,\vec{r}_m)+\rho(\vec{r}_k)C(\vec{r}_j,\vec{r}_m)\right] \\
&+ \ldots
\end{aligned}
$$

Equation 7.8-4

Note that the double integrals may be combined, as well as the triple integrals, etc. By neglecting the terms involving triple scatter between two scatterers (Twersky approximation), etc. Just as was found for the single scatter approximation to the field correlation, the coherent fields in Equation 7.8-4 can be identified and separated. In addition, under this “extended Twersky approximation”, Equation 7.8-4 can be written in a more convenient, closed form [Tsolakis, 1985]. Hence, Equation 7.8-4 becomes [Tsolakis, 1985]

$$\left\langle \vec{E}(\vec{r}_a, k_1) \cdot \vec{E}^{\bar{*}}(\vec{r}_b, k_2) \right\rangle = \left\langle \vec{E}(\vec{r}_a, k_1) \right\rangle \cdot \left\langle \vec{E}^{\bar{*}}(\vec{r}_b, k_2) \right\rangle$$
$$+ \int_V d\vec{r}_j \, \overline{\overline{G}}{}^a_j(k_1) \cdot \left\langle \vec{E}(\vec{r}_j, k_1) \cdot \vec{E}^{\bar{*}}(\vec{r}_j, k_2) \right\rangle \left(\overline{\overline{G}}{}^b_j(k_1) \right)^{\bar{*}} \rho\left(\vec{r}_j\right)$$
$$+ \int_V d\vec{r}_j \int_V d\vec{r}_k \, \overline{\overline{G}}{}^a_j(k_1) \cdot \left\langle \vec{E}(\vec{r}_j, k_1) \cdot \vec{E}^{\bar{*}}(\vec{r}_k, k_2) \right\rangle \cdot \left(\overline{\overline{G}}{}^b_k(k_2) \right)^{\bar{*}} C\left(\vec{r}_j, \vec{r}_k\right)$$

Equation 7.8-5

Here, the mean Green's function, G, has been defined in Equation 7.3-28. Including the configuration averaging, the Bethe-Salpeter equation for the mutual coherence tensor becomes [Tsolakis, 1985]

$$\left\langle \vec{E}(\vec{r}_a, k_1) \cdot \vec{E}^{\bar{*}}(\vec{r}_b, k_2) \right\rangle = \left\langle \vec{E}(\vec{r}_a, k_1) \right\rangle \cdot \left\langle \vec{E}^{\bar{*}}(\vec{r}_b, k_2) \right\rangle$$
$$+ \int_V d\vec{r}_j \left\langle \left\langle \overline{\overline{G}}(\vec{r}_a, \vec{r}_j; k_1) \right\rangle \right\rangle \cdot \left\langle \vec{E}(\vec{r}_j, k_1) \cdot \vec{E}^{\bar{*}}(\vec{r}_j, k_2) \right\rangle \left\langle \left\langle \overline{\overline{G}}(\vec{r}_b, \vec{r}_j; k_2) \right\rangle \right\rangle^{\bar{*}} \rho\left(\vec{r}_j\right)$$
$$+ \int_V d\vec{r}_j \int_V d\vec{r}_k \left\langle \left\langle \overline{\overline{G}}(\vec{r}_a, \vec{r}_j; k_1) \right\rangle \right\rangle \cdot \left\langle \vec{E}(\vec{r}_j, k_1) \cdot \vec{E}^{\bar{*}}(\vec{r}_k, k_2) \right\rangle \cdot \left\langle \left\langle \overline{\overline{G}}(\vec{r}_b, \vec{r}_k; k_2) \right\rangle \right\rangle^{\bar{*}} C\left(\vec{r}_j, \vec{r}_k\right)$$

Equation 7.8-6

7.8.2 Two Frequency, Bethe-Salpeter Equation

At this point rather than pursuing a case with depolarization, we will concentrate on *scalar wave propagation*. Hence, assuming no depolarization, the components of the coherency matrix can be written

$$\left\langle E(\vec{r}_a, k_1) E^*(\vec{r}_b, k_2) \right\rangle = \left\langle E(\vec{r}_a, k_1) \right\rangle \left\langle E^*(\vec{r}_b, k_2) \right\rangle$$
$$+ \int_V d\vec{r}_j \left\langle \left\langle G(\vec{r}_a, \vec{r}_j; k_1) \right\rangle \right\rangle \left\langle E(\vec{r}_j, k_1) E^*(\vec{r}_j, k_2) \right\rangle \left\langle \left\langle G(\vec{r}_b, \vec{r}_j; k_2) \right\rangle \right\rangle^* \rho\left(\vec{r}_j\right)$$
$$+ \int_V d\vec{r}_j \int_V d\vec{r}_k \left\langle \left\langle G(\vec{r}_a, \vec{r}_j; k_1) \right\rangle \right\rangle \left\langle E(\vec{r}_j, k_1) E^*(\vec{r}_k, k_2) \right\rangle \left\langle \left\langle G(\vec{r}_b, \vec{r}_k; k_2) \right\rangle \right\rangle^* C\left(\vec{r}_j, \vec{r}_k\right)$$

Equation 7.8-7

First we note that operating on the mean field, with the $\left(\nabla^2 + k^2\right)$ and recalling that this operates on the observation coordinate $\vec{r}_a$ only, the equation for the mean field becomes

$$\left(\nabla_{\vec{r}_a}^2 + k_1^2\right)\left\langle E(\vec{r}_a, k_1)\right\rangle = \left(\nabla_{\vec{r}_a}^2 + k_1^2\right)E_i(\vec{r}_a, k_1) + \int_V d\vec{r}_j \left(\nabla_{\vec{r}_a}^2 + k_1^2\right)\left\langle\left\langle u_j^a\right\rangle\right\rangle\left\langle E(\vec{r}_j, k_1)\right\rangle\rho(\vec{r}_j)$$
$$+ \int_V d\vec{r}_j \int_V d\vec{r}_k \left(\nabla_{\vec{r}_a}^2 + k_1^2\right)\left\langle\left\langle u_j^a\right\rangle\right\rangle\left\langle\left\langle G(\vec{r}_a, \vec{r}_j; k_1)\right\rangle\right\rangle\left\langle E(\vec{r}_k, k_1)\right\rangle C(\vec{r}_j, \vec{r}_k)$$

$$= 0 - f\left(\hat{k}_i\right)\left\langle E(\vec{r}_a, k_1)\right\rangle\rho(\vec{r}_a) - f\left(\hat{k}_i\right)\int_V d\vec{r}_k \left\langle\left\langle G(\vec{r}_a, \vec{r}_j; k)\right\rangle\right\rangle\left\langle E(\vec{r}_a, k_1)\right\rangle C(\vec{r}_a, \vec{r}_k)$$

Equation 7.8-8

Note that when this operator is applied to an incident field, it yields zero. In addition, this expression explicitly shows the frequency dependence in the Green's function as well as the field quantities.

Recall that under one of the propagation conditions assumed in this chapter, the waves are scattered in the forward direction only. Since the incident wave is assumed to be propagating in the z-direction, the Laplacian, the field quantities and the green's function reduce to a z-variation only, and the wave equation will reduce to a one-dimensional form. For example, Equation 7.8-8 becomes

$$\left(\frac{d^2}{dz_a^2} + k_1^2\right)\left\langle E(z_a, k_1)\right\rangle = \left(\frac{d^2}{dz_a^2} + k_1^2\right)E_i(z_a, k_1) + \int_V d\vec{r}_j \left(\frac{d^2}{dz_a^2} + k_1^2\right)\left\langle\left\langle u_j^a\right\rangle\right\rangle\left\langle E(z_j, k_1)\right\rangle\rho(\vec{r}_j)$$
$$+ \int_V dz_j \int_V dz_k \left(\frac{d^2}{dz_a^2} + k_1^2\right)\left\langle\left\langle u_j^a\right\rangle\right\rangle\left\langle\left\langle G(z_a, z_j; k_1)\right\rangle\right\rangle\left\langle E(z_k, k_1)\right\rangle C(z_j, z_k)$$

$$= 0 - f\left(\hat{k}_i\right)\left\langle E(z_a, k_1)\right\rangle\rho(z_a) - f\left(\hat{k}_i\right)\int_V dz_k \left\langle\left\langle G(z_a, z_j; k)\right\rangle\right\rangle\left\langle E(z_a, k_1)\right\rangle C(z_a, z_k)$$

Equation 7.8-9

However, the three dimensional problem is more general and will apply to both the isotropic and the forward/backward cases (within a constant).

Defining the two-point, two-frequency coherence function

$$\Gamma'(\vec{r}_a, \vec{r}_b, k_1, k_2) \equiv \left\langle E(\vec{r}_a, k_1) E^*(\vec{r}_b, k_2) \right\rangle$$

We apply the operator twice to Equation 7.8-8; once with respect to the observation coordinate at $\vec{r}_a$ and then with respect to the observation coordinate at $\vec{r}_b$; forming the difference

$$\begin{aligned}
&\left(\nabla^2_{\vec{r}_a} + k_1^2\right)\Gamma'(\vec{r}_a, \vec{r}_b, k_1, k_2) - \left(\nabla^2_{\vec{r}_b} + k_2^2\right)\Gamma'(\vec{r}_a, \vec{r}_b, k_1, k_2) \\
&\quad = \quad \left(\nabla^2_{\vec{r}_a} + k_1^2\right)\left\langle E(\vec{r}_a, k_1)\right\rangle\left\langle E^*(\vec{r}_b, k_2)\right\rangle - \left(\nabla^2_{\vec{r}_b} + k_2^2\right)\left\langle E(\vec{r}_a, k_1)\right\rangle\left\langle E^*(\vec{r}_b, k_2)\right\rangle \\
&\qquad + \left(\nabla^2_{\vec{r}_a} + k_1^2\right)\int_V d\vec{r}_j \left\langle\left\langle U(\vec{r}_a, \vec{r}_j; k_1)\right\rangle\right\rangle \Gamma'(\vec{r}_j, \vec{r}_j, k_1, k_2)\left\langle\left\langle U(\vec{r}_b, \vec{r}_j; k_2)\right\rangle\right\rangle^* \rho\left(\vec{r}_j\right) \\
&\qquad - \left(\nabla^2_{\vec{r}_b} + k_2^2\right)\int_V d\vec{r}_j \left\langle\left\langle U(\vec{r}_a, \vec{r}_j; k_1)\right\rangle\right\rangle \Gamma'(\vec{r}_j, \vec{r}_j, k_1, k_2)\left\langle\left\langle U(\vec{r}_b, \vec{r}_j; k_2)\right\rangle\right\rangle^* \rho\left(\vec{r}_j\right) \\
&\qquad + \left(\nabla^2_{\vec{r}_a} + k_1^2\right)\int_V d\vec{r}_j \int_V d\vec{r}_k \left\langle\left\langle U(\vec{r}_a, \vec{r}_j; k_1)\right\rangle\right\rangle \Gamma'(\vec{r}_j, \vec{r}_k, k_1, k_2)\left\langle\left\langle U(\vec{r}_b, \vec{r}_k; k_2)\right\rangle\right\rangle^* C\left(\vec{r}_j, \vec{r}_k\right) \\
&\qquad - \left(\nabla^2_{\vec{r}_b} + k_2^2\right)\int_V d\vec{r}_j \int_V d\vec{r}_k \left\langle\left\langle U(\vec{r}_a, \vec{r}_j; k_1)\right\rangle\right\rangle \Gamma'(\vec{r}_j, \vec{r}_k, k_1, k_2)\left\langle\left\langle U(\vec{r}_b, \vec{r}_k; k_2)\right\rangle\right\rangle^* C\left(\vec{r}_j, \vec{r}_k\right)
\end{aligned}$$

Equation 7.8-10

using the result for the mean field (first two terms on the left) from Equation 7.8-8, Tsolakis [1985],

$$\begin{aligned}
&\left[\left(\nabla^2_{\vec{r}_a} - \nabla^2_{\vec{r}_b}\right) + \left(k_1^2 - k_2^2\right) + \left(f\left(\hat{k}_i, k_1\right)\rho(\vec{r}_a) - f^*\left(\hat{k}_i, k_2\right)\rho(\vec{r}_b)\right)\right] \Gamma'(\vec{r}_a, \vec{r}_b, k_1, k_2) \\
&\quad = \; - f\left(\hat{k}_i, k_1\right)\Gamma'(\vec{r}_a, \vec{r}_a, k_1, k_2)\left\langle\left\langle U^*(\vec{r}_b, \vec{r}_a; k_2)\right\rangle\right\rangle \rho\left(\vec{r}_a\right) \\
&\qquad + \left\langle\left\langle U(\vec{r}_a, \vec{r}_b; k_1)\right\rangle\right\rangle \Gamma'(\vec{r}_b, \vec{r}_b, k_1, k_2)\, f^*\left(\hat{k}_i, k_2\right)\rho\left(\vec{r}_b\right) \\
&\qquad - \int_V d\vec{r}_k \left[f\left(\hat{k}_i, k_1\right) C\left(\vec{r}_a, \vec{r}_k\right) - f^*\left(\hat{k}_i, k_2\right) C(\vec{r}_j, \vec{r}_b) \right] \\
&\qquad\qquad \cdot \left[\left\langle\left\langle U(\vec{r}_a, \vec{r}_j; k_1)\right\rangle\right\rangle \Gamma'(\vec{r}_j, \vec{r}_b, k_1, k_2) + \left\langle\left\langle U^*(\vec{r}_b, \vec{r}_j; k_2)\right\rangle\right\rangle \Gamma'(\vec{r}_a, \vec{r}_j, k_1, k_2) \right]
\end{aligned}$$

Equation 7.8-11

This closed equation is the desired form of the scalar-valued Dyson equation found in the papers by both Besieris [1981] and Tsolakis [1985]. The difference is in the form of the scattering amplitude function. Rather than assuming isotropic scattering as was done in the paper by Tsolakis [1985], a forward/backward scattering approximation is assumed for the scattering amplitude. Hence, rather than dipole-like scatterers in which the scatterer is small with respect to the wavelength, we have assumed that the scatterer is large with respect to the wavelength. We next follow in the footsteps of Besieris and Tsolakis in order to derive the two-frequency radiative transfer model.

7.8.3 The Quasi-Homogenous Assumption

The next step in deriving the transfer model is a transformation to center of mass coordinates. With this in mind, we substitute

$$\vec{R} \equiv \frac{1}{2}(\vec{r}_a + \vec{r}_b) \text{ and } \vec{r} \equiv (\vec{r}_a - \vec{r}_b)$$

$$k_s \equiv \frac{1}{2}(k_1 + k_2) \text{ and } k_d \equiv (k_1 - k_2)$$

Making the corresponding changes to the functional variables, we define the quantities; the first by straight substitution:

$$\rho\left(\vec{R} \pm \frac{1}{2}\vec{r}\right) \equiv \rho(\vec{r}_a), \rho(\vec{r}_b)$$

$$f\left(\hat{k}_i, k_s \pm \frac{1}{2}k_d\right) \equiv f(k_1) \text{ or } f(k_2)$$

For notational convenience, the modified expression for the scattering amplitude no longer includes a reference to the incidence direction. Starting with the Mutual Coherence Function, we define a new set of functions

$$\Gamma'(\vec{r}_a, \vec{r}_b, k_1, k_2) = \Gamma'\left(\vec{R} + \frac{1}{2}\vec{r}, \vec{R} - \frac{1}{2}\vec{r}, k_s + \frac{1}{2}k_d, k_s - \frac{1}{2}k_d\right)$$

$$\equiv \Gamma\left(\frac{1}{2}(\vec{r}_a + \vec{r}_b), (\vec{r}_a - \vec{r}_b), \frac{1}{2}(k_s + k_d), (k_s - k_d)\right) = \Gamma(\vec{R}, \vec{r}, k_s, k_d)$$

$$\Gamma'(\vec{r}_b, \vec{r}_b, k_1, k_2) = \Gamma'\left(\vec{R} - \frac{1}{2}\vec{r}, \vec{R} - \frac{1}{2}\vec{r}, k_s + \frac{1}{2}k_d, k_s - \frac{1}{2}k_d\right)$$

$$\equiv \Gamma\left(\frac{1}{2}(\vec{r}_b + \vec{r}_b), (\vec{r}_b - \vec{r}_b), \frac{1}{2}(k_s + k_d), (k_s - k_d)\right) = \Gamma\left(\vec{R} - \frac{1}{2}\vec{r}, 0, k_s, k_d\right)$$

the scatterer correlation:

$$C(\vec{r}_a, \vec{r}_b) = C\left(\vec{R} + \frac{1}{2}\vec{r}, \vec{R} - \frac{1}{2}\vec{r}\right)$$

$$\equiv B\left(\frac{1}{2}(\vec{r}_a + \vec{r}_b), (\vec{r}_a - \vec{r}_b)\right) = B(\vec{R}, \vec{r})$$

the “Mass Kernel:”

$$f(k_1)C(\vec{r}_a, \vec{r}_b)\langle\langle U(\vec{r}_a, \vec{r}_b;\ k_1)\rangle\rangle$$

$$= f\left(k_s + \frac{1}{2}k_d\right)C\left(\vec{R} + \frac{1}{2}\vec{r}, \vec{R} - \frac{1}{2}\vec{r}\right)\left\langle\left\langle U\left(\vec{R} + \frac{1}{2}\vec{r}, \vec{R} - \frac{1}{2}\vec{r}; k_s + \frac{1}{2}k_d\right)\right\rangle\right\rangle$$

$$\equiv M\left(\frac{1}{2}(\vec{r}_a + \vec{r}_b), (\vec{r}_a - \vec{r}_b); k_s + \frac{1}{2}k_d\right) = M\left(\vec{R}, \vec{r}\,; k_s + \frac{1}{2}k_d\right)$$

the Mean Green’s Function:

$$\langle\langle U(\vec{r}_a, \vec{r}_b;\ k_1)\rangle\rangle = \left\langle\left\langle U\left(\vec{R} + \frac{1}{2}\vec{r}, \vec{R} - \frac{1}{2}\vec{r}; k_s + \frac{1}{2}k_d\right)\right\rangle\right\rangle$$

$$\equiv \left\langle\left\langle G\left(\frac{1}{2}(\vec{r}_a + \vec{r}_b), (\vec{r}_a - \vec{r}_b); k_s + \frac{1}{2}k_d\right)\right\rangle\right\rangle = \left\langle\left\langle G\left(\vec{R}, \vec{r}\,; k_s + \frac{1}{2}k_d\right)\right\rangle\right\rangle$$

$$\left\langle\left\langle U(\vec{r}_a, \vec{r}';\ k_1)\right\rangle\right\rangle = \left\langle\left\langle U\left(\vec{R} + \frac{1}{2}\vec{r}, \vec{r}'; k_s + \frac{1}{2}k_d\right)\right\rangle\right\rangle$$

$$\equiv \left\langle\left\langle G\left(\frac{1}{2}(\vec{r}_a + \vec{r}_b), (\vec{r}_a - \vec{r}_b); k_s + \frac{1}{2}k_d\right)\right\rangle\right\rangle = \left\langle\left\langle G\left(\frac{1}{2}(\vec{r}_a + (\vec{r}_a - \vec{r}')), \vec{r}'; k_s + \frac{1}{2}k_d\right)\right\rangle\right\rangle$$

$$\equiv \left\langle\left\langle G\left(\vec{R} + \frac{\vec{r} - \vec{r}'}{2}, \vec{r}'; k_s + \frac{1}{2}k_d\right)\right\rangle\right\rangle$$

where we have let $\vec{r}_b = \vec{r}_a - \vec{r}'$, so that the second argument is simply $\vec{r}'$.

Here, we have shown two specific sets of arguments; several different argument sets appear in Equation 7.8-10; these are derived in a similar fashion. Next, we transform the operator:

$$\left(\frac{d^2}{dz_a^2} - \frac{d^2}{dz_b^2}\right) = \left(\frac{\partial}{\partial Z}\frac{\partial Z}{\partial z_a} + \frac{\partial}{\partial z}\frac{\partial z}{\partial z_a}\right)^2 - \left(\frac{\partial}{\partial Z}\frac{\partial Z}{\partial z_b} + \frac{\partial}{\partial z}\frac{\partial z}{\partial z_b}\right)^2$$

$$= \left((1)\frac{\partial}{\partial Z} + \frac{1}{2}\frac{\partial}{\partial z}\right)^2 - \left((1)\frac{\partial}{\partial Z} - \frac{1}{2}\frac{\partial}{\partial z}\right)^2 = 2\frac{\partial}{\partial Z}\frac{\partial}{\partial z}$$

$$\text{(extrapolating)} \Rightarrow \left(\nabla^2_{\vec{r}_a} - \nabla^2_{\vec{r}_b}\right) = 2\nabla_{\vec{R}} \cdot \nabla_{\vec{r}}$$

Substituting, the reformulated equation for the mutual coherence becomes

$$\left[2\nabla_{\vec{R}}\cdot\nabla_{\vec{r}}+2k_sk_d+f\left(k_s+\frac{1}{2}k_d\right)\rho\left(\vec{R}+\frac{1}{2}\vec{r}\right)-f^*\left(k_s-\frac{1}{2}k_d\right)\rho\left(\vec{R}-\frac{1}{2}\vec{r}\right)\right]\Gamma\left(\vec{R},\vec{r},k_s,k_d\right)$$

$$\begin{aligned}
= & -f\left(k_s+\frac{1}{2}k_d\right)\rho\left(\vec{R}+\frac{1}{2}\vec{r}\right)\left\langle\left\langle G^*\left(\vec{R},-\vec{r};k_s-\frac{1}{2}k_d\right)\right\rangle\right\rangle\Gamma\left(\vec{R}+\frac{1}{2}\vec{r},0,k_s,k_d\right)\\
& -f^*\left(k_s-\frac{1}{2}k_d\right)\rho\left(\vec{R}-\frac{1}{2}\vec{r}\right)\left\langle\left\langle G\left(\vec{R},\vec{r};k_s+\frac{1}{2}k_d\right)\right\rangle\right\rangle\Gamma\left(\vec{R}-\frac{1}{2}\vec{r},0,k_s,k_d\right)\\
& -\int_V d\vec{r}'\, M\left(\vec{R}+\frac{\vec{r}-\vec{r}'}{2},\vec{r}',k_s+\frac{1}{2}k_d\right)\Gamma\left(\vec{R}-\frac{1}{2}\vec{r}',\vec{r}-\vec{r}',k_s,k_d\right)\\
& +\int_V d\vec{r}'\, M^*\left(\vec{R}-\frac{\vec{r}+\vec{r}'}{2},\vec{r}',k_s-\frac{1}{2}k_d\right)\Gamma\left(\vec{R}-\frac{1}{2}\vec{r}',\vec{r}+\vec{r}',k_s,k_d\right)\\
& -\int_V d\vec{r}'\, f\left(k_s+\frac{1}{2}k_d\right)B\left(\vec{R}-\frac{1}{2}\vec{r}',\vec{r}+\vec{r}'\right)\\
& \qquad\cdot\left\langle\left\langle G^*\left(\vec{R}+\frac{\vec{r}-\vec{r}'}{2},\vec{r}',k_s+\frac{1}{2}k_d\right)\right\rangle\right\rangle\Gamma\left(\vec{R}-\frac{1}{2}\vec{r}',\vec{r}-\vec{r}',k_s,k_d\right)\\
& -\int_V d\vec{r}'\, f^*\left(k_s-\frac{1}{2}k_d\right)B\left(\vec{R}-\frac{1}{2}\vec{r}',\vec{r}-\vec{r}'\right)\\
& \qquad\cdot\left\langle\left\langle G\left(\vec{R}+\frac{\vec{r}-\vec{r}'}{2},\vec{r}',k_s+\frac{1}{2}k_d\right)\right\rangle\right\rangle\Gamma\left(\vec{R}-\frac{1}{2}\vec{r}',\vec{r}-\vec{r}',k_s,k_d\right)
\end{aligned}$$

Equation 7.8-12

Considering a “smoothly inhomogeneous” medium, we may simplify the expressions by assuming that these quantities vary rapidly with the difference variable and slowly with the sum variables. Expanding these functions in a Taylor series (truncated to the second term) about the value

$$\text{Taylor Series}: \rho(\vec{\xi})\ \text{about}\ \vec{\xi}=\vec{R}:$$

$$\rho\left(\vec{r}_1\right)=\rho\left(\vec{R}+\frac{1}{2}\vec{r}\right)=\rho(\vec{R})+\frac{1}{2}\left[\nabla_{\vec{R}}\rho(\vec{R})\right]_{\vec{r}=0}\cdot\vec{r}+\dots$$

$$\rho\left(\vec{r}_2\right)=\rho\left(\vec{R}-\frac{1}{2}\vec{r}\right)=\rho(\vec{R})-\frac{1}{2}\left[\nabla_{\vec{R}}\rho(\vec{R})\right]_{\vec{r}=0}\cdot\vec{r}+\dots$$

$$\text{Taylor Series}: f(k) \text{ about } k = k_s:$$

$$f(k_1) = f(k_s) + \frac{1}{2} k_d \frac{df(k_s)}{dk_s} + \ldots$$

$$f(k_2) = f(k_s) - \frac{1}{2} k_d \frac{df(k_s)}{dk_s} + \ldots$$

Equation 7.8-13

Substituting into the equation for the two-frequency mutual coherence function and truncating after the first term, we arrive at the following form of Equation 7.8-11

$$
\begin{aligned}
&\left\{ 2\nabla_{\vec{R}} \cdot \nabla_{\vec{r}} + \frac{1}{2} k_s k_d \right\} \Gamma(\vec{R}, \vec{r}, k_s, k_d) + \\
&\left\{ f_R(k_s) \nabla_{\vec{R}} \rho(\vec{R}) \cdot \vec{r} + j2f_I(k_s) \rho(\vec{R}) + \frac{df_R(\hat{k}_i, k_s)}{dk_s} k_d \rho(\vec{R}) \right\} \Gamma(\vec{R}, \vec{r}, k_s, k_d) + \\
&\left\{ f(k_s) \rho(\vec{R}) \left\langle\left\langle G^*(\vec{R}, \vec{r};\ k_s) \right\rangle\right\rangle - f^*(k_s) \rho(\vec{R}) \left\langle\left\langle G(\vec{R}, \vec{r};\ k_s) \right\rangle\right\rangle \right\} \Gamma(\vec{R}, \vec{r}, k_s, k_d) \\
&+ \int d\vec{r}'\, M\left(\vec{R}, \vec{r}', k_s + \frac{1}{2} k_d \right) \Gamma(\vec{R}, \vec{r} - \vec{r}', k_s, k_d) \\
&+ \frac{1}{2} \int d\vec{r}'\, (\vec{r} - \vec{r}') \cdot \nabla_{\vec{R}} M\left(\vec{R}, \vec{r}', k_s + \frac{1}{2} k_d \right) \Gamma(\vec{R}, \vec{r} - \vec{r}', k_s, k_d) \\
&- \frac{1}{2} \int d\vec{r}'\, M(\vec{R}, \vec{r}', k_s)\, \vec{r}' \cdot \nabla_{\vec{R}} \Gamma(\vec{R}, \vec{r} - \vec{r}', k_s, k_d) \\
&- \int d\vec{r}'\, M^*\left(\vec{R}, \vec{r}', k_s - \frac{1}{2} k_d \right) \Gamma(\vec{R}, \vec{r} + \vec{r}', k_s, k_d) \\
&+ \frac{1}{2} \int d\vec{r}'\, (\vec{r} + \vec{r}') \cdot \nabla_{\vec{R}} M^*\left(\vec{R}, \vec{r}', k_s - \frac{1}{2} k_d \right) \Gamma(\vec{R}, \vec{r} + \vec{r}', k_s, k_d) \\
&+ \frac{1}{2} \int d\vec{r}'\, M^*(\vec{R}, \vec{r}', k_s)\, \vec{r}' \cdot \nabla_{\vec{R}} \Gamma(\vec{R}, \vec{r} + \vec{r}', k_s, k_d) \\
&- \int d\vec{r}'\, f(k_s) B(\vec{R}, \vec{r} - \vec{r}') \left\langle\left\langle G(\vec{R}, \vec{r}', k_s) \right\rangle\right\rangle \Gamma(\vec{R}, \vec{r} - \vec{r}', k_s, k_d) \\
&+ \int d\vec{r}'\, f(k_s) B(\vec{R}, \vec{r} + \vec{r}') \left\langle\left\langle G^*(\vec{R}, \vec{r}', k_s) \right\rangle\right\rangle \Gamma(\vec{R}, \vec{r} + \vec{r}', k_s, k_d) = 0
\end{aligned}
$$

Equation 7.8-14

In this form, a narrowband pulse assumption has been incorporated. Hence, under this assumption, the scattering amplitude is peaked at the carrier frequency.

7.8.4 Phase Space Analysis

A Fourier transform of Equation 7.8-14 with respect to the fast (difference) variable changes our solution space to "phase space" [Besieris, 1981]. This particular transform, the Wigner Transform, is accomplished for the two-frequency coherence function as follows

$$W(\vec{R},\vec{u},k_s,k_d)=\frac{1}{2\pi}\int d\vec{r}\,\Gamma\left(\vec{R},\vec{r},k_s,k_d\right)e^{-j\vec{u}\cdot\vec{r}}$$

The result, W, will be referred to as the ***two-frequency Wigner distribution function***. where the transform variable has been identified as the vector, $\vec{u}$. The other quantities of interest transform as follows [Tsolakis, 1985],

$$\begin{aligned}
\phi(\vec{R},\vec{u}) \quad &= \frac{1}{(2\pi)^3}\int d\vec{r}\,B\left(\vec{R},\vec{r}\right)e^{-j\vec{u}\cdot\vec{r}} \\
\tilde{M}(\vec{R},\vec{u},\ldots) \quad &= \frac{1}{(2\pi)^3}\int d\vec{r}\,M\left(\vec{R},\vec{r},\ldots\right)e^{-j\vec{u}\cdot\vec{r}} \\
\left\langle\left\langle\tilde{G}(\vec{R},\vec{u},\ldots)\right\rangle\right\rangle &= \frac{1}{(2\pi)^3}\int d\vec{r}\left\langle\left\langle G(\vec{R},\vec{r},\ldots)\right\rangle\right\rangle e^{-j\vec{u}\cdot\vec{r}}
\end{aligned}$$

Equation 7.8-15

The ellipsis in Equation 7.8-15 has been added to indicate placeholders for additional (dummy) variables. The "equation of evolution" for the two-frequency Wigner distribution function is now written from the Wigner transform of Equation 7.8-14 (taking advantage of the convolutional property of the Fourier transform to eliminate several integrals) [Tsolakis, 1985]

$$
\begin{aligned}
&\left\{ j2\vec{u}\cdot\nabla_{\vec{R}} + \frac{1}{2}k_s k_d + 2j\left[f_I(k_s)\rho(\vec{R}) + \tilde{M}_I\left(\vec{R},\vec{u}',k_s\right)\right]\right\} W(\vec{R},\vec{u},k_s,k_d) \; + \\
&\left[\frac{df_R(k_s)}{dk_s}\rho(\vec{R}) + \frac{d\tilde{M}_R\left(\vec{R},\vec{u}',k_s\right)}{dk_s}\right] k_d W(\vec{R},\vec{u},k_s,k_d) \; + \\
&j\left[f_R(k_s)\nabla_{\vec{R}}\rho(\vec{R}) + \nabla_{\vec{R}}\tilde{M}_R\left(\vec{R},\vec{u}',k_s\right)\right]\cdot\nabla_{\vec{u}} W(\vec{R},\vec{u},k_s,k_d) - \\
&j\nabla_{\vec{u}}\tilde{M}_R\left(\vec{R},\vec{u}',k_s\right)\cdot\nabla_{\vec{R}} W(\vec{R},\vec{u},k_s,k_d) \; + \\
&\frac{1}{(2\pi)^3}\int d\vec{u}'\left[\phi\left(\vec{R},\vec{u}-\vec{u}'\right) + \rho(\vec{R})\right] W(\vec{R},\vec{u}',k_s,k_d) \\
&\quad\cdot\left\{ f(k_s)\rho(\vec{R})\left\langle\left\langle \tilde{G}^*(\vec{R},\vec{u};\,k_s)\right\rangle\right\rangle - f^*(k_s)\rho(\vec{R})\left\langle\left\langle \tilde{G}(\vec{R},\vec{u};\,k_s)\right\rangle\right\rangle \right\} \\
&= 0
\end{aligned}
$$

Equation 7.8-16

In this development, the following Fourier property was employed

$$
\Im_{\vec{r}}\left\{ \vec{r}\,\Gamma(\vec{R},\vec{r},k_s,k_d)\right\} = j\nabla_{\vec{u}} W(\vec{R},\vec{u},k_s,k_d)
$$

The configurationally averaged Wigner-transformed Green’s function is found from the Dyson equation of **Equation 7.3-30** (suitably transformed to center of mass coordinates)

$$
\left(\nabla_{\vec{r}}^2 + k^2 + f(k_s)\rho(\vec{r})\right)\left\langle\left\langle G(\vec{R},\vec{r})\right\rangle\right\rangle = -f\left(\hat{k}_i\right)\delta(\vec{r}) - f\left(\hat{k}_i\right)\int_V d\vec{r}'\,M(\vec{r}-\vec{r}')\left\langle\left\langle G(\vec{R},\vec{r}')\right\rangle\right\rangle
$$

Equation 7.8-17

and the solution via Fourier transform yields

$$\left\langle\left\langle G(\vec{R},\vec{r},k)\right\rangle\right\rangle = \frac{f(k_s)}{\left[u^2 - k^2 - f_R(k_s)\rho(\vec{R}) - \tilde{M}_R(\vec{R},\vec{u},k_s)\right] - j\left[f_I(k_s)\rho(\vec{R}) + \tilde{M}_I(\vec{R},\vec{u},k_s)\right]}$$

$$= f(k_s)\left[2\,H(\vec{R},\vec{u},k_s)\right]^{-1} = \frac{1}{2} f(k_s)\left[\,H_R(\vec{R},\vec{u},k_s) + jH_I(\vec{R},\vec{u},k_s)\,\right]^{-1}$$

Equation 7.8-18

The quantity $H(\vec{R},\vec{u},k_s)$ is the "complex Hamiltonian" of the effective medium, as defined in the paper by Besieris [1981]. Here, the complex Hamiltonian has been broken down into its real and imaginary portions. The parts,

$$f_R(k_s)\rho(\vec{R}) + \tilde{M}_R(\vec{R},\vec{u},k_s)$$

are identified as refraction terms [Tsolakis, 1985]. The scattering loss terms are identified as [Tsolakis, 1985]:

$$f_I(k_s)\rho(\vec{R}) + \tilde{M}_I(\vec{R},\vec{u},k_s)$$

In this expression, the imaginary portion of the transformed mass operator kernel accounts for scattering loss. Like Besieris and Tsolakis, we assume that the regular and scattering loss terms are small, but not negligible. Hence, a constant energy surface is defined by setting the Hamiltonian equal to zero

$$\begin{aligned} &H_R(\vec{R},\vec{u},k_s) + jH_I(\vec{R},\vec{u},k_s) = 0 \\ &\cong H_R(\vec{R},\vec{u},k_s) = 0 \end{aligned}$$

This equation defines the surface in the (R, u) coordinate space where the wavenumber is equal to the effective wavenumber. This is directly reminiscent of the definition for the effective wavenumber from Equation 7.3-32. In addition, the term,

$$\left\{ f(k_s)\rho(\vec{R})\left\langle\left\langle \tilde{G}^*(\vec{R},\vec{u};\ k_s)\right\rangle\right\rangle - f^*(k_s)\rho(\vec{R})\left\langle\left\langle \tilde{G}(\vec{R},\vec{u};\ k_s)\right\rangle\right\rangle \right\}$$

appears in the purely scattering integral. “It is reasonable then for its computation to neglect completely the imaginary part of the effective complex Hamiltonian. [Tsolakis, 1985]” Consequently, the following approximation is used

$$f^*(k_s)\rho(\vec{R})\left\langle\left\langle \tilde{G}(\vec{R},\vec{u};\ k_s)\right\rangle\right\rangle \cong |f(k_s)|^2\left[2H_R(\vec{R},\vec{u};\ k_s)\right]^{-1}$$

Employing this approximation, and evaluating the inverse Fourier transform into a principal value, P{*}, and the associated singularity

$$f^*(k_s)\rho(\vec{R})\left\langle\left\langle \tilde{G}(\vec{R},\vec{u};\ k_s)\right\rangle\right\rangle \cong P\left\{ \left| f(k_s) \right|^2 \left[2H_R(\vec{R},\vec{u};\ k_s)\right]^{-1}\right\} + j\pi\delta\left\{H_R(\vec{R},\vec{u};\ k_s)\right\}$$

Hence, we make the following approximation

$$\begin{aligned}&\left\{ f(k_s)\rho(\vec{R})\left\langle\left\langle \tilde{G}^*(\vec{R},\vec{u};\ k_s)\right\rangle\right\rangle - f^*(k_s)\rho(\vec{R})\left\langle\left\langle \tilde{G}(\vec{R},\vec{u};\ k_s)\right\rangle\right\rangle \right\}\\ &\qquad \cong -j2\pi\left| f(k_s) \right|^2\delta\left[u^2 - k^2 - f_R(k_s)\rho(\vec{R}) - \tilde{M}_R(\vec{R},\vec{u},k_s)\right]\end{aligned}$$

Equation 7.8-19

Including this approximation, the equation of evolution of the two-frequency Wigner distribution reduces to

$$\left\{\vec{u}\cdot\nabla_{\vec{R}} - j\frac{1}{4}k_s k_d + \left[f_I(k_s)\rho(\vec{R}) + \tilde{M}_I\left(\vec{R},\vec{u}',k_s\right)\right]\right\}W(\vec{R},\vec{u},k_s,k_d)$$

$$-j\frac{k_d}{2}\left[\frac{df_R(k_s)}{dk_s}\rho(\vec{R}) + \frac{d\tilde{M}_R\left(\vec{R},\vec{u}',k_s\right)}{dk_s}\right]W(\vec{R},\vec{u},k_s,k_d)$$

$$+\frac{1}{2}\left[f_R(k_s)\nabla_{\vec{R}}\rho(\vec{R}) + \nabla_{\vec{R}}\tilde{M}_R\left(\vec{R},\vec{u}',k_s\right)\right]\cdot\nabla_{\vec{u}}W(\vec{R},\vec{u},k_s,k_d)$$

$$-\frac{1}{2}\nabla_{\vec{u}}\tilde{M}_R\left(\vec{R},\vec{u}',k_s\right)\cdot\nabla_{\vec{R}}W(\vec{R},\vec{u},k_s,k_d)$$

$$-\frac{1}{4}\left|f(k_s)\right|^2\delta\left\{\left[H_R(\vec{R},\vec{u};\,k_s)\right]^{-1}\right\}\int d\vec{u}'\left[\phi\left(\vec{R},\vec{u}-\vec{u}'\right)+\rho(\vec{R})\right]W(\vec{R},\vec{u}',k_s,k_d)$$

$$= 0$$

Equation 7.8-20

The following interesting observations were added in the paper by Tsolakis [1985],

> The effects of deterministic absorption are subsumed in the term $f_I(k_s)\rho(\vec{R})\,W(\vec{R},\vec{u},k_s,k_d)$. On the other hand, absorption due to pair correlations (randomness) among scatterers enters through the factors involving $\tilde{M}_R\left(\vec{R},\vec{u},k_s\right)$, $\tilde{M}_I\left(\vec{R},\vec{u},k_s\right)$ and $\phi\left(\vec{R},\vec{u}-\vec{u}'\right)$. The interaction between the deterministic absorption and the statistical fluctuations in the medium has been neglected completely.

Given the "weak absorption" approximation, the scattering integral is significant only on the energy surface $H_R\left(\vec{R},\vec{u},k_s\right)=0$ [Besieris, 1981]. "Let specifically, dl, be the differential of a curvilinear ray that passes the point $\vec{R}$ in the direction of the group velocity $\nabla_{\vec{u}}H_R\left(\vec{R},\vec{u},k_s\right)=0$" [Tsolakis, 1985]. Then the Hamilton-Jacobi equations corresponding to the effective Hamiltonian, $H_R\left(\vec{R},\vec{u},k_s\right)$, assume the form

$$\frac{d}{dl}\vec{R} = \frac{\nabla_{\vec{u}} H_R\left(\vec{R},\vec{u},k_s\right)}{\left|\nabla_{\vec{u}} H_R\left(\vec{R},\vec{u},k_s\right)\right|}$$

$$\frac{d}{dl}\vec{u} = -\frac{\nabla_{\vec{R}} H_R\left(\vec{R},\vec{u},k_s\right)}{\left|\nabla_{\vec{u}} H_R\left(\vec{R},\vec{u},k_s\right)\right|}$$

Equation 7.8-21

These results are expected since the ray path is similarly defined in ray optics. Hence, the these results are comparable to the ray equation result [Marcuse, 1982]

$$n\frac{d\vec{r}}{dl} = \nabla S$$

where the function S defines the constant phase surface, n is the refractive index and the vector $\vec{r}$ points from a fixed origin to all points on the light ray. However, in the development of this chapter, the surfaces of constant energy and constant phase may not coincide. Hence, these Hamilton-Jacobi equations apply to the ray path with respect to the constant energy and phase surfaces, respectively. In addition, we can see that an effective index of refraction may be defined as follows

$$n_{eff}\left(\vec{R},\vec{u},k_s\right) = \left|\nabla_{\vec{u}} H_R\left(\vec{R},\vec{u},k_s\right)\right|_{u=k_{eff}}$$

This form will be slightly modified in a later section in order to comply with the definitions given by Tsolakis [1985].

Combining the Hamilton-Jacobi equations with the results for the evolution of the two-frequency Wigner distribution and noting that

$$\begin{aligned}\frac{d}{dl}W(\vec{R},\vec{u},k_s,k_d) &= \nabla_{\vec{R}} W(\vec{R},\vec{u},k_s,k_d)\cdot\frac{d\vec{R}}{dl} + \nabla_{\vec{u}} W(\vec{R},\vec{u},k_s,k_d)\cdot\frac{d\vec{u}}{dl} \\ &= \nabla_{\vec{R}} W(\vec{R},\vec{u},k_s,k_d)\cdot\frac{\nabla_{\vec{u}} H_R\left(\vec{R},\vec{u},k_s\right)}{\left|\nabla_{\vec{u}} H_R\left(\vec{R},\vec{u},k_s\right)\right|} - \nabla_{\vec{u}} W(\vec{R},\vec{u},k_s,k_d)\cdot\frac{\nabla_{\vec{R}} H_R\left(\vec{R},\vec{u},k_s\right)}{\left|\nabla_{\vec{u}} H_R\left(\vec{R},\vec{u},k_s\right)\right|}\end{aligned}$$

Equation 7.8-22

we arrive at the transport equation for the two-frequency Wigner distribution

$$
\begin{aligned}
&\left|\nabla_{\vec{u}} H_R\left(\vec{R},\vec{u},k_s\right)\right| \frac{dW(\vec{R},\vec{u},k_s,k_d)}{dl} + \left[f_I(k_s)\rho(\vec{R}) + \tilde{M}_I\left(\vec{R},\vec{u}',k_s\right)\right] W(\vec{R},\vec{u},k_s,k_d) \\
&- 2\left|f(k_s)\right|^2 \delta\left\{\left[H_R(\vec{R},\vec{u};\,k_s)\right]^{-1}\right\} \int d\vec{u}' \left[\phi\left(\vec{R},\vec{u}-\vec{u}'\right)+\rho(\vec{R})\right] W(\vec{R},\vec{u}',k_s,k_d) \\
&- jk_d\left[\frac{k_s}{4} + \frac{1}{2}\frac{df_R(k_s)}{dk_s}\rho(\vec{R}) + \frac{1}{2}\frac{d\tilde{M}_R\left(\vec{R},\vec{u}',k_s\right)}{dk_s}\right] W(\vec{R},\vec{u},k_s,k_d) = 0
\end{aligned}
$$

Equation 7.8-23

This is the “generalized transport equation.” This is not the same as the transport equation for the photometric intensity. That relationship is developed in the next section.

7.8.5 The Two-frequency Radiative Transfer Equation

In order to derive an equation of transfer that is similar to that given in literature, the coherent power must be separated from the incoherent power. This is a requirement since the standard radiative transfer equations are based primarily on the propagation of incoherent power. The first step in producing a radiative transfer formulation will be to split the two-frequency Wigner distribution into a coherent, W_C, and an incoherent, W_I, portion.

$$
\begin{aligned}
W(\vec{R},\vec{u},k_s,k_d) &= \frac{1}{2\pi}\int d\vec{r}\,\Gamma\left(\vec{R},\vec{u},k_s,k_d\right)e^{-j\vec{u}\cdot\vec{r}} \\
&= W_C(\vec{R},\vec{u},k_s,k_d) + W_I(\vec{R},\vec{u},k_s,k_d)
\end{aligned}
$$

the coherent portion obeys a generalized transport equation derived by Tsolakis [1985],

$$
\begin{aligned}
&\left|\nabla_{\vec{u}} H_R\left(\vec{R},\vec{u},k_s\right)\right| \frac{dW_C(\vec{R},\vec{u},k_s,k_d)}{dl} + \left[f_I(k_s)\rho(\vec{R}) + \tilde{M}_I\left(\vec{R},\vec{u}',k_s\right)\right] W_C(\vec{R},\vec{u},k_s,k_d) \\
&- jk_d\left[\frac{k_s}{4} + \frac{1}{2}\frac{df_R(k_s)}{dk_s}\rho(\vec{R}) + \frac{1}{2}\frac{d\tilde{M}_R\left(\vec{R},\vec{u}',k_s\right)}{dk_s}\right] W_C(\vec{R},\vec{u},k_s,k_d) = 0
\end{aligned}
$$

Equation 7.8-24

Notice that this equation behaves just as expected. The form is the same as the overall transport equation with the exception of the scattering integral. Hence, as proposed in previous chapters concerning classical radiative transfer formulation, the coherent power propagates, losing power but no power is scattered back into its path. There are differences with the radiative transfer formulation that will be acknowledged in an upcoming discussion.

The incoherent portion of the two-frequency Wigner distribution is chosen as follows [Tsolakis, 1985].

$$W_I\left(\vec{R}, \vec{u}, k_s, k_d\right) = k_s \frac{\left|\nabla_{\vec{u}} H_R\left(\vec{R}, \vec{u}, k_s\right)\right|}{\left|\nabla_{\vec{u}} H_R\left(\vec{R}, \vec{u}, k_s\right)\right|^3} \delta\left\{\left[H_R(\vec{R}, \vec{u};\ k_s)\ \right]^{-1}\right\} I\left(\vec{R}, \vec{s}, k_s, k_d\right)$$

Equation 7.8-25

In Equation 7.8-25, the ***two-frequency incoherent power density*** at a point $\vec{R}$ propagating in the direction, $\vec{s} = \vec{u}/u$, has been defined. Adopting the effective wavenumber, k_{eff}, as the value of u for which $H_R\left(\vec{R}, u\vec{s}, k_s\right) = 0$, the definition for

$$n_{eff}\left(\vec{R}, \vec{s}, k_s\right) = \left[\frac{\left|\nabla_{\vec{u}} H_R\left(\vec{R}, u\vec{s}, k_s\right)\right|}{k_s}\right]_{u = k_{eff}\left(\vec{R}, \vec{s}, k_s\right)}$$

Equation 7.8-26

In an anisotropic medium, the phase velocity and the group velocity are not in the same direction. This case has been derived for the isotropic scatterers by Tsolakis [1985] but will not be addressed here. In the case of isotropic pair correlations, the quantities, $\tilde{M}_R\left(\vec{R}, \vec{u}, k_s\right), \tilde{M}_I\left(\vec{R}, \vec{u}, k_s\right)$ and $\phi\left(\vec{R}, \vec{u} - \vec{u}'\right)$, no longer depend on a vector, u, only on its magnitude. Consequently, the two-frequency radiative transfer equation reduces to [Tsolakis, 1985]

$$n_{eff}^2(\vec{R},k_s)\frac{d}{dl}\left[I(\vec{R},\vec{s},k_s,k_d)n_{eff}^{-2}(\vec{R},k_s)\right] = -\alpha(\vec{R},\vec{s},k_s)I(\vec{R},\vec{s},k_s,k_d)$$

$$+\ j\frac{k_d}{k_s n_{eff}(\vec{R},k_s)}\left[\frac{k_s}{4}+2\pi\frac{d}{dk_s}\left[\rho(\vec{R})f_R(k_s)+\tilde{M}'(\vec{R},k_{eff}(\vec{R},k_s)\vec{s},k_s)\right]\right]I(\vec{R},\vec{s},k_s,k_d)$$

$$+\ \iint_{\substack{\text{solid}\\\text{angle}}} d\Omega(\vec{s}')p(\vec{R},\vec{s},\vec{s}',k_s)I(\vec{R},\vec{s},k_s,k_d)$$

$$+\ \iint_{\substack{\text{solid}\\\text{angle}}} d\Omega(\vec{s}')p(\vec{R},\vec{s},\vec{s}',k_s)W_C(\vec{R},\vec{s},k_s,k_d)$$

Equation 7.8-27

In Equation 7.8-27, we see that this looks like the classical radiative transfer equations. The extinction coefficient is given by

$$\alpha(\vec{R},\vec{s},k_s)=\frac{1}{k_s n_{eff}(\vec{R},k_s)}\left[f_I(k_s)\rho(\vec{R})+\tilde{M}_I(\vec{R},\vec{u}',k_s)\right]$$

Equation 7.8-28

The first term represents the true absorption and the second term is the loss due to scattering. There is an extra factor, which accounts for frequency offset effects.

$$j\frac{k_d}{k_s n_{eff}(\vec{R},k_s)}\left[\frac{k_s}{4}+\frac{1}{2}\frac{d}{dk_s}\left[\rho(\vec{R})f_R(k_s)+\tilde{M}'(\vec{R},k_{eff}(\vec{R},k_s)\vec{s},k_s)\right]\right]$$

Equation 7.8-29

Recall, however, that the frequency dependence of this solution is limited due to a narrowband assumption. The “power” scattering amplitude (or “phase matrix” from radiometry) is given by

$$p(\vec{R},\vec{s},\vec{s}',k_s)=\frac{2|f(k_s)|^2 k_{eff}^2(\vec{R},k_s)}{k_s^2\, n_{eff}^2(\vec{R},k_s)}\left[\phi(\vec{R},\vec{u}-\vec{u}',k_{eff}(\vec{R},k_s))+\rho(\vec{R})\right]$$

Equation 7.8-30

An obvious difference from the classical transfer formulation is the extinction. When the difference frequency is zero, the extinction coefficient is real as expected; on the other hand, a non-zero difference frequency yields a complex extinction coefficient.

Chapter 8 Surface-Volume Interaction

The interaction of the foliage with the underlying rough surface can be handled in many ways. The simplest is to assume that the random medium above the rough surface does not interact with the rough surface. This has been the approach in the convolutional method. After this level of approximation, comes single scatter interaction, double scatter interaction, etc. Finally, the most complete model is a full interaction. Thus far, this level has only been achieved numerically with a simple closed body above a rough surface.

The returned power from the volume must be modified by the addition of the time-delayed return from the rough surface under the random medium. As previously seen, the radiative transfer method accounts for this second scattering event simply by assuming that the incident wave to the rough surface is due to an attenuated version of the original, free-space, time-delayed incident power waveform. The attenuation is due to the collection of scatterers along each radial from the antenna.

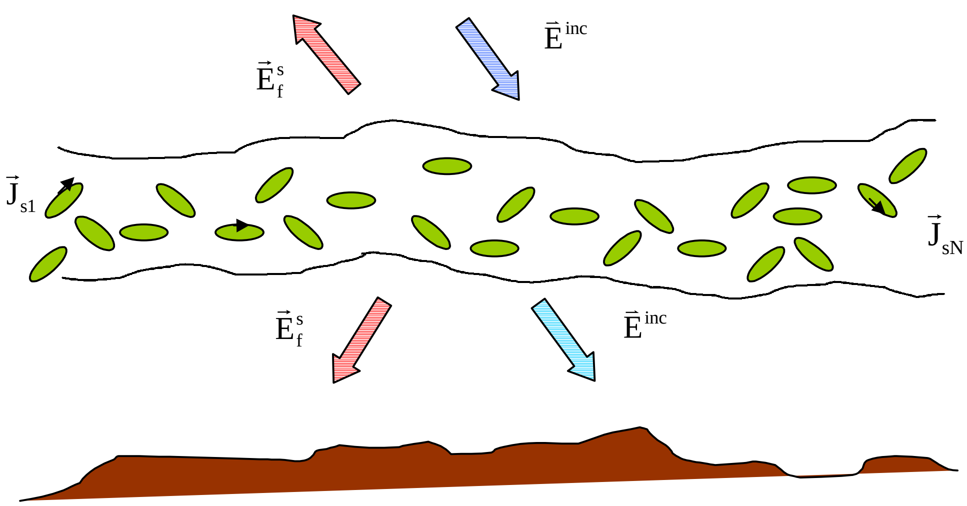

Figure 7.8-1: The total incident field with respect to the surface

After the power waveform is then scattered by the surface, it again travels back up through the foliage, suffering the same attenuation. The details of this approach were developed in the Section 4.3.

Since there are many assumptions are inherent in the radiative transfer result, there is a question as to the validity of this approach. Can the interaction between the foliage and surface be modeled simply by this single interaction? This question may be addressed by interpreting the interaction in the context of equivalent currents and multiple scattering. Referring to Figure 7.8-1, the incident field induces currents in the volume which reradiate to the surface and toward the antenna (single scatter interpretation). This is the foliage, single-scattered field, $\vec{E}_f^s$. This foliage scattered field, $\vec{E}_f^s$, is also incident on the rough surface in addition to the free space incident field $\vec{E}^{inc}$. It is then scattered back through the foliage, (see Figure 7.8-2) resulting in a second scattered field returned to the radar, $\vec{E}_{fsf}^s$, due to the foliage-surface-foliage interaction (a second order interaction).

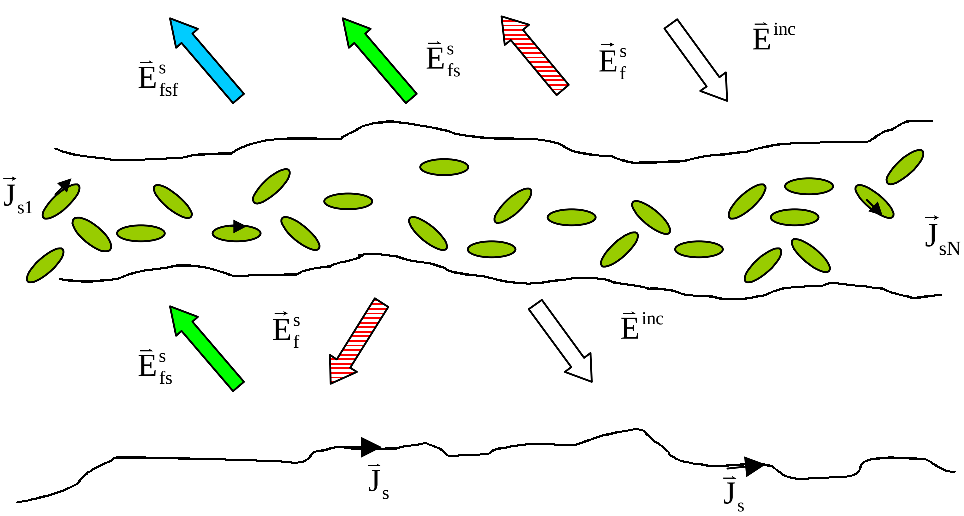

Figure 7.8-2: the first order approximate scattered field from the foliage and surface combination

Naturally, the question arises: are the multiple interactions between the foliage and the surface a necessary component in this portion of the model? That is, is there a significant second order surface interaction due to incidence of the field $\vec{E}^s_{fsf}$, the foliage-surface-foliage field, to the surface? When $\vec{E}^s_{fsf}$ is incident on the surface (note the *addition* of $\vec{E}^s_{fsf}$ into Figure **7.8-3** with respect to Figure 7.8-2) will there be a significant correction to the surface scattered field? This additional incident field will modify the surface currents, which will radiate, $\vec{E}^s_{fsfs}$, creating a new foliage scattered field, $\vec{E}^s_{fsfsf}$. The third order approximation to the interaction between the foliage and the surface would repeat this process again. This process will continue indefinitely, or until the corrections become negligible. Notice that with each iteration, the final foliage scattered field is not used as an incident field for the surface.

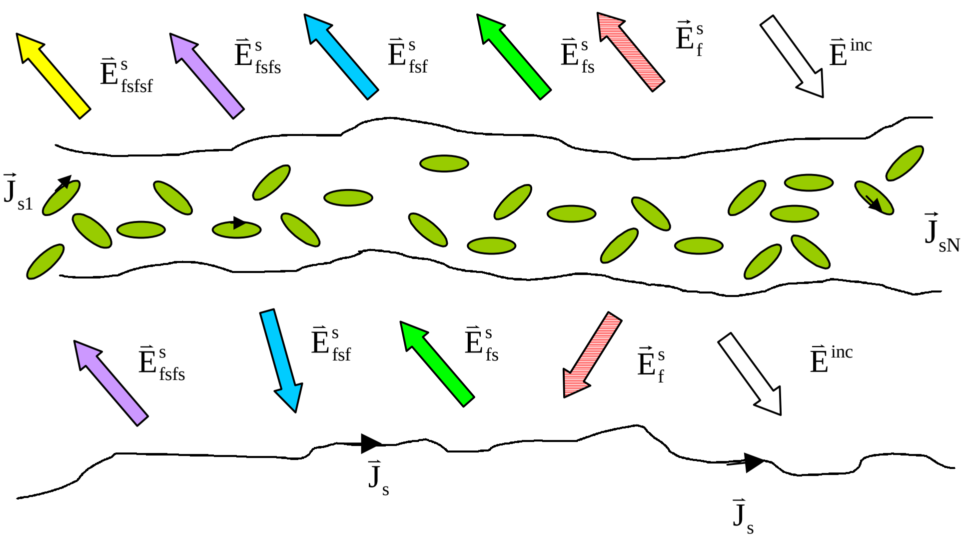

Figure 7.8-3: the second order approximate scattered field from the foliage and surface combination

Hence, extensions of this single passage event would include an infinite series of interactions between the foliage and the surface in the case of single scattering theory or fully coupled integral equations in the integral equation approach. Is the first order scattering interaction term adequate? Three methods of approximation to the second term have been examined in this study:

1. Modified "First Order Multiple Scattering" theory
2. Exact formulation using the Method of Moments (MOM)
3. Reduced integral equation approach

Due to the complexity of the second approach listed only a limited number of scatterers can be placed above the surface. Hence, we will investigate the higher order interactions based on a single scatterer above a rough surface. Since the radiative transfer approach cannot simulate this situation, another approach was required. After some investigation the first listed approach was found to not only support the single scatterer investigation, but also turned out to be a more general version of the radiative transfer result as developed in Chapter 4 . This first order multiple scattering approach, under certain assumptions reduces to the result given for the radiative transfer approach. This is detailed in Chapter 6 .

The first approach, the modified first order multiple scattering result, does begin with a single scatterer. Hence, since the convolutional, radiative transfer approach is related to this method, we need only show that the foliage to surface to foliage interaction requires only the first order interaction, i.e. truncate the infinite series of interactions as previously described with only the first interaction to verify the assumption. In addition, if this method were successfully implemented as a convolution, it would serve as a more general approach than the radiative transfer method as developed in the first section of this chapter.

Verification of the first order multiple scattering result will require a comparison with an exact solution. Consequently, the next section of this chapter examines the exact formulation for a single scatterer above a rough surface and solution via the efficient MOMI method as previously described. This result may serve as an exact result when compared with the first order multiple scattering solution obtained for a single scatterer above a rough surface.

Finally, in the following section, the exact integral equation method is simplified using some reasonable assumptions. This method will result in a more accurate method to simulate interaction between a single scatterer above a rough surface than the first order multiple scattering approach. In addition, it may also yield a more tractable numerical model when it is extended to a collection of scatterers above a rough surface than the full Method of Moments approach. This more accurate representation of the interaction may be required at some level of simulation.

8.1 Single Scatterer above a Rough Surface

The impulse response model, like most radiative transfer models, does not account for any interaction between the scatterers (foliage) and the boundary (surface). In establishing a range of validity for this assumption, a measure and threshold of "no interaction" must be established. Once this measure is established, numerous simulations of the exact scattered field must be examined in order to verify this assumption over a large parameter space including

- the scatterer's size normalized to wavelength
- the scatterer's separation from the rough surface normalized to wavelength
- the scatterer's orientation (if it is not circular)

Consequently, we must assess the magnitude of the contribution of multiple scattering interactions between the scatterer and the rough surface. One approach to establishing the measure of significant interaction would be to include each level of multiple scattering and measure its contribution to the exact solution. Hence, we begin with the assumption that the surface and the scatterer do not interact. Next, we assess the correction for a single scatter interaction.

In order to verify this assumption of independent scattering, an "exact" numerical model has been created using the method of moments (MOM); the numerical solution for the currents on the scatterer and the rough surface accounts for all orders of interactions. After the problem is cast into the proper integral equation, the geometry is discretized in preparation for a solution via the familiar Method of Moments (MOM). Specifically, the Method of Ordered Multiple Interactions (MOMI) has been modified and is implemented as a solution method. This will be described in Section 3.1. Once the currents are found from the integral equation, the scattered fields can be simply found using the proper radiation integral; the far-field formulation has been used. A brief description of the MOMI as originally applied to rough surfaces can be found in Section 3.1.

Extension of the MOMI to Closed Bodies

The MOMI method, as discussed in Section 3.1, is a solution method for the MOM derived matrix equation of the following form:

$$\psi = \psi^{inc} + P\psi$$

Equation 8.1-1

where P is a propagator matrix, ψ is an unknown scalar field and ψ^{inc} is the known incident field. In it original form, , the MOMI neglected self-interaction terms P_{ii} [Kapp, 1996]. The propagator matrix (P) was thus decomposed into lower triangular (L) and upper triangular (U) matrices, each having zero entries along the diagonal,

$$P \rightarrow L + U$$

Equation 8.1-2

Consistent discretization of (1) requires that the diagonal elements P_{ii} be retained [Toporkov, 1998]. This modification was incorporated by decomposing the propagator matrix as

$$P \rightarrow L + \hat{D} + U$$

Equation 8.1-3

where $\hat{D}$ is a diagonal matrix with $\hat{D}$ = P_{ii} [Adams, 1999]. In the application of MOMI to integral equations having singular kernels, Adams has been found that optimal convergence properties are obtained in the decomposition . Physically, maintaining the self interaction terms in $\hat{D}$ separate from (L) and (U) provides better convergence properties when applying the method to integral equations having singular kernels because these equations exhibit strong coupling between oppositely directed fields on the surface of a scatterer [Adams, 1999]. The decomposition leads to the matrix equation

$$\psi = (D - U)^{-1} D (D - L)^{-1} \psi^{inc} + P_M \psi$$

Equation 8.1-4

where D = I - $\hat{D}$ and the MOMI propagator, P_M, is defined as

$$P_M = (D-U)^{-1}D(D-L)^{-1}LD^{-1}U$$

Equation 8.1-5

Neumann iteration of Equation 8.1-4 yields the candidate solution

$$\psi = \sum_{n=0}^{\infty} {P_M}^n (D-U)^{-1}D(D-L)^{-1}\psi^{inc}$$

Equation 8.1-6

which is the same as equation (28) of [Kapp, 1996] under the substitution $D \to I$. The MOMI series (6) provides a very robust and rapidly convergent solution to the MFIE for scattering from extended rough surfaces in two dimensions. The series has never been observed to diverge [Adams, 1999]. These desirable properties have been attributed to the manner in which the MOMI series re-sums the multiple scattering terms present in the Neumann series for the original integral equation.

The Born term in the MOMI series, $(D-U)^{-1}D(D-L)^{-1}\psi^{inc}$, includes the contributions to the current due to all orders of continuous forward scattering $(D-L)^{-1}$, all orders of backscattering, $(D-U)^{-1}$. In addition, it accounts for one order of interaction between the backward and forward traveling waves on the surface (resulting from the multiplication of these operators). The largest effect neglected by the order zero iterate of the MOMI series is that of a wave which twice changes directions on the rough surface before again interacting with the currents on the surface - a triple scattering event.

Consequently, the ordering of the unknowns in the original matrix Equation 8.1-1 is found to have a drastic effect on the convergence of the MOMI series. A different ordering of unknowns in the MOMI series will result in the summation of different multiple scattering terms. In the case of a random ordering of the unknowns in the original matrix Equation 8.1-1 for the rough surface scattering problem, the number of MOMI iterations required to converge to a given error tolerance can be orders of magnitude larger than in the case of the physically based forward-backward ordering. It is not immediately clear how the unknowns in Equation 8.1-1 should be ordered for the application of MOMI to closed body scattering problems. Adams describes two methods of ordering the unknowns in the matrix equation, illustrated in Figure 8.1-1. An ordering which is sequential-in-ϕ (SIP) produces an iterative series that mimics the progression of creeping waves around the surface of the cylinder [Adams, 1999]. However, Adams finds that the ordering which is sequential-in-x (SIX) is somewhat analogous to the forward-backward approach used in [Kapp and Brown, 1996] and is preferred in convergence tests.

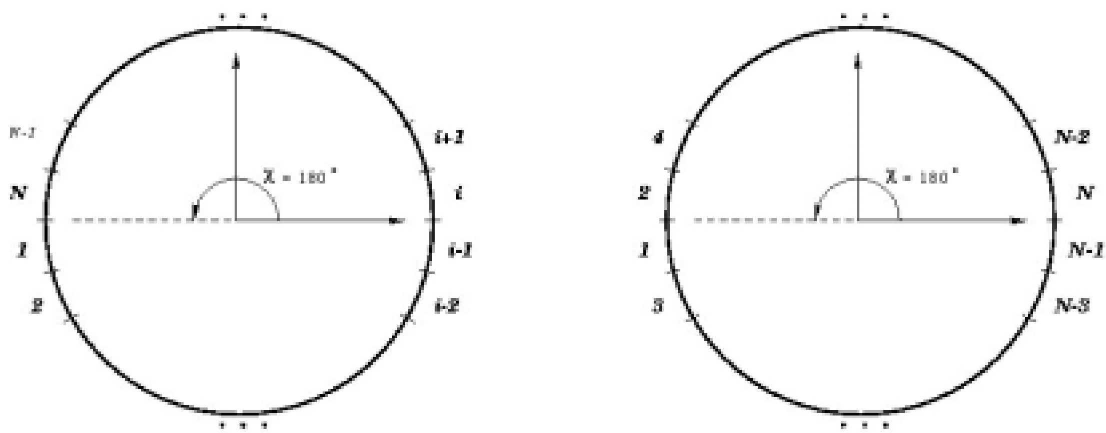

SIP Ordering SIX Ordering

Figure 8.1-1 : Ordering of the Unknowns [Adams, 1999]

8.1.1 A Combined Field Formulation

The scattering problem is formulated in a way that does not give rise to a singular or nearly singular integral equation [Adams, 1999]. In the following, we consider a combined field integral equation (CFIE) representation. The CFIE is a linear combination of the magnetic field integral equation (MFIE) and the electric field integral equation (EFIE) as indicated below.

$$\alpha \text{EFIE} + \text{MFIE} = \text{CFIE}_{\alpha}$$

While the CFIE can be used to provide a unique solution to the scattering problem, the use of MOMI as formulated with a combined field description of the scattering problem introduces additional difficulties associated with the kernels of the EFIEs. These difficulties are explored and settled in the paper by Adams [1999]. He finds that the singularity of the EFIE kernel for TE scattering is much weaker than that for the TM cases and is therefore more amenable to the MOMI series solution technique. Hence, only the TE case is treated here.

The electric field integral equation (EFIE) for TE scattering from a PEC object is

$$0 = E^{inc} - \iint_S \frac{\partial E}{\partial n_0} G \, dS_0$$

Equation 8.1-7

The CFIE for the TE case is obtained by adding this to the MFIE for this problem using the complex constant α. This leads to

$$\frac{\partial E}{\partial n} = 2\alpha E^{inc} + 2\frac{\partial E^{inc}}{\partial n} - 2\iint_S \frac{\partial E^{inc}}{\partial n_0} K_\alpha dS_0$$

Equation 8.1-8

where

$$K_\alpha \equiv \left(\alpha G + \frac{\partial G}{\partial n} \right)$$

Equation 8.1-9

Discretization of this equation is discussed in [Adams, 1998]. The resulting matrix equation can be put in the MOMI form.

The CFIE is guaranteed to have a unique solution whenever α is complex. This requirement provides significant freedom in the choice of α. We further constrain α by requiring that it provide optimal convergence properties for an arbitrary incident field. Adams that stipulates that the choice of α is made in order to minimize the maximum eigenvalue of the propagator (accelerates convergence for arbitrary incidence angles). In addition, the optimal α for the surface (MFIE) α is different from that for the cylinder. Therefore, we choose α as a function of position: $\alpha = \alpha(\rho)$. Surface scattering using the MOMI approach in the past used only the MFIE formulation which is consistent with α= 0, and becomes exact in the flat surface limit.

8.1.2 Example Results for TE Polarization

Simulations that follow demonstrate the investigations into an elliptical cylinder above a rough surface. A MOMI code was produced which includes unknowns on both an elliptical cylinder and a rough surface. The coupling parameter, α, on each surface was chosen to be the optimum for the observation point on the surface. Consequently, α is the asymptotic value described above on the cylinder and $\alpha = 0$ on the surface. The cylinder was chosen to be elliptical in order to resemble the foliage problem. All of the simulations which follow use TE Polarization and $\lambda/10$ sampling. Other parameters depend upon the size of the scatterer and its separation from the surface; these include the following

- incident spot size = 20λ to 30λ
- surface length = 100λ to 200λ
- ellipse: major axis = 10λ , minor axis = 2.5λ
- height of the ellipse = 5λ to 60λ above the mean surface

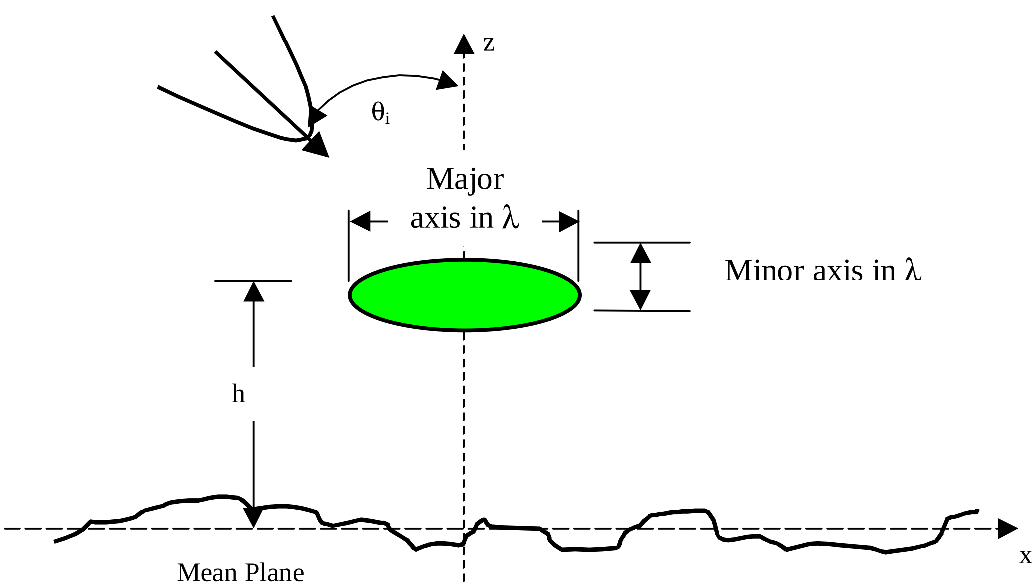

These variables are identified in Figure 8.1-2.

Figure 8.1-2: Scatterer over a Randomly Rough Surface

The total cross section of the elliptical cylinder and rough surface combination is plotted in the figures that follow. The far field form of the Hankel function normalizes this value:

$$\sqrt{\frac{2}{\pi k\rho}}\, e^{jk\rho - j\frac{\pi}{4}}$$

This solution which includes the full interaction will be referred to as the “exact solution”.

In addition to the total cross section of the full interaction problem, the total cross section of various stages of interaction are also included. First, the simple incoherent addition of scatter power is included; this case will be referred to as “incoherent addition” (IA) in the examples that follow. This curve will allow the assumptions of the impulse response method (no interaction) to be compared with a full interaction solution. Hence, it is equivalent to calculating the total cross of the ellipse and the surface in isolation and simply adding the resulting power, see Figure 8.1-3(a) and Figure 8.1-3(b), respectively. The source in this case is will be referred to as the “free-space incident field” and the resulting induced currents as the “incident currents.”

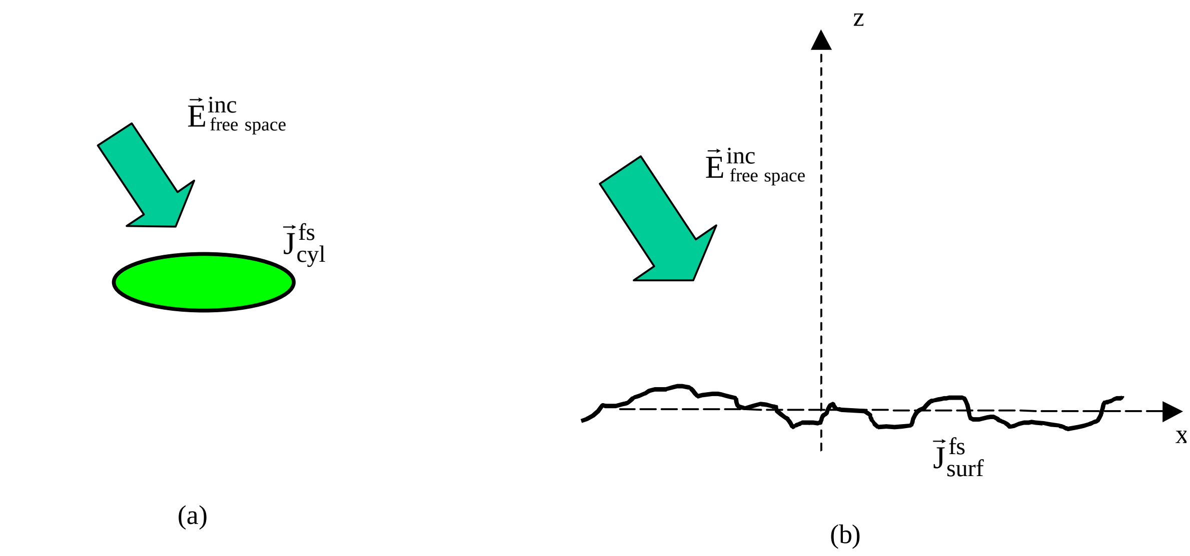

Figure 8.1-3: The Single Scatter Approximation: (a) Currents induced on the cylinder in isolation (b) Currents induced on the surface in isolation

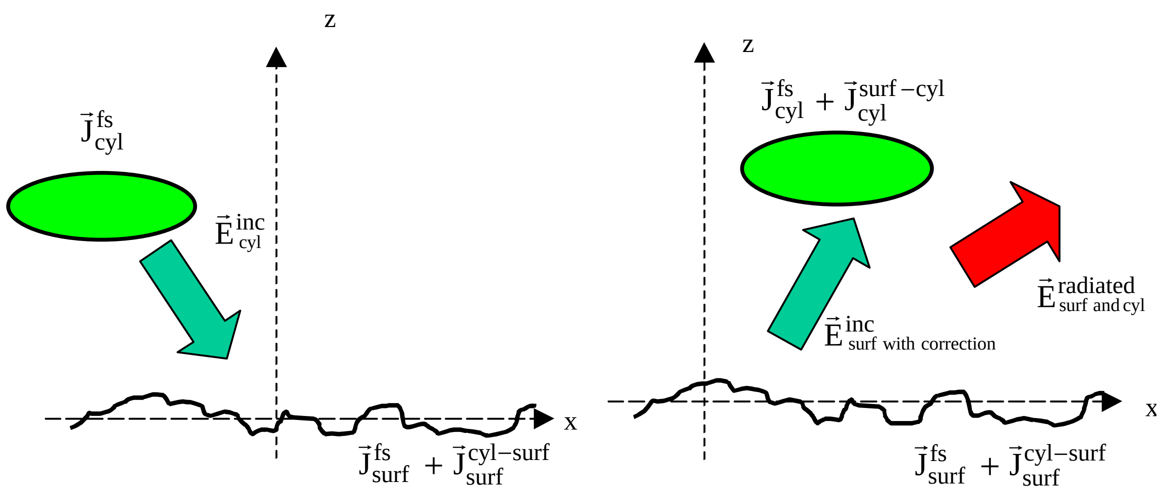

Figure 8.1-4: The Single Scatter Approximation: (a) Corrections to currents induced on the surface (b) Correction to Currents induced on the cylinder

The next step is the addition of the first order correction to both the current on the surface and the ellipse. Thus, after the current on the ellipse is calculated in isolation, its radiated field is added to the free-space field incident on the surface, see Figure 8.1-4(a).

This results in the simple correction of the incident currents and the single scatter currents due to the ellipse. In turn, this corrected current on the surface is permitted to radiate and induce a correction to the current on the ellipse. This results in a double scatter event, yet is still a first order correction to the incident current on the ellipse, see Figure 8.1-4(b). Finally, the composite system with the first order corrected currents is allowed to radiate. This result is referred to as the double scatter result in the following example results.

In Figure 8.1-5 through Figure 8.1-7, we see the effect of separation on the total cross section for the elliptical scatter/rough surface system by varying the separation between a 6 wavelength elliptical cylinder and the surface.

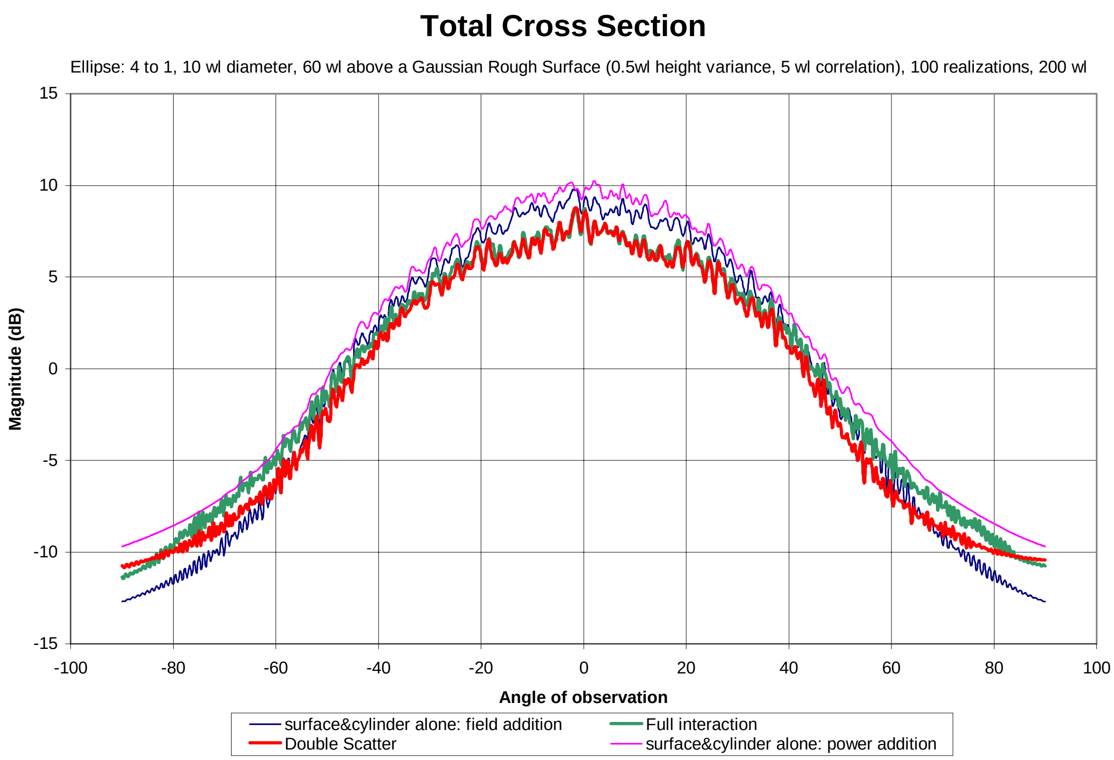

Figure 8.1-5: 10 wavelength ellipse, 60 wavelengths above a Gaussian rough surface

In these figures, the exact total cross-section can be compared with the incoherent addition of the surface and the scatterer (radiative transfer assumption) and the first order interaction between these parts. It is obvious from the figures that the double scatter approximation provides a better estimate of the total cross section of the composite system than the simple incoherent addition of the cross sections of the individual elements. It can also be seen that a larger the separation between the ellipse and the surface results in an increasingly better approximation by the incoherent addition with respect to the exact result. This fact has been verified by examining the cumulative root mean square error (cumulative with respect to the observation angles).

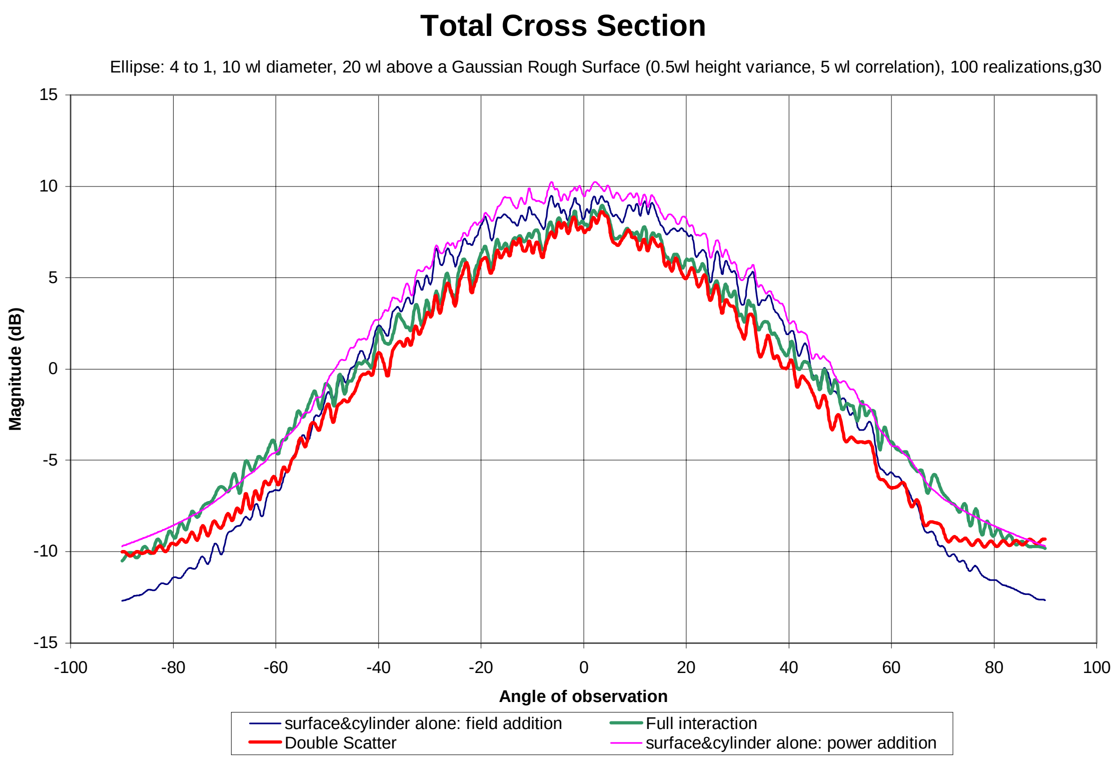

Figure 8.1-6: 10 wavelength ellipse, 20 wavelengths above a Gaussian rough surface

Since the agreement between the incoherent addition of the parts and the exact total cross section becomes closer, we can expect a threshold for the distance at which higher order interactions become significant. In addition to the separation, this threshold will most likely depend on the observation direction, the illumination direction and the orientation of the ellipse. Further numerical studies will be required to find these relationships. We can see that the calculation of the returned power for most foliage components will probably not require accounting the higher order interactions. However, a land-based target buried beneath the foliage, may require accounting for these interactions.

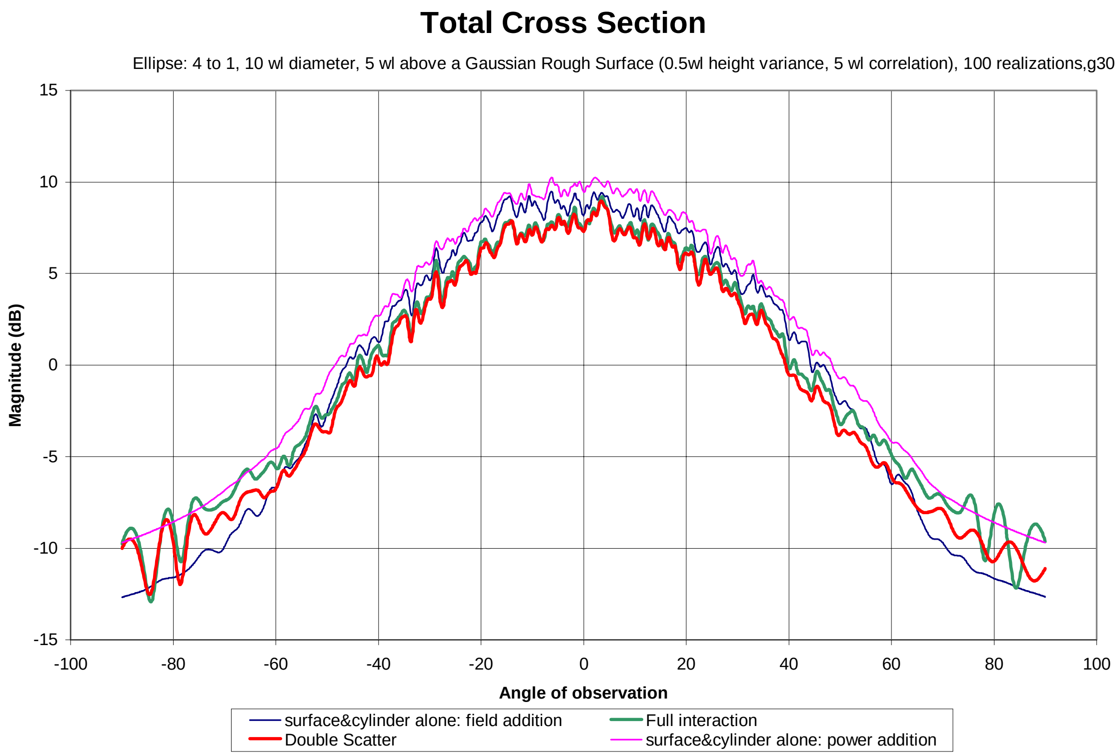

Figure 8.1-7: 10 wavelength ellipse, 5 wavelengths above a Gaussian rough surface

It seems apparent that the farther the scatterer is from the surface, the less interactions become important. In Figure 8.1-8 and Figure 8.1-9, the full interaction problem and the simple power addition are examined for large separations and off-nadir incidence (30 degrees). These results show good agreement and indicate very little interaction.

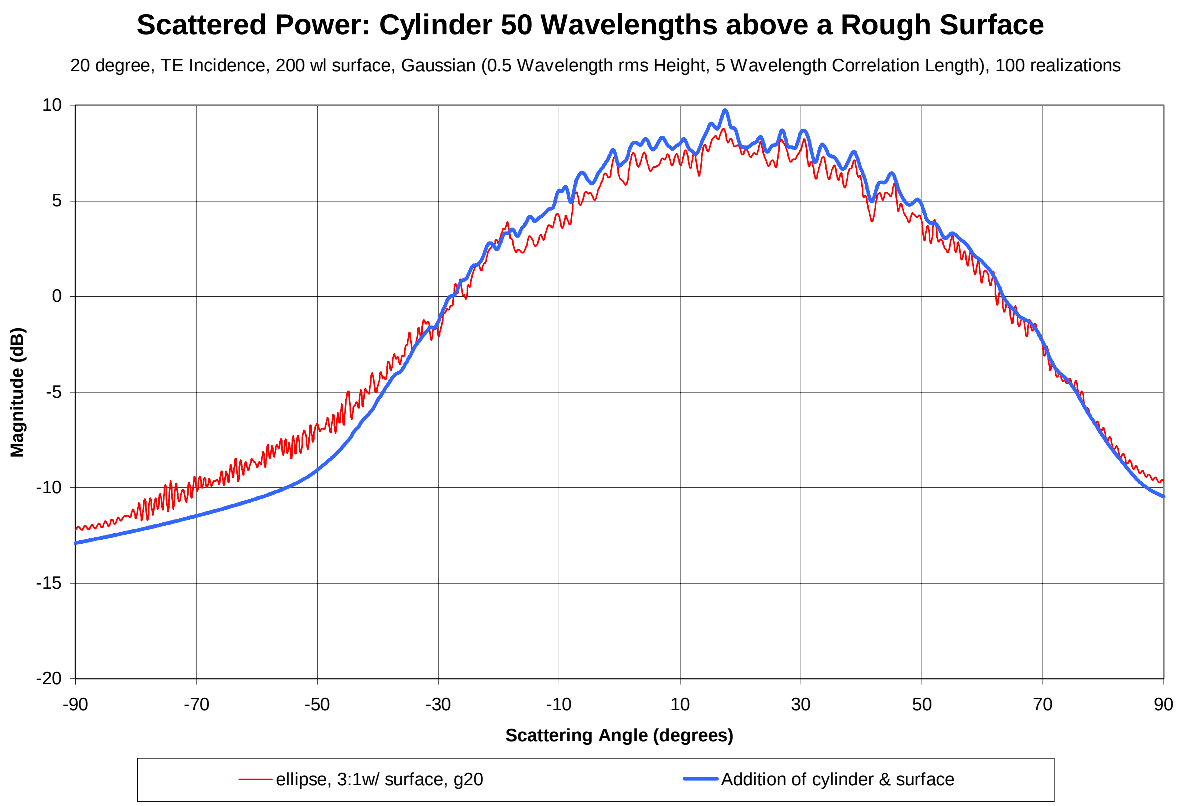

Figure 8.1-8: 10 wavelength ellipse, 50 wavelengths above a Gaussian rough surface

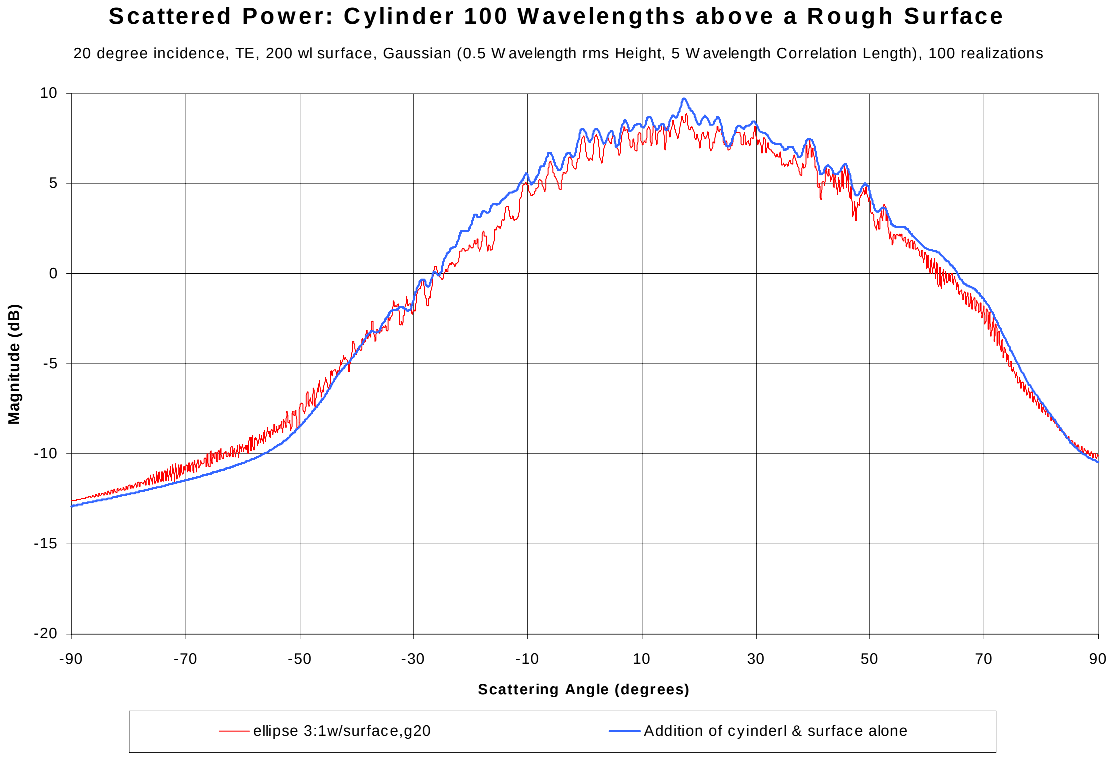

Figure 8.1-9: 10 wavelength ellipse, 100 wavelengths above Gaussian rough surface

8.1.3 Conclusions and Future Efforts

The solution of the cylinder above a rough surface serves as a basis for comparison with the first order multiple scattering approach and ultimately the radiative transfer approach. The results from these simulations will justify the requirements for higher order interactions in the foliage-surface scattering problem. As one would expect, we have seen an increased importance for the higher order interactions as the scatterer is moved closer to the surface or its size increases. This method is obviously inadequate as the number of scatterers increases or as the incidence angle increases since the problem becomes numerically intractable. The conclusions drawn from the example are not surprising and include the following

- the iterations required increased as the ratio of the body size to height above the surface decreased
- the interaction between the surface and the cylinder decreases as the separation is increased and incidence angle is decreased (measured from the vertical)
- the beamwidth must be significantly larger than the ellipse to see the effects of multiple scattering
- the single/double scatter corrections significantly improve the estimate for power returned relative to the simple power addition (at least for small roughness)

In addition, we have seen slower convergence in our technique as the scatterer is moved closer to the surface. Consequently, a stabilized bi-conjugate gradient solution (BiCSTAB) in combination with the MOMI has been implemented as an aide for the convergence of the problem. We note that the application of the BiCSTAB routine to the MOM equations in one particular example (16λ cylinder major axis, 3λ above the rough surface) did not converge within the number of iterations allotted. Likewise, the straight MOMI solution required 30 iterations. However, when the BiCSTAB routine was applied to the MOM equations *after* the MOMI preconditioner was applied, the ellipse and rough surface system required only 10 MOMI/BiCSTAB iterations.

Two final notes: since these simulations occur with monochromatic waves and the interest in this work involves pulsed energy, the pulse chosen for comparison will be slowly varying and of long duration. Primarily, we are interested in the importance of the interactions, not the solution; consequently, until a time-dependent code is introduced, we will assume that the importance of the interactions in the pulsed energy problem is similar to that in the monochromatic problem. In addition, one further assumption of the impulse response model requires our attention; the assumption of no wide-angle scattering. This may be significant for all components of foliage and ground-based targets.

8.2 Approximate Analytical Solution for the Moments of a Single Scatterer above a Rough Surface

If it is found that the scatterer above the rough surface includes important interactions that are not included in the modified first order multiple scattering solution, this solution must be refined. In addition, if the return from a strong scattering object, such as a vehicle, under the vegetation is desired, then the coherent return may be desired. The exact solution for the problem of multiple scatterers above a rough surface will become numerically intractable as the number of scatterers increase. *Consequently, alternative methods must be used or the exact solution must be simplified.* As we have seen in the previous sections, the exact solution for a single scatterer above the rough surface in combination with the first order multiple scattering will produce some insight into the validity of the radiative transfer result. An alternate approach that simplifies the exact results, yet unlike the first order multiple scattering result, maintains the coherent response, begins with the exact integral equations and incorporates some reasonable assumptions. Like the first order multiple scattering response, we begin with a single scatterer over a rough surface and propose an extension to N scatterers above a rough surface.

We start with coupled integral equations: one representing the current on the rough surface and the other representing that on the scatterer. From equivalence, the MFIE for the current on the scatterer in the presence of the rough surface can be written

$$\begin{aligned}\bar{J}_{s1}(\bar{r}_1) = 2\hat{n}_1 \times \bar{H}^i(\bar{r}_1) + 2\hat{n}_1 \times \iint_{\substack{\text{Scatterer}\\ \text{Surface}}} \bar{J}_{s1}(\bar{r}_1') \times \nabla' G(\bar{r}_1, \bar{r}_1')\, dS_1 \\ + 2\hat{n}_1 \times \iint_{\substack{\text{Rough}\\ \text{Surface}}} \bar{J}_{s2}(\bar{r}_2') \times \nabla' G(\bar{r}_1, \bar{r}_2')\, dS_2\end{aligned}$$

Equation 8.2-1

where the subscripts 1 and 2 will indicate points or currents on the scatterer and the rough surface, respectively. The current is evaluated at the observation point, which is on the scatterer. Note the presence of the term, the last term. From equivalence, the MFIE for the current on the rough surface in the presence of the scatterer can be written

$$\vec{J}_{s2}(\bar{r}_2) = 2\hat{n}_2 \times \vec{H}^i(\bar{r}_2) + 2\hat{n}_2 \times \iint_{\substack{\text{Scatterer}\\\text{Surface}}} \vec{J}_{s1}(\bar{r}_1') \times \nabla' G(\bar{r}_2, \bar{r}_1')\, dS_1$$
$$+ 2\hat{n}_2 \times \iint_{\substack{\text{Rough}\\\text{Surface}}} \vec{J}_{s2}(\bar{r}_2') \times \nabla' G(\bar{r}_2, \bar{r}_2')\, dS_2$$

Equation 8.2-2

The current is evaluated at the observation point, which is on the scatterer. Note the presence of the coupling, the second term. The geometric quantities in these two equations are defined in Figure 8.2-1.

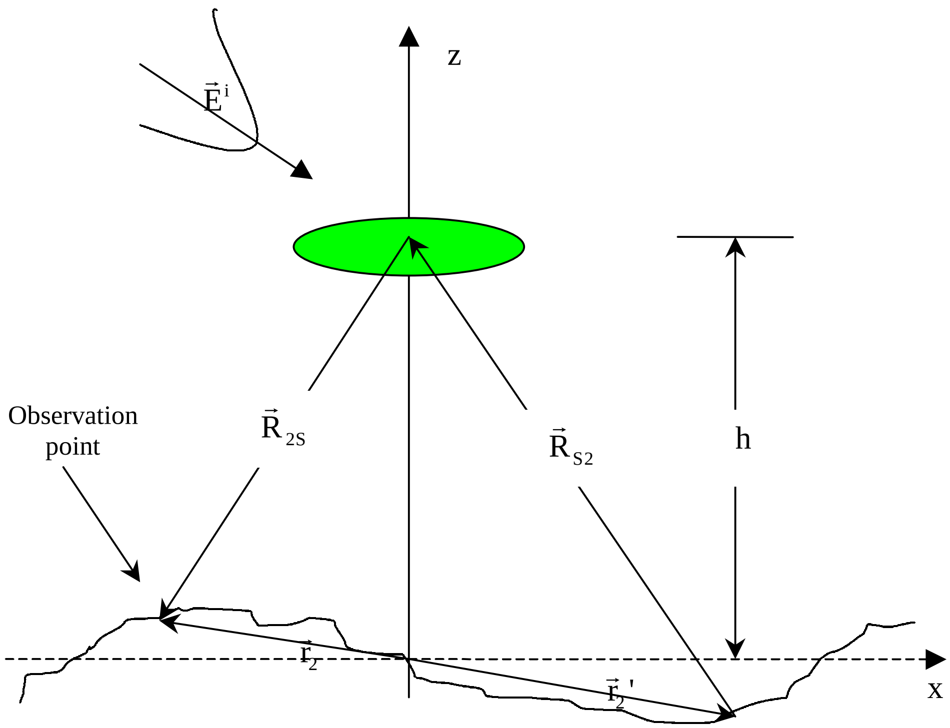

Figure 8.2-1: Geometry for the Reduced Integral Equation Approach

8.2.1 The Reduced Integral Representation

The overall goal is to simplify the solution for a single scatterer over a rough surface. Since the scatterer is assumed to be small with respect to the distance to the surface, the far-field form of the Green's function will be used for interactions involving the scatterer as the source and the surface as the observation location. In addition, when the object is modeled as a smooth ellipse or a disc, the Physical Optics (PO) approximation will be used to estimate the induced currents on the scatterer due to the incident field. In all remaining sections, these two simplifications shall be considered accurate. Starting with the coupled integral equations and substituting into the integrands of (1) and (2) in the previous section, we find for the scatterer

$$\vec{J}_{s1}(\vec{r}_1) = 2\hat{n}_1 \times \vec{H}^i(\vec{r}_1) + 2\hat{n}_1 \times \iint\limits_{\substack{\text{Rough}\\\text{Surface}}} \vec{J}_{s2}(\vec{r}_2\,') \times \nabla' G(\vec{r}_1, \vec{r}_2\,')\, dS_2$$

Equation 8.2-3

In this formulation, the integral equation for the current on the scatterer still involves two unknowns. For the currents on the rough surface, we find the following equation

$$\begin{aligned}\vec{J}_{s2}(\vec{r}_2) &= 2\hat{n}_2 \times \vec{H}^i(\vec{r}_2)\\ &+ 2\hat{n}_2 \times \iint\limits_{\substack{\text{Scatterer}\\\text{Surface}}} \left[2\hat{n}_1 \times \vec{H}^i(\vec{r}_1) + 2\hat{n}_1 \times \iint\limits_{\substack{\text{Rough}\\\text{Surface}}} \vec{J}_{s2}(\vec{r}_2\,') \times \nabla' G(\vec{r}_1, \vec{r}_2\,')\, dS_2 \right] \times \nabla' G_{ff}(\vec{r}_2, \vec{r}_1\,')\, dS_1\\ &+ 2\hat{n}_2 \times \iint\limits_{\substack{\text{Rough}\\\text{Surface}}} \vec{J}_{s2}(\vec{r}_2\,') \times \nabla' G(\vec{r}_2, \vec{r}_2\,')\, dS_2\end{aligned}$$

Equation 8.2-4

where $G_{ff}(r,r')$ is the far-field form of the free space Greens Function. Those vales with a subscripted “1” are in reference to the scatterer and those with a “2” are with respect to the surface. In addition, the primed coordinates reference the sources and unprimed reference the observation points. This integral equation consists of three terms

1. The first term is the well-known Kirchhoff term
2. The second term couples the currents of the surface to that of the scatterer
3. The third term is the familiar multiple scattering term for the surface to surface interactions

Notice that the PO current on the scatterer is known; consequently, the only unknown in the integral equation for the surface current is the surface current itself. Moving the normal unit vectors inside the integrals and using the vector identity

$$\vec{A} \times \vec{B} \times \vec{C} = \vec{B}(\vec{A}\cdot\vec{C}) - \vec{C}(\vec{A}\cdot\vec{B})$$

Equation 8.2-5

Expanding the gradient of the Greens Function:

$$\nabla' G(\vec{r},\vec{r}\,') = \left[\frac{1}{|\vec{r}-\vec{r}\,'|} + jk\right] G(\vec{r},\vec{r}\,') \frac{(\vec{r}-\vec{r}\,')}{|\vec{r}-\vec{r}\,'|} = \left[\frac{1}{|\vec{r}-\vec{r}\,'|} + jk\right] G(\vec{r},\vec{r}\,')\,\hat{k}_s$$

Equation 8.2-6

where, following the notation of [Ishimaru, 1978], the direction from the source point to the observation point is given by

$$\hat{k}_s \equiv \frac{(\vec{r}-\vec{r}\,')}{|\vec{r}-\vec{r}\,'|} = \text{the scattering direction}$$

Employing the far-field approximation, the Greens function and its gradient become

$$G(\vec{r},\vec{r}\,') \cong \frac{e^{-jkR}}{4\pi R} e^{-j\vec{k}\hat{r}\cdot\vec{r}\,'} \equiv G_{ff}(\vec{r},\vec{r}\,')$$

$$\nabla' G(\vec{r},\vec{r}\,') \cong jk \frac{e^{-jkR}}{4\pi R} e^{-j\vec{k}\hat{r}\cdot\vec{r}\,'}\,\hat{k}_s = jk\,G(\vec{r},\vec{r}\,')\,\hat{k}_s$$

Equation 8.2-7

where $\vec{R} \equiv \vec{r} - \vec{r}\,'$. Further reduction of integral equations is accomplished by assuming the scatterer has a definite geometrical shape (disc, etc.). In this case the backscatter and forward scatter from known scatterer geometry may have an analytical result, further simplifying the integral equations.

8.2.2 Reduction for a Circular Disk (3-D) Scatterer above a Rough Surface

In 3-D, the integral equations were specialized to a circular disc with random tilt and height above a randomly rough surface and in 2-D, the integral equations were specialized to a strip with random tilt above a corrugated surface. Only the results of these derivations will be given in this report. These results should include more interaction terms with the surface than the first order multiple scattering theory but with less computational demand than the exact solution. For a flat disc, horizontally suspended over a rough surface, the current on the rough surface is

$$\vec{J}_S(\vec{r}_2) = 2\hat{n}_2 \text{ x } \vec{H}_i(\vec{r}_2) \ + \ jk\frac{\exp\{-jkR_{2S}\}}{2\pi R_{2S}}\exp\{-jk\hat{R}_{2S}\cdot\hat{z}h\}$$

$$\cdot \iint_{S1}\left[\left(-\hat{n}_2\cdot\hat{R}_{2S}\right)\left(\hat{z}\text{ x }\vec{H}_i(\vec{r}_1')\right) + \hat{R}_{2S}\left(\hat{n}_2\cdot\left[\hat{z}\text{ x }\vec{H}_i(\vec{r}_1')\right]\right)\right]\exp\{-jk\hat{R}_{2S}\cdot\vec{r}_1'\}dS_1'$$

$$+ \ 2\iint_{S2}\left\{\vec{J}_S(\vec{r}_2')\ \left(\hat{n}_2\cdot\hat{R}_{22'}\right) - \left(\hat{n}_2\cdot\vec{J}_S(\vec{r}_2')\right)\hat{R}_{22'}\right\}\left|\nabla' G(\vec{r}_2,\vec{r}_2')\right|dS_2'$$

$$+ \ \frac{\exp\{-jkR_{2S}\}}{4\pi^2 R_{2S}}kA\exp\left\{\frac{-jkh^2}{R_{2S}}\right\}J_1(kA)$$

$$\cdot\iint_{S2}\ \{\left[\vec{J}_S(\vec{r}_2')\left(\hat{n}_2\cdot\hat{R}_{2S}\right) - \left(\hat{n}_2\cdot\vec{J}_S(\vec{r}_2')\right)\hat{R}_{2S}\right]\frac{h}{R_{S2}}$$

$$-\left[\left(\hat{n}_2\cdot\hat{R}_{2S}\right)\hat{R}_{S2} - \left(\hat{n}_2\cdot\hat{R}_{S2}\right)\hat{R}_{2S}\right]\left(\hat{z}\cdot\vec{J}_S(\vec{r}_2')\right)\}\frac{\exp\{-jkR_{S2}\}}{4\pi^2 R_{S2}}\exp\left\{\frac{-jkh^2}{R_{S2}}\right\}dS_2'$$

Equation 8.2-8

where the Bessel Function of the first kind, $J_1(x)$, has arisen due to the circular disk and A is the area of one face of the disk. It has been assumed that the disk is very thin. The first term is the Kirchhoff current on the surface. The second term, the first integral term, is an additional Kirchhoff current term due to the incident field from the Kirchhoff current on the disc: the Kirchhoff current on the disk radiates to the surface. Shadowing must be accounted for in the use of this term: the Physical optics current on the underside of the disc, due to the incident field will typically be zero. The third term is the surface in isolation. Finally, the fourth term is a multiple interaction result: the current on the surface radiates to the disk and is re-radiated to the surface again … ad nauseum. Note that this integral equation has only one unknown: the current on the surface.

The integral equation for the disk simply involves Kirchhoff current and the current due to the surface radiating to the disk. Note that this equation is fully coupled to the solution for the current on the surface

$$\vec{J}_1(\vec{r}_1) = 2\hat{z} \times \vec{H}_i(\vec{r}_1)$$
$$+ \ 2\iint_{S2}\left\{\vec{J}_{S2}(\vec{r}_2')\left[\left(\frac{1}{|\vec{r}_1-\vec{r}_2'|} + jk\right)\frac{h}{|\vec{r}_1-\vec{r}_2'|}G(\vec{r}_1,\vec{r}_2')\right] + \nabla' G(\vec{r}_1,\vec{r}_2')\left(\hat{z}\cdot\vec{J}_{S2}(\vec{r}_2')\right)\right\}dS_2'$$

Equation 8.2-9

If the surface is gently undulating, the z-directed currents will be nearly zero, hence, the integral equations for the currents become

$$\vec{J}_S(\vec{r}_2) = 2\hat{n}_2 \times \vec{H}_i(\vec{r}_2) \ + \ jk\frac{\exp\{-jkR_{2S}\}}{2\pi R_{2S}}\exp\left\{-jk\hat{R}_{2S}\cdot\hat{z}h\right\}$$

$$\cdot\iint_{S1}\left[\left(-\hat{n}_2\cdot\hat{R}_{2S}\right)\left(\hat{z}\times\vec{H}_i(\vec{r}_1')\right) + \hat{R}_{2S}\left(\hat{n}_2\cdot\left[\hat{z}\times\vec{H}_i(\vec{r}_1')\right]\right)\right]\exp\left\{-jk\hat{R}_{2S}\cdot\vec{r}_1'\right\}dS_1'$$

$$+ \ 2\iint_{S2}\left\{\vec{J}_S(\vec{r}_2')\left(\hat{n}_2\cdot\hat{R}_{22'}\right) - \left(\hat{n}_2\cdot\vec{J}_S(\vec{r}_2')\right)\hat{R}_{22'}\right\}\left|\nabla' G(\vec{r}_2,\vec{r}_2')\right|dS_2'$$

$$+ \ \frac{\exp\{-jkR_{2S}\}}{4\pi^2 R_{2S}}kA\exp\left\{\frac{-jkh^2}{R_{2S}}\right\}J_1(kA)$$

$$\cdot\iint_{S2}\left\{\left[\vec{J}_S(\vec{r}_2')\left(\hat{n}_2\cdot\hat{R}_{2S}\right) - \left(\hat{n}_2\cdot\vec{J}_S(\vec{r}_2')\right)\hat{R}_{2S}\right]\frac{h}{R_{S2}}\right\}\frac{\exp\{-jkR_{S2}\}}{4\pi^2 R_{S2}}\exp\left\{\frac{-jkh^2}{R_{S2}}\right\}dS_2'$$

Equation 8.2-10

And

$$\vec{J}_1(\vec{r}_1) = 2\hat{z} \times \vec{H}_i(\vec{r}_1) \ + 2\iint_{S2}\vec{J}_{S2}(\vec{r}_2')\left[\left(\frac{1}{|\vec{r}_1-\vec{r}_2'|} + jk\right)\frac{h}{|\vec{r}_1-\vec{r}_2'|}G(\vec{r}_1,\vec{r}_2')\right]dS_2'$$

Equation 8.2-11

A more complex result is available for a disk with arbitrary tilt and in 2-D, a strip with arbitrary tilt.

8.2.3 Conclusions and Future Work

This section has started with the exact coupled integral equations for a rough surface in the presence of a single scatterer and reduced these using the far-field form of the Green's function for the scattered field due to the scatterer and the physical optics solution to the scatterer's current. Furthermore, we have isolated an approximate integral equation for the surface scattering in the presence of the disk. This integral equation only involves one unknown, the current on the rough surface.

In addition, we have simplified the expression for a scatterer that is a circular disk. In addition, the term that represents the multiple interactions between the scatterer and the surface has been isolated and should be evaluated relative to the surface in isolation. This investigation will yield an analytical solution as to the validity of the single interaction assumption for the radiative transfer result. The next step in this process is to numerically implement the above integral equations. These results may then be compared with those obtained with MOM/MOMI. Concurrently, the average results will be attempted analytically for a random height and then the random orientation. These results should be implemented numerically.

In the extension to N scatterers above a rough surface, no interaction between scatterers will be accommodated; the result will include interaction with the surface, like the first order multiple scattering result. Unlike the first order multiple scattering result discussed earlier, these results will include a more comprehensive treatment of the interaction with the surface in addition to the preservation of the coherent field. Numerical solutions and comparison with MOM results for two to three scatterers can be performed in an effort to assess the mutual interactions among the scatterers themselves (ignored by the presented single scatter theory). An attempt to derive analytic expressions for the field moments from these equations will be made, including the mutual coherence functions.

Chapter 9 Summary and Future Efforts

This dissertation has covered a large variety of subjects, all concerning the interaction of waves with rough edges, surfaces and random media. First, a method for predicting the total field beyond a rough knife edge was presented. Using a spectral approach in combination with the paraxial approximation and the Kirchhoff approximation, we can predict the field, total power and its coherent and incoherent components in the line-of-sight direction beyond the obstruction. The mean diffraction field is a result of an effectively smooth knife edge; hence, this term is present even in the absence of roughness on the edge. The fluctuating portion results from the roughness on the knife edge. Hence, for small relative roughness, the diffracted field is equivalent to the mean diffracted field. As the roughness on the edge increases, the edge diffracted-field becomes more incoherent and the phase interference consequently diminishes, leading to an attenuation of the oscillations in the coherent or mean total field.

The wide angle scattering from a rough knife edge may be interpreted in a similar manner. The paraxial approach and the stationary phase result agree in magnitude under narrow (but reasonable) beamwidths and for large observation distances. In order to increase the applicability of this model, the saddle point evaluation of the spectral integration must be completed. This task can be completed using a transformation found in Banos [1966]. Finally, the propagation of a pulse past the rough knife edge was presented. In reducing the problem to a usable form, it was found that a narrowband approximation was necessary. The received pulse, in both the smooth and rough edge result was found to be an amplitude-weighted replica of the transmitted pulse., due to the narrow band assumption, several integrals were dismissed as insignificant; as the bandwidth grows, these integrals will assume a greater role and consequently pulse distortion and dispersion may become an issue. As a future effort, the results presented in this dissertation should be generalized for larger bandwidths.

Extending the idea of the knife edge diffraction, this thesis builds on the topic of a wedge on a plane by extending the Method of Multiple Ordered Interactions (MOMI) to the dielectric surface. This model is developed as a more exact alternative to the

Impedance (Leontovich) Boundary Condition (IBC). In this development, the coupled integral equations governing the scattering by a dielectric surface are combined into a single equation where the lossy dielectric enters the solution as a perturbation of solution for a perfectly conducting surface. Hence, the solution is not only exact, but as the loss increases, the convergence is rapid. Other interesting results are possible when this formulation is extended to the TM polarization.

In predicting the radar return from vegetation, a number of approaches have been developed: radiative transfer, single scatter, and multiple scatter. In this dissertation, the focus has been on the formulation a simple model from radiative transfer theory that is numerically efficient and depends on the empirical identification of effective parameters. However, there are a number of verification studies that were performed and several different levels of verification have been outlined in this dissertation. The Impulse Response (Convolutional) model allows a superposition of surface and volume responses. Its numerical implementation is via the Fast Fourier transform, FFT, which allows a fast numerical solution. This approach, although originally derived from the radar equation and then by the radiative transfer equations, has been shown to be equivalent to the "first order multiple scattering theory." This equivalence has been derived under the assumptions of narrow-band and narrow-beamwidth with a limited scattering pattern.

The beam wave solutions presented have indicated that beam broadening will become significant when the discrete objects scatter isotropically or the medium is electrical deep. Isotropic scattering, however, is expected to yield a large beam spread. Hence, further examination of beam broadening for more general power scattering amplitudes, such as the one proposed by Schwering (see Section 4.4), are necessary. This is a work in progress; although the theory is developed, it has only been tested for forward-backward and isotropic scattering. In addition, there is still room for original work in extending the solutions to polarized waves and pulsed waves.

The single scatter approximation was examined next in the simulation of volume scattering. This approach has exposed several of the major assumptions of the convolutional model, since the single scatter result also leads to the same convolutional equations. The narrow-band and narrow-beamwidth approximations are the primary limitations, beyond the forward-backward scattering approximation. However, using the full expression for two-frequency mutual coherence function, the impulse response approach may be extended to broader bandwidth pulses in addition to broader beamwidth antenna patterns while maintaining some convolutional aspects. In addition, it was demonstrated that the single scatter solution could be extended to include polarization effects. This effort looks feasible and should be attempted.

The multiple scattering approach will yields further insight into the physical parameters that make up the extinction and effective medium parameters. The multiple scattering approach has yielded two useful results with respect to the convolutional model: the Distorted Wave Born Approximation (DWBA), and the two-frequency radiative transfer equation. From the calculation of the mean Green's function, the DWBA will provide an avenue to calculate the scattered power. More specifically, however, using the mean Green's function in the convolutional result from the single scatter development will yield a more predictable and interpretable convolutional model. In this development, the simple far field form of the Green's function in combination with the scattering amplitude would be replaced by the mean Green's function. Finally, the two-frequency radiative transfer equation was reduced to a forward-backward result and is expected to be easily manipulated into the convolutional form, which will include the effects of surface and foliage roughness. Consequently, the result will be a more general, physically interpretable form of the convolutional model. This section of the dissertation has created a host of possible avenues to explore. First, the DWBA should be implemented, first for uncorrelated scatterers and then with pair correlated scatterers. This result will lend some physical interpretation to the convolutional solution. Then the solution must be implemented (along with the two-frequency rough surface result) and compared with the simple convolutional result. Not only will this provide further insight into the physical mechanisms, but it will also add some new dimensions to the analysis – frequency dependence. Obviously, implementing this solution will add complexity to the simple convolutional result, in the form of some difficult inverse Fourier transforms.

In the third region of interaction, the volume and surface interaction, an exact solution to the single scatterer above a rough surface has been implemented via the MOMI method of solution to the MOM problem. This effort is necessary in order to compare the first order multiple scattering result with a result with known accuracy. It has been observed that the interaction is certainly present, particularly when the scatterer is closer to the surface and as incidence angle is further removed from nadir. These results provide a basis of comparison for the impulse response. The results presented are restricted to the TE incidence and must be extended to the construction of the MOMI model for TM polarization for an elliptical cylinder over a rough surface. It is apparent that foliage components well above the rough surface may be treated as non-interacting; this includes components other than the trunk region, which was not simulated. However, it is evident that multiple scattering effects may be significant for a large conducting object near the rough surface. In addition to the impulse response approach, a second analytical approach has been formulated which begins with the exact integral equations. We hope to find an analytical, or at least computationally efficient, solution to both the mean and second order, time dependent power density for the single scatterer above a rough surface.

References

1. Abramowitz, M. and I.A. Stegun, Handbook of Mathematical Functions, Dover Publications, New York, 1972.
2. Adams, R.J., G.S. Brown, "A model for altimeter returns from penetrable geophysical media," *IEEE Transactions on Geoscience and Remote Sensing*, vol. 36, no. 5, 1998.
3. Adams, R.J., G.S. Brown, "A class of Robust and Efficient Iterative Methods for Wave Scattering Problems," Ph.D. Dissertation, Virginia Tech, Blacksburg, VA, December 1998.
4. Adams, R.J., discussions, 2000.
5. Banos, A., Dipole Radiation in the Presence of a Conducting Half-Space, Pergamon Press, Oxford, 1966.
6. Barabanenkov, Yu N., A.G. Vinogradov, Yu. Kravtsov, and V.I. Tatarskii, "Application of the theory of multiple scattering of waves to the derivation of the radiative transfer equation for a statistically inhomogenious medium," Izv. Vyssh. Ucheb. Zaved. Radiofiz., 15, 1852-1860, 1971.
7. Besieris, I.M., and W.E. Kohler, "Two frequency radiative transfer equation for a statistically inhomogeneous and anisotropic absorptive medium," in Multiple Scattering and Waves in Random Media, edited by P.L. Chow, W.E. Kohler, and G.C. Papanicolaou, North Holland, Amsterdam, 1981.
8. Boyce, W.E., Diprima, R.C, Elementary Differential Equations and Boundary Value Problems, Third Edition, Wiley, New York, 1977.
9. Brown, G.S., "The average impulse response of a rough surface and its applications," *IEEE Transactions on Antennas and Propagation*, pp. 67-74, Vol. AP-25, January, 1977.
10. Brown, G.S. & W.J. Curry, "A Theory and Model for Propagation Through Foliage", *Radio Science*, Vol. 17, No. 5, pp. 1027-1036, 1982.
11. Brown, G.S. Class notes, "Rough Surface Scattering," 1997.
12. Chauhan, N.S., R.H. Lang, "Radar Modeling of a Boreal Forest," *IEEE Transactions on Geoscience and Remote Sensing*, v.29, no.4, pp. 627-637, 1983.

13. Chang, H., Ishimaru, A., " Beam wave propagation and scattering in random media based on the radiative transfer theory," Journal of Wave Material Interaction, vol. 2, no. 1, pp. 41-69, 1987.
14. Collin, R.E., Antennas and Radiowave Propagation, McGraw-Hill, New York, 1985.
15. Cole, Randal H., Theory of Ordinary Differential Equations, Appleton, Century, Crofts, New York, 1968.
16. Dagurov, P.N., A.S. Zayakhanov, N.B. Chimitdorzhiev, "A Model of Multibeam Diffractive Propagation of Radio Waves," *Journal of Communications Technology and Electronics*, Vol. 39, No. 6, 8-16, 1994.
17. DeWolf, D.A., "Electromagnetic reflection from an extended turbulent medium: cumulative forward-scatter single–backscatter approximation," *IEEE Transactions on Antennas and Propagation*, Vol. AP-19, No. 2, pp. 254-262, March 1971.
18. Fung, A.K., M.F.Chen, K.K. Lee, "Fresnel field interaction applied to scattering from a vegetation layer, " *Remote Sensing of the Environment*, v. 23, p.35-50, 1987.
19. Fung, A.K., F.T. Ulaby, "A scatter model for leafy vegetation," *IEEE Transactions on Geoscience and Remote Sensing*, v. GE-16, p.281-285, 1978.
20. Fung, A.K., F.T. Ulaby, "Scattering from a vegetation layer," *IEEE Transactions on Geoscience and Remote Sensing*, v. GE-17, p.1-6, 1979.
21. George, N., G.M. Morris, "Diffraction by Serrated Apertures," *Journal of the Optical Society of America*, Vol. 70, No. 1, 6-17, January 1980.
22. Zardecki, A., S.A.W. Gerstl, "Applicatio of the 2-D Discrete Ordinate Method to Multiple Scattering of Laser Radiation," Applied Optics, vol. 22, pp. 1346-1353, 1985.
23. Goodman, J.W., Statistical Optics, John Wiley & Sons, New York, 1985.
24. Ishimaru, A., L. Ailes-Senger, P. Phu, D. Winebrenner, "Pulse scattering by rough surfaces," Ultra-Wideband, Short-Pulse Electromagnetics, ed. Carin, L. and Felsen, L.B., Plenum Press, New York, 1995.
25. Ishimaru, A., Wave Propagation and Scattering in Random Media, IEEE Press, 1997.
26. Johnson, R. and F. Schwering, A Transport Theory of Millimeter Wave Propagation Through Woods and Forests, CECOM Report # CECOM-TR-85-1, February 1985.

27. Johnson, R. and F. Schwering, “A Transport Theory of Millimeter Wave Propagation Through Woods and Forests,” *Journal of Wave-Material Interaction*, v.1, no.2, p.205-236, 1986.

28. Karam, M.A., A.K. Fung, “Scattering from randomly oriented circular discs with application to vegetation,” *Radio Science*, v.18, no.4, p.557-565, 1983.

29. Karam, M.A., A.K. Fung, R.H. Lang, N.S. Chauhan, “A microwave scattering model for layered vegetation,” *IEEE Transactions on Geoscience and Remote Sensing*, v.30, no.4, p.767-784, 1992.

30. Karam, M.A., “A physical model for microwave radiometry of vegetation,” *IEEE Transactions on Geoscience and Remote Sensing*, pp. 1045-1058, Vol. 35, July 1997.

31. Kapp, D.A., G.S. Brown, “A new numerical method for rough surface scattering calculations,” *IEEE Transactions on Antennas and Propagation*, Vol. AP-44, pp. 711-721, May 1996.

32. Karam, M.A., “A physical model for microwave radiometry of vegetation,” IEEE Transactions on Geoscience and Remote Sensing, pp. 1045-1058, Vol. 35, July 1997.

33. Lang, R.H., “Electromagnetic backscattering from a sparse distribution of lossy dielectric scatterers,” *Radio Science*, v.16, no.1, p. 15-30, 1981.

34. Lang, R.H., “Electromagnetic backscattering from a layer of vegetation: a discrete approach,” *IEEE Transactions on Geoscience and Remote Sensing*, v.GE-21, no.1, p.62-71, 1983.

35. LeVine, D.M., R.H. Lang, “Transient response of a layer of discrete random media over a dielectric half space,” *IEEE Transactions on Geoscience and Remote Sensing*, v.30, no.5, p.1034-1045, 1992.

36. Marcuse, D., Light Transmission Optics, Second Edition, Van Nostrand, New York, 1982.

37. McDonald, K.C., Ulaby, F.T., “Radiative transfer modeling of discontinuous tree canopies at microwave frequencies,” *International Journal of Remote Sensing*, Vol. 14, no. 11, pp. 2097-2128, 1993.

38. Newkirk and Brown, “Issues Related to Waveform Computations for Radar Altimeter Applications.” *IEEE Transactions on Antennas and Propagation*, Vol. 40 , No. 12, 1992.

39. Polischuk, Y.M., "Fresnel Diffraction at n Half-planes with Statistically Non-uniform Edges," *Radio Engineering and Electronic Physics*, Vol. 16, 728 – 736, 1971.
40. Polischuk, Y.M., "Fresnel Diffraction at n rough Screens in a Medium with Large-scale Nonhomogeneities," *Radio Engineering and Electronic Physics*, Vol. 19, 2038-2045, 1974.
41. Stutzman, W.L., G.A. Theile, Antenna Theory and Design (2/e), John Wiley and Sons, New York, 1998.
42. Toporkov, J.V., R.T. Marchand, G.S. Brown, "On the Discretization of the Integral Equation Describing Scattering by Rough Conducting Surfaces*.*" *IEEE Transactions on Antennas and Propagation*, Vol. 46, No. 1, 1998.
43. Tsang, L., J.A. Kong, "Radiative transfer theory for active remote sensing of a half-space random media," *Radio Science*, v.13, no. 5, p.763-773, 1978.
44. Tsang, L., M.C. Kubacsi, J.A. Kong, "Radiative transfer theory for active remote sensing of a layer of small ellipsoidal scatterers," *Radio Science*, v.16, no. 3, pp. 321-329, 1981.
45. Tsang, L., J.A. Kong, Shin, R.T., Theory of Microwave Remote Sensing, John Wiley and Sons, New York, 1985.
46. Tsolakis A.I., I.M. Besieris, W.E. Kohler, "Two-frequency radiative transfer equation for scalar waves in a random distribution of discrete scatterers with pair correlations," *Radio Science*, vol. 20, no. 5, pp. 1037-1052, 1985.
47. Twersky, V. "On propagation in random media of discrete scatterers*,*" *Proc. Am. Math. Soc*., vol. 16, pp. 84-116, 1964.
48. Ulaby, F.A., R.K. Moore, A.K. Fung, Microwave Remote Sensing, Volume 2, Artech House, Norwood, MA, 1986.
49. Ulaby, F.A., "Measurement and modeling of millimeter-wave scattering from tree foliage," *Radio Science,* Vol. 25, no. 3, pp. 193-203, May-June, 1990
50. Ulaby, F.A., "Michigan microwave canopy scattering model*,*" *International Journal of Remote Sensing*, Vol. 11, no. 7, pp. 1223-1253, 1990.
51. Whitman G.M., Schwering, F., Triolo, A.A., "A Transport Theory of Pulse Propagation in a Strongly Forward Scattering Random Medium," *IEEE Transactions on Antennas and Propagation*, Vol. 44, No. 1, 1996.

Vita

Bradley A. Davis

PhD. Electrical Engineering, June, 2000.
Virginia Polytechnic Institute and State University (Virginia Tech), Blacksburg, VA

Research I have developed and implemented scattering codes for radar waveform prediction for scattering from rough surfaces and from vegetation covered rough surfaces using a variety of techniques including advanced numerical simulation, multiple scattering, and radiative transfer. In addition, I have developed and produced results for the application of propagation of electromagnetic waves over a statistically rough knife edge.

M.S. Electrical Engineering, August, 1988.
Virginia Polytechnic Institute and State University (Virginia Tech), Blacksburg, VA

Research I assessed the use of Doppler processing in a NASA sponsored multibeam radar altimetry study and developed an algorithm for Doppler clutter mapping. (MS)

B.S. Electrical Engineering, June, 1986.
Virginia Polytechnic Institute and State University (Virginia Tech), Blacksburg, VA

Honors and Certifications

- Registered Professional Engineer, State of Maine, #7823
- Fellowships: Bradley, NSF, Virginia Space Grant to pursue Ph.D.
- Tau Beta Pi, Eta Kappa Nu, Phi Kappa Phi, Phi Eta Sigma

Employment History:

1/96 - Present	**Graduate Research Assistant**; Dr. Gary Brown, Virginia Tech
10/90 – 12/95	**Engineer III**, System Engineering; Central Maine Power Company
9/88 - 9/90	**Associate Engineer**, Antenna Engineering; Westinghouse Electronics
9/86 - 8/88	**Graduate Research Assistant**; Dr. Gary Brown, Virginia Tech
6/87 - 9/87	**Staff Engineer Trainee**, System Survivability; The BDM Corporation
6/86 - 9/86	**Staff Engineer Trainee**, System Survivability; The BDM Corporation
6/84 - 9/84	**Programmer**, Satellite Missions and Payload; GTE Spacenet